

Synthesis and Potency of Long End-Associative Polymers for Mist Control

Thesis by

Ming-Hsin Wei

In Partial Fulfillment of the Requirements for the Degree of Doctor of Philosophy

California Institute of Technology
Pasadena, California
2014

(Defended on September 4, 2013)

© 2014
Ming-Hsin Wei
All Rights Reserved

Dedicated to:

*Jesus Christ, for His salvation and unlimited grace,
and my family, for their unconditional love and support.*

Acknowledgements

I am very grateful for having the opportunity to come to the US in pursuit of my doctoral education. My journey at Caltech has been a wonderful experience, thanks to many fine people and outstanding scientists in the Caltech community. I would love to express my appreciation for the support and contributions I received from the following individuals: my advisor, Professor Julia Kornfield, for her invaluable guidance on research and personal life, and for her kindness; Dr. Virendra Sarohia, for his guidance on research and his unwavering support to my research project; Dr. R. L. Ameri David, Dr. Simon Jones and Dr. Yan Xia, for giving me training on synthetic chemistry; the member of the Kornfield group, for their technical and emotional support; fellow students Paul Pirogovsky and Boyu Li, for their invaluable intellectual input and providing assistance to my research; undergraduate researchers Rachel Moore, Steven Wilke, Ashley Guo and Shuaili Li, for their direct involvement in my research and assistance in lab; and the members of my research committee, Professor Mark Davis and Professor Zhen-Gang Wang, for their guidance and invaluable insights. I would also like to acknowledge Mr. Joel Schmitigal of the US Army Tank Automotive Research, Development and Engineering Center (TARDEC) for sponsoring my research. I express appreciation to my friends of the Radiant Glory group at Evangelical Formosan Church, Los Angeles, for their emotional support and remembering me in their prayers. Finally, I express my appreciation to my family and my wife Wei-Ling, for their unconditional love and support.

Abstract

Long linear polymers that are end-functionalized with associative groups were studied as additives to hydrocarbon fluids to mitigate the fire hazard associated with the presence of mist in a crash scenario. These polymers were molecularly designed to overcome both the shear-degradation of long polymer chains in turbulent flows, and the chain collapse induced by the *random* placement of associative groups along polymer backbones. Architectures of associative groups on the polymer chain ends that were tested included clusters of self-associative carboxyl groups and pairs of hetero-complementary associative units.

Linear polymers with clusters of discrete numbers of carboxyl groups on their chain ends were investigated first: an innovative synthetic strategy was devised to achieve unprecedented backbone lengths and precise control of the number of carboxyl groups on chain ends (N). We found that a very narrow range of N allows the co-existence of sufficient end-association strength and polymer solubility in apolar media. Subsequent steady-flow rheological study on solution behavior of such soluble polymers in apolar media revealed that the end-association of very long chains in apolar media leads to the formation of flower-like micelles interconnected by bridging chains, which trap significant fraction of polymer chains into looped structures with low contribution to mist-control. The efficacy of very long 1,4-polybutadiene chains end-functionalized with clusters of four carboxyl groups as mist-control additives for jet fuel was further tested. In addition to being shear-resistant, the polymer was found capable of providing fire-protection to jet fuel at concentrations as low as 0.3wt%. We also found that this polymer has excellent solubility in jet fuel over a wide range of

temperature (-30 to +70°C) and negligible interference with dewatering of jet fuel. It does not cause an adverse increase in viscosity at concentrations where mist-control efficacy exists.

Four pairs of *hetero-complementary* associative end-groups of varying strengths were subsequently investigated, in the hopes of achieving supramolecular aggregates with both mist-control ability and better utilization of polymer building blocks. Rheological study of solutions of the corresponding complementary associative polymer pairs in apolar media revealed the strength of complementary end-association required to achieve supramolecular aggregates capable of modulating the rheological properties of the solution.

Both self-associating and complementary associating polymers have therefore been found to resist shear degradation. The successful strategy of building soluble, end-associative polymers with either self-associative or complementary associative groups will guide the next generation of mist-control technology.

Table of Contents

Acknowledgements.....	iv
Abstract.....	v
Table of Contents.....	vii
List of Illustrations and Tables.....	xii
Chapter I Introduction.....	I-1
1.1 Technological Need for Safer Kerosene-Based Fuel.....	I-1
1.2 Development of Mist-control Additives for Fuels-A Historical Review.....	I-2
1.2.1 Early Research Efforts.....	I-2
1.2.2 Renewed Motivation and Efforts After the 9-11 Terrorist Attack.....	I-6
1.3 Overview of the Present Work.....	I-11
1.3.1 Objective.....	I-12
1.3.2 Organization.....	I-13
1.4 Figures and Tables.....	I-14
References.....	I-26
Chapter II Opening the Way to Very Long Telechelic Polymers.....	II-1
2.1 Introduction.....	II-1
2.1.1 Background.....	II-1
2.1.2 Scope of the Present Work.....	II-6
2.2 Experimental.....	II-7
2.2.1 Materials and Instrumentation.....	II-7
2.2.2 Synthesis of Chain Transfer Agents (CTAs) and Intermediates.....	II-8
2.2.3 Polymer Synthesis (Scheme 2.2).....	II-15
2.3 Results.....	II-18

2.3.1 Synthesis of Chain Transfer Agents (CTAs).....	II-18
2.3.2 Monomer Purification.....	II-19
2.3.3 Polymer Synthesis	II-21
2.3.4 Hydrolysis of <i>tert</i> -Butyl Ester Groups on Polymer Chain Ends	II-23
2.4 Discussion	II-25
2.4.1 Aspects of the CTA Design	II-25
2.4.2 Molecular-Weight Control	II-29
2.4.3 Hydrolysis of <i>tert</i> -Butyl Ester Terminal Groups of Polymers	II-34
2.5 Conclusions	II-37
2.6 Figures, Schemes, and Tables	II-38
References	II-52
Chapter III End-Associative Polymers in Apolar Aprotic Solvents	III-1
3.1 Introduction	III-1
3.2 Experimental	III-2
3.2.1 Materials	III-2
3.2.2 Procedure for Sample Preparation.....	III-3
3.2.3 Viscosity Measurements.....	III-3
3.3 Results	III-4
3.3.1 Dissolution Behavior	III-4
3.3.2 Steady-Flow Shear Viscosity of 1wt% Polymer Solutions	III-4
3.3.3 Concentration Dependence of Specific Viscosity	III-5
3.3.4 Shear-Thinning Behavior of Solutions of Carboxyl-Terminated Polymers..	III-6
3.4 Discussions.....	III-6
3.4.1 Importance of Precise Control of Chain-End Structure.....	III-6

3.4.2 Relationship between Rheology Modification and Supramolecular Structures	III-8
3.5 Conclusions	III-13
3.6 Figures and Tables	III-15
References	III-23
Chapter IV Structure-Property Relationships for Hetero-Complementary	
Hydrogen-Bonding Partners	IV-1
4.1 Introduction	IV-1
4.1.1 <i>Directional</i> Noncovalent Bonding	IV-2
4.1.2 Methods to Characterize Noncovalent Bonding	IV-5
4.1.3 Scope of the Present Work	IV-8
4.2 Results	IV-9
4.2.1 Synthesis of Tertiary Amine-Terminated Telechelic 1,4-PBs	IV-9
4.2.2 Synthesis of Complementary Hydrogen-Bonding Polymer Pairs	IV-11
4.2.3 ¹ H NMR Study on Complementary End-Association in Deuterated Chloroform	IV-14
4.2.4 Shear Viscometric Study of Complementary End-Association	IV-17
4.3 Discussions	IV-20
4.3.1 Insights into Hydrogen-Bonding-Based Complementary Association	IV-20
4.3.2 Reconciliation between ¹ H NMR Results and Viscosity Data	IV-26
4.3.3 Connection between Shear Viscosity and Supramolecular Assembly	IV-29
4.4 Conclusions	IV-31
4.5 Experimental	IV-32
4.5.1 Triple Hydrogen-Bonding THY/DAAP Pair	IV-33
4.5.2 Sextuple Hydrogen-Bonding HR/CA Pair	IV-39

4.5.3 CAHB-Based DA/DB and TA/TB Pairs.....	IV-48
4.5.4 ¹ H NMR Study of Hetero-Complementary End-Association.....	IV-52
4.5.5 Shear Viscometric Study of Hetero-Complementary End-Association	IV-53
4.6 Figures, Schemes, and Tables	IV-55
References	IV-82
Chapter V Towards A Viable Fuel Additive to Mitigate Post-Impact Fires.....	V-1
5.1 Introduction	V-1
5.2 Experimental	V-2
5.2.1 Materials.....	V-2
5.2.2 Preparation of Test Solutions	V-2
5.2.3 Shear Stability Test.....	V-3
5.2.4 Shear Viscosity Measurements.....	V-4
5.2.5 Dewatering Test.....	V-4
5.2.6 Impact/Flame Propagation Test.....	V-4
5.3 Results	V-6
5.3.1 Phase Behavior	V-6
5.3.2 Effect of End-Association in Jet-A.....	V-6
5.3.3 Shear Stability.....	V-7
5.3.4 De-Watering	V-8
5.3.5 Impact/Flame Propagation Test.....	V-8
5.4 Discussions.....	V-10
5.4.1 Successful Molecular Design	V-10
5.4.2 Optimizing the Strength of Association	V-12
5.4.3 The Advantages of An Unsaturated Hydrocarbon Backbone	V-14
5.4.4 Factors That Affect Resistance to Mechanical Degradation	V-16

5.4.5 Anti-Misting or Mist-Control?	V-17
5.4.6 Potential for Large-Scale Production	V-18
5.5 Conclusions	V-20
5.6 Figures	V-21
References	V-36
Appendix A Supplemental Information	A-1
A.1 Measurements of Polymer Molecular Weights	A-1
A.2 Effect of COD Purity on the Proceeding of ROMP with CTAs	A-5
A.3 Synthesis of 76K, 264K and 300K Di- TE 1,4-PBs	A-8
A.4 Hydrolysis of <i>tert</i> -Butyl Ester-Terminated Telechelic 1,4-PBs Using Ground KOH	A-10
A.5 Synthesis of Multi-Functional Chloro-Terminated 1,4-PBs	A-14
References	A-21

List of Illustrations and Tables

Figures

Chapter I

Figure 1.1 Illustration of the effect of poly(ethylene glycol) (PEG) with $M_w = 4 \times 10^6$ g/mol on the breakup behavior of water droplets under air flow traveling at 432 m/s...	I-14
Figure 1.2 Polymers with associative groups randomly grafted along their backbones.	I-15
Figure 1.3 Crash test comparison of Jet-A and Jet-A containing 0.3% FM-9 polymer .	I-16
Figure 1.4 Preparation of carboxyl- and tertiary amine-functionalized 1250KPBs <i>via</i> thiol-ene addition	I-17
Figure 1.5 Schematics of chain collapse of polymers with associative groups randomly grafted along the backbones at dilute and semi-dilute regimes.....	I-18
Figure 1.6 Schematics for the characterization of drop splashing, spreading, and breakup.....	I-19
Figure 1.7 High-speed imaging of drop breakup of polymer solutions at 180 ppm in Jet-A (I).....	I-20
Figure 1.8 High-speed imaging of drop breakup of polymer solutions at 180 ppm in Jet-A (II).....	I-21
Figure 1.9 Schematic of supramolecular aggregation of telechelic complementary associative polymers	I-22
Figure 1.10 Computational predictions of equilibrium composition of equimolar blend of A---A and B---B as a function of MW_p , concentration, and strength of interaction $\epsilon k_B T$	I-23
Figure 1.11 Computational predictions of equilibrium concentrations of linear chains and loops in the mixture of A---, A---A and B---B in a 2:1:2 ratio as a function of strength of interaction $\epsilon k_B T$	I-24

Chapter II

Figure 2.1 Schematics of ring-opening metathesis polymerization.....	II-38
Figure 2.2 Possible configurations to cluster associative groups at polymer chain ends	II-39
Figure 2.3 GPC traces of bis-dendritic CTAs.....	II-40
Figure 2.4 ¹ H NMR spectra of (a) COD after BH ₃ ·THF treatment and vacuum distillation (b) COD further purified with Magnesol®/CaH ₂ treatments.	II-41
Figure 2.5 Incorporation of G2 CTA into polymer as a function of reaction time during the first stage of two-stage ROMP of COD.....	II-42
Figure 2.6 ¹ H NMR spectra of telechelic 1,4-PB of M _w = 226 kg/mol with 1 <i>tert</i> -butyl ester group at each chain end before and after TFA hydrolysis of <i>tert</i> -butyl ester groups.....	II-43
Figure 2.7 Effect of the number of carboxyl groups on chain ends (N) on the appearance of telechelic 1,4-PBs of M _w = 230 kg/mol.....	II-44
Figure 2.8 GPC-LS traces of 230K di- TE 1,4-PB and the corresponding polymers after TFA hydrolysis (carboxyl-terminated) and further LAH reduction (hydroxyl- terminated).....	II-45
Figure 2.9 GPC-LS traces of 143K di- DE 1,4-PB and the corresponding polymers after TFA hydrolysis with and without the addition of BHT.....	II-46

Chapter III

Figure 3.1 Schematic representation of the concentration-dependent self-association of telechelic associative polymers	III-15
Figure 3.2 Structures of telechelic 1,4-PBs investigated in the present study.....	III-16
Figure 3.3 Specific viscosity of 1wt% solutions of test polymers in 1-chlorododecane (CDD) and tetralin (TL).....	III-17
Figure 3.4 Effect of number of chain-end functional groups (N) on the concentration dependence of the specific viscosity of solutions of telechelic associative polymers with M _w ~ 230 kg/mol in (a) 1-chlorododecane (CDD) and (b) tetralin (TL).....	III-18

Figure 3.5 Concentration dependence of specific viscosity of solutions of telechelic 1,4-PBs with non-associative and associative chain ends (N=4) as a function of M_w	III-19
Figure 3.6 Shear-thinning behavior of CDD solutions of di- TA 1,4-PBs at three concentrations (0.4, 0.7 and 1.0 wt%) as a function of M_w	III-20
Figure 3.7 Shear-thinning behavior of TL solutions of di- TA 1,4-PBs at three concentrations (0.4, 0.7 and 1.0 wt%) as a function of M_w	III-21

Chapter IV

Figure 4.1 Representative examples of directional noncovalent bondings.....	IV-55
Figure 4.2 (a) Structures of polymers PA , PB , PC and step-wise self-assembly of supramolecular triblock copolymer. (b) Plot of specific viscosity versus concentration for PB and supramolecular block copolymers	IV-56
Figure 4.3 GPC-LS traces of di- THY macro CTA and the corresponding 288K di- THY 1,4-PB.....	IV-57
Figure 4.4 GPC-LS traces of di- DAAP macro CTA and the corresponding 219K di- DAAP 1,4-PB.	IV-58
Figure 4.5 GPC-LS traces of di- CA macro CTA and the corresponding 200K di- CA 1,4-PB.	IV-59
Figure 4.6 GPC-LS traces of di- HR macro CTA and the corresponding 240K di- HR 1,4-PB.	IV-60
Figure 4.7 Expanded ^1H NMR (500 MHz) spectra of CDCl_3 solutions of telechelic polymers that have a 10 kg/mol 1,4-PB backbone with end groups that are (a) THY , (b) DAAP , and (c) a mixture of the two polymers with a mass ratio of 1:2, which represents a stoichiometric ratio of approximately 1:2.....	IV-61
Figure 4.8 Expanded ^1H NMR (500 MHz) spectra of CDCl_3 solutions of telechelic polymers that are (a) 1,4-PB of $M_w = 50$ kg/mol with CA end groups, (b) 1,4-PB of $M_w = 24$ kg/mol with HR end groups, and (c) a mixture of the two polymers with a mass ratio of 1:1.4, which represents a stoichiometric ratio of CA:HR of approximately 1:2	IV-62

- Figure 4.9 Expanded ^1H NMR (500 MHz) spectra of CDCl_3 solutions of telechelic polymers that are (a) 1,4-PB of $M_w = 22$ kg/mol with **TB** end groups, (b) a mixture of 1,4-PB of $M_w = 22$ kg/mol with **TB** end groups and 1,4-PB of $M_w = 22$ kg/mol with **TA** end groups two polymers with a mass ratio of 1:1IV-63
- Figure 4.10 Expanded ^1H NMR (500 MHz) spectra of CDCl_3 solutions of telechelic polymers that are (a) 1,4-PB of $M_w = 288$ kg/mol with **THY** end groups, (b) 1,4-PB of $M_w = 219$ kg/mol with **DAAP** end groups, and (c) a mixture of the two polymers with a mass ratio of 1:2IV-64
- Figure 4.11 Expanded ^1H NMR (500 MHz) spectra of CDCl_3 solutions of telechelic polymers that are (a) 1,4-PB of $M_w = 200$ kg/mol with **CA** end groups, (b) 1,4-PB of $M_w = 240$ kg/mol with **HR** end groups, and (c) a mixture of the two polymers with a mass ratio of 1:2IV-65
- Figure 4.12 Expanded ^1H NMR (500 MHz) spectra of CDCl_3 solutions of telechelic polymers that are (a) 1,4-PB of $M_w = 250$ kg/mol with **TB** end groups, (b) a mixture of 1,4-PB of $M_w = 250$ kg/mol with **TB** end groups and 1,4-PB of $M_w = 230$ kg/mol with **TA** end groups two polymers with a mass ratio of 1:1IV-66
- Figure 4.13 Specific viscosity (25°C) of 1wt% 1-chlorododecane (CDD) and dodecane solutions of 288K di-**THY** 1,4-PB, 219K di-**DAAP** 1,4-PB, and 1:2 (w/w) mixture of 288K di-**THY** 1,4-PB and 219K di-**DAAP** 1,4-PB.IV-67
- Figure 4.14 Specific viscosity (25°C) of 1wt% 1-chlorododecane (CDD) and Jet-A solutions of 240K di-**HR** 1,4-PB, 200K di-**CA** 1,4-PB, and 1:2 and 2:1 (w/w) mixtures of 240K di-**HR** 1,4-PB and 200K di-**CA** 1,4-PB.IV-68
- Figure 4.15 Specific viscosity (25°C) of 1wt% CDD solutions of 230K di-**TE** 1,4-PB, 230K di-**TA** 1,4-PB, 250K di-**TB** 1,4-PB, and the 1:1 (w/w) mixture of 230K di-**TA** 1,4-PB and 250K di-**TB** 1,4-PB at shear rates 1-3000 s^{-1} IV-69
- Figure 4.16 Specific viscosity (25°C) of 1wt% CDD solutions of 230K di-**DE** 1,4-PB, 230K di-**DA** 1,4-PB, 204K di-**DB** 1,4-PB, and the 1:1 (w/w) mixture of 230K di-**DA** 1,4-PB and 204K di-**DB** 1,4-PB at shear rates 1-3000 s^{-1}IV-70
- Figure 4.17 Specific viscosity (25°C) of 1wt% Jet-A solutions of 430K di-**TE** 1,4-PB, 430K di-**TA** 1,4-PB, 430K di-**TB** 1,4-PB, and the 1:1 (w/w) mixture of 430K di-**TA** 1,4-PB and 430K di-**TB** 1,4-PB at shear rates 1-3000 s^{-1} IV-71

Figure 4.18 Secondary-electrostatic-interaction (SEI) analysis of all possible hydrogen-bond donor (D) and acceptor (A) site arrangements for triple-hydrogen-bonding hetero-complementary associative pairs and their representative examples	IV-72
Figure 4.19 SEI analysis of D/A site arrangements for multiple-hydrogen-bonding hetero-complementary associative pairs.....	IV-73

Chapter V

Figure 5.1 Experimental setup for shear stability test.....	V-21
Figure 5.2 Results of de-watering test	V-22
Figure 5.3 Experimental setup for high-speed impact and flame propagation test	V-23
Figure 5.4 Appearance of 0.5wt% Jet-A solution of 264K di- TA 1,4-PB stored at -30°C for 18 months.	V-24
Figure 5.5 Shear viscosity of Jet-A solutions of 430K di- TE 1,4-PB and 430K di- TA 1,4-PB	V-25
Figure 5.6 Shear viscosity of samples from shear stability test and their unsheared controls.....	V-26
Figure 5.7 Results of Jet-A in impact/flame propagation test	V-27
Figure 5.8 Results of 0.35wt% Jet-A solution of 4.2M PIB in flame propagation test	V-28
Figure 5.9 Results of 0.3wt% Jet-A solution of 430K di- TA 1,4-PB in flame propagation test. Left: results of unsheared solution. Right: results of sheared solution.	V-29
Figure 5.10 Results of 0.5wt% Jet-A solution of 430K di- TA 1,4-PB in flame propagation test. Left: results of unsheared solution. Right: results of sheared solution.	V-30
Figure 5.11 Results of 0.7wt% Jet-A solution of 430K di- TA 1,4-PB in flame propagation test.....	V-31
Figure 5.12 Effect of concentration of 430K di- TA 1,4-PB in Jet-A on fire suppression.....	V-32

Figure 5.13 Effect of M_w on fire resistance of unsheared 0.5wt% Jet-A solutions of di- TA 1,4-PBs.....	V-33
Figure 5.14 Effect of concentration on fire resistance of sheared Jet-A solutions of 430K di- TA 1,4-PB	V-34
Figure 5.15 Cumulative weight-average molecular weight distribution of 430K di- TE 1,4-PB	V-35

Appendix A

Figure A.1 GPC-LS (THF, 35°C) traces of 230K di- TE 1,4-PB, 230K di- TA 1,4-PB and the resultant polymer of LAH reduction of 230K di- TA 1,4-PB.....	A-4
Figure A.2 Synthesis of di- TE 1,4-PB <i>via</i> two-stage ROMP of COD as the benchmark reaction for the influence of the purity of VCH-free COD.....	A-6
Figure A.3 Reaction scheme of hydrolysis of di- TE 1,4-PBs using the KOH/HCl protocol.	A-11
Figure A.4 Expanded ^1H NMR (500 MHz) spectra of CDCl_3 solutions of 287K di- TE 1,4-PB and 287K di- TA 1,4-PB prepared <i>via</i> the KOH/HCl protocol.....	A-12
Figure A.5 Specific viscosity of 1wt% solutions of test polymers in 1-chlorododecane (CDD)	A-14
Figure A.6 Synthesis of tetra-functional chloro-terminated bis-dendritic CTA.	A-15
Figure A.7 Synthesis of octa-functional chloro-terminated bis-dendritic CTA.	A-16
Figure A.8 Two-stage synthesis of telechelic 1,4-PB of $M_w = 204$ kg/mol with di-functional chloro-terminated dendritic end groups.....	A-17
Figure A.9 Synthesis of telechelic 1,4-PB of $M_w = 22$ kg/mol with tetra-functional chloro-terminated dendritic end groups.	A-18
Figure A.10 Two-stage synthesis of telechelic 1,4-PBs of $M_w = 254$ and 430 kg/mol with tetra-functional chloro-terminated dendritic end groups.	A-19

Schemes

Chapter II

Scheme 2.1 Synthesis of Bis-Dendritic, <i>tert</i> -Butyl Ester-Terminated Chain Transfer Agents	II-47
Scheme 2.2 ...Two-stage Synthesis of <i>tert</i> -Butyl Ester-Terminated Telechelic 1,4-PBs	II-48
Scheme 2.3 TFA Hydrolysis of <i>tert</i> -Butyl Ester Polymer End Groups.....	II-48
 Chapter IV	
Scheme 4.1 Synthesis of Di- DB and Di- TB 1,4-PBs <i>via</i> Two-stage, Post-Polymerization End-Functionalization	IV-74
Scheme 4.2 Synthesis of THY -Functional Acid, Di- THY Macro CTA, and Di- THY 1,4-PB of $M_w \sim 200$ kg/mol	IV-75
Scheme 4.3 Synthesis of DAAP -Functional Acid, Di- DAAP Macro CTA, and Di- DAAP 1,4-PB of $M_w \sim 200$ kg/mol	IV-76
Scheme 4.4 Synthesis of CA -Functional Acid, Di- CA CTA, Di- CA Macro CTA, and Di- CA 1,4-PB of $M_w \sim 200$ kg/mol	IV-77
Scheme 4.5 Synthesis of HR -Functional Azide, Di- HR Macro CTA, and Di- HR 1,4-PB of $M_w \sim 200$ kg/mol	IV-78

Tables

Chapter I

Table 1.1 Fundamental Requirements of an Ideal Polymer Additive for Mist Control of Fuel	I-25
--	------

Chapter II

Table 2.1 Representative Example of Commercially Available Cyclic Olefins as ROMP Monomers	II-49
Table 2.2 Conditions and Results of Two-stage Synthesis of Telechelic 1,4-Polybutadienes (PBs) Using Bis-Dendritic CTAs	II-50
Table 2.3 Molecular Weight and PDI Data of <i>tert</i> -Butyl Ester- and Carboxyl-Terminated Telechelic 1,4-PBs.....	II-51

Chapter III

Table 3.1 Molecular Weight (M_w) and Number of Chain-End Functional Groups (N) of <i>tert</i> -Butyl Ester- and Carboxyl-Terminated Telechelic 1,4-PBs Investigated in the Present Study	III-22
--	--------

Chapter IV

Table 4.1 Representative Examples of Multiple OHB-Based Hetero-Complementary Associative Pairs	IV-79
Table 4.2 pKa Values of Common Organic Acids and Conjugated Acids of Organic bases	IV-80
Table 4.3 List of Attempted Strategies for Synthesizing Tertiary-amine-Terminated 1,4-PBs and Corresponding Problems	IV-81

Appendix A

Table A.1 Molecular Weight Measurement Methods.....	A-1
Table A.2 Results of Synthesis of Di-TE 1,4-PB <i>via</i> ROMP of Batch 1 and Batch 2 VCH-free COD	A-6

Chapter I Introduction

1.1 Technological Need for Safer Kerosene-Based Fuel

Kerosene-based fuels (i.e., jet fuel and diesel) have historically been, and are currently the main fuel source for aviation and ground transportation. Unfortunately, however, these fuels have also been a major source of fire hazard and vulnerability when they are released in an uncontrolled manner (for example in scenarios involving impacts, such as aircraft crashes and improvised explosive device (IED) attacks on military ground vehicles). It is estimated that 40% of the fatalities in so-called “survivable aircraft crashes,” which make up approximately 70% of accidents that occur on takeoff and landing, are due to fire caused by combustion of aviation fuel.¹ Similarly, the violent and catastrophic combustion of leaked fuel after the direct or indirect ballistic penetration of a vehicle’s fuel tank or fuel line by shrapnel in IED attacks has inflicted heavy casualties on US military over the last decade. The destructive power of an uncontrolled energy release of kerosene has also been demonstrated to be an issue of homeland security: in the 911 terrorist attack the Twin Towers of the World Trade Center survived the initial impact, but both later collapsed due to structure weakening by the immense heat released from combustion of fuel from the two hijacked aircrafts.²

Why are fuel fires in the aforementioned scenarios so lethal? It turns out that the fine fuel mist generated by impact will burn in an uncontrollable manner when ignited, and the resultant fire can rapidly propagate away from the ignition source, involve more fuel, and trigger deadly pool fires that are very violent and difficult to contain. Such fires often accompany tank explosions, leaving no chance for firefighters to intervene. Hence,

the reduction of the fire hazard of fuels, and especially the suppression of impact-induced atomization of fuels, can never be over-emphasized.

A variety of safety features have been incorporated into the designs of aircrafts and ground combat vehicles, including firewalls, shrouded and break-away fuel lines, flame arrestors, fuel-line isolation, explosion-proof electromechanical equipment, detectors and extinguishing systems, and fire-resistant materials, but only limited success has been achieved.³ Burning of fuel has dominated most post-accident fire scenarios and causes even the most fire-resistant material to burn readily. A 1997 National Research Council (NRC) reports, “The reduction of the fire hazard of [the] fuel [itself] is critical in improving survivability in past crashes.”³ This perspective is supported by a recent comprehensive review of technologies towards mitigation of impact-induced fuel fires (authored by Bernard Wright, one of the leaders in the field), which identifies that the use of mist-control additives in fuels is the most promising one and the highest priority.⁴ To minimize loss of life in aircraft crashes or IED attacks on troops in war zone, it is paramount to have a fuel that “burns but doesn't burn”-that is, after ignition from an incendiary threat, it self-extinguishes and slows the spread of fire so that fire-extinguishing systems can intervene, and personnel can have time to escape.⁵

1.2 Development of Mist-control Additives for Fuels-A Historical Review

1.2.1 Early Research Efforts

Efforts for reducing the fire hazard of fuels have been underway since the late 1960's.⁴ Among them, the use of a small amount of ultra-high molecular weight (on the order $\sim 10^7$ g/mol) polymers as anti-misting additives in kerosene, also known as *anti-*

misting kerosene (AMK) then, attracted the most attention.^{4,5} It has been known that these polymers, even at very low concentration, have potent effects on the breakup of liquid jets and drops (Figure 1.1),⁶ since they are long enough to exhibit elasticity and sustain tensile stress.⁷⁻¹⁰ When fluids are subject to elongational deformation (e.g., impact-induced atomization and liquid jets), such a property provides them a means to resist the pinching caused by capillary action (also known as Rayleigh instability), and consequently promotes the formation of filaments that connect ejected fluid elements, keeping the fluid together.⁷ A classic example of AMK was reported by Chao and coworkers in 1984: They found that linear polyisobutylene (PIB) with a molecular weight of $5\text{-}10 \times 10^6$ g/mol was effective at reducing flammability of sprays of a commercial jet fuel, Jet-A, at concentrations as low as 50 ppm, and the mist-suppressing ability increases with both increasing molecular weight and concentration of PIB.¹¹ To be more specific, when an AMK is released in scenarios involving impact, the aforementioned mist-suppressing action of ultra-high molecular weight PIB leads to a reduction in the total surface area of fuel droplets available for vaporization by several orders of magnitude compared to that of the fine mist generated by conventional fuels. The combination of tremendous reduction in vapor and the increase of thermal mass per drop results in slow energy release in the presence of transient ignition source, and thus further reduces vaporization relative to untreated fuels.¹² Consequently, the resultant fire is cooler, unlikely to propagate away from ignition sources, and can even be self-quenching if the ignition source is removed. The likelihood of igniting pool fuel fires is thus either eliminated or significantly delayed, which provides precious time for firefighting and evacuation of personnel.

Unfortunately, polymers with molecular weights high enough to provide mist-control effect are vulnerable to shear degradation, presenting a major technical obstacle to the implementation of AMK over the past 30 years.^{13,14} Specifically, during fuel transportation and dispensing processes, these very long polymers shear-degrade rapidly and lose their mist-suppressing capability after the fuel is pumped. The research focus of AMK has thus shifted from ultra-high molecular weight polymers to *associative polymers*: polymer chains that capable of interacting through non-covalent bonding (e.g., hydrogen bonding).^{11,14-16} The underlying principle of design, then, is to use shear-stable polymer chains that have molecular weight less than 10^6 g/mol but can aggregate into larger clusters (which could be effective mist-control agents) *via* hydrogen bonding and respond to turbulent flow *via* reversible dissociation.

The prevailing design principle in the 1980's was to use linear chains possessing hydrogen-bonding functional groups (e.g., carboxylic acid) grafted at random positions along the entire chains (Figure 1.2 (a)). The most representative examples of such a design are ICI's proprietary polymer FM-9 (Figure 1.2 (b)) and Exxon's poly alpha-olefin polymer (Figure 1.2 (c)).^{11,14,17,18} FM-9, a random copolymer of *tert*-butyl styrene, methyl acrylate, and acrylic acid with a $M_w \sim 3 \times 10^6$ g/mol (acid content of ~ 5 mol%, but exact composition remains undisclosed),¹⁶ was extensively tested as a mist-suppressing polymer additive for aviation fuels in the FAA-funded Anti-Misting Kerosene (AMK) program during the period 1978-1984.^{1,3,17} Indeed, on December 1, 1984, a *full-scale*, controlled-impact demonstration (CID) was performed by the FAA and NASA as an attempt to evaluate the effectiveness of AMK under realistic conditions of a survivable crash: A remotely piloted Boeing 720 aircraft fueled with Jet-A fuel containing 0.3 wt%

FM-9 was crashed at Edwards Air Force Base. Although a fireball emerged on impact and briefly trailed the aircraft (Figure 1.3 (B)), it quickly self-extinguished within 10 s, allowing photographers to walk up to the aircraft to take pictures which showed that the paint was still intact (Figure 1.3 (C)), an indication that the fire was of low temperature and did not penetrate the interior of the aircraft. The pool fire did not emerge until several minutes later, indicating there would be sufficient time for complete evacuation of passengers and fire-fighting to control the pool fire. In contrast, in a similar controlled crash conducted earlier than the CID test, with unmodified Jet-A, an intense fireball approximately 10 times the length of the crashed aircraft emerged (Figure 1.3 (A)), and the fire continued even after ignition sources ceased, melting the fuselage and engulfing its contents in flames. The fire was so intense that firefighters could not even approach the scene. The sharp contrast between the results of AMK and those of unmodified Jet-A in controlled crash tests clearly indicates that the AMK's fire suppression qualities are significant.

Despite the success revealed in the aforementioned CID test, the FAA cancelled the AMK program due to the difficulty in implementing AMK: considerable additional development was found required to make the FM-9-based AMK operationally acceptable.^{1,5} The empiricism-based AMK program was focused on practical testing and engineering approaches were utilized in the development of AMK formulation; the lack of scientific effort to acquire fundamental understanding of how to make necessary adjustments eventually led the program to its failure. Despite its observed efficacy, FM-9 has a very poor solubility in jet fuels due to the constituents of its backbone: methacrylate and acrylic acid; therefore, a package of "carrier fluid"- that is, a mixture of water,

glycerol, ethylene glycol, and formic or acetic acid- is required to prevent it from phase-separating from jet fuels.^{16,17} FM-9's high acid content (~ 5 mol%) not only contributes to its tendency to phase separate, but also imparts high water uptake and unacceptably large enhancement in shear viscosity to the resultant AMK at concentrations of anti-misting effectiveness. The FM-9-induced AMK was observed to be more like a gel bound into a matrix which shows shear-thickening behavior, creating numerous problems, including difficulty in mixing, clogging of filters, and the need for aircraft modification (e.g., installation of "polymer degraders" before the engines).⁵ The high molecular weight of FM-9 ($\sim 3 \times 10^6$ g/mol) also renders it vulnerable to shear degradation and thus it was found required to be mixed carefully into the fuel immediately prior to use because it degraded during pumping. Consequently, these technical issues associated with FM-9 rendered the effort of the AMK program a prohibitively complicated and costly mode of implementation.

1.2.2 Renewed Motivation and Efforts After the 9-11 Terrorist Attack

After the terrorist attack on September 11, 2001, fuel-laden aircrafts were identified as a new category of "weapons of mass destruction" (WMD) that present a threat, not only to passenger survivability, but also against buildings and large gatherings of people.⁵ Since then, fuel and flammability specialists have been investigating the possibility of developing a fire-safe fuel that would prevent another catastrophic event and eliminate this form of terrorism. Such an urgent need for safer fuels is also shared by military ground vehicles, given the fact that IED attacks and the subsequent fire hazard of fuel leaked from ruptured fuel tanks have been the deadliest form of weapon against troops deployed in Afghanistan and Iraq since 2001. A new term called "mist-control

kerosene” (MCK) has therefore been proposed by the California Institute of Technology (Caltech) as a response to the demand for fire-safe fuels and a more accurate description of such fuels compared to AMK since the 2003 NASA/FAA/TSA workshop on Aircraft Fire/Fuel Safety and Security.¹⁹

Investigation of MCK has been actively conducted in the Kornfield group at Caltech since 2005. The research efforts were focused on generating scientific understanding of the relationship between the molecular design of mist-control polymers and solution behavior. In order to avoid repeating the failure of the AMK program in the 1980’s, diverse criteria (summarized in Table 1.1) for ideal fuel additives have also been imposed on the development of MCK technology in the Kornfield group.²⁰ Our research began with the examination of the prevailing molecular designs of anti-misting polymers in the literature: linear chains possessing carboxylic acid groups grafted at random positions along the entire chains,^{16,18} and randomly functionalized chains with complementary side-groups (carboxylic acid/tertiary amine or pyridine, Figure 1.2 (d)).^{14,15,21,22} The Kornfield group utilized a concept called “analogous chemistry” to prepare model polymer molecules that allowed isolation of the effect of association from those of other parameters, such as chain size. More specifically, homologous series of associative polymers identical in every respect (backbone length, architecture, chemical makeup, etc.), except for the nature and number of associative groups, were prepared *via* functionalization of the pendant vinyl groups of a narrow-disperse polybutadiene (PB, $M_n = 1.25 \times 10^6$ g/mol, containing 92% 1,4-adduct and 8% 1,2-adduct; referred to as 1250KPB hereinafter) through thiol-ene coupling with carboxyl- and tertiary amine-functional thiols (Figure 1.4).^{23,24} The PB backbone was selected due to its excellent

solubility in fuels, and thiol-ene chemistry was chosen for its versatility that allowed the control of degree of functionalization of PB and caused minimal damage to the backbone. The degree of functionalization of PB with carboxyl groups was limited within 0.6 mol% of the repeating units of PB backbone; further functionalization led to poor solubility of resultant polymers in Jet-A. In the case of tertiary amine-functionalized PB, the degrees of functionalization were significantly higher (up to 5.4 mol%) since tertiary amine groups did not adversely affect the solubility of resultant polymers in Jet-A.

Studying the behaviors of solutions of carboxyl-functionalized PB in Jet-A, however, uncovered an intrinsic flaw in the design of associative polymers with carboxylic acid group randomly grafted along polymer backbone (*i.e.*, the molecular architecture of FM-9): Chain collapse caused by intramolecular association (Figure 1.5 (a)). This phenomenon led to a supramolecular aggregate of the associative polymer that was *less* elastic than the unmodified 1250KPB, as revealed in the droplet impact experiments, in which individual drops of each test solution were forced out from a needle and impacted a smooth, solid surface, and the splashing, spreading, and breakup processes were recorded using a high-speed camera at frame rate of 4 kHz (Figures 1.6). At 180 ppm in Jet-A, the reference polymer PIB with $M_w \sim 4.2 \times 10^6$ g/mol (referred to as 4200KPIB) completely suppressed the ejection of satellite droplets (Figure 1.7 (a)), while unmodified 1250KPB exhibited limited elasticity to hinder the necking and pinching of ejected fluid and thus resulted in the formation of beads-on-a-string morphology, of which the filaments survived for ~ 2 ms (Figure 1.7 (b)). In the cases of 1250KPB functionalized with 0.3 mol% and 0.6 mol% of carboxyl groups, same morphologies were observed, but the survival times of filaments were reduced to 1.5 and 1 ms,

respectively (Figure 1.7 (c) and (d)). The reduction of filament lifetime due to the increase in carboxyl content clearly indicates that random positioning of carboxyl groups along polymer backbone *cannot* lead to the formation of supramolecular aggregates that are more elastic than the individual polymer chains. Using polymers with these molecular architectures as mist-control additives for kerosene was therefore shown to be infeasible.

Results of the second system studied in the Kornfield group, a complementary blend of polymer chains functionalized with carboxylic acid and tertiary amine groups, respectively, revealed that the combination of directional, complementary acid/base association and random positioning of functional groups along polymer backbone only makes matters worse (Figure 1.5 (b)).²⁰ Even though both viscometry and dynamic light scattering (DLS) studies showed that the carboxyl- and amino-functionalized PB polymer pair can form shear-stable clusters at concentrations well below the overlap concentration (c^*) of the backbone 1250KPB, and that the size of clusters increase with polymer concentration, the detrimental effect of chain collapse on the elasticity of formed supramolecular aggregates was clearly revealed in drop impact experiments (Figure 1.8). At 180 ppm in Jet-A, the mixtures of carboxyl-functionalized 1250KPB (0.3 mol%) and tertiary amino-functionalized 1250KPB (2.6 mol%) at ratios of 3:1 and 1:1 exhibited far worse abilities to suppress the breakup of ejected fluid compared to the unmodified 1250KPB backbone (Figure 1.8 (b)-(d)). Directional interchain acid/base interaction was found to be capable of driving the formation of interpolymer complexes (IPCs) even at concentrations $\ll c^*$, and inevitably led to even more severe chain collapse, which significantly inhibited the stretching of polymer chains when subjected to elongational flow and caused loss of elasticity of the solution (Figure 1.6 (b)).

The experimental work by the Kornfield group has thus clearly indicated that using polymers with associative groups randomly grafted along the backbone as mist-control additives for kerosene is *not* a viable solution because the chain collapse inherent in the molecular architecture interferes with the mechanism of mist control. To eliminate chain collapse and to achieve elastic supramolecular polymer aggregates that can be useful in mist-control applications, we have thus proposed an innovative molecular design where associative groups are clustered to the ends of linear polymer chains (Figure 1.9). A computational model was subsequently constructed in order to provide insights for designing mist-control polymers *via* understanding the equilibrium partitioning of long, mono-disperse linear chains end-capped with strongly associative A and B groups (A---A and B---B) into supramolecular linear chains and supramolecular loops of all sizes.²⁰ In this model, A and B end-groups were assumed to be in equal amount and associate with each other pair-wise with interaction energy $\epsilon k_B T$ (k_B : Boltzmann constant, $= 1.38 \times 10^{-23}$ J/K), but that neither the A nor the B end-groups self-associate. The following parameters crucial for mist-control kerosene were selected in the study: molecular weight of polymer (MW_p), total volume concentration of polymer (ϕ_{total}), and binding energy ($\epsilon k_B T$). Parameter values were chosen in order to represent the practically “best-case” scenario in mist control of kerosene that can be tested experimentally: $MW_{A---A} = MW_{B---B} = MW_p = 5 \times 10^5$ and 10^6 g/mol, $\phi_{total} = 800$ and 1400 ppm, and $14 \leq \epsilon \leq 20$. Based on the guideline reported by Chao and coworkers that PIB chains with $M_w \sim 5 \times 10^6$ g/mol were satisfactory mist-suppressing agents at concentrations as low as 50 ppm in kerosene,¹¹ the theoretical prediction was focused on the cumulative amount of linear supramolecules with $M_w > 5 \times 10^6$ g/mol and that of

cyclic supramolecules with $M_w > 10 \times 10^6$ g/mol. In other words, the total concentration of these supramolecular species should be ≥ 50 ppm to achieve mist-control effectiveness. The simulation revealed that in the case of equimolar blend of A---A and B---B, the formation of linear aggregates that are useful in mist-control applications is comparatively favored at high MW_p and high φ_{total} ; nevertheless the majority of polymer building blocks are lost in small loops (Figure 1.10). In addition, only a narrow range, $16 \leq \varepsilon \leq 18$, is predicted to yield “good” results, that is, a total concentration of linear supramolecules with $M_w > 5 \times 10^6$ g/mol and cyclic supramolecules with $M_w > 10 \times 10^6$ g/mol over 50 ppm. The model also predicted that the use of end-capping, mono-telechelic chains A--- would solve the above problems because the presence of A--- favors the formation of linear supramolecular aggregates and lowers the fraction of polymer chains lost in loops due to symmetry breaking. Computational results showed that when $MW_p = 10^6$ g/mol, $\varphi_{total} = 800$ ppm and $\varepsilon \geq 20$, a mixture of A---, A---A and B---B in a ratio of 2:1:2 is expected to lead to an equilibrium concentration of linear supramolecules with $M_w > 5 \times 10^6$ g/mol greater than 100 ppm and that of cyclic supramolecules with $M_w > 7 \times 10^6$ g/mol greater than 50 ppm (Figure 1.11), indicating the possibility to achieve mist-suppression effectiveness.

1.3 Overview of the Present Work

Previous experimental and theoretical works carried out by the Kornfield group have clearly suggested a direction towards a viable design of mist-control polymers for kerosene-based fuels. As a crucial part of our continued effort to pursue MCK, in this thesis we address the experimental realization of the molecular design illustrated in Figure 1.9. There has not been any report in the literature, to the best of our knowledge,

on the preparation of fuel-soluble, end-associative polymers with high molecular weights and high strength of end-association that are described in our model. We are keen to develop a method that can provide shear-resistant, mist-control polymers for kerosene based on our molecular design, and to establish scientific understanding of the relationship between molecular designs and rheological solution properties which are important in regards to mist-control applications.

1.3.1 Objective

As mentioned above, our previous theoretical work has provided a guideline for the design of shear-resistant, effective mist-control polymers for kerosene. Accordingly, the first objective in this thesis is to establish an economically feasible and scalable way to synthesize polymers with architectures recommended by the theory. Given the determining role of the strength of end-association in the formation of supramolecular aggregates useful in mist suppression, our second objective is to develop a strategy that allows precise engineering of the structure of polymer chain ends and the ability to control the corresponding strength of end-association. To provide insights for the design of an effective formulation of MCK, our next objective is to generate understanding of the relationship between molecular properties (e.g., molecular weight, the nature and strength of end-associative units) and solution behavior, such as aggregate structures, rheological properties, shear resistance, and performance in mist suppression. Our technological objective is the eventual development of an effective formulation of MCK that satisfies the requirements listed in Table 1.1.

1.3.2 Organization

Chapter 2 tackles the challenge of preparing fuel-soluble, end-associative polymers with unprecedentedly high molecular weights which meet the requirements of MCK using mild conditions that are economically viable. As an intermediate step in the fulfillment of the molecular design in Figure 1.9, *self*-associative carboxyl group is used as the end-associative group in this chapter. A unique approach to achieve well-defined end-group structures with tunable strength of association is also presented. The rheological properties of these polymers in apolar media are investigated in Chapter 3. In Chapter 4, we apply the synthetic strategy developed in Chapter 2 to prepare fuel-soluble polymers end-functionalized with *complementary* associative units. Four such pairs with different association strengths are studied in order to generate understanding of the required strength to achieve the molecular design described in Figure 1.9. Chapter 5 then presents the testing results of our high-molecular-weight end-associative polymers as mist-control additives for Jet-A. Emphasis is placed on key properties in the regard of MCK, including resistance to shear degradation and the ability to impart fire-safety to Jet-A.

1.4 Figures and Tables

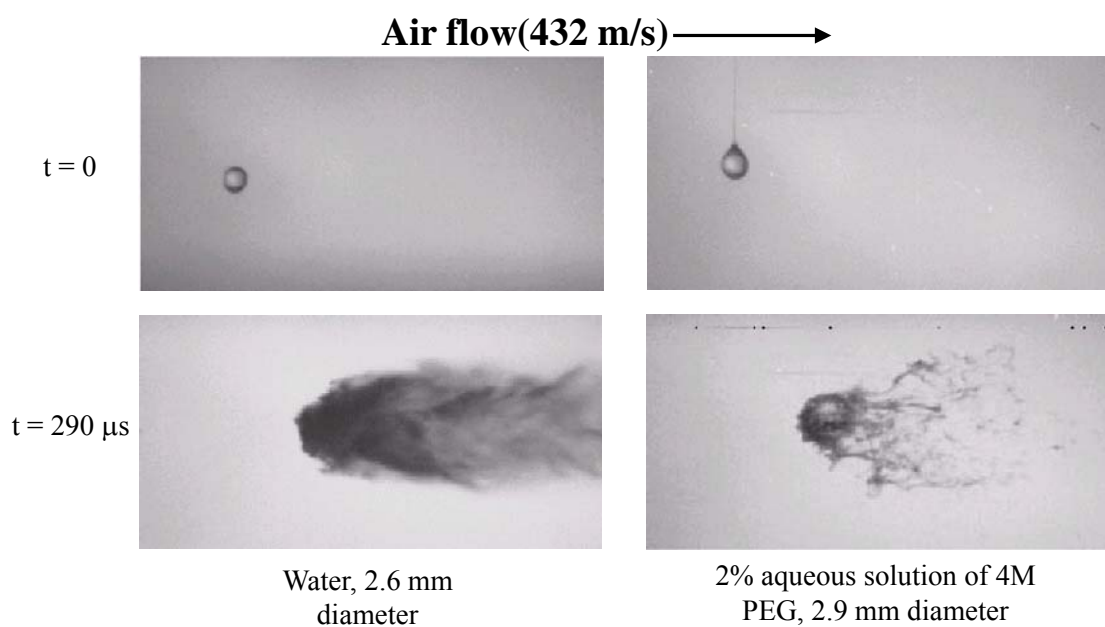


Figure 1.1 Illustration of the effect of poly(ethylene glycol) (PEG) with $M_w = 4 \times 10^6$ g/mol on the breakup behavior of water droplets under air flow traveling at 432 m/s. Left: water; Right: 2wt% aqueous solution of 4M PEG.⁶

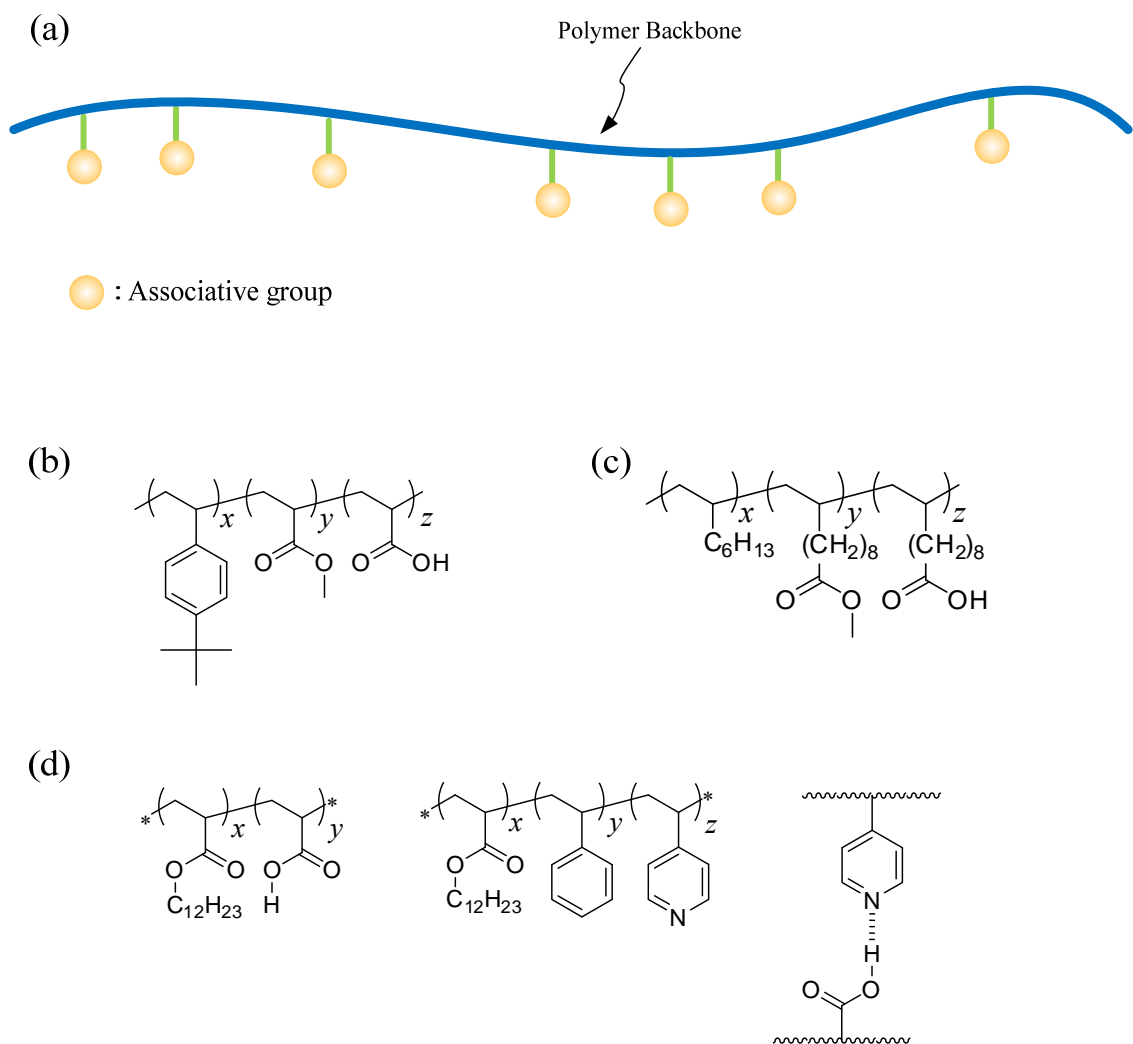


Figure 1.2 Polymers with associative groups randomly grafted along their backbones. (a) A general schematic. (b) Structure of ICI's FM-9 polymer. (c) Structure of Exxon's poly(α -olefin) derivative. (d) Complementary pair of polymer chain of $M_w \sim 4.7 \times 10^5$ g/mol with ~ 3 wt % of acrylic acid and polymer chain of $M_w \sim 2.1 \times 10^6$ g/mol with ~ 4 wt% of pyridine groups developed by Malik and Mashelka.²²

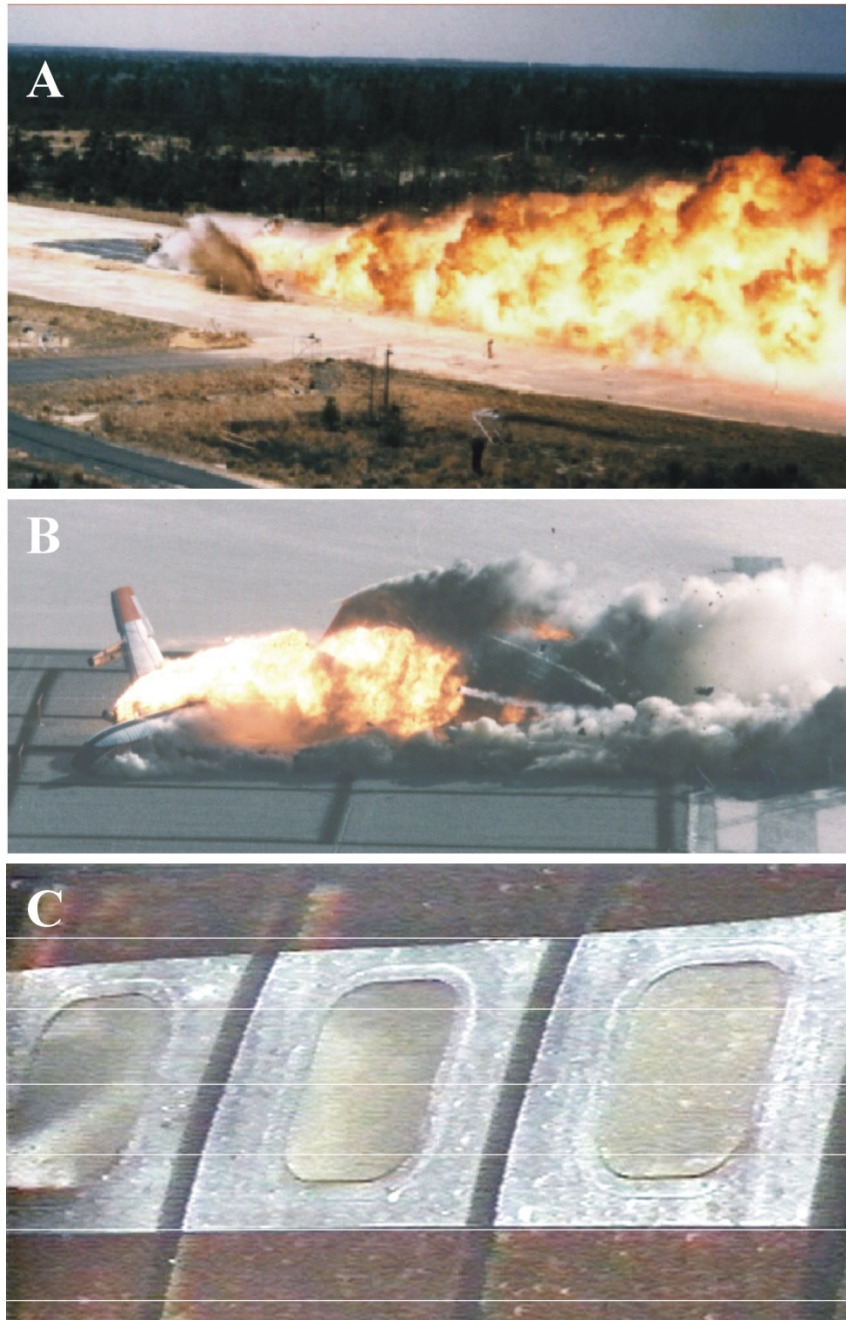


Figure 1.3 Crash test comparison of Jet-A and Jet-A containing 0.3% FM-9 polymer. (A) A sled-driven aircraft fueled with Jet-A. (B) A B-720 fueled with Jet-A containing 0.3% FM-9. (C) Appearance of fuselage after the initial fireball was extinguished.

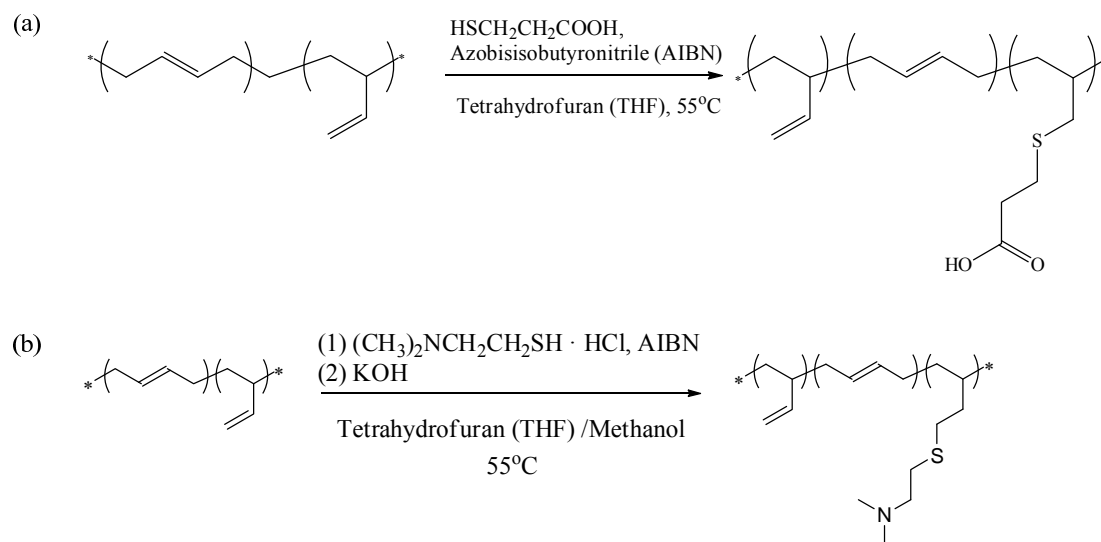


Figure 1.4 Preparation of carboxyl- and tertiary amine-functionalized 1250KPBs *via* thiol-ene addition. (a) Carboxyl-functionalized. (b) Tertiary amine-functionalized.

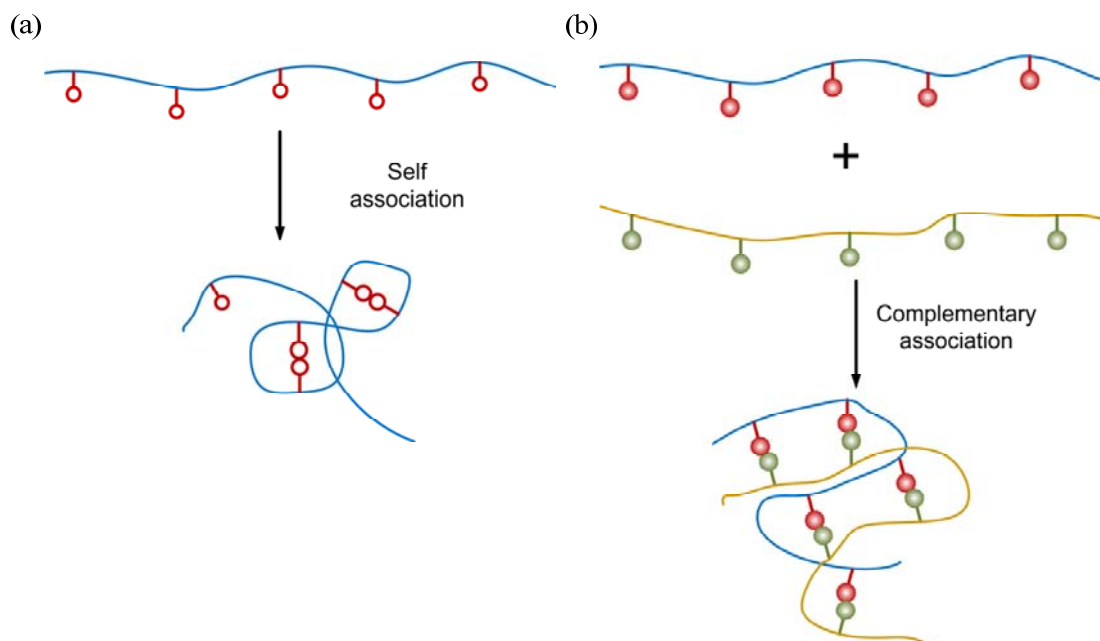


Figure 1.5 Schematics of chain collapse of polymers with associative groups randomly grafted along the backbones at dilute and semi-dilute regimes. (a) Chain collapse induced by self-association. (b) Chain collapse induced by inter-chain complementary association.

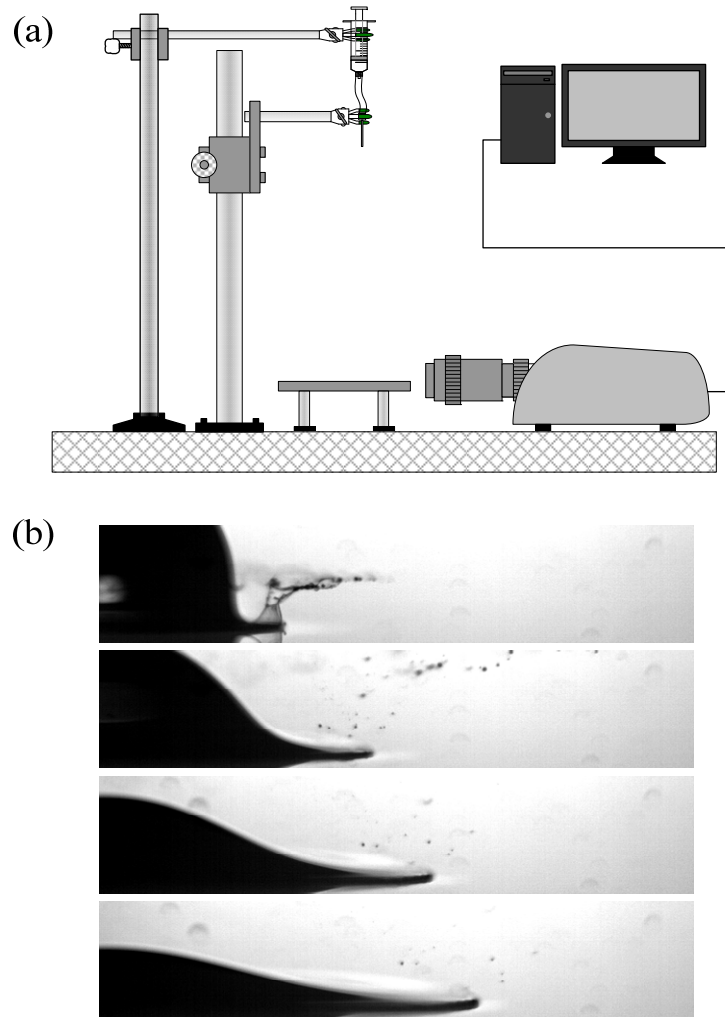


Figure 1.6 Schematics for the characterization of drop splashing, spreading, and breakup. (a) Experimental setup. (b) The results for Jet-A with an interval of 0.5 ms between frame. Note that the ejected fluid breaks up so quickly that only a small number of individual droplets can be resolved after 0.5 ms.

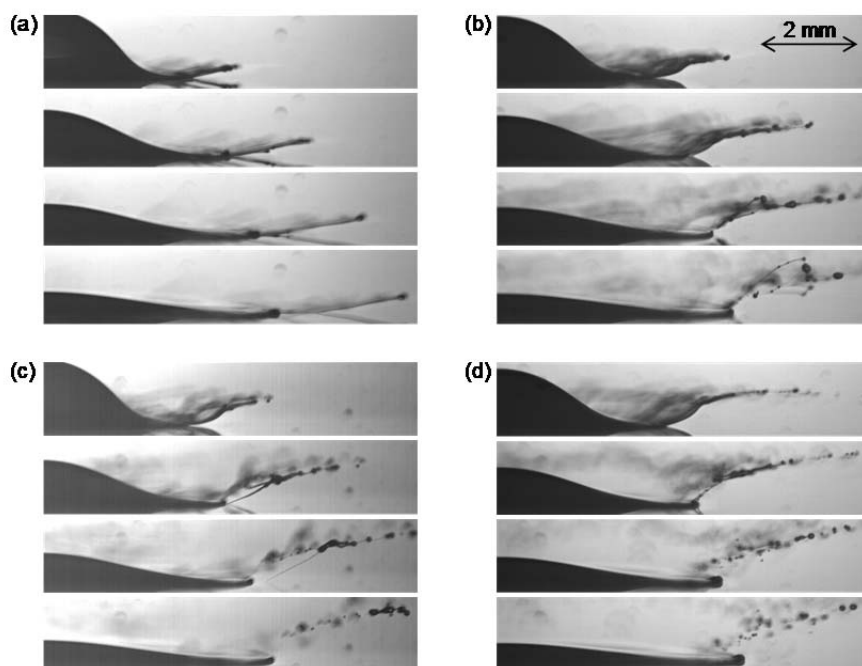


Figure 1.7 High-speed imaging of drop breakup of polymer solutions at 180 ppm in Jet-A (I). (a) 4200KPIB. (b) Unmodified 1250KPB. (c) 1250KPB functionalized with 0.3mol% carboxyl groups. (d) 1250KPB functionalized with 0.6 mol% carboxyl groups. The interval between frame is 0.5 ms in all cases.

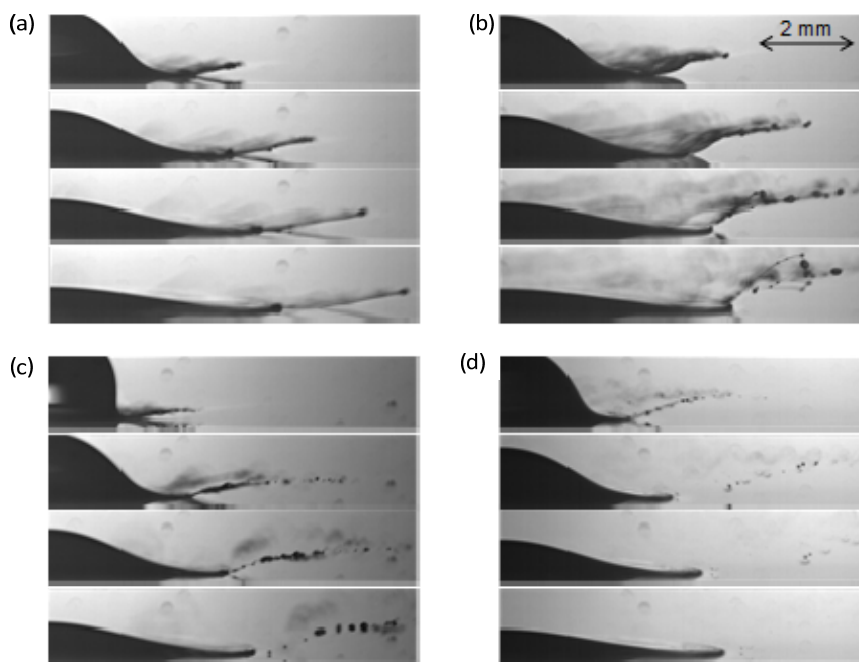
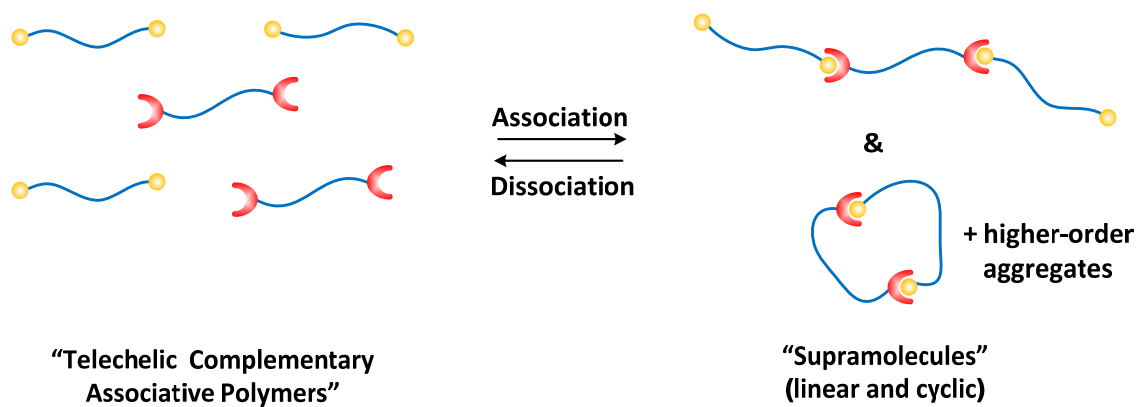


Figure 1.8 High-speed imaging of drop breakup of polymer solutions at 180 ppm in Jet-A (II). (a) 4200KPIB. (b) Unmodified 1250KPB. (c) 3:1 blend of 1250KPB functionalized with 0.3 mol% of carboxyl groups and 1250KPB functionalized with 2.6 mol% of amine groups. (d) 1: 1 blend of 1250KPB functionalized with 0.3 mol% of carboxyl groups and 1250KPB functionalized with 2.6 mol% of amine groups. The interval between frame is 0.5 ms in all cases.



●, ◐ : Complementary Associative Units

Figure 1.9 Schematic of supramolecular aggregation of telechelic complementary associative polymers.

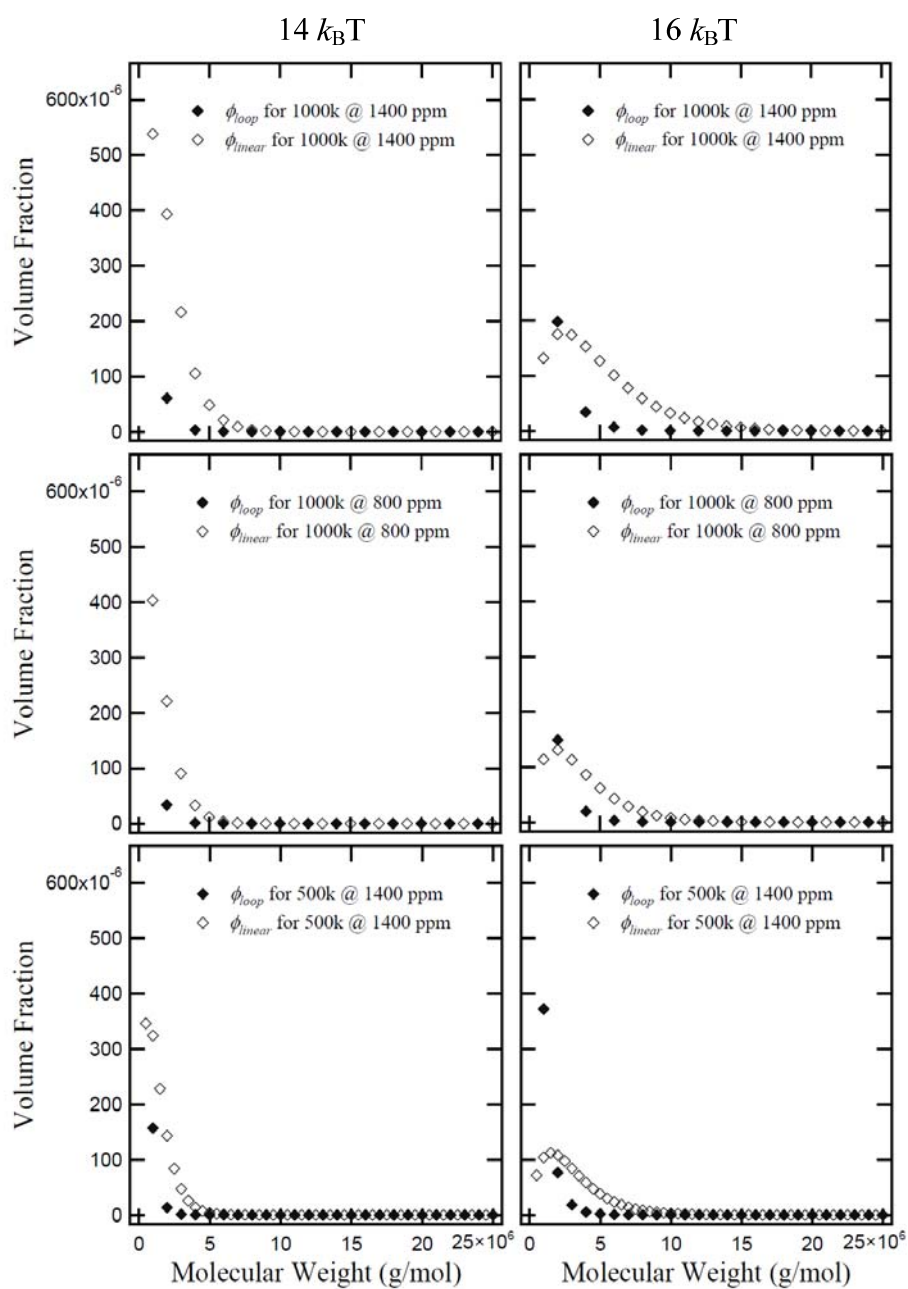


Figure 1.10 Computational predictions of equilibrium composition of equimolar blend of A---A and B---B as a function of MW_p , concentration, and strength of interaction $\epsilon k_B T$. Left: $\epsilon k_B T = 14k_B T$; Right: $\epsilon k_B T = 16k_B T$.

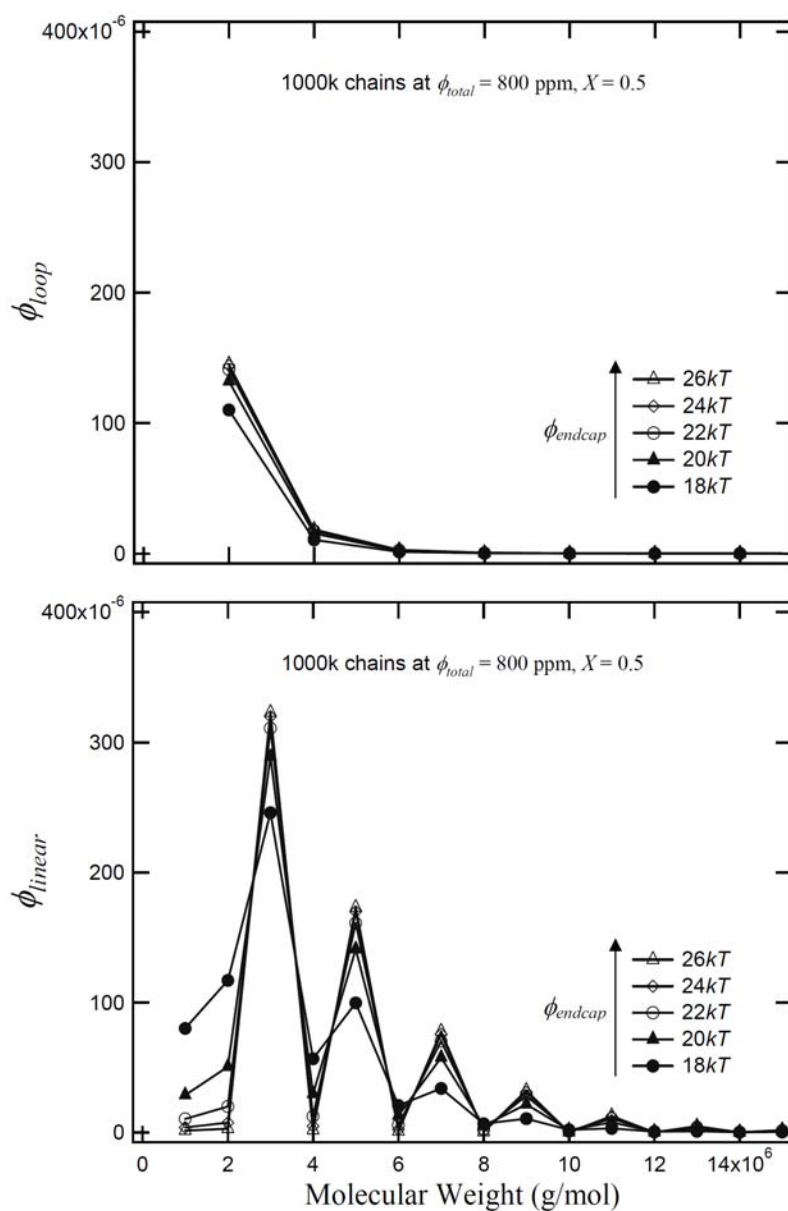


Figure 1.11 Computational predictions of equilibrium concentrations of linear chains and loops in the mixture of A---, A---A and B---B in a 2:1:2 ratio as a function of strength of interaction $\epsilon k_B T$.

Table 1.1 Fundamental Requirements of an Ideal Polymer Additive for Mist Control of Fuel.²⁰

Criteria	Fluid Physical and Chemical Requirements
Improved fire safety	Fuel must not produce fine drops when accidentally released during a crash.
Compatibility with fuel system	Addition of mist-control agent must not cause significant changes to other fuel physical and chemical properties, such as shear viscosity, acidity, etc. Fuel must remain single-phase over a wide range of use conditions.
Ease of transport, storage, and use	Polymer design must confer sufficient stability that additives introduced at the point of production survive to the point of delivery.
Low cost	Selection of polymer backbone and functional groups must take into account feasibility and cost of large scale production.
Environmentally friendly	Polymer must burn cleanly.
Marginal water uptake	Polymer must have low affinity for water.

References

- (1) Yaffee, M. L. *Antimisting Research and Development for Commercial Aircraft—Final Summary Report*, Federal Aviation Administration Technical Center, 1986.
- (2) Eagar, T. W.; Musso, C. *Jom-J Min Met Mat S* 2001, 53, 8.
- (3) *Aviation Fuels with Improved Fire Safety: A Proceedings*, 1997.
- (4) Wright, B. *Assessment of Concepts and Research for Commercial Aviation Fire-Safe Fuel*, NASA Lewis Research Center, 2000.
- (5) Wright, B. R. *The Forensic Examiner* 2004, 13, 14.
- (6) Joseph, D. D.; Beavers, G. S.; Funada, T. *Journal of Fluid Mechanics* 2002, 453, 109.
- (7) Anna, S. L.; McKinley, G. H. *Journal of Rheology* 2001, 45, 115.
- (8) Goldin, M.; Yerushal.J; Pfeffer, R.; Shinnar, R. *Journal of Fluid Mechanics* 1969, 38, 689.
- (9) Yu, J. H.; Fridrikh, S. V.; Rutledge, G. C. *Polymer* 2006, 47, 4789.
- (10) Christanti, Y.; Walker, L. M. *Journal of Rheology* 2002, 46, 733.
- (11) Chao, K. K.; Child, C. A.; Grens, E. A.; Williams, M. C. *Aiche Journal* 1984, 30, 111.
- (12) Willauer, H. D.; Ananth, R.; Hoover, J. B.; Foote, A. B.; Whitehurst, C. L.; Williams, F. W. *Combust Sci Technol* 2007, 179, 1303.
- (13) Brostow, W. *Polymer* 1983, 24, 631.
- (14) Schulz, D. N.; Kitano, K.; Duvdevani, I.; Kowalik, R. M.; Eckert, J. A. *Acs Symposium Series* 1991, 462, 176.
- (15) Ilan Duvdevani, L. N. J.; Dennis G. Peiffer, E. B. N. J.; John A. Eckert, M. N. J.; Robert D. Lundberg, B. N. J. Antimisting system for hydrocarbon fluids. US 4516982, 1985.
- (16) John Knight, F. Antimisting additives for aviation fuels. US 4396398, 1983.
- (17) Peng, S. T. J.; Landel, R. F. *Journal of Non-Newtonian Fluid Mechanics* 1983, 12, 95.
- (18) Schulz, D. N.; Bock, J. *J Macromol Sci Chem* 1991, A28, 1235.
- (19) *First Fire/Fuel Safety Security Workshop*, 2003.

- (20) David, R. L. A. Dissertation (Ph.D.), California Institute of Technology, 2008.
- (21) Kowalik, R. M.; Duvdevani, I.; Peiffer, D. G.; Lundberg, R. D.; Kitano, K.; Schulz, D. N. *Journal of Non-Newtonian Fluid Mechanics* 1987, 24, 1.
- (22) Malik, S.; Mashelkar, R. A. *Chemical Engineering Science* 1995, 50, 105.
- (23) David, R. L. A.; Wei, M. H.; Liu, D.; Bathel, B. F.; Plog, J. P.; Ratner, A.; Kornfield, J. A. *Macromolecules* 2009, 42, 1380.
- (24) David, R. L. A.; Wei, M. H.; Kornfield, J. A. *Polymer* 2009, 50, 6323.

Chapter II Opening the Way to Very Long Telechelic Polymers

2.1 Introduction

The molecular design of associative polymers is essential when synthesizing fuel additives for mist-control. Based on our previous experimental and theoretical studies, we have determined that associative groups need to be clustered around the chain ends of a high-molecular-weight fuel-soluble polymer backbone, in order to eliminate undesired chain collapse and to favor the formation of high-order linear and cyclic supramolecules that are useful to suppress misting.¹ In this chapter, we begin by examining the simplest design: high-molecular-weight linear polymers that are end-capped with clusters of *self-associative* groups.

2.1.1 Background

Polymers that are end-capped with reactive functional groups are referred to as *telechelic polymers*,²⁻¹¹ a term originating from the junction of two Greek words: *tele*, meaning ‘remote,’ and *chele*, meaning lip, claw, or nipper.¹² These polymers have been used to modify the thermal and mechanical properties of condensation polymers, to form polymeric networks, and as components in the synthesis of block copolymers.^{6,12} When end-capping reactive terminal groups are capable of intra-molecular, as well as inter-molecular association, their corresponding linear telechelic polymers, which fulfill the theoretical criteria of ideal mist-control polymers developed in the Kornfield group, are referred to as *telechelic associative polymers*.¹³⁻¹⁷ The simplest example of such polymers is an ABA amphiphilic triblock copolymer, which, when dispersed in an appropriate solvent, will result in the aggregation of the terminal A blocks.^{12,13} As a result of the

association of the end groups, telechelic associative polymers can act, even at low concentrations, as effective modifiers for low-shear rheological properties without considerably altering the high-shear properties.^{18,19} They therefore have been used for a number of industrial applications where careful control of rheological properties is required, e.g., paints, coating, cosmetics, foods, and pharmaceuticals.^{19,20} A representative example of a telechelic associative polymer used in aqueous systems is hydrophobically-modified ethoxylated urethanes (HEURs), where the main chain is water-soluble poly(ethylene oxide) (PEO) and the chain ends are capped with hydrophobic groups such as long alkyl or fluoroalkyl groups through urethane groups.¹⁵ As for apolar systems, linear hydrophobic chains (such as polystyrene, polyisoprene, and poly(ethylene butylene)) end-capped with ionic groups (also known as *ionomers*) serve as good examples of telechelic associative polymers.^{21,22} A variety of techniques have been reported in the literature to prepare telechelic polymers, including anionic and cationic polymerizations, conventional radical polymerization, controlled radical polymerizations, polycondensation, and ring-opening metathesis polymerization.^{12,23}

The demand for an effective mist-control fuel additive calls for telechelic associative polymers with high-molecular-weight ($100 \text{ kg/mol} \ll M_w < 1000 \text{ kg/mol}$), fuel-soluble backbones, and terminal groups that can effectively associate in fuels, as well as an economically feasible route to prepare these polymers (see Chapter 1). These requirements distinguish ring-open metathesis polymerization (ROMP), one of many valuable applications of the highly recognized olefin metathesis chemistry (2005 Nobel Prize in Chemistry), from the other methods discussed above as the ideal approach to prepare such high-molecular-weight telechelic associative polymers. In ROMP, cyclic

olefin monomers are polymerized into unsaturated linear polyolefins that are chemically similar to fuels.^{24,25} When acyclic functional olefins are used in small quantities as chain-transfer agents (CTAs) along with cyclic monomers in ROMP, they not only permit the regulation of polymer molecular weight, but also effectively transfer functional groups to the ends of the polymer chains, yielding a high degree of end-functionalization (> 95%) (see Figure 2.1).^{6,9,10} The built-in ability of ROMP to directly end-functionalize a growing polymer chain provides a huge advantage over the other competing techniques, since most, if not all, of them require post-polymerization functionalization, which can be inefficient and expensive for polymer chains with molecular weights in the range of interest for mist-control applications.²³ Recent advances in ruthenium-based catalysts for olefin metathesis, also known as Grubbs catalysts, have achieved high tolerance towards a variety of functional groups and allowed ROMP to be performed under extremely mild and user-friendly conditions.²⁶ Consequently, ROMP has become a popular approach in recent years to prepare polymers with well-defined and complex structures.²⁷⁻³⁰

Key aspects of the design of telechelic associative polymers for mist-control of fuels include the size and chemical nature of the backbone and structures of the terminal associative groups. The former factors are determined by the selection of cyclic olefin monomers, the metathesis catalyst, and the monomer:CTA:catalyst ratio; while the latter solely rely on the design of CTAs. Mechanistically, ROMP is thermodynamically driven by the release of ring strain in cyclic olefins, and thus a highly strained monomer is preferred to achieve polymer backbones with high molecular weights (cyclic olefins with ring strains less than 5 kcal/mol have been reported to not readily polymerize).³¹⁻³³ Representative examples of commercially available cyclic olefins that possess sufficient

ring strain as ROMP monomers are given in Table 2.1.³¹ Among these monomers, *cis,cis*-1,5-cyclooctadiene (referred to as COD hereinafter) is considered the most appropriate one for building mist-control polymers as additives for fuels, because it possesses a high ring strain (13.3 kcal/mol) and its corresponding polymer backbone, 1,4-polybutadiene (1,4-PB), has been shown to have excellent solubility in fuels over a wide range of temperature.³⁴ Although norbornene has an even higher ring strain (27.2 kcal/mol) and can be easily polymerized into very high molecular weights (>1,000 kg/mol), the poor solubility of its corresponding polymer, polynorbornene, in common organic solvents renders it an inappropriate building block for mist-control polymers.³⁵ Despite of the advantages provided by COD, the monomer has historically been shown to be *not* viable to polymerize into polymer with $M_w > 100$ kg/mol due to the interference with the metathesis catalyst by the isomer of COD, 4-vinylcyclohexene (VCH) (which is usually found at 0.05-0.1 mol% in commercial “redistilled” grade of COD), and the difference in boiling point between COD (150°C) and VCH (129°C) is too small to allow effective removal of VCH by means of fractional distillation on a bench-top scale.^{36,37} In 2004, the Macosko group at the University of Minnesota reported a ground-breaking approach to synthesize telechelic 1,4-PBs with M_w up to 260 kg/mol *via* ROMP of chemically purified COD. Specifically, they found that after treating redistilled-grade COD with ≥ 12 mol% of $\text{BH}_3 \cdot \text{THF}$ complex, the level of VCH was reduced below the detection limit of ^1H NMR (<100 ppm), and the subsequent polymerization of purified COD could easily afford the aforementioned high polymer when a 2000:1 monomer:CTA ratio was used; nevertheless a higher monomer:CTA ratio did not yield higher molecular weight.³⁸ The effects of other contaminants in COD (such as peroxides³⁹ and *n*-butanol introduced by

$\text{BH}_3\cdot\text{THF}$ complex⁴⁰) on the highest achievable molecular weight of telechelic 1,4-PBs, however, were not addressed in the work by the Macosko group. To the best of our knowledge, the M_w of telechelic 1,4-PB reported by the Macosko group (260 kg/mol) is the highest ever in the literature. The value, however, merely reaches the lower bound for mist-control applications. A method to prepare telechelic 1,4-PB with even higher molecular weights, for instance, 500 kg/mol, is needed.

The design of CTA is also an important factor in the development of high-molecular-weight telechelic 1,4-PBs as mist-control additives for fuels. As addressed previously, CTAs regulate the polymer molecular weight and transfer functional groups (in this case, associative groups or their precursors), to polymer chain ends in ROMP. Carboxyl groups are ideal associative groups for *self*-associative telechelic 1,4-PBs because they are able to perform pair-wise self-association in apolar media, and they can be burnt in an engine cleanly.^{34,41} In practice, they need to be “protected” by functional groups that can be easily removed afterwards, for instance, *tert*-butyl group, because of the poor solubility of carboxylic acids in solvents suitable for ROMP of COD (e.g., dichloromethane (DCM) and toluene) and the interference of carboxyl groups with metathesis catalysts.⁶

It should be noted that the binding strength provided by a pair of associative carboxylic acid groups may not be strong enough to hold polymer chains with $M_w \gg 100$ kg/mol together, therefore ideal CTAs for preparing self-associative telechelic polymers as mist-control additives will possess multiple *tert*-butyl ester groups, and the resultant telechelic 1,4-PBs end-capped with multiple *tert*-butyl ester groups will need to be

deprotected so as to recover the carboxyl groups on chain ends. There are two possible configurations to cluster multiple *tert*-butyl ester groups: (1) a short, narrow-disperse functional block of *tert*-butyl ester (e.g., poly(*tert*-butyl acrylate), PtBA); (2) a dendron terminated with *tert*-butyl ester groups (Figure 2.2). A dendron configuration is preferable due to (1) the unparalleled structural uniformity of dendrons which provides precise control of the number of self-associative groups on polymer chain ends, and (2) the dendritic configuration allows very low number of self-associative groups (e.g., 1, 2, and 4) on polymer chain ends that cannot be achieved in the configuration of short functional block, a feature that could potentially prevent the poor solubility of the resultant telechelic polymers in fuels due to having too many associative groups on chain ends. An example of such dendritic CTAs and corresponding telechelic polymers by ROMP was reported by Sill and Emrick in 2005.⁴² In their work, they prepared bis-dendritic CTAs with 1st to 3rd generations (**G1-G3**) of benzyl bromide-terminated poly(benzyl ether) dendrons (or “Fréchet” dendrons, Figure 2.2 (c)) and used these CTAs in ROMP of cyclooctene to prepare dendron-poly(cyclooctene)-dendron ABA triblock copolymers. Such a molecular architecture, to the best of our knowledge, has never been employed to prepare fuel-soluble telechelic polymers with well-defined, dendritic end-associative units.

2.1.2 Scope of the Present Work

In this chapter, we focus on the development of a series of bis-dendritic CTAs that can precisely end-functionalize 1,4-PB chains with desired number of carboxyl groups, as well as the pursuit of a synthetic method that can prepare telechelic 1,4-PBs with M_w well beyond the currently known limit (260 kg/mol). In light of the ease of

purification and the possibility for future scale-up production, a divergent approach is used in the present study to prepare a series of *tert*-butyl ester-terminated bis-dendritic CTAs that have 2 (**G0**), 4 (**G1**), 8 (**G2**), and 16 (**G3**) *tert*-butyl ester terminal groups, respectively. Based on the protocol developed by the Macosko group,³⁸ we devise a strategy to synthesize telechelic 1,4-PB with $M_w \gg 260$ kg/mol starting from rigorous purification of COD which removes not only VCH, but also peroxides and *n*-butanol introduced by $\text{BH}_3\cdot\text{THF}$ complex; **G0-G3** CTAs are subsequently used to synthesize telechelic 1,4-PBs with 1, 2, 4, and 8 *tert*-butyl ester groups on chain ends, respectively. The recovery of carboxyl groups on chain ends of prepared telechelic 1,4-PBs by means of removing *tert*-butyl groups is also studied.

2.2 Experimental

2.2.1 Materials and Instrumentation

Except for *cis* 1,4-dichloro-2-butene (Aldrich, 95%), potassium *tert*-butoxide (Aldrich, 98%), 5-hydroxyisophthalic acid (Aldrich, 97%), dimethyl 5-hydroxyisophthalate (Aldrich, 98%), lithium aluminum hydride (Aldrich, 95%), all reagents were obtained at 99% purity from Sigma-Aldrich, Alfa Aesar, or Mallinckrodt Chemicals. ^1H and ^{13}C NMR spectra were obtained using a Varian Inova 500 spectrometer (500 MHz for ^1H and 125.7 MHz for ^{13}C); all spectra were recorded in CDCl_3 , DMSO-d_6 , or 16:1 $\text{CDCl}_3/\text{acetone-d}_6$ mixture. Chemical shifts were reported in parts per million (ppm, δ) and were referenced to residual solvent resonances. Polymer molecular weight measurements were carried out in tetrahydrofuran (THF) at 35°C eluting at 0.9 mL/min (pump: Shimadzu LC-20AD Prominence HPLC Pump) through four PLgel 10- μm analytical columns (Polymer Labs, 10^6 to 10^3 Å in pore size)

connected in series to a DAWN EOS multi-angle laser light scattering (MALLS) detector (Wyatt Technology, Ar laser, $\lambda = 690$ nm) and a Waters 410 differential refractometer detector ($\lambda = 930$ nm).

2.2.2 Synthesis of Chain Transfer Agents (CTAs) and Intermediates

***tert*-Butyl 4-hydroxybenzoate (1).** 4-hydroxybenzoic acid (3.0g, 21.5 mmol) was added into a 100-mL RBF, followed by 50 mL of anhydrous THF. Thionyl chloride (3.15 mL, 43 mmol) was then added dropwise into the RBF through a 25 mL addition funnel over a period of 30 min, and the RBF was placed in an oil bath at 67°C and left to stir at reflux temperature for 2 h to form 4-hydroxybenzoyl chloride. The gaseous byproducts, sulfur dioxide and hydrogen chloride, were scavenged by directing them into a water bath. Excess thionyl chloride and THF were removed under reduced pressure. The resultant brown syrup was dissolved in 40 mL of anhydrous THF, and the solution was slowly added to an anhydrous THF solution of potassium *tert*-butoxide (*t*BuOK) in a 250 mL round-bottom flask (RBF) in an ice bath over 10 min. The RBF was taken out of the ice bath and left to stir at room temperature overnight. 60 mL of de-ionized (DI) water was then added in small portions into the RBF over 5 min, to quench the excess *t*BuOK. 100 mL of 1M HCl_(aq) was added to neutralize the mixture. The mixture was then extracted with 150 mL of ethyl acetate (EA) in a 500-mL separatory funnel. The organic phase was washed thrice with 200 ml water + 6 g of sodium bicarbonate (NaHCO₃) (discarding the aqueous phase after each wash). The resultant organic phase was dried over 6 g of MgSO₄ and filtered, followed by solvent evaporation at 40°C. The crude product was then purified by dissolving in 20 mL boiling 4:1 hexane/EA mixture and allowing it to recrystallize in the freezer for 1 day. Filtration of the crystals and removal of solvent

under reduced pressure gave analytically pure **1** as fine, off-white crystals (3.3 g, 17.2 mmol, 80.0% yield). $^1\text{H NMR}$ (500 MHz, DMSO- d_6): δ = 10.22 (s, ArOH, 1H), 7.75 (m, ArH, 2H), 6.82 (m, ArH, 2H), 1.52 (s, COOC(CH $_3$) $_3$, 9H).

Di-*tert*-butyl 5-hydroxyisophthalate (2). It was synthesized according to literature procedures.⁴³ Specifically, 5-hydroxyisophthalic acid (10.0 g, 53.3 mmol) was added into a 250-mL RBF, followed by 60 mL of anhydrous THF. Thionyl chloride (16 mL, 218 mmol) was added dropwise into the RBF through a 25 mL addition funnel over a period of 30 min, and then the RBF was placed in an oil bath at 67°C and left to stir at reflux temperature for 2 h to form 5-hydroxyisophthaloyl chloride. The gaseous byproducts, sulfur dioxide and hydrogen chloride, were scavenged by directing the gases into a water bath. The excess thionyl chloride and THF were removed under reduced pressure. The resultant brown syrup was dissolved with 40 mL of anhydrous THF. To 35.0 g of *t*BuOK (303 mmol) in 120 mL of anhydrous THF in a 500 mL RBF in an ice bath was slowly added the THF solution of isophthaloyl chloride over 10 min. The RBF was then taken out of the ice bath and left to stir at room temperature overnight. 100 mL of DI water was added in small portions into the RBF over 5 min to quench the excess *t*BuOK. 200 mL of 1M HCl_(aq) was added to neutralize the mixture. The mixture was extracted with 200 mL of EA in a 1 L separatory funnel. The organic phase was washed thrice with 300 ml water + 11 g of NaHCO $_3$ (discarding the aqueous phase after each wash). The resultant organic phase was first dried over 11 g of MgSO $_4$ then filtered, and the solvent was rotary-evaporated at 40°C. The crude product was then purified by dissolving in 50 mL boiling 4:1 hexane/EA mixture and allowing it to recrystallize in the freezer for 2 days. Filtration of the crystals and removal of solvent under reduced pressure gave analytically pure **2** as

fine, off-white crystals (12.59 g, 42.8 mmol, 80.4% yield). ^1H NMR (500 MHz, DMSO- d_6): δ = 10.18 (s, ArOH, 1H), 7.85 (t, J = 1.5 Hz, ArH, 1H), 7.49 (d, J = 1.5 Hz, ArH, 2H), 1.54 (s, COOC(CH₃)₃, 18H).

Di-*tert*-butyl ester CTA (G0, 3). *tert*-Butyl 4-hydroxybenzoate (0.9 g, 4.34 mmol), dry potassium carbonate (K₂CO₃, 1.67 g, 6.52 mmol), and *cis* 1,4-dichloro-2-butene (0.26 g, 1.98 mmol) were stirred at 80°C in 10 mL of *N,N*-dimethylformamide (DMF) in a 50 mL RBF for 5 h. 30 mL of DCM was added into the reaction mixture after it was cooled to room temperature, and the mixture was poured into a 100 mL separatory funnel, washed thrice with 30 mL of water, and then thrice with 1M HCl_(aq) (discarding the aqueous phase after each wash). The resultant organic phase was dried over 3 g of MgSO₄ and filtered, and the solvent was removed under reduced pressure at 25°C to afford crude product **3** in ~95% purity (0.65 g, 14 mmol, ~80.0% yield). ^1H NMR (500 MHz, CDCl₃) : δ = 7.96 (m, ArH, 4H), 6.92 (m, ArH, 4H), 5.97 (ddd, J = 4.3, 3.3, 0.9 Hz, CH₂CH=CHCH₂, 2H), 4.74 (m, -OCH₂CH=, 4H), 1.60 (s, COOC(CH₃)₃, 18H).

Tetra-methyl ester butene (4). Dimethyl 5-hydroxyisophthalate (**2'**, 7.28g, 34 mmol) and dry K₂CO₃ (7.06 g, 51 mmol) were weighed and loaded into a 100 mL RBF. Then, 40 ml of DMF, followed by *cis* 1,4-dichloro-2-butene (2.00 g, 15.3 mmol) were added into the flask. The RBF was placed in an oil bath at 80°C and left to stir for 5 h. The reaction mixture was poured into a 250 mL separatory funnel, diluted with 100 mL of DCM, washed with 100 mL of water, and then thrice with 100 mL of 1M HCl_(aq) (discarding the aqueous phase after each wash). The resultant organic phase was dried over MgSO₄, filtered, and the solvent was removed under reduced pressure at room

temperature. The crude product was purified by dissolving in 30 mL of boiling ethanol and allowing it to recrystallize in the freezer overnight, yielding analytically pure **4** (6.0 g, 12.7 mmol, 83.0% yield) as white crystals after filtration and solvent removal. ^1H NMR (500 MHz, CDCl_3) : δ = 8.30 (t, J = 1.4 Hz, ArH, 2H), 7.77 (d, J = 1.4 Hz, ArH, 4H), 5.99 (ddd, J = 4.3, 3.2, 0.9 Hz, $-\text{CH}_2\text{CH}=\text{CHCH}_2-$, 2H), 4.83 – 4.75 (m, $-\text{OCH}_2\text{CH}=\text{}$, 4H), 3.94 (s, COOCH_3 , 12H).

Tetra-*tert*-butyl ester CTA (G1, 5). 2 (2.55g, 8.49 mmol) and dry K_2CO_3 (2.25 g, 16.28 mmol) were weighed and loaded into a 50 mL RBF (RBF, charged with a magnetic stir bar). Then 20 ml of DMF, followed by *cis* 1,4-dichloro-2-butene (0.51 g, 3.86 mmol) were added into the flask. The RBF was placed in an oil bath at 80°C and left to stir for 5 h. The reaction mixture was poured into a 125 mL separatory funnel, diluted with 50 mL of dichloromethane (DCM), washed twice with 50 mL of water, and then four times with 50 mL of 1M $\text{HCl}_{(aq)}$ (discarding the aqueous phase after each wash). The resultant organic phase was dried over MgSO_4 , filtered, and the solvent was removed under reduced pressure at room temperature. The crude product was purified by dissolving in 25 mL of boiling methanol and allowing it to recrystallize in the freezer overnight, yielding analytically pure **5** (1.80 g, 2.81 mmol, 72.8% yield) as white crystals after filtration and solvent removal. ^1H NMR (500 MHz, CDCl_3) : δ = 8.9 (t, J = 1.5 Hz, ArH, 2H), 7.69 (d, J = 1.5 Hz, ArH, 4H), 6.00 (ddd, J = 4.3, 3.3, 0.9 Hz, $-\text{CH}_2\text{CH}=\text{CHCH}_2-$, 2H), 4.81 – 4.72 (m, $-\text{OCH}_2\text{CH}=\text{}$, 4H), 1.59 (s, $\text{COOC}(\text{CH}_3)_3$, 36H).

Tetra-hydroxy butene (6). A suspension of lithium aluminum hydride (LiAlH_4 , 1.75 g, 43.8 mmol) in THF (30 mL) was slowly added to a THF (40 mL) solution of **4** (5.01 g,

10.4 mmol in a 250 mL RBF in an ice bath. The flask was taken out of the ice bath and left to stir at room temperature overnight. 6 mL of 35% HCl_(aq) in 50 mL of water was slowly added to the reaction mixture to quench excess LiAlH₄. The mixture was poured into a 250 mL separatory funnel containing 50 mL of water and extracted with 100 mL of 2-butanone (MEK). The aqueous phase was extracted twice with 100 mL MEK, and the organic extracts were combined, concentrated by rotary evaporation to remove ~200 mL of solvent, dried over 6 g of MgSO₄, and filtered. The solvent was removed under reduced pressure at 45 °C, and the crude was purified by dissolving in boiling 1:1 acetone/MEK mixture, and allowing it to recrystallize in the freezer overnight. Vacuum filtration and removal of solvents under reduced pressure gave analytically pure **6** (2.97g, 8.24 mmol, 79.5% yield) as fine, white crystals. ¹H NMR (500 MHz, DMSO-d₆): δ = 6.87 (tt, J = 1.5, 0.8 Hz, 2H), 6.78 (dt, J = 1.5, 0.7 Hz, 4H), 5.86 (ddd, J = 4.1, 3.2, 0.8 Hz, -CH₂CH=CHCH₂-, 2H), 5.16 (t, J = 5.7 Hz, 4H), 4.75 – 4.66 (m, -OCH₂CH=, 4H), 4.45 (d, -O-CH₂-OH, 8H).

Octa-methyl ester butene (7). To an anhydrous THF (60 mL) suspension of **6** (2.00g, 5.55 mmol), triphenylphosphine (PPh₃, 8.87g, 33.82 mmol) and **2'** (7.15g, 33.34 mmol) in a 100 mL RBF in a water bath at room temperature was drop-wise added diisopropyl azodicarboxylate (DIAD, 7.13g, 33.50 mmol) in anhydrous THF (20 mL). The RBF was taken out of water bath and placed in an oil bath at 50°C. The mixture was stirred at the bath temperature overnight. The solvent was removed under reduced pressure, and the residue was dissolved with 30 mL of DCM. The solution was cooled to 0°C, and precipitated into 300 mL of cold methanol at -20°C. After vacuum filtration and removal of solvents under reduced pressure at 40°C overnight, the crude product was redissolved

with 40 mL of THF and precipitated into 200 mL of cold methanol at -20°C , and vacuum filtered. Drying *in vacuo* overnight at 40°C afforded analytically pure **7** (5.74g, 5.08 mmol, 91.5%) as off-white powder. ^1H NMR (500 MHz, CDCl_3): δ = 8.27 (t, J = 1.4 Hz, ArH, 4H), 7.80 (d, J = 1.4 Hz, ArH, 8H), 7.11 (t, J = 1.4 Hz, ArH, 2H), 6.98 (d, J = 1.4 Hz, ArH, 4H), 5.96 (ddd, J = 4.1, 3.2, 0.8 Hz, $-\text{CH}_2\text{CH}=\text{CHCH}_2-$, 2H), 5.10 (s, $-\text{O}-\text{CH}_2-\text{O}-$, 8H), 4.77 – 4.72 (m, $-\text{OCH}_2\text{CH}=\text{}$, 4H), 3.92 (s, COOCH_3 , 24H).

Octa-tert-butyl ester CTA (G2, 8). To an anhydrous THF (45 mL) suspension of **6** (0.75g, 2.08 mmol), PPh_3 (3.32g, 12.53 mmol) and **2** (3.75g, 12.74 mmol) in a 100 mL RBF in a water bath at room temperature was drop-wise added DIAD (2.66g, 12.5 mmol). The RBF was taken out of water bath and placed in an oil bath at 40°C . The mixture was stirred at 40°C overnight. The solvent was removed under reduced pressure, and the residue was dissolved with 15 mL of DCM. The solution was cooled to 0°C , and precipitated into 200 mL of cold methanol at -20°C . After vacuum filtration and removal of solvents under reduced pressure at 40°C overnight, the crude was redissolved with 5 mL of THF and precipitated into 150 mL of cold methanol at -20°C , and vacuum filtered. Drying *in vacuo* overnight at 40°C afforded analytically pure **8** (1.21g, 0.83 mmol, 39.7% yield) as off-white powder. ^1H NMR (500 MHz, CDCl_3): δ = 8.19 (t, J = 1.4 Hz, ArH, 4H), 7.74 (d, J = 1.4 Hz, ArH, 8H), 7.13 (t, J = 1.4 Hz, ArH, 2H), 7.00 (d, J = 1.4 Hz, ArH, 4H), 5.97 (ddd, J = 4.3, 3.2, 0.9 Hz, $-\text{CH}_2\text{CH}=\text{CHCH}_2-$, 2H), 5.10 (s, $-\text{O}-\text{CH}_2-\text{O}-$, 8H), 4.76 – 4.68 (m, $-\text{OCH}_2\text{CH}=\text{}$, 4H), 1.59 (s, $\text{COOC}(\text{CH}_3)_3$, 72H).

Octa-hydroxy butene (9). LiAlH_4 (0.28g, 7.1 mmol) in THF (10 mL) was slowly added into the THF (20 mL) solution of **7** (1.01g, 0.89 mmol) in a 100 mL RBF in an ice bath

over 10 min. The reaction mixture was stirred at room temperature overnight. 0.3 mL of DI water was added into the reaction mixture to quench excess LiAlH_4 . 0.3 mL of 15% $\text{NaOH}_{(aq)}$, followed by 0.9 mL of DI water, was added. The mixture was stirred at room temperature for 1 h to allow the granular salt of aluminum hydroxide ($\text{Al}(\text{OH})_3$) to form. The reaction mixture was filtered and dried over MgSO_4 , and the solvent was removed under reduced pressure at 35°C to afford **9** (0.63 g, 0.70 mmol, 78.7% yield) as glassy, faint-yellow solid. ^1H NMR (500 MHz, DMSO-d_6): δ = 7.12 (d, J = 1.4 Hz, ArH , 4H), 7.02 (d, J = 1.4 Hz, ArH , 8H), 6.87 (t, J = 1.5 Hz, ArH , 8H), 6.83 (d, J = 1.5 Hz, ArH , 16H), 5.93 – 5.82 (m, $-\text{CH}_2\text{CH}=\text{CHCH}_2-$, 2H), 5.17 (t, J = 5.7 Hz, $-\text{O}-\text{CH}_2-\text{OH}$, 8H), 5.05 (s, $\text{Ar}-\text{O}-\text{CH}_2-\text{O}-$, 8H), 4.77 (d, J = 3.6 Hz, $-\text{OCH}_2\text{CH}=\text{}$, 4H), 4.45 (d, J = 5.6 Hz, $-\text{O}-\text{CH}_2-\text{OH}$, 16H).

Hexadeca-*tert*-butyl ester CTA (G3, 10). To a THF (40 mL) solution of **9** (0.63g, 0.69 mmol), PPh_3 (2.24g, 8.3 mmol) and **2** (2.46g, 8.3 mmol) in a 100 mL RBF in a water bath at room temperature was drop-wise added DIAD (1.76g, 8.3 mmol). The RBF was taken out of water bath and placed in an oil bath at 40°C . The mixture was stirred at 40°C overnight. The solvent was removed under reduced pressure, and the residue was dissolved with 5 mL of DCM. The solution was cooled to 0°C , and precipitated into 150 mL of cold methanol at -78°C . After vacuum filtration and removal of solvents under reduced pressure at 40°C overnight, the crude was redissolved with 5 mL of THF and precipitated into 150 mL of cold methanol at -20°C , and vacuum -filtered. Drying *in vacuo* overnight at 40°C afforded analytically pure **10** (1.39g, 0.45 mmol, 64.6% yield) as white powder. ^1H NMR (500 MHz, CDCl_3): δ = 8.18 (t, J = 1.3 Hz, ArH , 8H), 7.74 (d, J = 2.7, 1.4 Hz, ArH , 16H), 7.14 (t, J = 7.3, 1.4 Hz, ArH , 4H), 7.12 (t, J = 7.3, 1.4 Hz, ArH ,

2H), 7.05 (d, $J = 1.5$ Hz, ArH , 8H), 6.99 (d, $J = 1.5$ Hz, ArH , 4H), 5.99 – 5.91 (m, $-CH_2CH=CHCH_2-$, 2H), 5.09 (s, $-O-CH_2-O-$, 16H), 5.06 (s, $-O-CH_2-O-$, 8H), 4.73 (d, $J = 3.6$ Hz, $-OCH_2CH=$, 4H), 1.58 (s, $COOC(CH_3)_3$, 144H).

2.2.3 Polymer Synthesis (Scheme 2.2)

Purification of Monomer. Redistilled-grade COD (72.3 g, 0.67 mol) was syringe-transferred to a 250 ml Schlenk flask in an ice bath at 0°C under argon atmosphere. Under argon flow, 1M $BH_3 \cdot THF$ complex in THF (108 mL, 0.11 mol) was then slowly added into the flask over 10 min. The flask was taken out of the ice bath, and left to stir under argon atmosphere at room temperature for 2 h. THF was evaporated under reduced pressure at room temperature to an extent that the concentration of residual THF in the mixture was below 300 ppm (verified by 1H NMR analysis). The monomer was vacuum distilled from the mixture at 40°C and 100 mTorr into a 100 mL Schlenk flask (loaded with 9 g of Magnesol® xl and a magnetic stir bar) in a dry-ice tub. The mixture was stirred under argon atmosphere at room temperature overnight. The monomer was vacuum distilled again at 45°C and 100 mTorr from the mixture into a 100 mL Schlenk flask (loaded with 10 g of calcium hydride (CaH_2) and a stir bar) in a dry ice tub in order to remove moisture introduced by Magnesol® xl. After stirring at room temperature for 3 h under argon flow, the monomer was once again vacuum distilled (45°C, 100 mTorr) from the mixture into a 100 mL Schlenk flask in a dry-ice tub. After being warmed to ambient temperature, the flask was sealed with a Suba-Seal rubber septum while argon stream was flowing through the flask, and placed in a freezer at -30°C for storage of the rigorously purified COD (40.0 g, 55.3% yield). The rigorously purified monomer was vacuum-distilled again at 35°C prior to use.

Representative procedure for synthesis of *tert*-butyl ester-terminated telechelic 1,4-PBs of $M_w < 300$ kg/mol. G2 CTA **8** (13.0 mg, 9.15 μmol) was placed in 50 mL Schlenk flask (charged with a magnetic stir bar), and degassed by 5 cycles of pulling vacuum/filling argon. Deoxygenated, anhydrous DCM was syringe-transferred into the flask to dissolve the CTA. The flask was placed in an oil bath at 40°C. 0.26 mL of 1 mg/mL anhydrous DCM solution of second-generation Grubbs Catalyst (0.26 mg, 0.31 μmol ; referred to as Grubbs II, hereafter) was injected into the mixture to equilibrate with the CTA, followed immediately by the addition of a small amount of degassed, freshly vacuum-distilled rigorously purified COD (0.10 g, 0.92 mmol) to the mixture to start the polymerization reaction. The mixture was stirred at 40°C for 1 h. A large amount of degassed, freshly vacuum-distilled rigorously purified COD (2.00 g, 18.3 mmol) in degassed, anhydrous DCM (4 mL) was injected into the mixture. The mixture was stirred at 40°C overnight. Additional DCM (20 mL) and 0.1 g of BHT were added, and the mixture was precipitated into 300 mL of acetone at room temperature. The precipitated polymer was collected and dried *in vacuo* at room temperature overnight.

Representative procedure for synthesis of *tert*-butyl ester-terminated telechelic 1,4-PBs of $M_w > 400$ kg/mol. G2 CTA **8** (6.5 mg, 4.58 μmol) was placed in a 50 ml Schlenk flask, and degassed by 5 cycles of pulling vacuum/filling argon. Degassed, anhydrous DCM (0.5 mL) was syringe-transferred into the flask to dissolve the CTA. 0.13 mL of 1 mg/mL anhydrous DCM solution of Grubbs II (0.13 mg, 0.16 μmol) was injected into the mixture to equilibrate with the CTA, followed immediately by the addition of a small amount of degassed, freshly vacuum-distilled rigorously purified COD (0.03 g, 0.23

mmol) to the mixture to start the polymerization reaction. The mixture was stirred at 40°C for 30 min. Another 0.13 ml of freshly prepared 1mg/ml DCM solution of Grubbs II is then injected, followed by a large amount of freshly vacuum-distilled, rigorously purified COD (5.00 g, 45.8 mmol) in degassed, anhydrous DCM (12 mL). The mixture was stirred at 40°C for 4-10 min. The reaction was stopped by exposure to air, and additional DCM (30 mL) + 0.1 g of BHT were added. The diluted mixture was precipitated into 400 mL of acetone at room temperature. The precipitated polymer was collected and dried *in vacuo* at room temperature overnight.

Representative procedure for preparation of carboxyl-terminated polymers. 1 g of *tert*-butyl ester-terminated polymer was loaded into a 50 mL Schlenk flask (charged with a magnetic stir bar), and degassed by 5 cycles of pulling vacuum/filling argon. 30 mL of deoxygenated, anhydrous DCM was syringe-transferred into the flask to dissolve the polymer. Once homogenization was achieved, 1.5 mL of deoxygenated trifluoroacetic acid (TFA) was slowly syringe-transferred to the mixture, which was stirred at room temperature for 12-16 h. Depending on the molecular weight of the starting material, the reaction mixture was diluted with 0-20 mL of DCM, and the resultant mixture was precipitated into 300-500 mL of acetone at room temperature. The precipitated polymer was collected, and further purified by 2 cycles of reprecipitation from THF (30-50 mL, with ~0.1 g of BHT) into acetone (300-500 mL), followed by drying *in vacuo* at room temperature overnight.

2.3 Results

2.3.1 Synthesis of Chain Transfer Agents (CTAs)

A series of bis-dendritic *cis*-olefinic CTAs with one (compound **3**), two (compound **5**), four (compound **8**), and eight (compound **10**) *tert*-butyl ester groups at each end were successfully synthesized in 40-80% yield. The protected form of the carboxyl group, *i.e.*, *tert*-butyl ester, was chosen for the sake of solubility of CTAs in the solvent for polymer synthesis (DCM in the present study). CTA **5**, **8**, and **10** are composed of first-, second- and third-generation poly(benzyl ether) dendrons terminated with *tert*-butyl ester groups, respectively. We did not proceed to the fourth-generation dendron due to the fact that the resultant carboxyl-terminated telechelic 1,4-PB from CTA **10** were found insoluble in apolar solvents for rheological study (refer to Chapter 3). GPC data showed that all three bis-dendritic CTAs **5**, **8** and **10** are mono-disperse (Figure 2.3).

Ideally, by repeating LAH reduction of peripheral *tert*-butyl ester groups and Mitsunobu coupling between the resultant bis-dendritic alcohols and **2**, CTA **10** can be synthesized from CTA **5** and CTA **8**. Given the fact that **2** is not commercially available, but di-methyl-5-hydroxyisophthalate (**2'**) is, intermediates **4** and **7** were prepared instead and used as the precursors for **6** and **9**, respectively (Scheme 2.1). They were not chosen as CTAs because of the comparative difficulty to hydrolyze methyl esters in the absence of a strong acid and the use of a high reaction temperature (>100°C).

The unique properties of poly(benzyl ether) dendrons allow easy purification of all bis-dendritic intermediates and CTAs without the need for chromatographic methods:

Compounds **4** and **5** were purified by recrystallization, whereas the purification of compounds **7**, **8**, and **10** was achieved by 2-3 times of reprecipitation from THF/DCM into cold methanol. The ease of purification, combined with mild reaction conditions for compounds **1-10**, demonstrate a scalable method to synthesize CTAs with discrete number of *tert*-butyl ester groups in quantity.

2.3.2 Monomer Purification

4-vinylcyclohexene (VCH), the isomer of COD produced as a by-product in synthesis of COD *via* nickel-catalyzed oligomerization of 1,3-butadiene, is present in commercially available, re-distilled grade COD at a concentration of 0.05-0.1 mol %.³⁷ Due to the adverse effects of vinyl impurities on syntheses of high molecular weights PBs *via* ROMP, the monomer needs to be purified in order to remove VCH. The Macosko group reported that by means of treating the commercial, re-distilled COD with ≥ 12 mol% of $\text{BH}_3 \cdot \text{THF}$ complex, the content of VCH can be effectively reduced below the detection limit of ^1H NMR because the vinyl group of VCH reacts with borane (*i.e.*, hydroboration) much faster than the internal C=C double bond of COD.³⁸ In this study, 16.4 mol% of $\text{BH}_3 \cdot \text{THF}$ complex (based on the crude monomer) was used. After the treatment, we found that the resonances of VCH (5.84, 5.73, 5.42, 5.02, and 4.94 ppm) were not present in the ^1H NMR spectra (500 MHz, CDCl_3) of the purified monomer vacuum-distilled from the reaction mixture.

To achieve telechelic 1,4-PBs with high molecular weights, all impurities that affect the activity of Grubbs II must be removed. In addition to VCH, peroxides and primary alcohols are also known to have adverse effects on the metathetical activity of

Grubbs catalysts, but none of them were addressed in the Macosko group's work.³⁸ When COD is exposed to air, it reacts with oxygen and forms peroxides, which are known to be inhibitors to Grubbs catalysts.³⁹ In addition, we have found that the 1M THF solution of $\text{BH}_3\cdot\text{THF}$ complex from Aldrich inevitably contains a small amount of *n*-butanol, possibly the product of ring-opening of THF by borane.⁴⁴ We also found that the resonances of *n*-butanol always appeared in the ^1H NMR spectra of COD purified according to the Macosko protocol. Ding and Mol have pointed out that both first- and second-generation of Grubbs catalysts react with primary alcohols and subsequently lose the active benzylidene motifs, and the reaction takes place more readily in the presence of triethylamine.⁴⁰ However, the small difference in boiling point between *n*-butanol (118°C) and that of COD (150°C) renders removal of *n*-butanol by vacuum distillation on a bench-top scale practically infeasible. Similar to the bench-top scale removal of VCH, the efficient way to remove *n*-butanol from VCH COD is to chemically consume it. In response to the issues caused by the aforementioned contaminants, we first stirred vacuum-distilled, VCH-free COD with Magnesol[®] (amorphous magnesium silicate hydrate) under argon at room temperature overnight in order to remove peroxides *via* adsorption. After the monomer was vacuum-distilled off from Magnesol[®], we stirred it with CaH_2 in order to deprotonate *n*-butanol and convert it to a non-volatile salt, as well as to remove the moisture introduced by Magnesol[®]. After Magnesol[®]/ CaH_2 treatment, ^1H NMR analysis showed the content of *n*-butanol is below the detection limit (Figure 2.4). We also found the ROMP reaction of COD purified in this manner proceeded significantly faster compared to that of monomer purified by mere $\text{BH}_3\cdot\text{THF}$ treatment

(i.e., the Macosko protocol). A full description of benchmark reactions is given in Appendix A.

The overall yield of the aforementioned rigorous purification of monomer was found to be 55%. Mechanistically, one $\text{BH}_3\cdot\text{THF}$ molecule is capable of consuming two molecules of COD. The use of 16.4 mol% of $\text{BH}_3\cdot\text{THF}$ accounted for at least 32.8% of loss of monomer. Vacuum evaporation of THF and multiple cycles of vacuum distillation of monomer after each treatment also contributed to the extra loss of monomer.

2.3.3 Polymer Synthesis

Scheme 2.2 depicts the two-stage strategy for ROMP of COD with the presence of a CTA developed by the Macosko group.³⁸ During the first stage, a small amount of COD (50-100 eq), along with a CTA, are given sufficient time to react with Grubbs II to full conversions of both monomer and CTA, turning the small-molecule CTA into a much more reactive macro CTA (*i.e.*, short telechelic 1,4-PB with $M_w < 20$ kg/mol). The majority of COD, along with required amount of deoxygenated, anhydrous DCM, are added to the living reaction mixture at the beginning of the second stage to drive the formation of telechelic 1,4-PBs with high molecular weights.

Based on Scheme 2.2, a series of telechelic 1,4-PBs were synthesized from rigorously purified COD using reaction conditions summarized in Table 2.2. The family of well-defined CTAs **3**, **5**, **8** and **10** offered precise control of the number of *tert*-butyl ester groups on polymer chain ends (N), which was later translated into the tunability of the strength of end-association after the removal of *tert*-butyl groups (refer to Chapter 3). ¹H NMR analysis of aliquots taken during the first stage showed that all four CTAs,

including the bulky CTA **10**, were able to be completely incorporated into the corresponding macro CTAs (Figure 2.5). In the case of target $M_w < 300$ kg/mol (entries 1-6 in Table 2.2), a reaction time of 16 h in conjunction with a total amount of 2000 eq of COD were used in the second-stage chain extension reaction. The freshness of such rigorously purified COD showed a crucial effect on the proceeding of polymerization reaction: When the monomer was freshly vacuum-distilled prior to use, the conversions of COD in the end of the second-stage reaction, as revealed by ^1H NMR analysis of aliquots taken at the end of each reaction, ranged from 94.8% to 97.6% (entries 2, 4, and 6 in Table 2.2); however, as the monomer stored for 30 h or longer at -30°C after being rigorously purified was used, the conversions of COD in the second-stage of ROMP were obviously lower, ranging from 76.9 to 90.6 % (entries 1, 3, 5 in Table 2.2). ^1H NMR analysis of aliquots taken at the end of each reaction showed the ratios of *cis* olefin to *trans* olefin in polymeric species in aliquots (referred to as the *cis/trans* ratios hereinafter) ranged from 1.71 to 2.64. A negative correlation was found between the conversion of COD and *cis/trans* ratio: The higher the conversion of COD, the lower the *cis/trans* ratio. The values of M_w of these polymers were found ranging from 142 to 230 kg/mol, and similarly a negative correlation between the conversion of monomer and M_w was observed.

In the case of target $M_w > 300$ kg/mol (entries 7 and 8 in Table 2.2), a different strategy was employed to break through the limit of M_w (~ 260 kg/mol) reported by the Macosko group.³⁸ A very large excess of monomer (10,000 eq) was used along with a very short reaction time (4-10 min) in the second-stage chain extension reaction in order to favor the formation of ultra-long, end-functionalized chains and minimize the

undesired reduction in molecular weight by intramolecular chain transfer (or “backbiting”, Figure 2.2 (c)).²⁵ The conversions of COD were 45.4% and 63.7% due to intentionally early termination of reaction. The *cis/trans* ratios were found ≥ 3 . With this strategy, we were able to achieve an unprecedented M_w of 430 kg/mol, and shear rheology study of the corresponding carboxyl-terminated polymer after deprotection of carboxyl groups on polymer chain ends in apolar media proved it was sufficiently end-functionalized (refer to Chapter 3). After deprotection of carboxyl groups on polymer chain ends, shear rheology study of the solutions of this polymer in apolar media proved that it was sufficiently end-functionalized (refer to Chapter 3).

2.3.4 Hydrolysis of *tert*-Butyl Ester Groups on Polymer Chain Ends

tert-Butyl esters are known to decompose readily into carboxylic acids in DCM solution of trifluoroacetic acid (TFA) at room temperature with loss of isobutylene.⁴⁵ This fact forms the foundation of Scheme 2.3, according to which the series of *tert*-butyl ester-terminated telechelic 1,4-PBs we prepared were turned into corresponding carboxyl-terminated telechelic polymers. We found by means of ¹H NMR analysis that for 1 g of *tert*-butyl ester-terminated 1,4-PB dissolved in 30 mL of DCM, 1.5 mL of TFA is needed to drive the removal of *tert*-butyl groups to completion, regardless of the value of N and polymer molecular weight. As a representative example, Figure 2.6 shows the ¹H NMR spectra (in CDCl₃) of telechelic 1,4-PB of $M_w = 226$ kg/mol with 1 *tert*-butyl ester group on each chain end (entry 1 in Table 2.1) before and after TFA hydrolysis using the aforementioned conditions. The resonance of *tert*-butyl protons at 1.58 ppm was not observed after hydrolysis, indicating complete deprotection of carboxyl groups on polymer chain ends. It is worth noting that telechelic 1,4-PBs with more than 1

carboxyl group on chain ends were found difficult to dissolve in CDCl_3 ; a small amount of polar acetone- d_6 (6.3 vol% of CDCl_3) was found needed to facilitate the dissolution of these carboxyl-terminated polymers.

All *tert*-butyl ester-terminated telechelic 1,4-PBs synthesized in the present study were found transparent at room temperature. In the case of telechelic 1,4-PBs synthesized from CTAs **8** and **10**, change in appearance was observed after TFA hydrolysis of *tert*-butyl ester groups on polymer chain ends: Their corresponding carboxyl-terminated polymers were observed to appear opaque at room temperature. For those synthesized from CTAs **3** and **5**, their resultant carboxyl-terminated polymers remained transparent. The observed transition took place as the number of carboxyl groups on polymer chain ends, N , increased from 2 to 4, as shown in Figure 2.7.

In order to understand if the polymer backbones stayed intact during TFA hydrolysis of *tert*-butyl ester groups, we performed GPC measurements of all the resultant carboxyl-terminated telechelic 1,4-PBs and found that all polymers showed apparent increases in M_w after TFA hydrolysis (Table 2.3). To investigate whether the observed increases in M_w were permanent, or merely the results of association of carboxyl-terminated dendritic end groups in THF, LAH reduction was performed on the carboxyl-terminated polymer from telechelic 1,4-PB of $M_w = 230 \text{ kg/mol}$ with 4 *tert*-butyl ester groups at each chain end (entry **3** in Table 2.2, referred to as 230K di-**TE** 1,4-PB hereinafter) as a representative example. GPC data (Figure 2.8) indicated that the apparent increase in M_w was the result of association of carboxyl-terminated end groups in THF, not the crosslinking of PB backbone: After LAH reduction of carboxyl groups on

polymer chain ends, the apparent M_w of polymer decreased from 375 kg/mol (PDI = 1.71) to 221 kg/mol (PDI = 1.66).

During the early stage of the present study, we used a small amount (ca. 15 wt% of polymer) of BHT in TFA hydrolysis of polymer end groups for the purpose of protecting polymer backbones from crosslinking by residual dissolved oxygen (in case of incomplete deoxygenation of reaction mixtures). We were surprised by the unexpected results: The combination of BHT and TFA *crosslinked* 1,4-PB backbones. Figure 2.9 shows the GPC results of TFA hydrolysis of telechelic 1,4-PB of $M_w = 143$ kg/mol with 2 *tert*-butyl ester groups at each chain end (referred to as 143K di-**DE** 1,4-PB hereinafter) *with* and *without* the use of BHT. When 15 wt% of BHT was used in combination with TFA (1.0 mL for 1 g of polymer), M_w of the polymer increased from 143 to 329 kg/mol, whereas the use of TFA only (1.5 mL for 1 g of polymer) resulted in a slightly increased $M_w = 183$ kg/mol. Consequently, all of the carboxyl-terminated telechelic polymers used in the present study, regardless of the number of acid groups and the backbone length, were prepared by treating the corresponding *tert*-butyl ester prepolymers with TFA in DCM only.

2.4 Discussion

2.4.1 Aspects of the CTA Design

A family of bis-dendritic CTAs **5**, **8** and **10** were developed for precise control of the strength of end-association of resultant polymers. In addition, aspects such as the ease of incorporation of CTAs into polymers and the feasibility of scale-up synthesis were also taken into consideration when designing the CTAs.

The CTAs employed in ROMP are required to be symmetric, acyclic olefins with terminal functional groups compatible with the catalysts.⁴⁶ Most CTAs reported in the literature are based on *cis*-2-butenediol derivatives for the following reasons: (1) they are commercially available and inexpensive; (2) the modification with desired functional groups is straightforward; (3) the incorporation of CTAs is not an issue when small terminal groups are used.^{5,7,27,47-49} These advantages are the reasons why we used *cis*-1,4-dichloro-2-butene as the core olefin unit to construct the entire family of bis-dendritic CTAs in the present study. We found that even though the spacer between the C=C double bond and the dendrons was a short methylene oxide unit (-CH₂-O-), all four CTAs we prepared were able to be completely incorporated into polymers during the first stage of ROMP of COD (Scheme 2.2). We originally expected that when the bulky CTA **10** was used, we would have observed the presence of unreacted **10** in the end of the first stage of ROMP. To our surprise, complete consumption of **10** was still observed, which suggests that the central olefin unit is sufficiently accessible to Grubbs II. We believe the comparatively easy access to the core olefinic unit of **10** is attributed to the cascade structure of the third-generation poly(benzyl ether) dendron, which leaves the core unhindered (Scheme 2.1).

The influence of steric hindrance from bulky dendrons on the reactivity of the central C=C double bond in ROMP can be reduced by having a long spacer between the C=C double bond and bulky terminal groups, as suggested by Higley and co-workers.⁴⁶ In their study a nonylalkyl spacer was used. In a similar fashion, Sill and Emrick used a succinic ester linkage between the central *cis*-2-butene unit and the third-generation poly(benzyl ether) dendrons.⁴² The problem is, however, that none of these functional

olefins are commercially available. Given that CTA **10**, which was synthesized from an inexpensive reagent *cis*-1,4-dichloro-2-butene, could be completely incorporated into polymers in two-stage ROMP of COD, the gain in reactivity of CTAs in ROMP from using a long spacer seems marginal. The extra cost and effort required to synthesize and purify starting olefins with long spacers render this approach comparatively *less* cost-effective, and inevitably counterbalance the benefit of higher reactivity of CTA provided by the use of long spacers.

In the literature, two distinct synthetic methodologies have been reported for the preparation of dendrimers: (i) The divergent approach, in which construction of dendrimers starts at the core and proceeds radially outward toward the dendrimer periphery, and (ii) the convergent approach, in which peripheral dendrons are built first and then attached to a suitable core to afford a complete dendrimer.⁵⁰ We chose the divergent approach because it is better suited to large-scale synthesis.⁵¹ As shown in Scheme 2.1, the divergent synthesis of the $n+1^{\text{th}}$ ($n = 1,2$) generation dendrimer in our work began with LAH reduction of terminal ester groups of the n^{th} generation. Then, the resultant alcohols were coupled with **2** or **2'** to form the $n+1^{\text{th}}$ generation dendrimer *via* Mitsunobu reaction. Alternatively, halogenation of bis-dendritic alcohols **6** and **9** followed by Williamson etherification with **2** under basic conditions may be used to synthesize CTAs **8** and **10**. The problem is, however, that Williamson etherification is not as a clean chemistry as Mitsunobu reaction. When Williamson etherification is used, oxygen-alkylation of the phenolate anion of **2** with the n^{th} generation dendritic halide affords the $n+1^{\text{th}}$ generation dendrimer, however the same phenolate anion of **2** can also undergo a resonance transformation and then undergo an *ortho*-carbon-alkylation (~1.5%

of oxygen-alkylation) with the n^{th} generation dendritic halide as well,^{52,53} resulting in the formation of polymeric byproducts. Consequently, the issue of over-alkylation compromises the precise structure control of polymer chain ends. On the contrary, Mitsunobu etherification only gives negligible amount of carbon-alkylation when reactive alcohols (such as **6** and **9**) are used.^{52,54} In our parallel study of synthesis of CTA **8** using both routes, by means of GPC analysis we found that Mitsunobu coupling of **6** with **2** afforded a monodisperse dendrimer, whereas Williamson etherification of the chloride of **6** with **2** gave a mixture of **8** and polymeric impurities that could not be removed by reprecipitation (Figure 2.3). Similar success of Mitsunobu reaction was also observed in the synthesis of CTA **10** (Figure 2.3). Therefore, direct etherification of **6** and **9** with **2** *via* Mitsunobu reaction is a better synthetic route for CTAs **8** and **10**.

Among the numerous types of dendrons reported in the literature, poly(benzyl ether) dendrons were chosen in the present study to construct the family of CTAs due to the following reasons: (i) The hyper-branched poly(benzyl ether) skeleton is highly hydrophobic, but still soluble in common organic solvents, which renders the resultant *tert*-butyl ester terminated CTAs soluble in solvents for ROMP of COD; (ii) poly(benzyl ether) dendrons are solid at room temperature even in the case of first generation. This property gives a significant advantage in purification: We found that CTAs prepared in this study could be purified by either recrystallization (CTAs **3** and **5**) or reprecipitation (CTAs **8** and **10**) to achieve reasonable purities without resorting to chromatographic separations, which is crucial for production on a large scale. (iii) The poly(benzyl ether) skeleton does not contain any moiety that interferes self-association of carboxyl groups. Neither the ether linkages nor the phenyl rings are capable of forming hydrogen bonds

with the resultant carboxyl groups on polymer chain ends after deprotection. Therefore, the end-association of polymers in this study is primarily controlled by the number of carboxyl groups on chain ends.

2.4.2 Molecular-Weight Control

In conventional polymerization techniques, such as controlled radical polymerizations (ATRP and RAFT) and anionic polymerization, molecular weight of growing polymer chains increases monotonically over the course of reaction. However, the mechanism of ROMP (see Figure 2.2) involves routes that allow molecular weights of polymer chains to *decrease*. In ROMP, the total number of polymer chains is determined by the number of available chain ends, which can only come from the CTA and the metathesis catalyst. Since the mechanism does not allow creation or elimination of chains, the number of chains remains unchanged if there is no new source of chain ends introduced to the reaction mixture.²⁵ Accordingly, individual chains increase or decrease in molecular weight so as to meet the above inherent constraint. The reaction between the ruthenium benzylidene unit on polymer chain end and the double bond of cyclic olefin (i.e., *primary* metathesis) contributes to the increase in molecular weight, whereas the reaction of formed polymer backbones with chain-end ruthenium benzylidene units, which is referred to as *secondary* metathesis or *cross metathesis*, can cause either increase or decrease in molecular weight, depending on whether it is *inter-* or *intra-*molecular (Figure 2.1). The latter is usually referred to as “backbiting,” and it results in the decrease in molecular weight and *cis*-content of the backbone, as well as the generation of cyclic byproducts.^{25,55} Polynorbornene (Table 2.2) is the only exception of polymer backbones that does not undergo backbiting reaction at any appreciable rate, but

its poor solubility in common organic solvents, as mentioned earlier in Section 2.1, renders it an inappropriate backbone for telechelic associative polymers as fuel additives.⁵⁶ Therefore, the presence of pathways in ROMP allowing growing polymer chains to lose molecular weight renders molecular-weight control of telechelic polymers comparatively complicated, especially when target molecular weight is > 200 kg/mol (which will be discussed later).

Previous studies on syntheses of telechelic polymers *via* ROMP of COD or COE in conjunction with *cis*-acyclic olefin CTAs using Grubbs II were focused only on varying the ratio of monomer to CTA ($[M]:[CTA]$) to achieve desired molecular weights (provided the amount of Grubbs II \ll CTA), and a linear relationship between M_n and $[M]:[CTA]$ has been reported up to a 2000:1 $[M]:[CTA]$ ratio by Ji and coworkers.^{10,38,42,55} However, the influences of other key aspects of ROMP (e.g., backbiting, effective turnover number (TON) of Grubbs II, and catalyst load) on molecular-weight control, were not addressed in these reports. As indicated by Dinger and Mol, ruthenium-based metathesis catalysts can only perform a finite number of metathesis reactions with substrates, *i.e.*, they have finite effective turnover numbers (TONs).⁵⁷ In a separate report, Dinger and Mol also pointed out that impurities such as primary alcohols, water and oxygen can cause Grubbs catalysts to degrade.⁴⁰ Nickel and coworkers further reported that the presence of peroxides in substrates for metathesis reactions has a dramatic effect on TONs of Grubbs catalysts, and removal of peroxides from substrates can lead to a 80-fold increase in effective TONs, allowing metathesis reactions to take place readily with extremely low catalyst load (on molar ppm level).³⁹ As mentioned earlier, the protocol developed by the Macosko group to remove VCH

from COD does not address the issue of peroxides, and it also inevitably introduces *n*-butanol into the monomer (Section 2.2.2). Therefore, we expect that the purity of COD, similar to the [M]:[CTA] ratio, has a crucial role in molecular-weight control in the synthesis of telechelic 1,4-PBs *via* ROMP of COD, since it directly affects the effective TONs of Grubbs II, which subsequently determines the proceeding of both primary and secondary metatheses.

The results of polymer synthesis in Table 2.2 and Appendix A illustrate the effects of the purity of COD on ROMP using Grubbs II. When VCH-free COD purified according to the Macosko protocol was used, we found that the conditions of entry 4 in Table 2.2 led to a conversion of COD of 85%, a M_w of 264 kg/mol (PDI = 1.58), and a *cis/trans* ratio of 2.20 (see Appendix A). It is worth noting that the same conditions gave very similar results to Ji and coworkers' report, despite the fact that a different CTA was used.³⁸ In the case of the rigorously purified, VCH-free COD (see Section 2.2.2), the same conditions resulted in a nearly quantitative conversion of COD (97.6%), a lower M_w of 142 kg/mol, and a lower *cis/trans* ratio of 1.73 (entry 4 in Table 2.2). Similar nearly-quantitative conversions of COD and *cis/trans* ratios <2 were also achieved (entries 2 and 6 in Table 2.2) as rigorously purified COD was vacuum-distilled again immediately prior to use. These results suggest that removal of *n*-butanol and peroxides from VCH-free COD boosts the effective TON of Grubbs II, and consequently a conversion of COD \geq 95% can be achieved. In addition, the results of *cis/trans* ratios and M_w reveal that as the majority of rigorously purified COD (>90%) was consumed, ruthenium benzylidene units on polymer chain ends could still possess sufficient activity to participate metathesis reactions thanks to the boosted effective TON of Grubbs II. Since the abundant species in

this circumstance were formed 1,4-PB backbones, they could undergo metathesis reaction with chain-end ruthenium benzylidene units, leading to the occurrence of backbiting and the subsequent decreases in *cis/trans* ratio and M_w . In other words, a delicate balance among factors that can affect the molecular weight of telechelic 1,4-PBs (e.g., [M]:[CTA], the amount of Grubbs II, reaction time, etc.) is needed for molecular-weight control as rigorously purified COD is used as the monomer. As for the control (i.e., *n*-butanol- and peroxides-containing VCH-free COD), Grubbs II may have lost its metathetical activity as the conversion of COD reached ~85% due to the influences of *n*-butanol and peroxides on the number of metathesis reactions it could perform; consequently, the loss of M_w due to backbiting was not as significant, and the aforementioned linear relationship between M_w and [M]:[CTA] still apparently held.

Although the use of rigorously purified COD seems to complicate the molecular-weight control when a [M]:[CTA] of 2000:1 is used, it provides invaluable access to telechelic 1,4-PBs with M_w useful in mist-control applications (entries 7 and 8 in Table 2.2). The implication of the results from rigorously purified COD at a 2000:1 [M]:[CTA] ratio is that when a very large excess of such monomer is used to suppress secondary metatheses that cause decrease in molecular weight, Grubbs II would be able to continuously react with COD until it reaches its maximum TON, leading the formation of telechelic chains with $M_w \gg 200$ kg/mol. Therefore, we tested a [M]:[CTA] of 10,000:1 using monomers purified according to the Macosko protocol and the protocol of rigorous purification of COD we developed in Section 2.2.2, respectively. We found that the monomer purified according to the Macosko protocol contained sufficient amount of *n*-butanol and peroxides to completely quench the metathetical activity of the ruthenium

benzylidene units on chain ends of macro CTAs (Scheme 2.2), leading no formation of any high-molecular-weight polymer chains. On the contrary, the second-stage addition of 10,000 eq of rigorously purified COD and required amount of deoxygenated DCM (Scheme 2.2) led to a rapid increase in viscosity of the reaction mixture, which is a sign of the rapid formation of telechelic chains with very high molecular weights. Relatively low conversions of COD ($< 65\%$) and high *cis/trans* ratios (≥ 3) were observed in both entries 7 and 8 in Table 2.2, suggesting that the extent of backbiting, which lowers the *cis* content of 1,4-PB backbone, was insignificant due to the presence of large excess of monomer. Fluctuation in reaction rate (in terms of the ratio of conversion of COD to reaction time) was observed between entries 7 and 8, nevertheless the values of M_w were found virtually the same. We believe that the aforementioned fluctuation may come from variation in the level of trace impurities (*e.g.*, oxygen) introduced into the reaction mixture during syringe transfer of monomer, solvent and catalyst solution, and we expect a better consistency when the polymer synthesis is carried out at a larger scale. The success observed in entries 7 and 8 also implies that an even higher M_w might be achieved if a higher $[M]:[CTA]$, say 20,000:1, is used.

Another intriguing property COD concerning molecular-weight control in the synthesis of telechelic 1,4-PBs *via* ROMP of COD is that it needs to be freshly vacuum-distilled immediately prior to use, even after all impurities capable of interfering with ROMP are removed. We found that COD underwent side-reactions which generated wax-like substances on a time scale ~ 1 day even when stored at -30°C , and the byproduct could interfere with ROMP as well. Examples are entries 1, 3, and 5 in Table 2.2, in which rigorously purified COD stored at -30°C for 1 day or longer after vacuum-

distillation was used. Conversion, *cis/trans* ratio and M_w data suggest a lower effective TON of Grubbs II compared to the cases in which freshly vacuum-distilled, rigorously purified COD was used. The composition of the wax-like byproducts and the mechanism accounting for their formation remain unclear, and currently investigation is underway.

2.4.3 Hydrolysis of *tert*-Butyl Ester Terminal Groups of Polymers

Benzoic acid and isophthalic acid are both highly polar chemical moieties, and thus the corresponding bis-dendritic acids of CTAs **3**, **5**, **8**, and **10**, as we found in the present study, are insoluble in reaction media for ROMP of COD. The solubility issue was circumvented by using the protected form of carboxyl group, *tert*-butyl ester, as the terminal group of all CTAs we studied. Post-polymerization hydrolysis of *tert*-butyl ester terminal groups is consequently necessary to recover the carboxyl groups on polymer chain ends. As noted previously, *tert*-butyl esters are known to decompose into the corresponding carboxylic acids and isobutylene gas readily in TFA/DCM mixture at room temperature.⁴⁵ The fact that such a hydrolysis reaction can be performed in DCM, a good solvent for 1,4-PBs, motivated us to adopt the TFA/DCM protocol (Scheme 2.3). Other acids, such as *p*-toluenesulfonic acid (PTSA) and 85wt% aqueous solution of phosphoric acid (H_3PO_4), have also been reported successful in deprotection of *tert*-butyl esters in organic solvents.⁵⁸ Compared to these acids, TFA is preferable due to its ease to remove thanks to its low boiling point (72.4°C) and the fact that it is strong enough ($pK_a = 0.3$ in water), but not as oxidative as mineral acids (e.g., H_2SO_4). It is worth noting that all reaction mixtures stayed homogeneous throughout the entire course of hydrolysis reaction. We believe such homogeneity contributes to the efficacy of the TFA/DCM protocol.

Alternatively, mixing *tert*-butyl ester-terminated compounds with ground KOH in THF at ambient temperatures, following by acidification has been reported as a safe and simple approach for cleavage of *tert*-butyl esters.⁵⁹ We tested this protocol for its compatibility with 1,4-PB backbones and its simplicity, and found it successful in the case of short *tert*-butyl ester-terminated telechelic 1,4-PBs ($M_w \sim 20$ kg/mol, refer to Chapter 4). However, incomplete removal of *tert*-butyl groups was observed when the size of 1,4-PB backbone increased to ~ 230 kg/mol (Appendix A) even with the use of a very large excess of KOH (ca. 400 eq based on *tert*-butyl ester groups). The extent of hydrolysis reaction may be limited by the mass transfer of *tert*-butyl ester-terminated chain ends to the surface of ground KOH thanks to the heterogeneous nature of this protocol. We also found that the hydrolysis reaction mixtures turned into gels within 1 h due to the aggregation of resultant potassium carboxylate salt on chain ends. We believe this further hindered unreacted *tert*-butyl ester groups from reaching the surface of ground KOH and eventually stopped the reaction from going to completion. These disadvantages render the KOH/THF protocol a *less* effective way to hydrolyze *tert*-butyl ester groups on polymer chain ends.

The appearance of carboxyl-terminated 1,4-PBs with $M_w \sim 230$ kg/mol (Figure 2.7) illustrated the effect of the number of carboxyl groups on polymer chain ends (N). The transition shown in Figure 2.7 suggests that it needs at least four carboxyl groups on chain ends of 1,4-PBs to achieve macro-phase separation between hydrophilic carboxyl-terminated chain ends and the hydrophobic 1,4-PB backbone. Similar trends were observed in GPC data of carboxyl-terminated telechelic 1,4-PBs in THF (Figure 2.8 and Table 2.3): In the cases of $N = 4$ and 8, telechelic 1,4-PBs with $M_w \sim 200$ kg/mol showed

significant apparent increases in apparent M_w (63.0% for $N = 4$ and 46.9% for $N = 8$, respectively) after carboxyl groups on polymer chain ends were deprotected, whereas $N = 1$ and $N = 2$ only led to increases in M_w by 22.1% and 30%, respectively. The occurrence of end-association is attributed to the fact that THF is a borderline polar aprotic solvent: its ability to solvate the carboxyl groups is not strong enough to completely turn off the pair-wise self-association of carboxyl groups. We also found that the increase in apparent M_w due to association of tetra-carboxyl-terminated chain ends in THF became *less* significant ($\sim 18.6\%$) as the M_w of 1,4-PB backbone increased to 430 kg/mol. It may be attributed to a diluted content of the highly polar, tetra-carboxyl polymer end groups due to a longer backbone. It is also worth noting that the GPC-LS data of carboxyl-terminated telechelic 1,4-PBs in THF may lead to a false conclusion that the TFA hydrolysis protocol shown in Scheme 2.3 results in the crosslinking of 1,4-PB backbones. As noted earlier, LAH reduction of carboxyl end groups clarified that such a hydrolysis protocol did not result in any noticeable extent of backbone crosslinking.

All TFA hydrolysis reactions in the present study were performed under oxygen-free conditions in order to prevent oxygen-induced crosslinking of 1,4-PB backbones. An anomaly was observed as we added antioxidant BHT (15-150 wt% of polymer) to the hydrolysis reaction mixtures to scavenge radicals induced by residual dissolved oxygen in case of incomplete deoxygenation of reaction mixtures. To our surprise, we found that the use of BHT in the presence of TFA induced crosslinking of 1,4-PB backbone (Figure 2.8), and the extent of crosslinking was positively correlated to the amounts of BHT and TFA. In the most extreme case, the hydrolysis reaction mixture irreversibly turned into a gel when large quantities of BHT and TFA were used. The mechanism accounting for

this counter-intuitive phenomenon remains unclear to us, and it is beyond the scope of this study.

2.5 Conclusions

In summary, we successfully devised a modular approach to synthesize telechelic 1,4-PBs with unprecedentedly high molecular weights (M_w up to 430 kg/mol) and to achieve precise control of the number of associative carboxyl groups on polymer chain ends. We found that the combination of ROMP chemistry and the use of *tert*-butyl ester-terminated bis-dendritic CTAs (Scheme 2.1) allowed end-functionalization of telechelic 1,4-PBs with discrete number of *tert*-butyl ester groups (1, 2, 4 and 8). The well-defined end-group structures, in conjunction with post-polymerization removal of the *tert*-butyl groups, present a novel way to achieve carboxyl-terminated telechelic 1,4-PBs, of which the end-association strength in apolar media can be tuned by means of varying the number of carboxyl groups on polymer chain ends, N . The present study also reveals the crucial role of the purity of COD in the pursuit of telechelic 1,4-PBs with M_w within the range useful in mist-control applications. In the next chapter, we will investigate the relationship between the end-association of carboxyl-terminated telechelic 1,4-PBs in apolar media and the key parameters in the design of mist-control polymers, , such as M_w and N , *via* steady-flow shear viscometry.

2.6 Figures, Schemes, and Tables

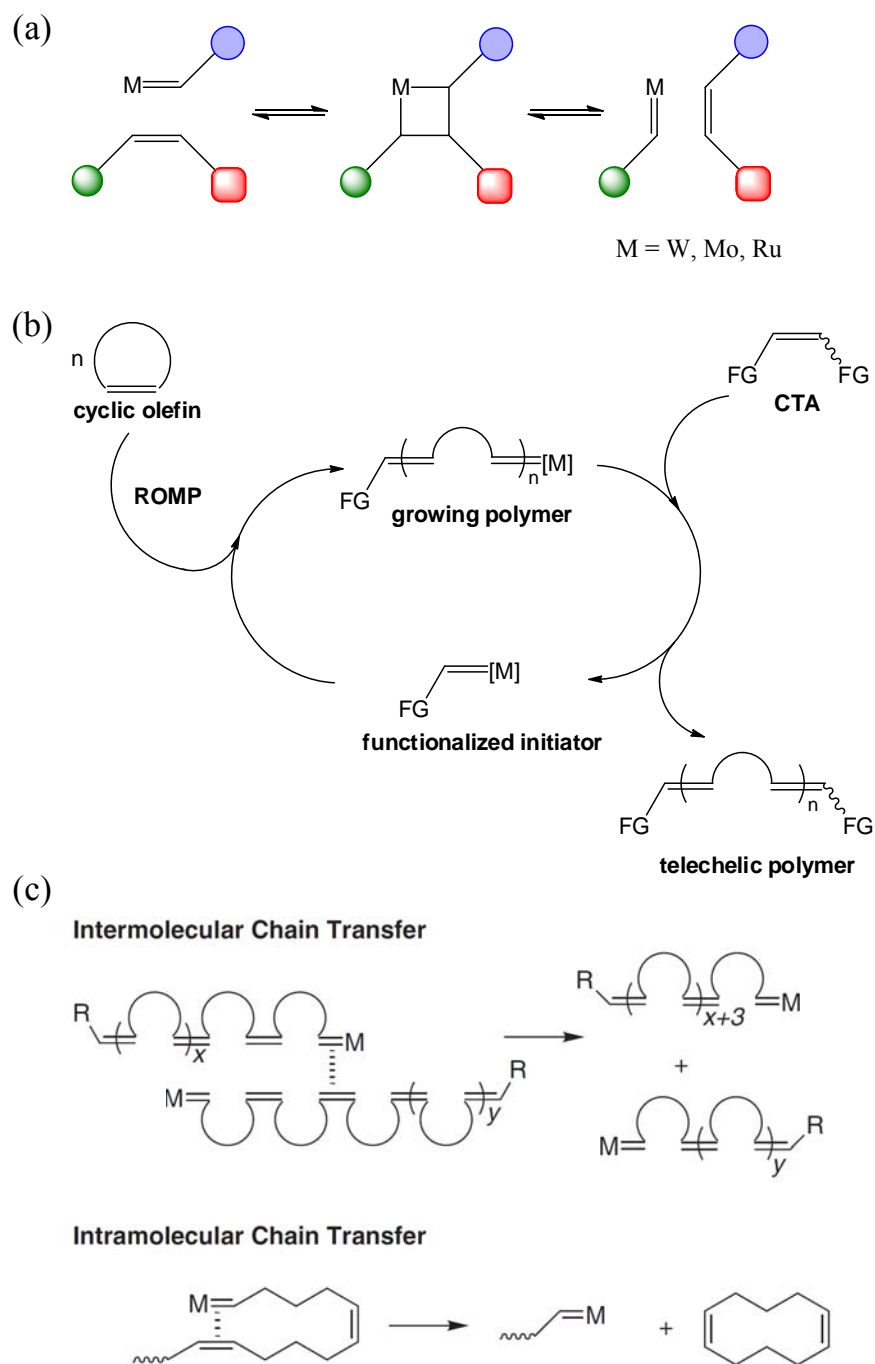


Figure 2.1 Schematics of ring-opening metathesis polymerization. (a) Illustration of metathesis process. (b) Primary metathesis processes in ROMP. (c) Secondary metathesis processes: Inter- and intra-molecular chain transfers (reproduced from Ref.55 with permission).

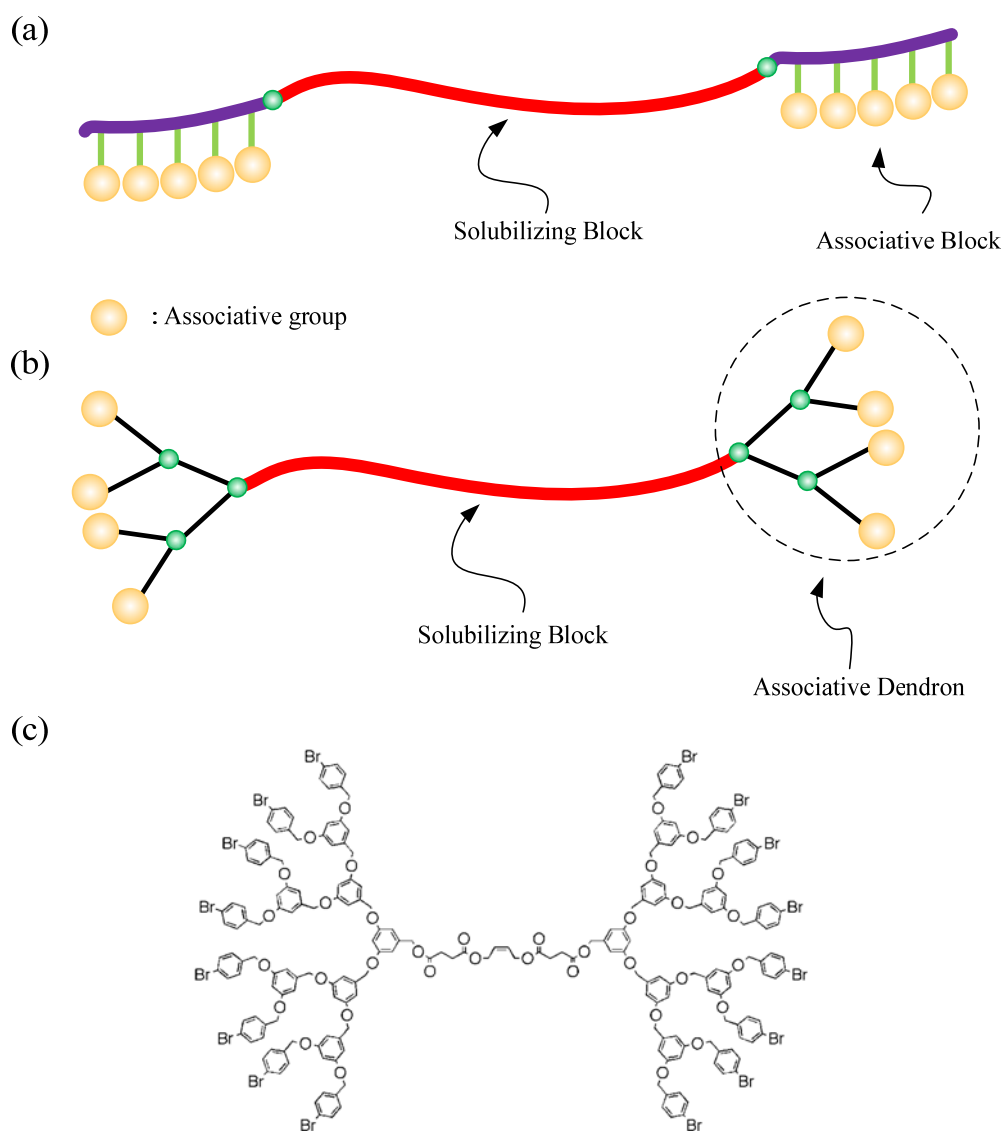


Figure 2.2 Possible configurations to cluster associative groups at polymer chain ends. (a) Linear block of associative groups. (b) Dendron terminated with associative groups. (c) Representative example of bis-dendritic CTA for ROMP (reproduced from Ref. 42 with permission).

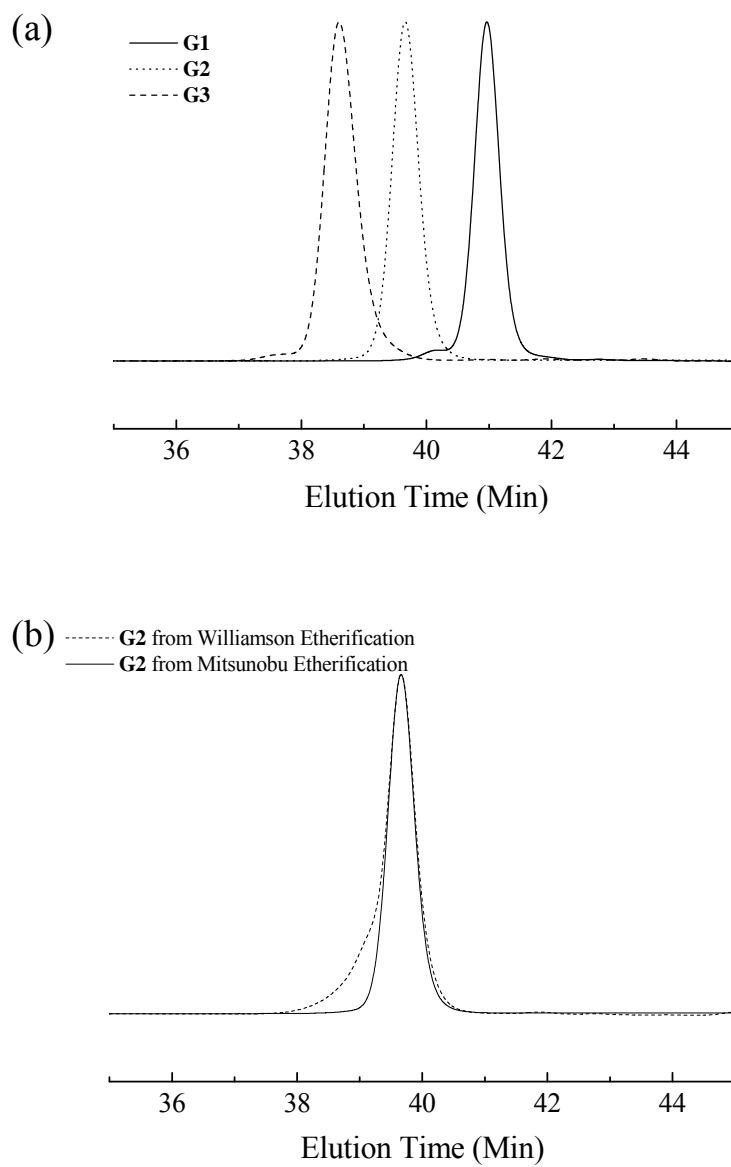


Figure 2.3 GPC traces of bis-dendritic CTAs. (a) **G1-G3** CTAs. (b) **G2** prepared *via* Williamson and Mitsunobu etherifications.

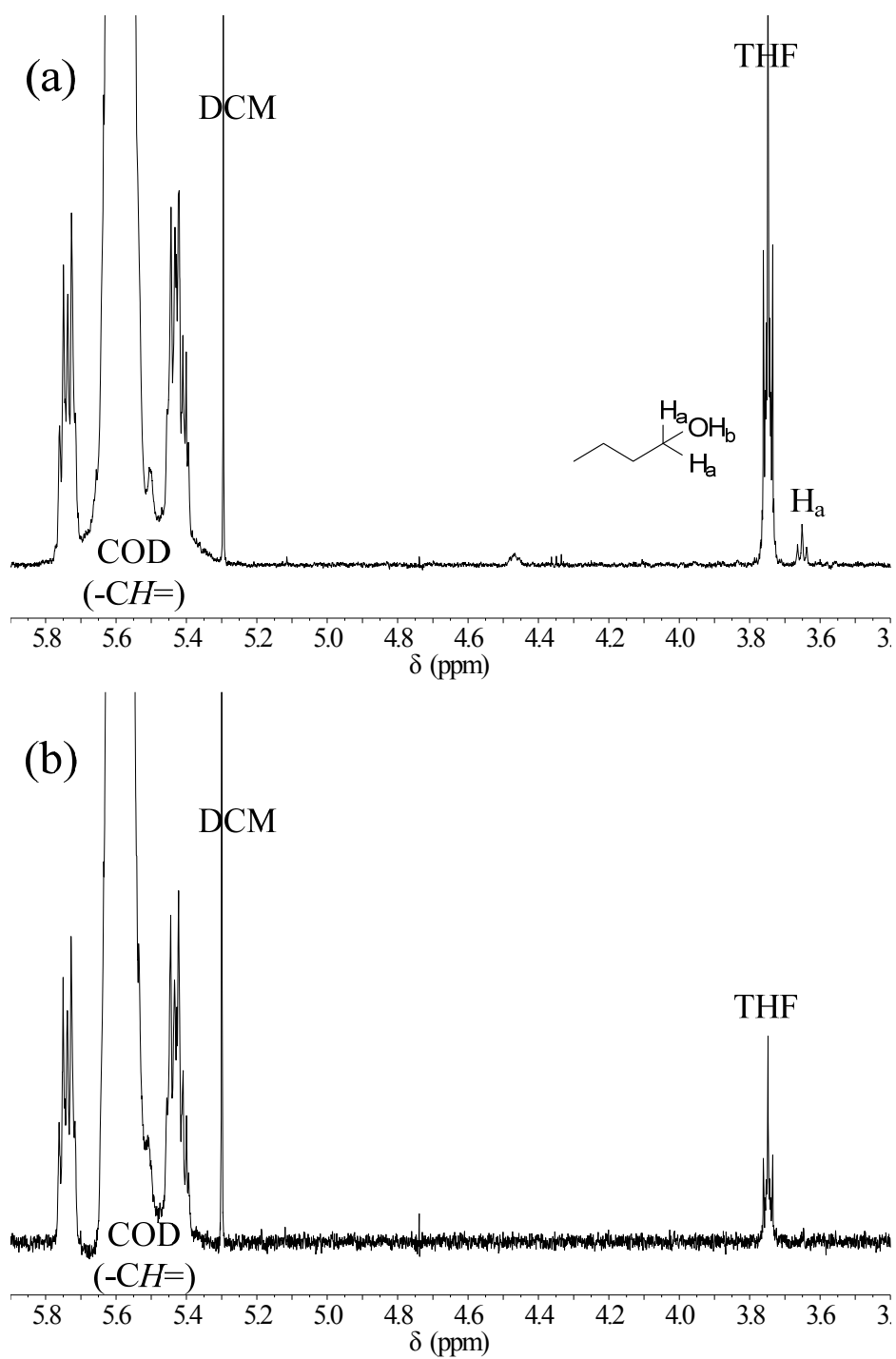


Figure 2.4 ^1H NMR spectra of (a) COD after $\text{BH}_3\cdot\text{THF}$ treatment and vacuum distillation (b) COD further purified with Magnesol $^{\text{®}}$ / CaH_2 treatments.

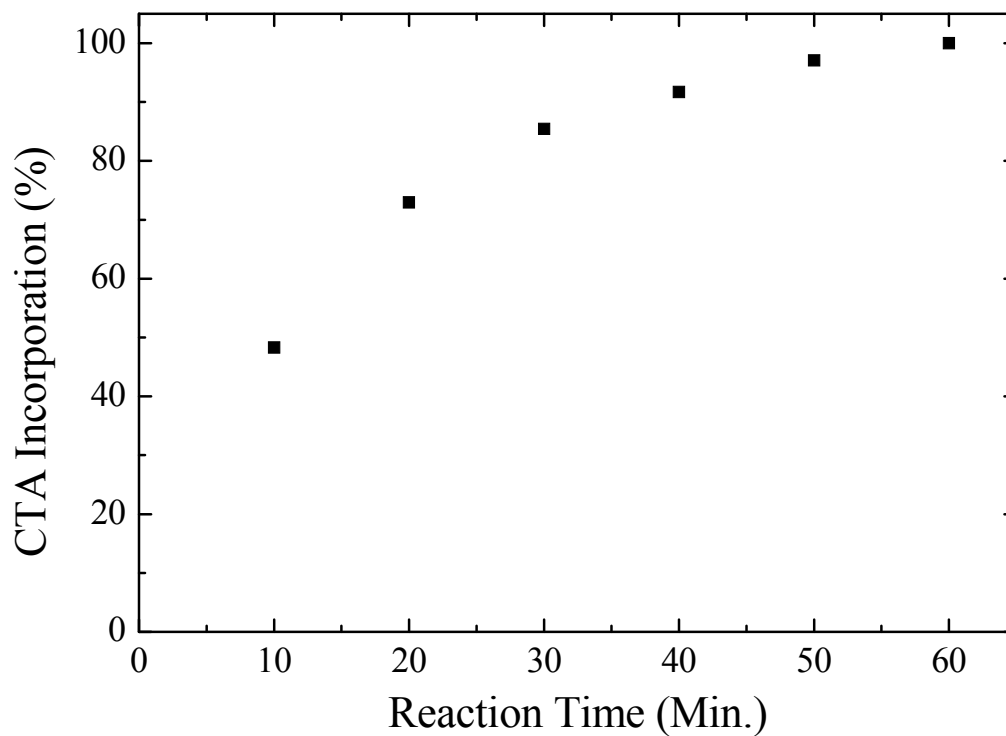


Figure 2.5 Incorporation of **G2** CTA into polymer as a function of reaction time during the first stage of two-stage ROMP of COD. Note that **G2** CTA is selected as a representative example to demonstrate the ease of incorporation of **G0-G3** bis-dendritic CTAs in ROMP.

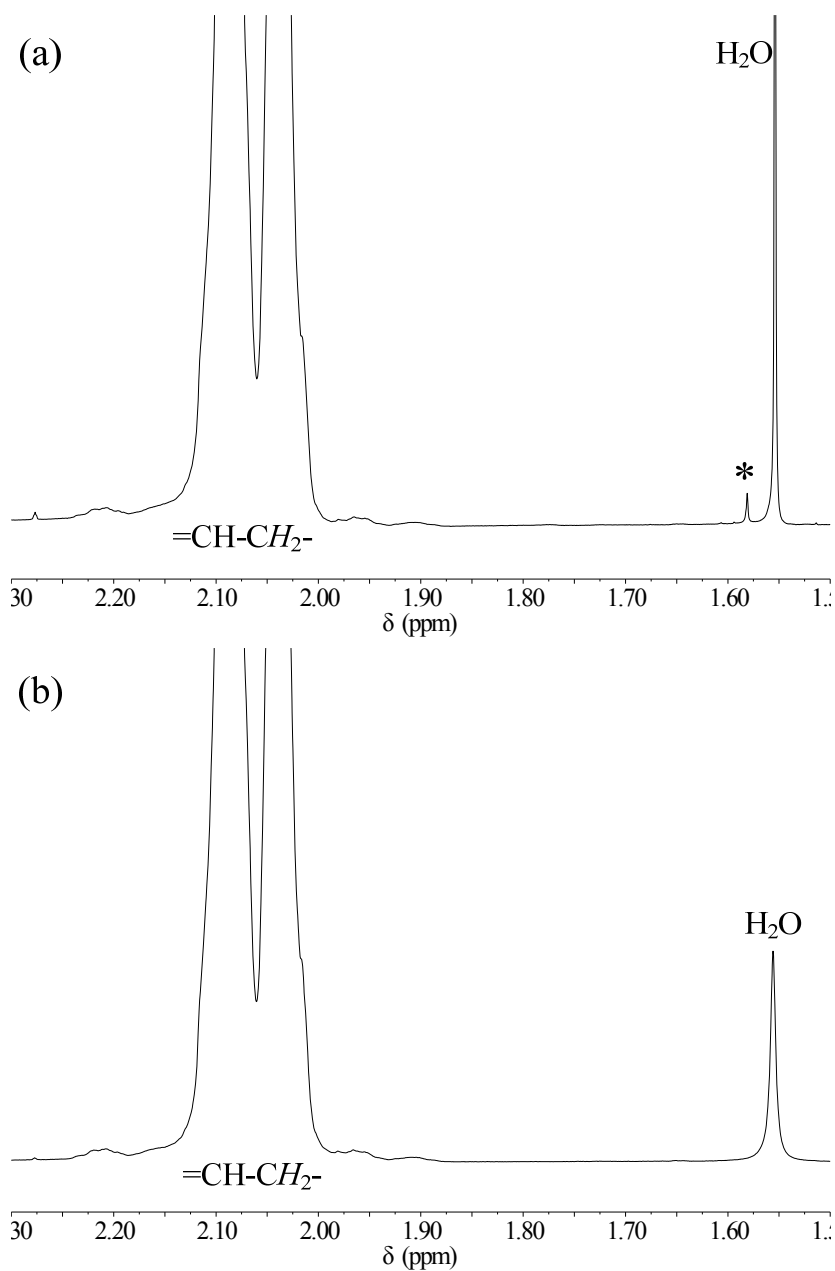


Figure 2.6 ^1H NMR spectra of telechelic 1,4-PB of $M_w = 226$ kg/mol with 1 *tert*-butyl ester group at each chain end before and after TFA hydrolysis of *tert*-butyl ester groups. (a) Before TFA hydrolysis (* = *tert*-butyl protons). (b) After TFA hydrolysis.

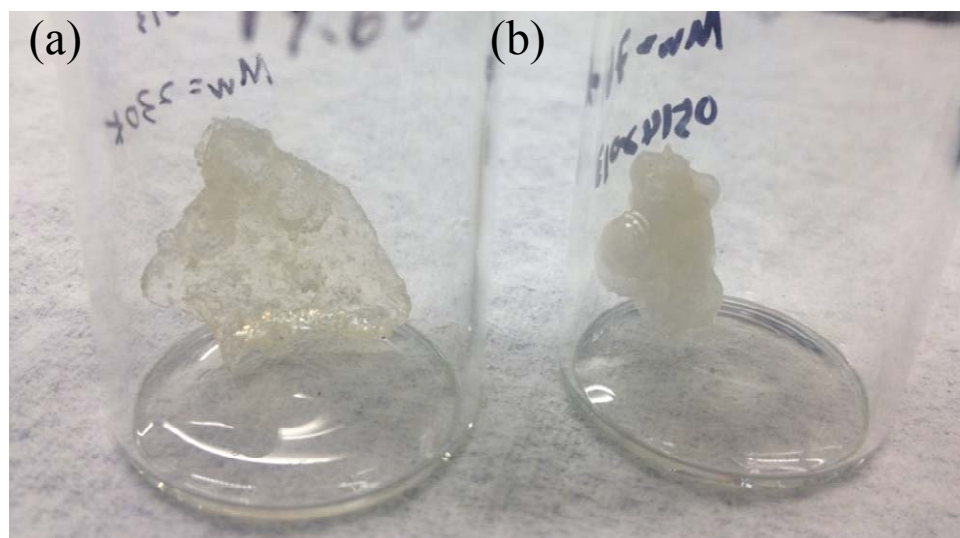


Figure 2.7 Effect of the number of carboxyl groups on chain ends (N) on the appearance of telechelic 1,4-PBs of $M_w = 230$ kg/mol. (a) $N = 2$. (b) $N = 4$.

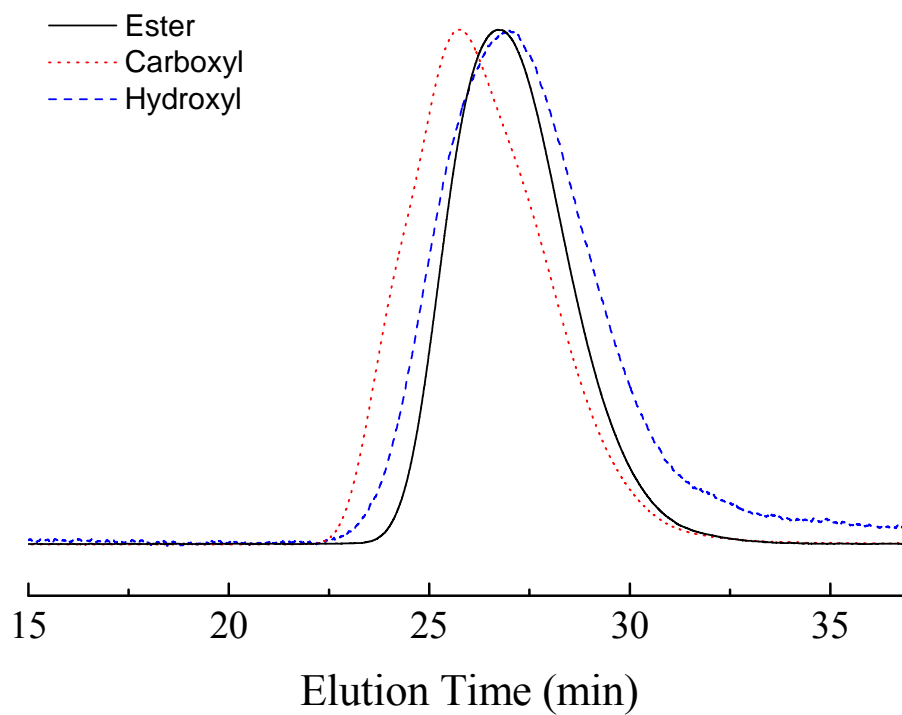


Figure 2.8 GPC-LS traces of 230K di-TE 1,4-PB and the corresponding polymers after TFA hydrolysis (carboxyl-terminated) and further LAH reduction (hydroxyl-terminated).

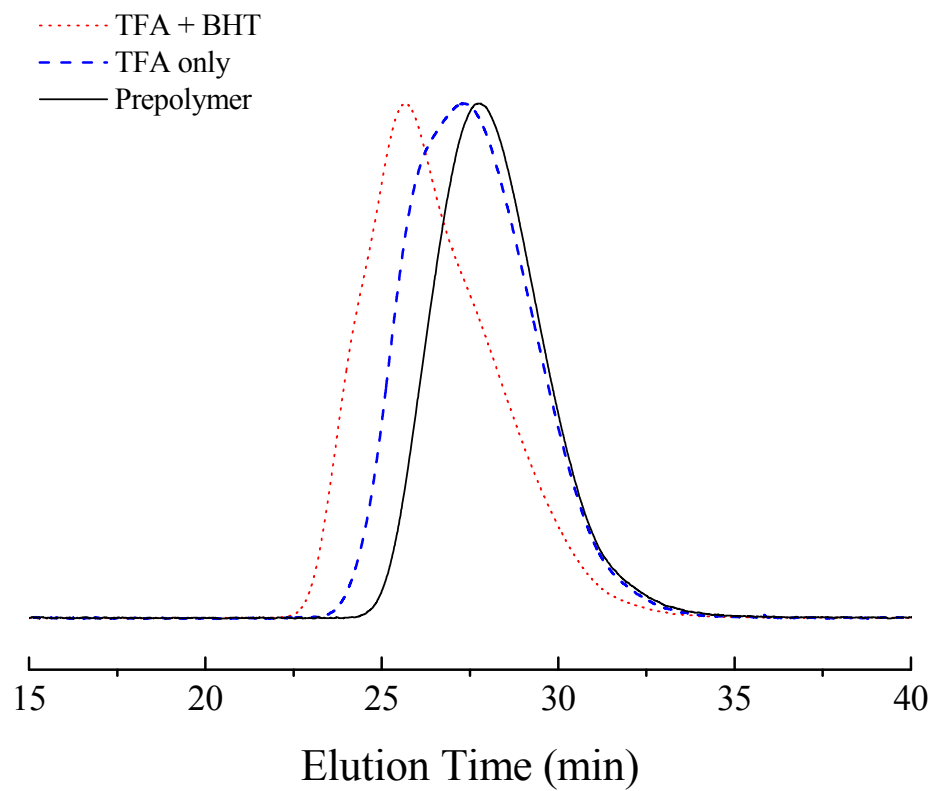
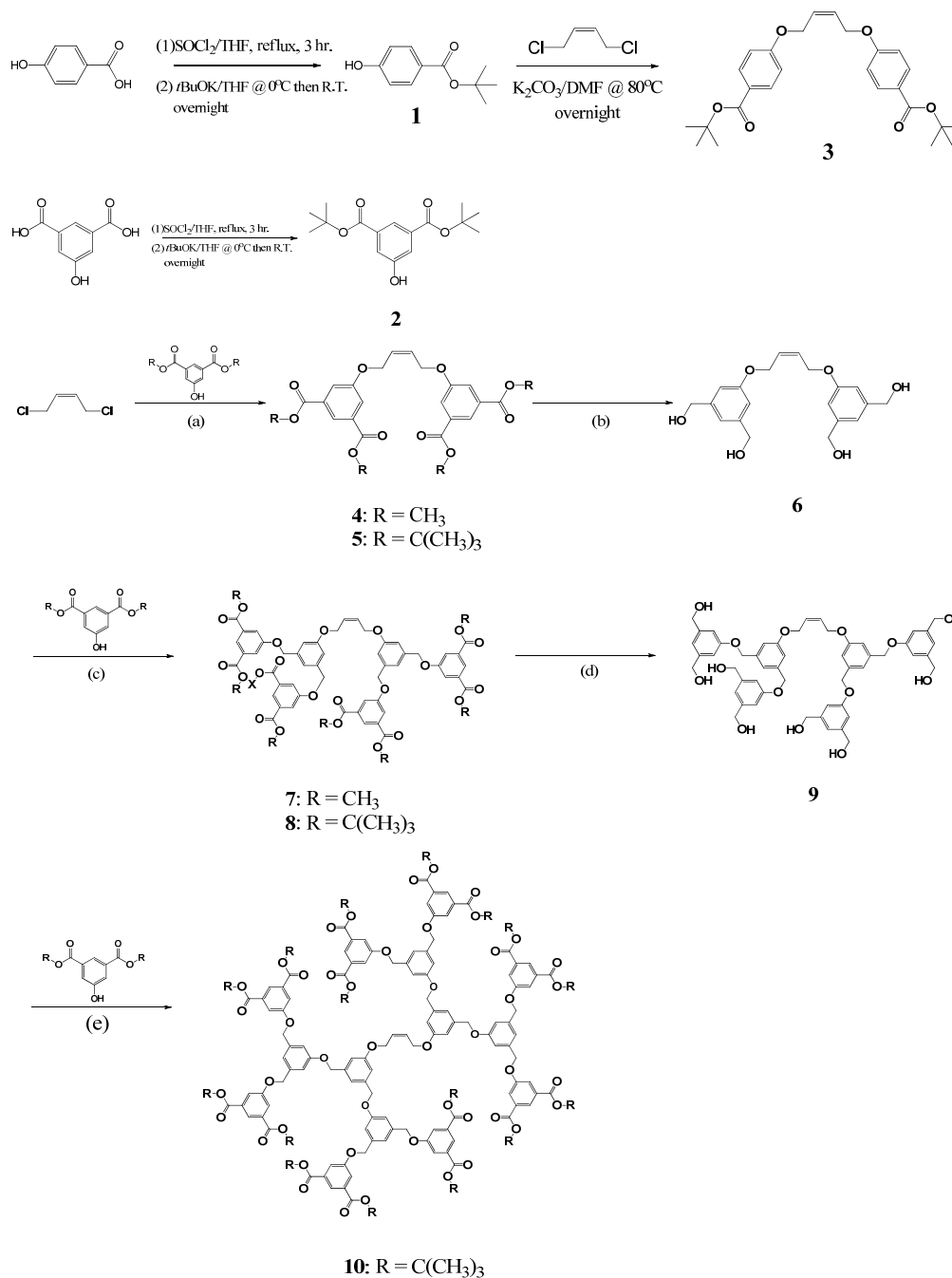


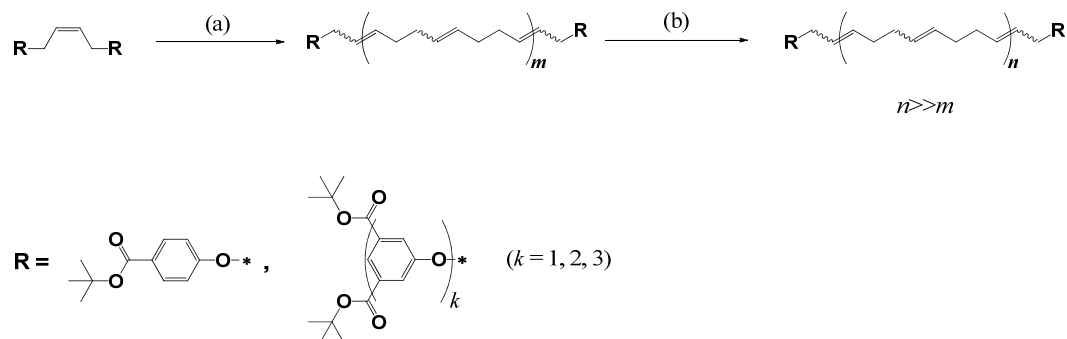
Figure 2.9 GPC-LS traces of 143K di-DE 1,4-PB and the corresponding polymers after TFA hydrolysis with and without the addition of BHT.

Scheme 2.1^a Synthesis of Bis-Dendritic, *tert*-Butyl Ester-Terminated Chain Transfer Agents



^aKey: (a) 2.2 eq. of **2** or **2'**, K_2CO_3 , *N,N*-dimethylformamide (DMF), 80°C , 5h; (b) 4 eq of LiAlH_4 , THF, R.T., overnight; (c) 6 eq of **2** or **2'**, 6 eq of PPh_3 , 6 eq of DIAD, THF, 0°C then 40°C , overnight; (d) 8 eq of LiAlH_4 , THF, R.T., overnight; (e) 12 eq of **3**, 12 eq. of PPh_3 , 12 eq. of DIAD, THF, 0°C then 40°C , overnight.

Scheme 2.2^a Two-stage Synthesis of *tert*-Butyl Ester-Terminated Telechelic 1,4-PBs



Key: (a) 50-100 eq of COD, 1/30 eq of Grubbs II, anhydrous dichloromethane (DCM), 40°C, 30-60 min. (b) 1000-2000 eq of COD for target $M_w < 300$ kg/mol, anhydrous DCM, 40°C, 16 h; 10,000 eq of COD for target $M_w > 400$ kg/mol, anhydrous DCM, 40°C, 4-10 min.

Scheme 2.3 TFA Hydrolysis of *tert*-butyl Ester Polymer End Groups

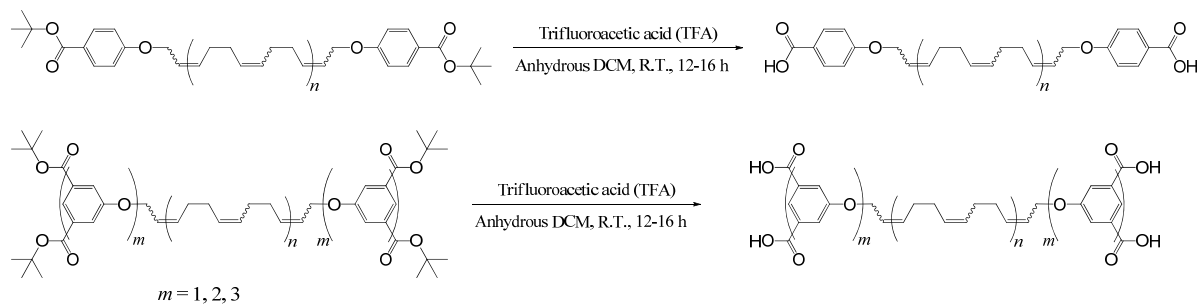


Table 2.1 Representative Example of Commercially Available Cyclic Olefins as ROMP Monomers³¹

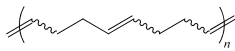
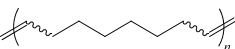
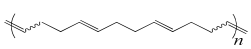
Monomer	Structure	Resulting polymer	Ring strain(kcal/mol)
norbornene			27.2
<i>cis,cis</i> -1,5-cyclooctadiene (COD)			13.3
<i>cis</i> -cyclooctene (COE)			7.4
<i>cis,trans,trans</i> -1,5,9-cyclododecatriene (CDT)			5.0

Table 2.2 Conditions and Results of Two-stage Synthesis of Telechelic 1,4-Polybutadienes (PBs) Using Bis-Dendritic CTAs

Entry	CTA	Monomer: CTA ratio	Catalyst Load (mol%) ^a	Chain Extensioin Time ^b	COD Conv(%) ^c	CTA Conv(%) ^d	<i>cis/trans</i> Ratio ^e	M _w ^f (kg/mol)	PDI
1	3	2000:1	3.3	16 h	90.7	100	2.20	226	1.43
2 [*]	5	2000:1	3.3	16 h	94.8	100	1.88	176	1.47
3	5	2000:1	3.3	2 h	76.9	100	2.64	230	1.53
4 [*]	8	2000:1	3.3	16 h	97.6	100	1.73	142	1.43
5	8	2000:1	3.3	16 h	84.2	100	2.35	231	1.43
6 [*]	10	2000:1	3.3	16 h	97.3	100	1.71	208	1.43
7 [*]	8	10000:1	6.6	10 min	45.4	100	3.19	430	1.49
8 [*]	8	10000:1	6.6	3.7 min	63.7	100	3.01	430	1.49

^a Based on CTA. ^b Reaction time of the second stage. ^c Measured by ¹H NMR spectroscopy. ^d measured by ¹H NMR spectroscopy. ^e by relative integration of the *cis*-allylic methylene peak to that of the *trans* methylene peak. ^{*} Carried out with freshly vacuum-distilled COD.

Table 2.3 Molecular Weight and PDI Data of *tert*-Butyl Ester- and Carboxyl-Terminated Telechelic 1,4-PBs

		N = 1	N = 2	N = 4	N = 8	N = 4
Before TFA Hydrolysis	M_w^a (kg/mol)	226	230	230	207	430
	PDI ^b	1.43	1.53	1.50	1.43	1.49
After TFA Hydrolysis	M_w (kg/mol)	276	299	375	304	510
	PDI	1.56	1.73	1.72	1.51	1.61
Increase in M_w (%)		22.12	30.00	63.04	46.86	18.60

^{a,b}: determined by GPC-LS

References

- (1) David, R. L. A. Dissertation (Ph.D.), California Institute of Technology, 2008.
- (2) Jerome, R.; Henriouille-Granville, M.; Boutevin, B.; Robin, J. J. *Progress in Polymer Science* **1991**, *16*, 837.
- (3) Chassenieux, C.; Tassin, J. F.; Gohy, J. F.; Jerome, R. *Macromolecules* **2000**, *33*, 1796.
- (4) Scherman, O. A.; Rutenberg, I. M.; Grubbs, R. H. *J Am Chem Soc* **2003**, *125*, 8515.
- (5) Bielawski, C. W.; Scherman, O. A.; Grubbs, R. H. *Polymer* **2001**, *42*, 4939.
- (6) Morita, T.; Maughon, B. R.; Bielawski, C. W.; Grubbs, R. H. *Macromolecules* **2000**, *33*, 6621.
- (7) Maughon, B. R.; Morita, T.; Bielawski, C. W.; Grubbs, R. H. *Macromolecules* **2000**, *33*, 1929.
- (8) Bielawski, C. W.; Morita, T.; Grubbs, R. H. *Macromolecules* **2000**, *33*, 678.
- (9) Bielawski, C. W.; Grubbs, R. H. *Angewandte Chemie-International Edition* **2000**, *39*, 2903.
- (10) Hillmyer, M. A.; Nguyen, S. T.; Grubbs, R. H. *Macromolecules* **1997**, *30*, 718.
- (11) Uraneck, C. A.; Hsieh, H. L.; Buck, O. G. *J Polym Sci* **1960**, *46*, 535.
- (12) Lo Verso, F.; Likos, C. N. *Polymer* **2008**, *49*, 1425.
- (13) Chassenieux, C.; Nicolai, T.; Benyahia, L. *Curr Opin Colloid In* **2011**, *16*, 18.
- (14) Uneyama, T.; Suzuki, S.; Watanabe, H. *Physical Review E* **2012**, *86*.
- (15) Suzuki, S.; Uneyama, T.; Inoue, T.; Watanabe, H. *Macromolecules* **2012**, *45*, 888.
- (16) Meng, X. X.; Russel, W. B. *Journal of Rheology* **2006**, *50*, 189.
- (17) Meng, X. X.; Russel, W. B. *Journal of Rheology* **2006**, *50*, 169.
- (18) Pellens, L.; Corrales, R. G.; Mewis, J. *Journal of Rheology* **2004**, *48*, 379.
- (19) Tripathi, A.; Tam, K. C.; McKinley, G. H. *Macromolecules* **2006**, *39*, 1981.
- (20) Koga, T.; Tanaka, F. *Macromolecules* **2010**, *43*, 3052.
- (21) Chassenieux, C.; Nicolai, T.; Tassin, J. F.; Durand, D.; Gohy, J. F.; Jerome, R. *Macromolecular Rapid Communications* **2001**, *22*, 1216.
- (22) Rahman, S. A.; Nemoto, N. *J Soc Rheol Jpn* **2003**, *31*, 219.

- (23) Tasdelen, M.; Kahveci, M.; Yagci, Y. *Progress in Polymer Science* **2011**, *36*, 455.
- (24) Grubbs, R. H. *Angewandte Chemie-International Edition* **2006**, *45*, 3760.
- (25) Sutthasupa, S.; Shiotsuki, M.; Sanda, F. *Polymer Journal* **2010**, *42*, 905.
- (26) Vougioukalakis, G. C.; Grubbs, R. H. *Chemical Reviews* **2010**, *110*, 1746.
- (27) Mahanthappa, M. K.; Bates, F. S.; Hillmyer, M. A. *Macromolecules* **2005**, *38*, 7890.
- (28) Switek, K. A.; Chang, K.; Bates, F. S.; Hillmyer, M. A. *J Polym Sci Pol Chem* **2007**, *45*, 361.
- (29) Hilf, S.; Grubbs, R. H.; Kilbinger, A. F. M. *Macromolecules* **2008**, *41*, 6006.
- (30) Xia, Y.; Kornfield, J. A.; Grubbs, R. H. *Macromolecules* **2009**, *42*, 3761.
- (31) Lerum, M. F. Z.; Chen, W. *Langmuir* **2011**, *27*, 5403.
- (32) Slugovc, C. *Macromolecular Rapid Communications* **2004**, *25*, 1283.
- (33) Ivin, K. J.; Mol, J. C. *Olefin metathesis and metathesis polymerization*; Academic Press: San Diego, 1997.
- (34) David, R. L. A.; Wei, M. H.; Liu, D.; Bathel, B. F.; Plog, J. P.; Ratner, A.; Kornfield, J. A. *Macromolecules* **2009**, *42*, 1380.
- (35) Frenzel, U. *Journal of polymer science. Part A, Polymer chemistry* **2002**, *40*, 2895.
- (36) Nubel, P. O.; Yokelson, H. B.; Lutman, C. A.; Bouslog, W. G.; Behrends, R. T.; Runge, K. D.; Elsevier Science Bv: 1997, p 43.
- (37) Bielawski, C. W.; Benitez, D.; Grubbs, R. H. *J Am Chem Soc* **2003**, *125*, 8424.
- (38) Ji, S. X.; Hoye, T. R.; Macosko, C. W. *Macromolecules* **2004**, *37*, 5485.
- (39) Nickel, A.; Ung, T.; Mkrtumyan, G.; Uy, J.; Lee, C. W.; Stoianova, D.; Papazian, J.; Wei, W. H.; Mallari, A.; Schrodi, Y.; Pederson, R. L. *Top Catal* **2012**, *55*, 518.
- (40) Dinger, M. B.; Mol, J. C. *Organometallics* **2003**, *22*, 1089.
- (41) Davis, M. M. *Acid-base Behavior in Aprotic Organic Solvents*; National Bureau of Standards, 1968.
- (42) Sill, K. *Journal of polymer science. Part A, Polymer chemistry* **2005**, *43*, 5429.
- (43) Mateo-Alonso, A.; Prato, M. *Eur J Org Chem* **2010**, 1324.
- (44) Li, F. B.; Shelly, K.; Kane, R. R.; Knobler, C. B.; Hawthorne, M. F. *Angew Chem Int Edit* **1996**, *35*, 2646.
- (45) Kocienski, P. J. *Protecting groups*; 3rd ed.; Thieme: Stuttgart ; New York, 2004.

- (46) Higley, M. N.; Pollino, J. M.; Hollebeak, E.; Weck, M. *Chemistry-a European Journal* **2005**, *11*, 2946.
- (47) Thomas, R.; Grubbs, R. *Macromolecules* **2010**, *43*, 3705.
- (48) Pitet, L. M.; Chamberlain, B. M.; Hauser, A. W.; Hillmyer, M. A. *Macromolecules* **2010**, *43*, 8018.
- (49) Pitet, L.; Amendt, M.; Hillmyer, M. *J Am Chem Soc* **2010**, *132*, 8230.
- (50) Matthews, O. A.; Shipway, A. N.; Stoddart, J. F. *Progress in Polymer Science* **1998**, *23*, 1.
- (51) Frechet, J. M. J. *P Natl Acad Sci USA* **2002**, *99*, 4782.
- (52) Elmer, S. L.; Zimmerman, S. C. *J Org Chem* **2004**, *69*, 7363.
- (53) Smith, M.; March, J. *March's advanced organic chemistry : reactions, mechanisms, and structure*; 5th ed.; John Wiley: New York, 2001.
- (54) Swamy, K. C. K.; Balaraman, E. *Chemical Reviews* **2009**, *109*, 2551.
- (55) Bielawski, C. W.; Grubbs, R. H. *Progress in Polymer Science* **2007**, *32*, 1.
- (56) Grubbs, R. H. *Tetrahedron* **2004**, *60*, 7117.
- (57) Dinger, M. B.; Mol, J. C. *Advanced Synthesis & Catalysis* **2002**, *344*, 671.
- (58) Li, B.; Berliner, M.; Buzon, R.; Chiu, C. K. F.; Colgan, S. T.; Kaneko, T.; Keene, N.; Kissel, W.; Le, T.; Leeman, K. R.; Marquez, B.; Morris, R.; Newell, L.; Wunderwald, S.; Witt, M.; Weaver, J.; Zhang, Z. J.; Zhang, Z. L. *J Org Chem* **2006**, *71*, 9045.
- (59) Filali, E.; Lloyd-Jones, G. C.; Sale, D. A. *Synlett* **2009**, 205.

Chapter III End-Associative Polymers in Apolar Aprotic Solvents

3.1 Introduction

Telechelic polymers with *self-associative* end groups form supramolecular aggregates *via* non-covalent association of end groups (Chapter 2) that make them excellent “rheology modifiers,” which are widely used in aqueous and to a lesser extent in apolar systems. In aqueous systems, water-soluble backbones (e.g., PEO) are functionalized with hydrophobic chain ends (alkyl or fluoroalkyl groups), whereas in apolar systems, hydrophobic (e.g., polystyrene) backbones are end-functionalized with polar or even ionic groups. Telechelic polymers with self-associative end groups tend to form “flower-like” micelles in dilute solution due to the aggregation of polymer chain ends, and with increasing concentration these flower-like micelles become increasingly interconnected by bridging polymer chains, forming a transient network (Figure 3.1).¹⁻¹⁰ The concentration-dependent topology of these supramolecules, combined with the dynamic nature of end-association confer rich features to the rheological properties of these solutions. For example, in steady flow, their shear viscosity depends nonlinearly on concentration, only reaches a Newtonian plateau at extremely low shear rates, and exhibits strong shear thinning at high shear rates.^{3,11,12} Although the rheological behavior of telechelic associative polymers in apolar systems has been documented, the polymer backbone sizes in the literature are well below 100 kg/mol. To the best of our knowledge, there are no reports on the solution behavior of hydrocarbon-soluble telechelic associative polymers in the molecular-weight regime (i.e., $M_w \gg 100$ kg/mol) of interest for mist-control applications.

Using the methods presented in Chapter 2 to synthesize telechelic 1,4-PBs with M_w up to 430 kg/mol capped at each end with well-defined *tert*-butyl ester-terminated dendrons (Scheme 2.2) provides facile access to *matched pairs* of non-associative and associative telechelic 1,4-PBs (Scheme 2.3). In this chapter we use these model polymers to study the relationship between molecular properties (e.g., polymer molecular weight and the number of carboxyl groups on chain ends) and association behavior, particularly its effects on the rheological properties in solution. The present study of the self-association behavior of carboxyl-terminated telechelic 1,4-PBs provides a foundation for comparative studies of complementary association illustrated in Figure 1.9 and considered further in Chapter 4.

3.2 Experimental

3.2.1 Materials

Solvents 1-chlorododecane (CDD) and tetralin (TL) were both obtained from Aldrich in 97% and 99% purity, respectively. All *tert*-butyl ester-terminated telechelic 1,4-PBs and their corresponding carboxyl-terminated telechelic 1,4-PBs were prepared as described in Chapter 2 and Appendix A. Four values of the number of functional groups on polymer chain ends, N , and three polymer backbone lengths (in terms of M_w by GPC-LS) were selected for the present study: A series of polymers with approximately matched backbone length (nominally 220kg/mol) were prepared with $N = 1, 2, 4$ and 8 ; and a series of polymers with $N=4$ was prepared with three backbone lengths of 76, 230, and 430 kg/mol. (Table 3.1). To simplify the nomenclature of materials, polymer end-groups with $N=1, 2, 4,$ and 8 *tert*-butyl ester groups are denoted **ME**, **DE**, **TE**, and **OE**

(for mono-, di-, tetra-, octa-ester end groups), respectively. Similarly, polymer end-groups with N=1, 2, 4, and 8 carboxyl groups are denoted **MA**, **DA**, **TA**, and **OA** (for mono-, di-, tetra-, octa-acid end groups), respectively

3.2.2 Procedure for Sample Preparation

Solutions of *tert*-butyl ester terminated polymers for viscosity measurements were prepared by combining polymer and solvent in clean 20 mL scintillation vials or larger 50 mL glass jars which were placed on a Wrist-Action Shaker (Burrell Scientific) for up to 24 h to allow complete homogenization.

Solutions of carboxyl-terminated polymers were prepared as follows: To 150 to 200 mg of carboxyl-terminated polymer in a 50-mL Schlenk flask was added necessary amount of solvent for 1 wt% stock. The contents of the Schlenk flask were degassed by 3 freeze-pump-thaw cycles, and then stirred overnight at 70 °C.

3.2.3 Viscosity Measurements

Steady shear viscosity was measured in a cone-plate geometry (60 mm diameter aluminum, 1° cone, 29 μm truncation) using an AR1000 rheometer from TA Instruments (temperature controlled at 25 °C). Solutions of *tert*-butyl ester terminated polymers were probed in the shear rate range 1 - 200 s⁻¹ logarithmically (5 shear rates per decade). The range was extended to 3000 s⁻¹ for carboxyl-terminated polymers to better capture shear-thinning behavior. All viscosity data were reported in terms of *specific viscosity* (η_{sp} , $\equiv (\eta_{solution} - \eta_{solvent})/\eta_{solvent}$, where $\eta_{solvent} = 2.72$ mPa·s for CDD and 2.02 mPa·s for TL at 25°C) which reflects the contribution of the polymer to the viscosity.¹³

3.3 Results

3.3.1 Dissolution Behavior

All six *tert*-butyl ester-terminated 1,4-PBs (Table 3.1) were found readily soluble in both CDD and TL. With increasing carboxyl content, it became more difficult to dissolve carboxyl-terminated polymers: For $N = 1$, the corresponding polymer (226K di-**MA** 1,4-PB) was found soluble in both CDD and TL at room temperature; at $N = 2$ and 4, the corresponding polymers (230K di-**DA** 1,4-PB; 76K, 230K, and 430K di-**TA** 1,4-PBs) were not soluble in either model solvent at room temperature, but they dissolved into CDD and TL when heated at 70°C and remained in solution thereafter. At $N = 8$, the polymer 207K di-**OA** 1,4-PB did not dissolve completely into either solvent even when heated at elevated temperatures (>110°C) overnight. The difficulty of dissolving 207K di-**OA** 1,4-PB is not due to crosslinking: The polymer dissolves readily in THF, it passes easily through filters, and GPC-LS analysis (Chapter 2) showed that 207K di-**OA** 1,4-PB has a unimodal distribution similar to the other polymers in the series of similar M_w (near 220kg/mol, Table 3.1).

3.3.2 Steady-Flow Shear Viscosity of 1wt% Polymer Solutions

Specific viscosity (η_{sp}) of 1wt% polymer solutions averaged over shear rates from 10-100 s^{-1} show that all solutions of carboxyl-terminated 1,4-PBs had higher η_{sp} than their *tert*-butyl ester-terminated (i.e., protected) counterparts, but the most dramatic increase was observed in the case of $N = 4$ (Figure 3.3). The lack of η_{sp} data for carboxyl-terminated 1,4-PB with $N = 8$ is due to the poor solubility of the polymer in both solvents. While η_{sp} for all of the non-associative ~230K *tert*-butyl ester-terminated polymers was

the same, the deprotection of carboxyl groups on polymer chain ends produced a threefold increase in specific viscosity in both CDD and tetralin for $N = 4$, whereas at $N = 1$ and 2 only marginal increases were observed after deprotection of carboxyl groups (Figure 3.3 a). Thus, there appears to be a minimum number of carboxyl groups on polymer chain ends to achieve the intermolecular association required for viscosity modification ($N > 2$) and a maximum number imposed by the solubility limit ($N < 8$). The effect of solvent quality on η_{sp} was also observed in Figure 3.3 (a). Increasing the length of 1,4-PB backbone, for identical **TA** end groups ($N = 4$) increases the specific viscosity strongly (Figure 3.3 (b)): In tetralin, for the 76 kg/mol polymer, deprotection of carboxyl groups only increases the specific viscosity by 90%, whereas the increase is more than 320% for the 430 kg/mol polymer. For each polymer, η_{sp} of its 1wt% tetralin solution was found nearly twice as high as that of its 1wt% 1-chlorododecane solution.

3.3.3 Concentration Dependence of Specific Viscosity

While the values of η_{sp} of three *tert*-butyl ester-terminated polymers in both CDD and TL showed a nearly linear dependence on polymer concentration, the CDD and TL solutions of the three carboxyl-terminated polymers (76K, 230K and 430K di-**TA** 1,4-PBs) exhibited nonlinear increases of η_{sp} with concentration, and the extent of such non-linearity was found positively correlated with the M_w of polymer backbone (Figure 3.4). In accord with the observation that associative polymers with 1 and 2 carboxyl groups at their ends have little effect on viscosity, comparison of the three 230K carboxyl-terminated 1,4-PBs with $N = 1, 2$ and 4 shows that the non-linear increase of η_{sp} with polymer concentration was obvious only in the case of $N = 4$ (Figure 3.5).

3.3.4 Shear-Thinning Behavior of Solutions of Carboxyl-Terminated Polymers

The onset and magnitude of shear-thinning depend on the molecular weight and concentration of polymer. Solutions of 76K di-**TA** 1,4-PB showed negligible shear-thinning (up to 3000 s^{-1}) (in either CDD or TL, Figures 3.6 (a) and 3.7 (a), respectively). In the case of 230K di-**TA** 1,4-PB, its CDD and TL solutions showed obvious shear-thinning at 1wt%, with onsets in the range $10\text{-}100 \text{ s}^{-1}$. With decreasing concentration, the magnitude of shear thinning decreased and the shear rate required to elicit it increased (e.g., relative to the 1wt% solution, at 0.7wt%, the extent of shear-thinning observed in both CDD and TL was less significant and the onset shifted to $>100 \text{ s}^{-1}$) (Figures 3.6 (b) and 3.7 (b)). Similar trends were observed for solutions of 430K di-**TA** 1,4-PBs, with greater extent of shear-thinning and onset of shear-thinning at lower shear rates compared to their 76K and 230K counterparts (in both CDD and TL, Figures 3.6 (c) and 3.7 (c), respectively).

An interesting shear-thickening feature followed by further shear-thinning was observed for 430K di-**TA** 1,4-PB at 1wt% in CDD and 0.7wt% in TL (see Figures 3.6 (c) and 3.7 (c)). The shear-thickening appeared at a higher shear rate in CDD than in TL (shear rates between 250 and 1000 s^{-1} in Figure 3.6 (c), compared to 160 and 630 s^{-1} in Figures 3.7 (c)).

3.4 Discussions

3.4.1 Importance of Precise Control of Chain-End Structure

The comparison of four well-defined, carboxyl-terminated telechelic 1,4-PBs with $M_w \sim 230 \text{ kg/mol}$ revealed a surprisingly narrow range of N that confers both complete

dissolution in CDD and TL, and the ability to form supramolecular polymer aggregates that significantly enhance shear viscosity (Figure 3.3 (a)): Among the four values of N investigated in the present study, only $N = 4$ satisfied this balance. At $N = 1$ and 2 , the strengths of end-association were not sufficient for their supramolecules to enhance viscosity; whereas the polymer with $N = 8$ failed to completely dissolve in either CDD or TL. Using a simple additive approximation for combined binding strength of multiple hydrogen bonds allows us to semi-quantitatively explain the effect of N revealed in Figure 3.3.¹⁴ Carboxyl groups undergo pair-wise association in apolar aprotic media, and each pair of carboxyl groups can be considered to form two $\text{O-H}\cdots\text{O}=\text{C}$ hydrogen bonds.^{15,16} As an estimate for the free energy (ΔG_{asso}) of pair-wise association of two carboxyl groups, we use the literature value for pair-wise association of benzoic acid in tetrachloromethane (CCl_4) at 25°C , that is, ~ -19 KJ/mol ($\equiv -7.6$ $k_{\text{B}}T$ at 25°C),¹⁵ leading to estimates of strength of end-association for $N = 1, 2, 4$ to be approximately $7.6, 15.2,$ and 30.4 $k_{\text{B}}T$, respectively. Our previous theoretical work (see Section 1.2.2) suggests that the strength of end-association for telechelic associative polymers to form a significant fraction of supramolecules greater than 2×10^6 g/mol has to be greater than 16 $k_{\text{B}}T$.¹⁷ Thus, the theory accords with the observation that carboxyl-terminated end groups with $N = 1$ and 2 do not provide sufficient strength to drive the formation of large supramolecules (Figure 3.3).

The narrow range of applicable values of N also provides validation of our choice of carboxyl-terminated dendrons as self-associative polymer end groups rather than using triblock polymers with long 1,4-PB mid-blocks and short blocks of carboxyl functional polymer at each end. Although the latter seems synthetically straightforward to

implement *via* controlled radical polymerization techniques, (e.g., atom-transfer radical polymerization (ATRP) and reverse-addition-fragmentation transfer polymerization (RAFT)), it gives substantial variations in oligomer lengths when used to grow very short end blocks (degree of polymerization (DP) of $2 < DP < 8$).¹⁸⁻²⁰ In view of the present study, the use of a short, polydisperse block of carboxyl groups as the associative end groups of telechelic 1,4-PBs would cause complications: The population of polymers with the appropriate number of carboxyl groups at both ends would be low, with polymers chains end-capped with blocks with > 4 carboxyl groups tending to be insoluble, and those having one end-capped with < 4 carboxyl groups acting as “stoppers” that interfere with formation of large supramolecules. In contrast, the dendritic CTA approach (see Scheme 2.1) offers precise control of the number of carboxyl groups on polymer chain ends. The use of well-defined structures with uniform, discrete values of N proved essential for discovering the narrow range of end-association strength for telechelic associative polymers that form supramolecules with a significant population $> 2 \times 10^6$ g/mol (e.g., for mist-control applications). We expect that this molecular toolkit will prove equally useful as we move on to the investigation of the use of complementary end-association in the development of telechelic polymers as mist-control additives (refer to Chapter 4).

3.4.2 Relationship between Rheology Modification and Supramolecular Structures

One of the complications in using self-association (rather than complementary association), is that it allows individual chains to form loops. While each individual carboxyl group forms pairwise association with another carboxyl group, it is possible for all of the carboxyl groups of a **TA** end group (Figure 3.2 (b), N=4) to participate in H-

bond pairs when an even number of chain ends are brought together (i.e., both ends of the same chain, or four chain ends contributed by two looped chains or by one looped chain and two bridging chains, and so on (Figure 3.1)). This type of association leads to a concentration-dependent topology.¹¹ Such a hypothesis is supported by the following features observed in steady-flow shear viscosity data of di-**TA** telechelic 1,4-PBs (Figures 3.4-3.7): non-linear dependence of the low shear rate η_{sp} on polymer concentration, a Newtonian plateau at low shear rates ($<10 \text{ s}^{-1}$), and strong shear thinning at high shear rates ($>100 \text{ s}^{-1}$).^{12,21,22} Furthermore, it explains the effect of polymer molecular weight on the magnitude and concentration-dependence of the rheological manifestations of association.

At low concentrations, chains that associate into flower-like micelles weakly affect viscosity—only as much as their non-associative counterparts: A power-law relationship between the specific viscosity and the polymer concentration was observed in solutions of non-associative di-**TE** 1,4-PBs and self-associative di-**TA** 1,4-PBs (Figure 3.5); as the concentration increases above a threshold value that correlates with the overlap concentration of non-associative chains, the probability that a telechelic chain has its two **TA** end groups located in two different micelles increases. As concentration increases further, the progressive increase in the proportion of bridging chains that interconnect flower-like micelles leads to the nonlinear increase in viscosity.^{3,10}

The significant role of bridging chains in the rheological properties of telechelic associative polymers also helps explain the highly-nonlinear M_w -dependence of shear viscosity of 1wt% solutions of di-**TA** 1,4-PBs (Figure 3.3 (b)). For telechelic chains, the

entropy cost of forming loops rises as the length of telechelic chains increases.¹⁷ And there is an interplay between the chain length and concentration in relation to the energy gained by having bridging chains, which increase the “exchange entropy” for the number of different configurations available to the number of chains participating in a particular micelle. As the concentration approached the overlap concentration c^* of the midblock (here, the di-**TE** counterpart of a particular di-**TA**), a significant number of micelle cores are “within reach” of the backbone (not penalized by chain stretching). For shorter chains, this requires a higher concentration (e.g., c^* of 76K di-**TE** 1,4-PB in TL is 1.4wt%—outside the range of interest in the present experiments, explaining the absence of shear thinning in Figures 3.6 (a) and 3.7 (a)). Thus, increasing chain length has two synergistic effects: it penalizes loops and lowers the concentration threshold (c^*) beyond which the exchange entropy favoring bridges becomes significant. These considerations account for the observation that—at fixed concentration in TL—increasing M_w of di-**TA** 1,4-PB from 76 to 230 kg/mol led to a staggering 430% increase in η_{sp} , and increasing M_w from 230 to 430 kg/mol produced a further 270% increase (Figure 3.3 (b)). Furthermore, it explains the absence of a nonlinear concentration effect in the 76 kg/mol solutions in the concentration range of interest here (1wt% or less) and the approximate concentrations for the onset of nonlinear concentration effects for the 230 and 430 kg/mol polymers (Figure 3.5).

A Newtonian plateau at low shear rates ($< 10 \text{ s}^{-1}$) was observed in the majority of di-**TA** 1,4-PB solutions, except the 0.7 and 1 wt% TL solutions of 430K di-**TA** 1,4-PB (Figure 3.7 (b)). There are two physical scenarios that can lead to a Newtonian plateau: a lack of bridging chains or, when significant bridging is present, a rapid exchange process

for end association (i.e., an exchange time less than the inverse shear rate). In view of the high value of c^* for the 76 kg/mol polymer, it is not surprising that the Newtonian plateau covers the entire range of shear rate for all of the concentrations examined: Very few bridging chains are expected since all of these concentrations are less than or approximately c^* . During steady shear, the fraction of bridging chains reflects the competition between the creation and destruction processes, as the ends of bridging chains continuously dissociate and re-associate due to the dynamic nature of the non-covalent aggregation of **TA** end groups.²³ In the regime of low shear rates, the dependence of the rates of these two processes is hardly perturbed from equilibrium; so, the free energy of association of **TA** end groups predominates and the fraction of bridging chains stays constant, which results in the Newtonian plateau.^{21,22}

At high deformation rates, shear imposed on a bridged cluster of micelles has a significant effect on the balance between creation and destruction of bridging chains, which are the elastically active parts of the transient network.²⁴ In the context of the transient network kinetic model developed by Tanaka and Edwards, the mechanism of shear thinning is the detachment of bridging chains from the transient network which is activated by the stretching of the bridging chains, causing the disengagement rate of bridging chains to increase with increasing shear rate.^{11,25} Since bridging chains carry most of the stress in transient network of self-associative telechelic polymers, the resulting decrease in the fraction of bridging chains with increasing shear rate is manifested as shear-thinning behavior.²¹ From the perspective of bridging chains, we could explain the shear-thinning behavior observed in all CDD and TL solutions of 230K and 430K di-**TA** 1,4-PBs at 0.4-1wt%, with magnitude positively correlated with

polymer concentration and molecular weight (see (b) and (c) in Figures 3.6 and 3.7). The difference addressed above suggests the presence of bridging chains in the supramolecular structures of the two high- M_w di-**TA** 1,4-PBs in CDD and TL at concentrations $\geq 0.4\text{wt}\%$. Marrucci and coworkers reported the effective relaxation time scale of the transient network as a function of polymer concentration and molecular weight as follows:

$$\tau_{\text{eff}} \sim \left(c\sqrt{M_w}\right)^{2/3}$$

Where τ_{eff} denotes the effective relaxation time of the network, c is the polymer concentration, and M_w is the weight-average molecular weight of telechelic chains. The above scaling relationship helps explain the observed temporary shear thickening in the η_{sp} data of 1wt% CDD and 0.7wt% TL solutions of 430K di-**TA** 1,4-PB (see (c) in Figures 3.6 and 3.7). The high concentration and M_w of telechelic chain give a long τ_{eff} , and thus leads to the possibility of incomplete relaxation of bridging chains from these long telechelic chains when subjected to high shear deformation. Vandenbrule and Hoogerbrugge reported that probability of dissociating chains to reattach to the network increases linearly with the length of the chain, and thus the combination of incomplete relaxation and a higher probability of reattachment leads to temporary shear thickening.²⁶

The topology of supramolecular aggregates of 230K and 430K di-**TA** 1,4-PBs in apolar media revealed by shear viscometry in the present study provides invaluable insights concerning the molecular design for polymers as mist-control additives. The implication of these results is that *directional* end-association of long telechelic chains is favored over *non-directional* types that lead to the formation of flower-like micelles

interconnected by bridging chains. As indicated in numerous reports, bridging chains, which are a small fraction of the transient network and only show up when polymer concentration is high enough, are the active parts of the transient network of interlinked flower-like micelles; telechelic chains trapped in looped structures have little contribution to rheological properties of the solution.^{10,11,24} In other words, a considerable fraction of telechelic chains are wasted in the flower-like micelles. Tripathi and coworkers reported that bridging chains carry most of the tensile stress in the transient network of self-associative telechelic polymers in extensional flow as well.²¹ Therefore, we can expect when di-TA 1,4-PBs with $M_w > 400$ kg/mol are used as mist-control additives for kerosene, a relative high polymer concentration, say on the order of 0.5wt%, will be required to allow the formation of bridging chains. To achieve an economically feasible MCK formulation, a more efficient way to utilize telechelic chains to form supramolecular aggregates that can provide elasticities needed for mist control applications is preferred.

3.5 Conclusions

For the purpose of rheology modification at very low concentration, very long telechelic polymers are an especially interesting class of molecules. Keeping the backbone of the polymer free of associative groups allows them to adopt open configurations that are necessary for efficacy at low concentration. Using long backbones penalizes loops (unproductive configurations) and brings the overlap concentration into the range below 1wt%. The end groups must provide strong enough association that withstands moderate hydrodynamic forces—a more strenuous condition than merely requiring very few groups are left unpaired (refer to Chapter 4). Consequently, there is a

surprisingly narrow range of the number of carboxyl groups (N) on the chain ends that confers both the ability to form supramolecular polymer aggregates *via* self-association of carboxyl-terminated end groups and solubility in apolar media. The *non-directional* self-association of **TA** end groups permits aggregation numbers greater than pairwise and, therefore, many of the chains adopt unproductive configurations (loops). Given the excellent performance of these self-associative polymers, it should be possible to achieve similar effects at even lower polymer concentration if end association were truly pairwise. The following chapter examines candidate end groups for *directional* complementary end-association to provide molecular insight for the design of complementary associative pairs of telechelic chains that may prove to be even more potent rheology modifiers than the best self-associative telechelic polymers.

3.6 Figures and Tables

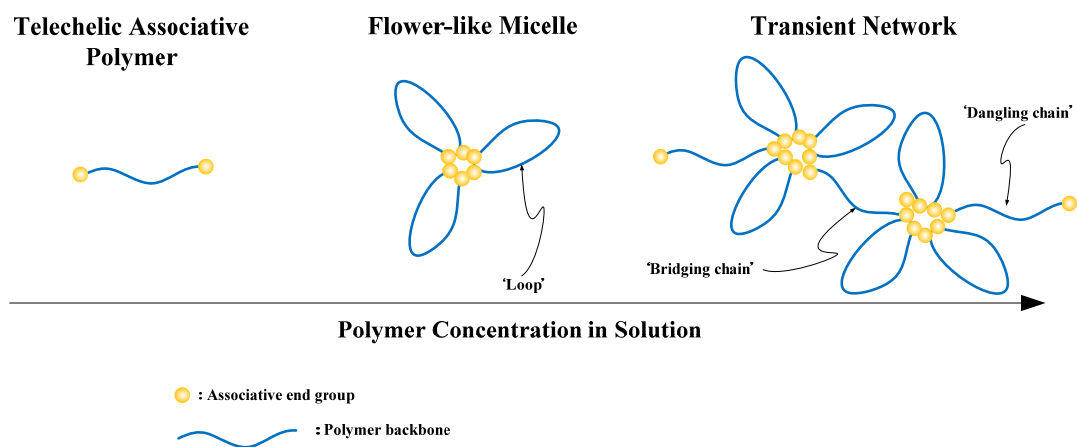


Figure 3.1 Schematic representation of the concentration-dependent self-association of telechelic associative polymers. Left: Telechelic associative chain at low concentration. Middle: Flower-like micelle above a critical concentration value. Right: Transient network at higher concentration.²

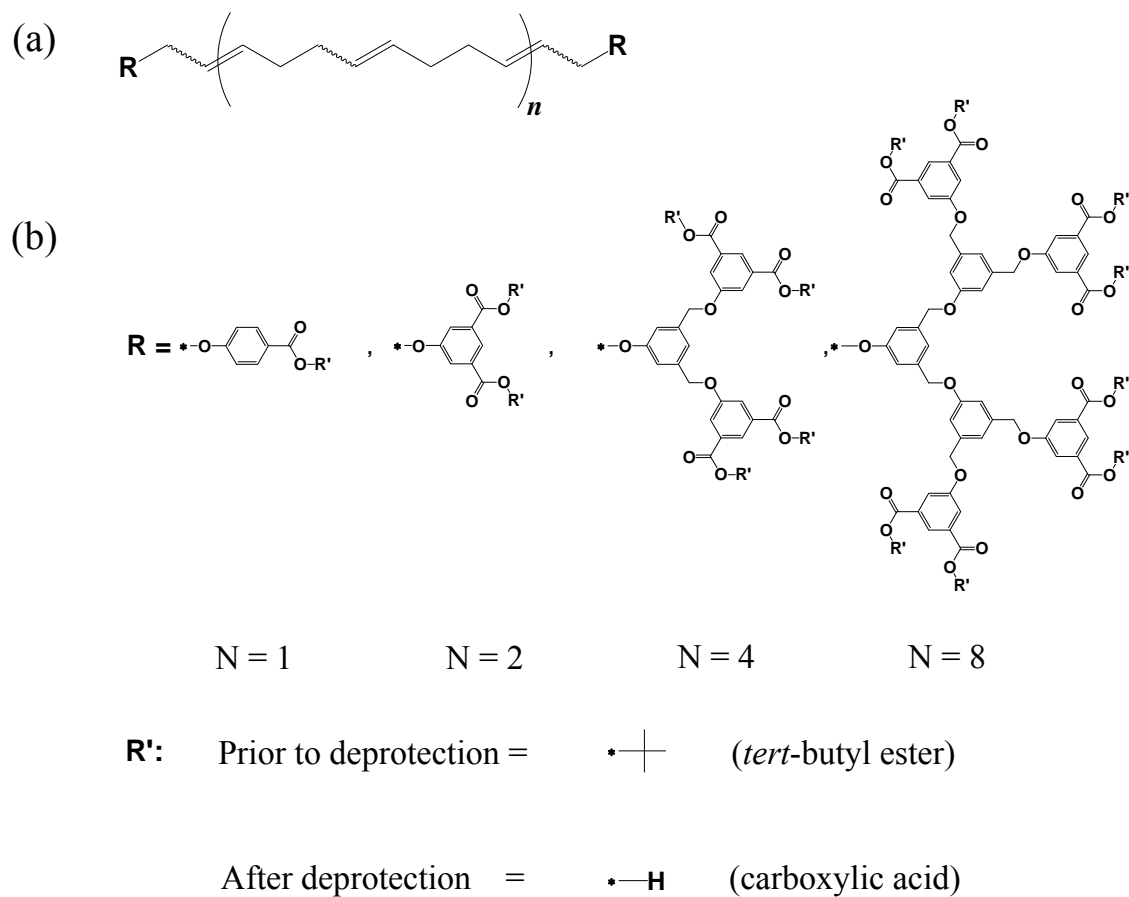


Figure 3.2 Structures of telechelic 1,4-PBs investigated in the present study. (a) General structure of telechelic 1,4-PBs. (b) Structures of end-groups corresponding to different number of functional groups (N = 1, 2, 4, and 8).

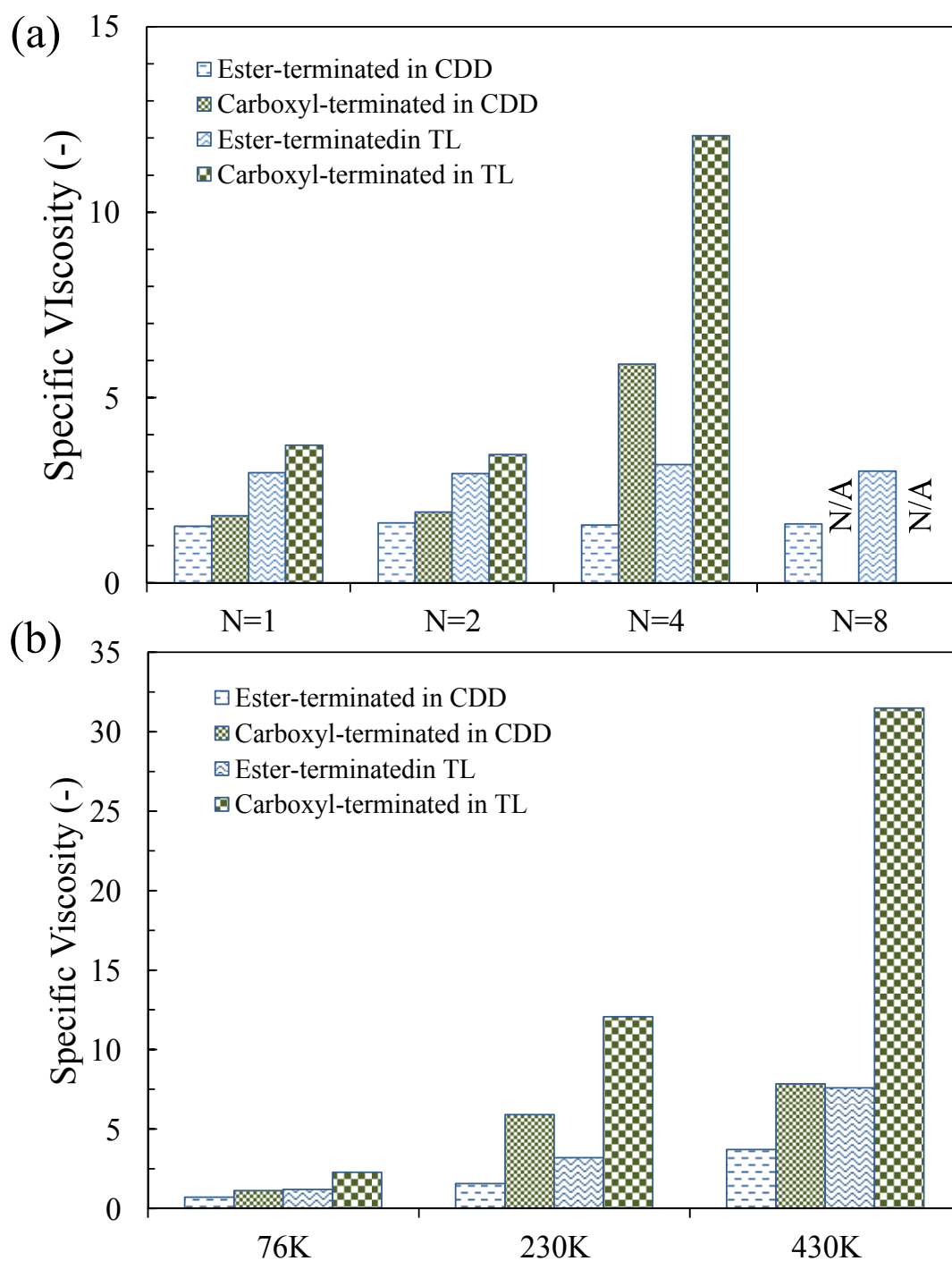


Figure 3.3 Specific viscosity of 1wt% solutions of test polymers in 1-chlorododecane (CDD) and tetralin (TL). (a) Effect of end functionality $N = 1, 2, 4, 8$ for polymers with $M_w \sim 220$ kg/mol (Table 3.1). Data are not available for octa-carboxyl end groups ($N = 8$) due to insolubility of the material in both in CDD and TL. (b) Results of $N=4$ at $M_w = 76, 230$ and 430 kg/mol. Note the difference in scale of the two graphs.

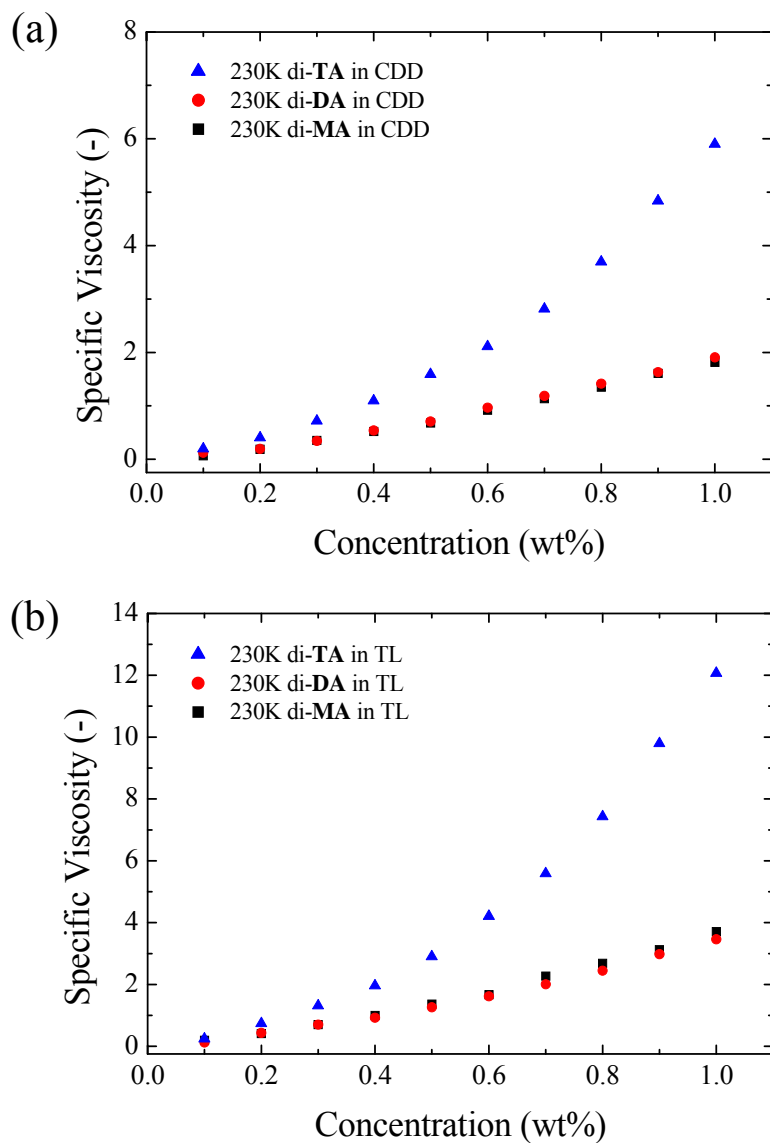


Figure 3.4 Effect of number of chain-end functional groups (N) on the concentration dependence of the specific viscosity of solutions of telechelic associative polymers with $M_w \sim 230$ kg/mol in (a) 1-chlorododecane (CDD) and (b) tetralin (TL). Note the difference in scale of the two graphs.

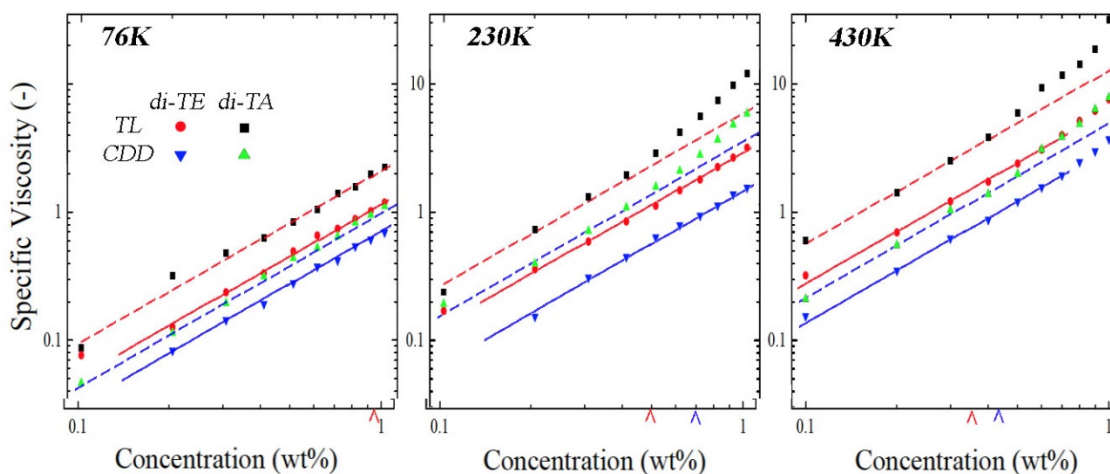


Figure 3.5 Concentration dependence of specific viscosity of solutions of telechelic 1,4-PBs with non-associative and associative chain ends ($N=4$) as a function of M_w : from left to right, 76 kg/mol, 230 kg/mol, and 430 kg/mol. The overlap concentration of the *tert*-butyl ester form of each polymer is indicated by the marks on the concentration axis, red for tetralin (TL) and blue for 1-chlorododecane (CDD); for 76K di-**TE** in CDD $c^*=1.4$ wt% (offscale). Solid lines indicate linear regression from 0.2 wt% to $1.5c^*$ for di-**TE**; dashed lines correspond to the solid line vertically shifted to the linear portion of the di-**TA** data: red for TL and blue for CDD.

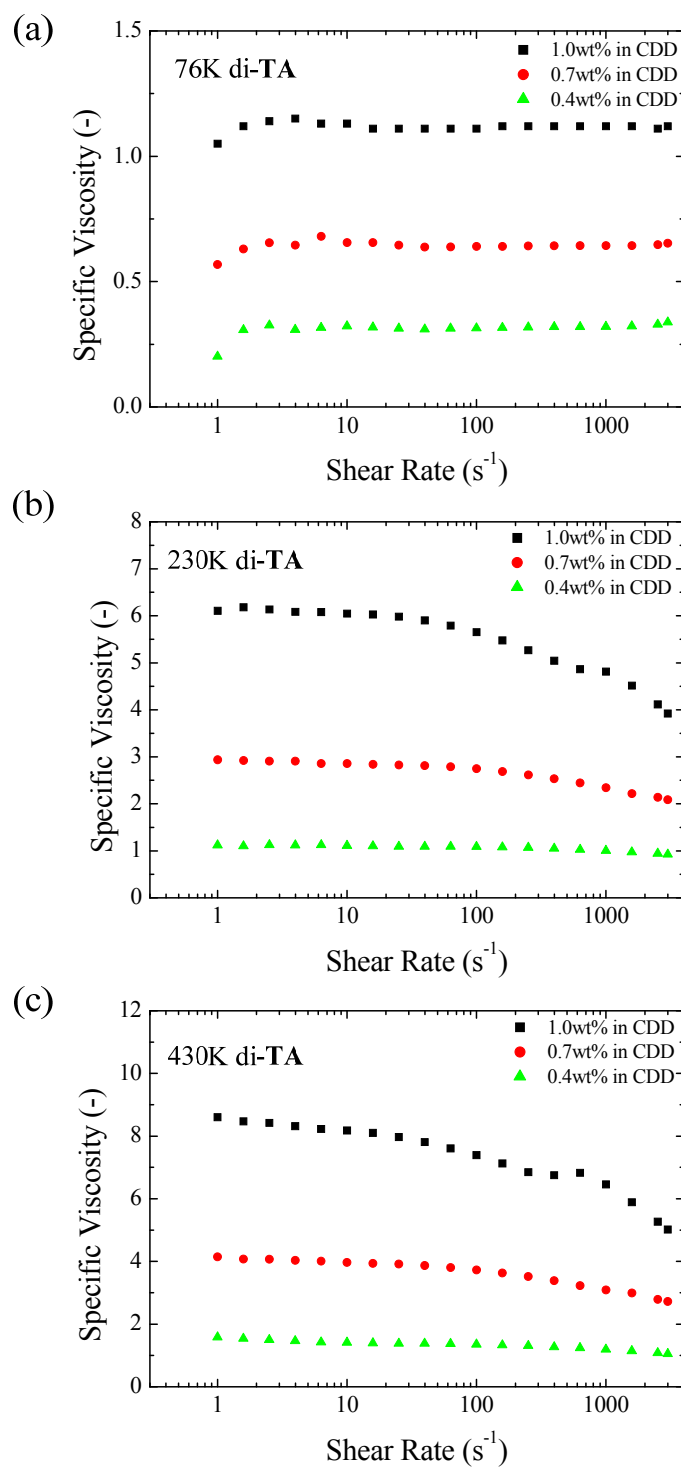


Figure 3.6 Shear-thinning behavior of CDD solutions of di-TA 1,4-PBs at three concentrations (0.4, 0.7 and 1.0 wt%) as a function of M_w : (a) 76 kg/mol, (b) $M_w = 230$ kg/mol, and (c) 430 kg/mol.

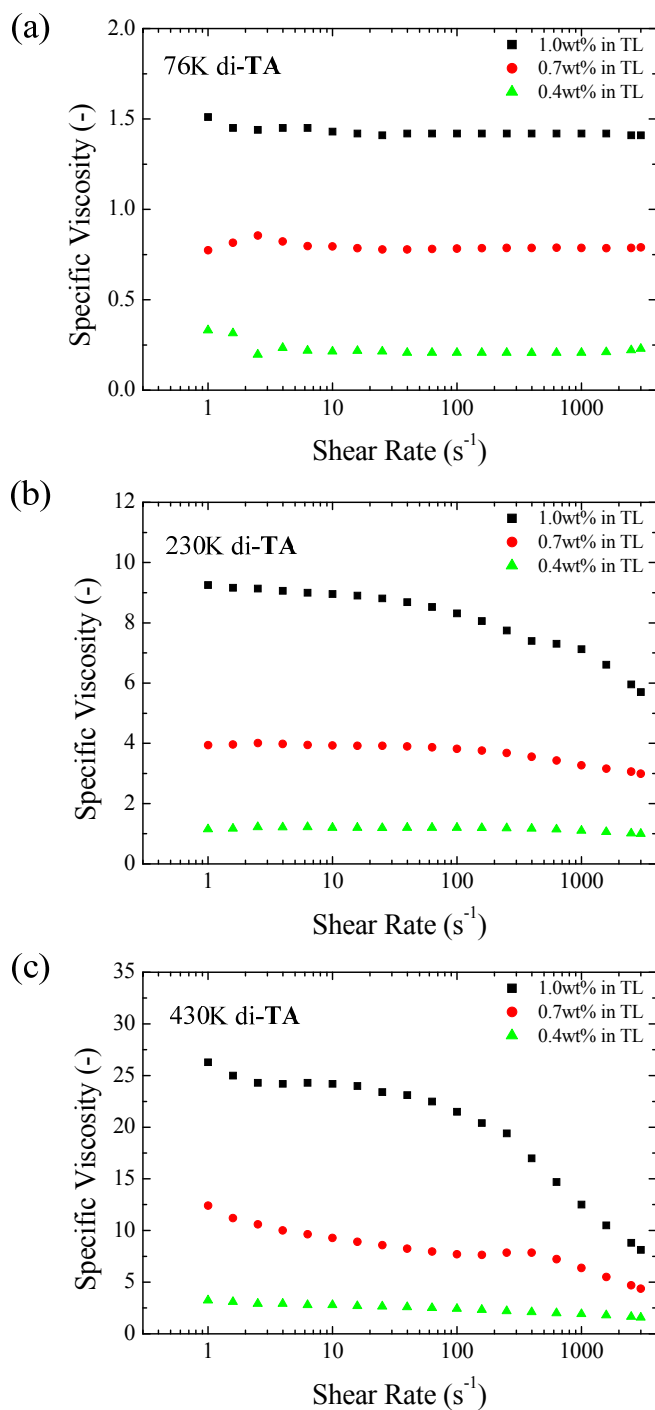


Figure 3.7 Shear-thinning behavior of TL solutions of di-TA 1,4-PBs at three concentrations (0.4, 0.7 and 1.0 wt%) as a function of M_w : (a) 76 kg/mol, (b) $M_w = 230$ kg/mol, and (c) 430 kg/mol. Note the difference in scale between these graphs and those in Figure 3.6 (solutions in CDD).

Table 3.1 Molecular Weight (M_w) and Number of Chain-End Functional Groups (N) of *tert*-Butyl Ester- and Carboxyl-Terminated Telechelic 1,4-PBs Investigated in the Present Study^a

Nominal M_w N	76	220	430
1		226 (1.4)	
2		230 (1.5)	
4	76 (1.5)	230 (1.4)	430 (1.5)
8		207 (1.5)	

^a GPC was performed for in THF for 35°C for the *tert*-butyl ester form; results are shown for M_w in kg/mol followed by PDI in parentheses.

References

- (1) Chassenieux, C.; Nicolai, T.; Benyahia, L. *Curr Opin Colloid In* **2011**, *16*, 18.
- (2) Lo Verso, F.; Likos, C. N. *Polymer* **2008**, *49*, 1425.
- (3) Cass, M. J.; Heyes, D. M.; Blanchard, R. L.; English, R. J. *J Phys-Condens Mat* **2008**, *20*.
- (4) Chassenieux, C.; Nicolai, T.; Tassin, J. F.; Durand, D.; Gohy, J. F.; Jerome, R. *Macromolecular Rapid Communications* **2001**, *22*, 1216.
- (5) Semenov, A. N.; Joanny, J. F.; Khokhlov, A. R. *Macromolecules* **1995**, *28*, 1066.
- (6) Stavrouli, N.; Aubry, T.; Tsitsilianis, C. *Polymer* **2008**, *49*, 1249.
- (7) Rahman, S. A.; Nemoto, N. *J Soc Rheol Jpn* **2003**, *31*, 219.
- (8) Suzuki, S.; Uneyama, T.; Inoue, T.; Watanabe, H. *Macromolecules* **2012**, *45*, 888.
- (9) Koga, T.; Tanaka, F. *Macromolecules* **2010**, *43*, 3052.
- (10) Sprakel, J.; Spruijt, E.; Stuart, M. A. C.; Besseling, N. A. M.; Lettinga, M. P.; van der Gucht, J. *Soft Matter* **2008**, *4*, 1696.
- (11) Annable, T.; Buscall, R.; Ettelaie, R.; Whittlestone, D. *Journal of Rheology* **1993**, *37*, 695.
- (12) Pellens, L.; Corrales, R. G.; Mewis, J. *Journal of Rheology* **2004**, *48*, 379.
- (13) Rubinstein, M.; Colby, R. H. *Polymer physics*; Oxford University Press: Oxford ; New York, 2003.
- (14) Hunter, C. A. *Angewandte Chemie-International Edition* **2004**, *43*, 5310.
- (15) Davis, M. M. *Acid-base Behavior in Aprotic Organic Solvents*; National Bureau of Standards, 1968.
- (16) David, R. L. A.; Wei, M. H.; Liu, D.; Bathel, B. F.; Plog, J. P.; Ratner, A.; Kornfield, J. A. *Macromolecules* **2009**, *42*, 1380.
- (17) David, R. L. A. Dissertation (Ph.D.), California Institute of Technology, 2008.
- (18) Skey, J.; O'Reilly, R. K. *Chemical Communications* **2008**, 4183.
- (19) Lai *Macromolecules* **2002**, *35*, 6754.
- (20) Davis, K. A.; Matyjaszewski, K. *Macromolecules* **2000**, *33*, 4039.
- (21) Tripathi, A.; Tam, K. C.; McKinley, G. H. *Macromolecules* **2006**, *39*, 1981.
- (22) Ma, S. O. X.; Cooper, S. L. *Macromolecules* **2001**, *34*, 3294.

- (23) Tam, K. C.; Jenkins, R. D.; Winnik, M. A.; Bassett, D. R. *Macromolecules* **1998**, *31*, 4149.
- (24) Michel, E.; Appell, J.; Molino, F.; Kieffer, J.; Porte, G. *Journal of Rheology* **2001**, *45*, 1465.
- (25) Tanaka, F.; Edwards, S. F. *Macromolecules* **1992**, *25*, 1516.
- (26) Vandenbrule, B. H. A. A.; Hoogerbrugge, P. J. *Journal of Non-Newtonian Fluid Mechanics* **1995**, *60*, 303.

Chapter IV Structure-Property Relationships for Hetero-Complementary Hydrogen-Bonding Partners

4.1 Introduction

Based on theoretical work of the Kornfield group at Caltech, the optimal design of shear-resistant associative polymers for mist control of fuels (Chapter 1) requires long, end-functionalized polymers bearing *directional, complementary* pairs of associative groups with association strength of 16-18 $k_B T$.¹ Therefore, we go beyond the *non-directional* self-association of carboxyl-terminated dendritic end groups (Chapters 2, 3 and 5) and investigate the structure-property relationships of complementary associative telechelic polymers. For use in organic liquids (e.g., fuel), hydrogen bonding is the *directional* noncovalent association of choice because it does not require the use of any activators or counterions (which could interfere with normal use of fuels). The present study compares simple carboxyl/tertiary amine association to selected polyvalent hydrogen-bonding-moieties drawn from the extensive literature on supramolecular architectures constructed using directional association.²⁻²³ The results show that carboxyl/tertiary amine association is superior to polydentate moieties (e.g., Hamilton receptor/cyanuric acid). Although this at first seems surprising, it agrees with prior literature on the roles of repulsive secondary interactions, which are present in most polyvalent hetero-complementary hydrogen-bond pairs, and the advantageous charge-assisted character of carboxyl/tertiary amine association.

4.1.1 *Directional* Noncovalent Bonding

The value of *directional* noncovalent association lies in its specificity, much like the value of mutually orthogonal “click” reactions in covalent bond formation: Association is pair-wise and joins two specific *hetero*-complementary partners. Supramolecular polymers held together by directional noncovalent association combine many of the attractive features of conventional polymers with responsiveness to their environment mediated by the reversibility of the noncovalent bonds.²⁴ Examples of such noncovalent associations include asymmetric hydrogen-bonding and asymmetric metal-coordination interaction (Figure 4.1). Among the directional interactions, hydrogen bonding is particularly important in the development of responsive supramolecular materials due to its high sensitivity to various external stimuli (e.g., solvent polarity, temperature, shear, and pH).^{19,21,25} Many creative applications of the above hetero-complementary associative pairs in supramolecular polymer chemistry have been reported, for instance, reversible and responsive polymer networks,²⁶ single-chain self-assembly,²⁷ self-healing materials,¹⁸ supramolecular multi-block copolymers,^{9,12,19,21,28-31} supramolecular star and miktoarm block (co)polymers,³² H-shape terpolymers,¹⁷ and compatibilized supramolecular polymer blends/networks of immiscible polymers.^{31,33} Among the various supramolecular architectures based on directional association reported, supramolecular multi-block copolymers from telechelic polymers end-capped with complementary associative units are particularly interesting in relation to mist-control applications. In principle, they have the potential to form high-molecular-weight linear supramolecular chains in non-polar solvents (such as hydrocarbons), which could provide both the elasticity needed for mist suppression and the reversibility that imparts

resistance to shear degradation (i.e., the supramolecules can dissociate reversibly into individual chains that are too short to undergo covalent bond scission due to flow).

Hydrogen bonding occurs between a proton donor D-H and a proton acceptor A, where D is an electronegative atom (usually O, N, or S), and the acceptor group is usually a lone pair of an electronegative atom (often a primary oxygen in a carbonyl or carboxyl group). Thus, a hydrogen bond can be characterized as a proton shared by two lone electron pairs.² The strength of a single hydrogen bond can be tuned by design of the chemical structure of the donor and the acceptor. One of the important design principles is that the strength of a single hydrogen bond is related to the difference in pK_a value between the proton donor and the conjugated acid of the proton acceptor, ΔpK_a . When the donor is less acidic than the conjugate acid of the acceptor ($\Delta pK_a \geq 0$), the proton remains predominantly with the donor, forming an *ordinary hydrogen bond* (OHB, D-H \cdots A) that is relatively weak (e.g., N-H \cdots O has strength ≤ 4 kcal/mol).^{2,34} In contrast, strong hydrogen bonds form when $\Delta pK_a < -4$, because the proton is largely transferred from the donor to the acceptor, forming a *charge-assisted hydrogen bond* (CAHB, D $^-$ \cdots H-A $^+$),² which can be exceptionally strong due to the accompanying electrostatic interaction. Typically, a CAHB (e.g., $^+N-H \cdots O^-$) is roughly 4 times stronger than an OHB (N-H \cdots O) and has strength ~ 15 kcal/mol (or $25 k_B T$ at 25°C).³ Thus, the equilibrium concentrations of unpaired acid and base are extremely low compared to the concentration of tight ion pairs resulting from transfer of the acidic proton to the base.

Generally, using one or two OHBs does not provide sufficient strength of association for the preparation of complex supramolecular structures. To achieve a high

degree of association (less than 1 in 10^5 building blocks is unpaired), the strength of association needs to be greater than $14 k_B T$ (8.3 kcal/mol), based on a Boltzmann distribution. This requirement has inspired a large body of literature devoted to the use of OHBs in multiple-hydrogen-bonding moieties, in which the strength of association depends on the number of hydrogen bonds, the arrangement of neighboring donor (D) and acceptor (A) sites, and whether the moieties are *self*-complementary or *hetero*-complementary. The former refers to the strong dimerization of an associative unit with itself (e.g., the ureidopyrimidone (**UPy**) motif used extensively by Meijer and coworkers is a DDAA motif with a self-dimerization constant of $K_d > 10^7 \text{ M}^{-1}$ in CDCl_3 at 25°C).^{16,35} Here we are interested in *hetero*-complementary hydrogen bonding, which enables the preparation of supramolecules with well-defined structures, such as block copolymers and dendrimers.²⁴ Hetero-complementary hydrogen bonding motifs, which show weak self-association ($K_d < 50 \text{ M}^{-1}$) and strong complementary association constants (K_{asso}) ranging from 10^2 to 10^8 M^{-1} in chloroform, have been devised using multiple hydrogen bonds.^{9,11-14,22,23,30,33,36,37} Representative examples of hetero-complementary hydrogen-bonding motifs are given in Table 4.1: (1) *triple* hydrogen-bonding: thymine (**THY**)/diamidopyridine (**DAP**)^{9,11} and **THY**/diaminotriazine (**DAT**),^{11,38} (2) *quadruple* hydrogen-bonding: 2,7-diamido-1,8-naphthyridine (**DAN**)/ ureidoguanosine (**UG**),^{12,13,33} and (3) *sextuple* hydrogen-bonding: Hamilton receptor (**HR**)/cyanuric acid (**CA**) or barbituric acid (**BA**).^{22,23}

Relatively less attention in supramolecular chemistry has been given to achieving strong association using hydrogen bonds reinforced by additional forces, such as electrostatic interaction (e.g., CAHBs).²⁴ As note earlier, when the donor is a sufficiently

strong acid relative to the conjugated acid of the acceptor (i.e., $\Delta pK_a < -4$, see Table 4.2 for pK_a values), a single hydrogen bond can meet or exceed the $14 k_B T$ (8.3 kcal/mol) requirement in non-polar aprotic solvents (e.g., chloroform and toluene), that is, a CAHB (which typically occurs when the donor is a carboxylic, phosphonic, or sulfonic acid and the acceptor is a primary, secondary or tertiary amine). The strength of CAHBs allows us to build supramolecular polymer structures using associative groups that are readily accessible and lend themselves naturally to construction of homologous series to elucidate structure-property relationships.^{2,6,7,39-45} Although CAHB-based hetero-complementary associative pairs have not received as much attention as those based on multiple OHBs, recent advances in polymer synthesis and the associated ability to prepare well-defined CAHB-based systems have led to a renaissance in this area.⁴ Representative examples of this category of supramolecular polymer structures include miktoarm supramolecular star copolymers of polystyrene (PS) and polyisoprene (PI),⁶ PI-PS-PI, supramolecular triblock copolymer and its thermo-responsive lamellar/cylindrical nanostructures,^{7,46} PS-PMMA supramolecular diblock copolymer and its application as anti-reflective coatings,⁴⁷ and supramolecular polymer gels *via* blending two polymers that are liquids at room temperature.⁴⁸

4.1.2 Methods to Characterize Noncovalent Bonding

The most widely adopted approach to characterize self-assembly of telechelic polymer building blocks in non-polar media is 1H NMR spectroscopy in non-polar deuterated solvents (e.g., $CDCl_3$ and toluene- d_8). Hydrogen-bonding can significantly alter electron environments of protons that participate in the association (e.g., amide protons in **THY** and **CA**), resulting in readily measured changes (> 3 ppm) in the

chemical shifts of these protons.^{11,49} Capillary (or “Ubbelohde”) viscometry at low shear rates ($<10^1 \text{ s}^{-1}$) has been used in few cases in conjunction with ^1H NMR spectroscopy to relate formation of supramolecular multiblock copolymers with their effects on macroscopic properties. Supramolecular block copolymers resulting from self-assembly are expected to possess higher solution viscosity compared to that of their individual blocks.^{12,21,22,30,50,51} Specifically, viscosity enhancement at low shear rates occurs when the product of the lifetime of the noncovalent bonds and the modulus of the associated structures is greater than the solvent viscosity, whereas the usual analysis of the peak shift observed in ^1H NMR spectra presumes “fast exchange” on a timescale of 1 ms.

The independent nature of the two observables (peak shift in ^1H NMR and low-shear-rate viscosity) is illustrated by recent results of Yang, Ambade and Weck on a non-covalent ABC triblock in which the three blocks were (A) poly(norbornene ester) with $M_n = 6.5 \text{ kg/mol}$, (B) poly(norbornene imide) with $M_n = 6.5 \text{ kg/mol}$, and (C) poly(ethylene oxide) with $M_n = 2.0 \text{ kg/mol}$, such that all three blocks have similar degrees of polymerization of approximately $\text{DP} = 25\text{-}45$ (Figure 4.2).²¹ The A-chains (**PA**) were monotelechelic with one end capped with **CA** (Table 4.1); the B-chains (**PB**) were heterotelechelic with a Hamilton receptor (**HR**) installed at one end (to connect with **PA**) and a 2,7-diamido-1,8-naphthyridine (**DAN**) group at the other end (to connect with **PC**), the C-chains were monotelechelic with a **UG** group at one end (to connect with the **DAN** end of **PB**). Association of **HR** and **CA** was demonstrated using ^1H NMR, which showed a roughly 5ppm shift of the protons of the **CA** unit in a stoichiometric solution of **PA** and **PB** (5 mM total polymer in CDCl_3 at 25°C), indicating that $>99\%$ of **HR** and **CA** were paired. Similarly, association of **DAN** and **UG** was evident in a shift of approximately 4

ppm of amide protons of the **UG** unit in a stoichiometric solution of **PB** and **PC** (5 mM total polymer in CDCl_3 at 25°C , which indicates >99% of **DAN** and **UG** were paired). These shifts occurred to the same extent when all three polymers were mixed at stoichiometric ratios, confirming that the **HR/CA** and **DAN/UG** associations were mutually orthogonal. Nevertheless, the specific viscosity ($\eta_{\text{sp}} \equiv \eta_{\text{solution}}/\eta_{\text{solvent}} - 1$) values only increased slightly upon association, consistent with approximately 20% of chains being connected (Figure 4.2 b). This apparent contradiction with respect to the high degrees of association suggested by ^1H NMR may simply reflect the rapid exchange among the associative groups.

Thus, the literature highlights the challenge of producing supramolecular polymers that confer effects provided by ultralong linear chains ($>10^6$ g/mol). Associations that give only a 10%-20% increase in the apparent molecular weight are not sufficient. Even if the non-associated chains are 250 kg/mol (over 20 times longer than those examined in prior literature on supramolecules), it is necessary to increase their apparent molecular weight by 800% to mimic effects that are conferred by chains of 2×10^6 g/mol. Furthermore, the concentration regime in which the effects of ultralong polymer are of particular interest is in the range of 1wt% or less, which has not been examined in the prior literature on supramolecules.

The literature is essentially silent in relation to long telechelic polymers (the longest we have found reported are <100 kg/mol). Nor are there reports of associative groups that have exchange times longer than approximately 0.1s. And the scant rheological data is limited to concentrations >1% and, with few exceptions, to shear

viscosity reported for only a single, low shear rate. As for CAHB-based supramolecular multiblock copolymers, to the best of our knowledge there are no reports on their applications as rheology modifiers in non-polar media. The lack of literature renders it unclear if the desired modification of rheological properties by hydrogen-bonding-based supramolecular multiblock copolymers can be achieved. In other words, it is uncertain whether the binding strengths of hydrogen-bonding-based complementary associative units discussed above are sufficient to hold longer polymer chains ($M_w > 100$ kg/mol) together at lower concentrations (1% or less) and comparatively higher shear rates (>10 s⁻¹). Motivated by the predictions of our previous theoretical work, we entered this unexplored regime of low concentrations of long telechelic chains and relatively strong associations (16-18 $k_B T$, see Chapter 1) to test the expectation that ultralong linear polymers could indeed be achieved, opening the way to various applications-including fire-safer fuels.

4.1.3 Scope of the Present Work

We are keen to answer the following question: How strong must a complementary association be to link telechelic polymers with $M_w \gg 100$ kg/mol to form supramolecular multiblock copolymers that are stable at comparatively high shear rates and useful as mist-control additives? To realize pairs of complementary associative telechelic polymers with different association strength, we choose OHB-based tridentate **THY**/diacetamidopyridine (**DAAP**) pair and hexadentate **HR/CA** pair (Table 4.1), and CAHB-based carboxyl/tertiary amine pair in bidentate and tetradentate configurations. The choice of **THY/DAAP** and **HR/CA** pairs is based on the fact that they have been widely adopted in supramolecular chemistry, and their ease of syntheses relative to other

multi-hydrogen-bonding pairs. 1,4-PB is chosen as the backbone of telechelic associative polymers for its excellent solubility in non-polar media, and the polymer syntheses are based on the strategy we developed for self-associative carboxyl-terminated telechelic 1,4-PBs (refer to Chapter 2). ^1H NMR spectroscopy and shear viscometry are employed in parallel to investigate if complementary association takes place when a backbone of $M_w \sim 200$ kg/mol and a polymer concentration $\sim 1\text{wt}\%$ are used, as well as if the association strength is strong enough to hold polymer chains together when exposed to moderate shear rates.

4.2 Results

4.2.1 Synthesis of Tertiary Amine-Terminated Telechelic 1,4-PBs

In non-polar aprotic solvents (e.g., chloroform), the basicity of amines follows the order: Tertiary > secondary > primary.⁵² In order to achieve sufficient strength of carboxyl/amine interaction in non-polar media (e.g., fuels), we need to have the tertiary amine-terminated counterparts of carboxyl-terminated telechelic 1,4-PBs. However, the high nucleophilicity of tertiary amines renders it a challenging task to synthesize tertiary amine-terminated bis-dendritic CTAs or telechelic polymers *via* coupling tertiary amine-functional compounds (e.g., *N,N*-dimethylaminoethanol) to precursors of bis-dendritic CTAs or the end groups of the pre-polymers, since tertiary amines can interfere with coupling reactions based on nucleophilic addition/substitution.⁵² Likewise, it is also difficult to synthesize tertiary amine motifs *via* direct *N*-alkylation of primary and secondary amines, which has been found plagued by the formation of quaternary amines as by-products.⁵³ Tertiary amines are also known to be capable of interfering with the

metathetical activities of ruthenium-based ROMP catalysts.^{54,55} The 3rd generation Grubbs catalyst (referred to as “Grubbs III” hereinafter) is comparatively tolerant towards tertiary amines, but it is not completely immune to the interference from tertiary amines.⁵⁶ In the present study, we tested a variety of strategies to synthesize multi-functional tertiary amine-terminated telechelic 1,4-PBs in order to meet the technical need for such polymers, as well as to address the possible synthetic difficulties associated with the aforementioned issues of tertiary amines. Table 4.3 summarizes all methods we attempted and the corresponding problems we encountered. We found that only the click chemistry-based, two-stage post-polymerization functionalization of multi-functional chloro-terminated telechelic 1,4-PB (Scheme 4.1; details of the syntheses of chloro-terminated telechelic 1,4-PBs are documented in Appendix A) successfully afforded the corresponding tertiary amine-terminated telechelic 1,4-PBs while keeping 1,4-PB backbones intact (verified by GPC-LS analysis). We also found that this strategy applied to a wide range of M_w of backbone (22 ~ 430 kg/mol). A series of tertiary amine-terminated telechelic 1,4-PBs were prepared accordingly: telechelic 1,4-PB of $M_w = 204$ kg/mol with *di*-functional tertiary amine-terminated dendritic end-groups (referred to as **DB** end-groups hereinafter; the polymer is referred to as 204K di-**DB** 1,4-PB), and telechelic 1,4-PBs of $M_w = 22, 250, \text{ and } 430$ kg/mol respectively with *tetra*-functional tertiary amine-terminated dendritic end groups (referred to as **TB** end groups hereinafter; the polymers are referred to as 22K, 250K, and 430K di-**TB** 1,4-PBs hereinafter). 22K di-**TB** 1,4-PB was used in ¹H NMR study of complementary end-association along with its carboxyl-terminated counterpart, 24K di-**TA** 1,4-PB (see Section 4.2.3); similarly, 204K di-**DB**, 250K di-**TB**, and 430K di-**TB** 1,4-PBs were used along with their carboxyl-

terminated counterparts 230K di-**DA**, 230K di-**TA**, and 430K di-**TA** 1,4-PBs (refer to Chapter 2), respectively, in shear viscometric study of end-association.

4.2.2 Synthesis of Complementary Hydrogen-Bonding Polymer Pairs

Triple-hydrogen-bonding **THY/DAAP** pair

The macro-CTA approach was employed to synthesize **THY**- and **DAAP**-terminated telechelic 1,4-PBs of $M_w \sim 200$ kg/mol **6** and **15** (referred to as di-**THY** 1,4-PB and di-**DAAP** 1,4-PBs hereinafter) in order to mitigate the influence from end-associative groups on polymerization reactions. The syntheses of di-**THY** and di-**DAAP** macro CTAs **5** and **14** commenced with the preparations of **THY**-functional acid **3**, **DAAP**-functional acid **13**, and di-hydroxyl 1,4-PB **4** ($M_w = 9.8$ kg/mol, PDI = 2.36). Subsequent coupling of the hydroxyl end groups of polymer **4** with **THY**-functional acid **3** via *N,N'*-diisopropylcarbodiimide (DIC)/4-dimethylaminopyridine (DMAP) mediated Steglich esterification at 40°C provided di-**THY** macro CTA **5**. The same approach was also employed to provide di-**DAAP** macro CTA **14**. The two macro CTAs **5** and **14** were also used as the model polymers in ^1H NMR spectral study of complementary association.

Scheme 4.2 details the synthesis of **THY**-functional acid **3**. Although thymine-1-acetic acid (**1**) is commercially available, its poor solubility in DCM and THF has prevented us to use it directly to prepare **5**. To prepare a **THY**-functional acid soluble in DCM and THF, thymine-1-acetic acid was esterified with allyl alcohol in bulk at reflux temperature using *p*-toluenesulfonic acid monohydrate (pTSA·H₂O) as the catalyst. Subsequent functionalization of the vinyl group with 3-mercaptopropionic acid (3MPA)

via photo-initiated thiol-ene reaction at room temperature provided the THF-soluble **THY**-functional acid **3**. The overall yield of **3** based on **1** was found reasonable (51.7%).

To the best of our knowledge, 2,6-diaminopyridine (**DAP**) functionalized intermediates with reactive functional groups (e.g., hydroxyl group) are not commercially available. We adopted the multi-step route (Scheme 4.3) developed by Shi and coworkers to synthesize 2,6-diacetamido-4-hydroxymethylpyridine (**12**),⁵⁷ of which the overall yield based on the starting material 4-picoline (**7**) was very low (3%) due to cumulative loss in multiple times of chromatographic separation along the course of synthesis (the 2,6-diacetamidopyridine motif of **12** is referred to as “**DAAP**” hereinafter). To overcome its poor solubility in THF, **DAAP**-functional alcohol **12** was further esterified with succinic anhydride to provide the THF-soluble **DAAP**-function acid **13**.

The preparations of macro CTAs **5** and **14** *via* Steglich esterification were performed under oxygen-free conditions in order to prevent the crosslinking of 1,4-PB backbones. DIC was chosen as the coupling reagent due to the good solubility of its corresponding urea in common organic solvents, which allowed complete removal of the urea byproduct during purification of the resultant polymers. Both polymers were afforded in ~ 42% yield after 3 cycles of reprecipitation from THF into methanol. In order to mitigate the adverse effects of the pyridine motif of **DAAP** on the kinetics and target molecular weight of ROMP, Grubbs III was used to synthesize high-molecular-weight telechelic associative polymers **6** and **15**.⁹ Very short reaction times were used in both cases (5 min for **6** and 18 min for **15**) because of the fast-initiating ability of Grubbs

III.⁵⁸ We found that macro CTAs **5** and **14** were completely incorporated into the resultant polymers (verified by GPC-LS analysis, Figures 4.3 and 4.4).

Sextuple-hydrogen-bonding **HR/CA** pair

Similar to the case of **THY/DAAP** pair, **HR**- and **CA**-terminated telechelic 1,4-PBs (referred to as di-**HR** and di-**CA** 1,4-PBs, respectively) **30** and **21** of $M_w \sim 200$ kg/mol were also synthesized *via* the macro-CTA approach in order to mitigate the influence of end groups on ROMP. The two macro CTAs **29** and **20** were also used as the model polymers for ¹H NMR spectral study of **HR/CA** complementary association.

What is different in the cases of **HR/CA** pair is that the di-**CA** macro CTA **20** was directly synthesized from ROMP of COD using small-molecule CTA **19**, and **19** was synthesized through Steglich esterification of **CA**-functional acid **18** with *cis*-2-butene-1,4-diol (Scheme 4.4) and used without chromatographic purification. **CA** unit has very poor solubility in common organic solvents except DMSO, and thus we functionalized it with a 1-undecenyl solubilizing unit to afford **17**. The vinyl group of **17** was further functionalized with 3MPA *via* photo-initiated thiol-ene coupling to provide the **CA**-functional acid **18** (Scheme 4.4). It is worth noting that a very large excess of cyanuric acid (~20 eq) was used in the synthesis of intermediate **17** in order to minimize the formation of di-substituted byproduct, but this inevitably resulted in the interference with the extraction of **17** from the reaction mixture: We observed that unreacted cyanuric acid precipitated during the extraction, and the precipitated solid was found adversely affecting the organic-aqueous phase separation. The low yield of **17** (15%) may be

attributed to the loss of product in extraction (possibly trapped in precipitated cyanuric acid solid) and in recrystallization.

HR-functional azide **27** was synthesized according to Scheme 4.5. The isophthalate core of the **HR** motif was functionalized with an azide group before it was coupled with two 2,6-diaminopyridine units for the following reasons: (i) the azide group is inert in all subsequent coupling/functionalization reactions and thus no tedious protection/deprotection steps for the terminal azide group are needed; (ii) the terminal azide group allows coupling of **HR** motif with propargyl-terminated telechelic 1,4-PB **28** ($M_w = 24$ kg/mol) *via* copper-catalyzed azide-alkyne cycloaddition (CuAAC, also known as “click chemistry”), a robust reaction insensitive to the interference from the pyridyl motifs of **HR**. Based on the aforementioned, post-polymerization end-functionalization *via* click chemistry was prepared the di-**HR** macro CTA **29**.

In the case of the **HR/CA** pair, Grubbs III was also used to synthesize telechelic associative polymers **21** and **30** (Schemes 4.4 and 4.5). Similar to the case of the **THY/DAAP** pair, macro CTAs **20** and **29** were also found completely incorporated into the resultant polymers (verified by GPC-LS analysis, Figures 4.5 and 4.6).

4.2.3 ^1H NMR Study on Complementary End-Association in Deuterated Chloroform

^1H NMR spectroscopy has been widely used to study the association of hydrogen-bonding-based hetero-complementary associative motifs in non-polar deuterated solvents (e.g., CDCl_3) because the resultant hydrogen bonds can cause significant changes in electron environments surrounding protons participating complementary associations; consequently, measurable changes in chemical shifts of those protons can be observed as

the results of such complementary associations.^{9-11,13,23,36,59} We adopted this widely accepted technique to investigate if the three pairs of hetero-complementary associative groups (**THY/DAAP**, **HR/CA**, and **TA/TB**) can perform complementary association in CDCl₃ at room temperature when attached to chain ends of 1,4-PB of M_w ~ 10-50 kg/mol, which was chosen to keep signals of end-groups recognizable. The results of each pair are described as follows:

(1) **THY/DAAP**: Figure 4.7 shows the expanded ¹H NMR spectra (500 MHz, CDCl₃) of 10K di-**THY** 1,4-PB **5**, 10K di-**DAAP** 1,4-PB **14**, and the mixture of **5** and **14** in a 1:2 wt ratio. In the absence of its complementary unit, the signal of the imide proton of **THY** end groups was observed at 8.05 ppm (Figure 4.7 (a)). Upon addition of ~ 2 eq of **DAAP** end groups, a large downfield shift to 11.05 ppm accompanied by signal broadening was observed (Figure 4.7 (c)). Similar shift was also observed for the signal of the amide protons of **DAAP** end groups (from 7.58 to 8.42 ppm, (b) and (c) in Figure 4.7). The observed association-induced shift (~2.9 ppm) of the imide proton signal of **THY** end groups is in good agreement with the literature,^{9,11,36} and it indicates that **THY** and **DAAP** end groups could find and associate with each other in CDCl₃.

(2) **HR/CA**: Figure 4.8 shows the expanded ¹H NMR spectra (500 MHz, CDCl₃) of 50K di-**CA** 1,4-PB, 24K di-**HR** 1,4-PB, and the mixture of 50K di-**CA** 1,4-PB and 24K di-**HR** 1,4-PB in a 1:1.4 wt ratio. In the absence of its complementary unit, the signal of the imide protons of the **CA** end group was observed at 7.75 ppm (Figure 4.8 (a)). A very large downfield shift to 12.90 ppm accompanied by peak broadening was observed (Figure 4.8 (c)) as ~ 2 eq of **HR** end groups were added. Similar to the case

of **THY/DAAP** pair, the observed association-induced shift (~5.2 ppm) of the signal of the imide protons of **CA** units indicates that **CA** and **HR** end groups could also find and associate with each other in CDCl_3 . The magnitude of the observed shift is in good agreement with the literature.^{21,22,32,37,60,61}

- (3) **TA/TB**: Due to the fact that 24K di-**TA** 1,4-PB is not soluble in CDCl_3 , we only performed ^1H NMR study on 22K di-**TB** 1,4-PB and its 1:1 (w/w) mixture with 24K di-**TA** 1,4-PB and monitored the association by tracking the shifts of the signals of the tertiary amine end group (H_1 and H_2 , see Figure 4.9). The results are shown in Figure 4.9. We found that the presence of 22K di-**TB** 1,4-PB assisted the dissolution of 24K di-**TA** 1,4-PB in CDCl_3 and thus rendered the ^1H NMR experiment possible. The signals of H_1 and H_2 were observed at 2.28 and 3.60 ppm respectively in the absence of 24K di-**TA** 1,4-PB (Figure 4.9 (a)). The addition of 24K di-**TA** 1,4-PB resulted in shifts of both signals: The signals of H_1 and H_2 shifted from 2.28 and 3.60 to 2.46 and 3.85 ppm, respectively. The observed shifts clearly indicate the association of **TA** and **TB** end groups.

In order to understand if the three pairs of complementary associative groups were still effective when attached to chain ends of 1,4-PBs of $M_w \sim 200\text{-}300$ kg/mol, we performed ^1H NMR analysis of the corresponding polymers and the complementary pairs at ~1wt% in CDCl_3 at room temperature. We found that in this case, signals of polymer end groups were barely recognizable due to their low contents in the test samples. In addition, association-induced signal broadening could cause signals of protons involved in complementary association to appear vanished. Nevertheless, evidence of end-association was observed in all three pairs of telechelic associative polymers of $M_w \sim 200$

kg/mol. In the case of the **THY/DAAP** pair, the signal of the imide proton of **THY** end group of 288K di-**THY** 1,4-PB was observed at 8.05 ppm with a very low intensity (Figure 4.10 (a)), and it was found disappeared in the ^1H NMR spectrum of the 1:2 (w/w) mixture of 288K di-**THY** and 219K di-**DAAP** 1,4-PBs. The disappearance of the signal indicates that **THY** and **DAAP** end groups could find and bind with each other in CDCl_3 , even when attached to chain ends of polymers of $M_w \sim 200$ kg/mol. Likewise, the signal of imide protons of the **CA** end groups of 200K di-**CA** 1,4-PB, along with those of the amide protons of the **HR** end groups of 240K di-**HR** 1,4-PB, were not observable in the ^1H NMR spectrum of the 1:1 (w/w) mixture of 200K di-**CA** and 240K di-**HR** 1,4-PBs (Figure 4.11). Signals of the **TB** end groups of 250K di-**TB** 1,4-PB were also found disappeared after the polymer was mixed with 230K di-**TA** 1,4-PB in a 1:1 wt ratio (Figure 4.12). These results suggest that all three complementary associative pairs can provide sufficient strength of end-association for telechelic 1,4-PB chains of $M_w \sim 200$ kg/mol to form supramolecular aggregates stable at least on the time scale of ^1H NMR spectroscopy.

4.2.4 Shear Viscometric Study of Complementary End-Association

Steady-flow shear viscometry at 25°C was used in parallel with ^1H NMR spectroscopy to investigate the ability of OHB-based and CAHB-based hetero-complementary associative pairs to afford supramolecular aggregates of telechelic 1,4-PBs of $M_w \geq 200$ kg/mol that are stable enough at low-moderate shear rates to provide modulation of rheological properties. In other words, we expected that at the same concentrations, the solution of complementary polymer pair would be *more* viscous than those of individual components. To avoid complication arising from the multi-component

nature of fuels, we chose 1-chlorododecane (CDD) as the model solvent, and prepared all polymer solutions at 1wt% in CDD. Surprising results were observed in both **THY/DAAP** and **HR/CA** complementary polymer pairs: None of them showed the expected enhancement in shear viscosity due to complementary end-association (Figures 4.13 and 4.14). To find out if the comparatively polar CDD (dielectric constant = 4.2 at 25°C) interferes with **THY/DAAP** and **HR/CA** complementary interactions, we repeated the experiments in *less* polar solvents: Dodecane (dielectric constant = 2.0 at 20°C) and Jet-A (dielectric constant = 1.8 at 20°C) were used for **THY/DAAP** pair and **HR/CA** pair, respectively. As shown in Figures 4.13 and 4.14, the expected enhancement in shear viscosity was still absent in both cases when *less* polar solvents were used.

Very different results were observed in the case of **TA/TB** pair. The 1:1 (w/w) mixture of 1wt% CDD solutions of 230K di-**TA** and 250K di-**TB** 1,4-PBs was found considerably more viscous than both solutions (Figure 4.15), and the observed enhancement in viscosity illustrated that the strength of **TA/TB** complementary end-association was sufficient to drive the formation of supramolecules stable at shear rates investigated in the present study. As discussed in preceding chapter (Section 3.3.2), strong self-association of 230K di-**TA** 1,4-PB resulted in significant difference in shear viscosity between the 1wt% CDD solution of 230K di-**TA** 1,4-PB and that of the non-associative pre-polymer 230K di-**TE** 1,4-PB (Figure 4.15). We observed that the addition of equal amount (by weight) of 250K di-**TB** 1,4-PB further enhanced the shear viscosity. What is also worth noting is the shear-thinning behavior observed in the 1wt% CDD solution of 1:1 mixture of 230K di-**TA** and 250K di-**TB** 1,4-PBs, which is a feature shared by aqueous solutions of water-soluble telechelic associative polymers.⁶²⁻⁶⁵ As for

the 1wt% CDD solution of 250K di-**TB** 1,4-PB, even though GPC-LS analysis confirmed no crosslinking of polymer backbone took place during end-functionalization with tertiary amine groups, we found that it was more viscous than that of the non-associative 230K di-**TE** 1,4-PB. Aggregation of triazole units resulting from the end-functionalization reaction (Scheme 4.1) may contribute to the above difference in shear viscosity.⁶⁶

Encouraged by the positive results of the pair of 230K di-**TA**/250K di-**TB** 1,4-PBs, we extended the viscometric study further to the complementary **DA/DB** association as an attempt to approach the limit of the strength of carboxyl/tertiary amine association. Figure 4.16 shows the results of 1wt% CDD solutions of the corresponding polymers (230K di-**DE**, 230K di-**DA**, and 204K di-**DB** 1,4-PBs) and the 1:1 (w/w) **DA/DB** mixture. Surprisingly, strong enhancement in shear viscosity induced by complementary **DA/DB** association was still observed in the 1:1 mixture. While only insignificant difference in shear viscosity was observed between the 1wt% CDD solution of 230K di-**DA** 1,4-PB and that of the non-associative 230K di-**DE** 1,4-PB, the considerable increase in viscosity due to **DA/DB** complementary end-association reaffirmed the promising strength of carboxyl/tertiary amine interaction.

The final part of the shear viscometric study of carboxyl/tertiary amine pairs is to investigate if the **TA/TB** complementary end-association was effective in Jet-A when the M_w of the 1,4-PB backbone increased to 430 kg/mol, and the results are shown in Figure 4.17. Strong enhancement in shear viscosity due to **TA/TB** complementary association was observed: At 1wt%, the 1:1 mixture of 430K di-**TA** and 430K di-**TB** 1,4-PBs in Jet-A was found significantly more viscous than the Jet-A solutions of the individual

polymers. These results clearly substantiate that when used in dendritic configurations, carboxyl/tertiary amine pair is suitable for building complementary pairs of telechelic associative polymers as mist-control additives for fuels.

4.3 Discussions

4.3.1 Insights into Hydrogen-Bonding-Based Complementary Association

The requirements for an ideal mist-control polymer additive for kerosene listed in Table 1.1 impose restrictions on the choice of hetero-complementary associative pairs as associative end-group for telechelic associative polymers as mist-control polymers. The expectation is that they are not only effective in enabling the formation of supramolecular aggregates capable of providing mist suppression and the subsequent fire protection to kerosene, but also able to render the implementation of MCK economically viable. Therefore, we selected **THY/DAAP**, **HR/CA**, **DA/DB** and **TA/TB** pairs for the sake that they are more synthetically and economically accessible as polymer end-groups compared to other hetero-complementary associative pairs reported in the literature. They also present a series of complementary end-associations varying in strength, which allow us to generate understanding of the strength of end-association required to achieve effective mist-control polymers for kerosene based on our design shown in Figure 1.9.

As noted earlier, the binding strength of a hetero-complementary associative pair is dictated by the strength and number of hydrogen bonds involved in the complementary interaction, as well as the arrangement of hydrogen-bond donor (D) and acceptor (A) sites. For OHB-based hetero-complementary associative pairs (e.g., **THY/DAAP** and **HR/CA**), the D/A site arrangement plays a crucial role in determining the resultant

binding strength.^{24,67} The pioneering work by the Jorgensen group on DNA nucleobase pairs reveals the influence of D/A site arrangement on their binding strengths.^{68,69} They proposed that partially charged atoms involved in hydrogen bonding in one partner can *electrostatically* interact with those in the other, and they further described such interactions as *secondary electrostatic interactions* (SEIs), which can be either attractive or repulsive depending on the pattern of D/A arrangement; the hydrogen bonds between the two partners were referred to as *primary interactions*. In addition, they suggested that attractive SEIs can provide additional stabilization to primary hydrogen bonds, whereas repulsive SEIs destabilize them. Based upon the above hypotheses, the Jorgensen group postulated that having all the hydrogen-bond donor groups in one partner and all the hydrogen-bond acceptor groups in the other would be the site arrangement that produces the strongest binding, since under this circumstance all SEIs would be attractive and able to contribute to the binding strength. Although Jorgensen's corollary has been criticized,⁷⁰ it has been found in good agreement with general experimental trends in triple-hydrogen-bonding hetero-complementary association,^{8,11,71,72} and it has also been applied quantitatively in empirical methods for predicting the strengths of hetero-complementary associative pairs.^{67,73}

Figure 4.18 illustrates all possible D/A site arrangements for triple-hydrogen-bonding hetero-complementary association, and their representative examples (including their K_{asso} values). Placing donors and acceptors in an alternating order (i.e., ADA-DAD, Figure 4.18 (a)) leads to 4 repulsive SEIs, and consequently the resultant value of K_{asso} ($\sim 10^3 \text{ M}^{-1}$ in CDCl_3) is the lowest among the three.¹¹ In the case of the AAD-DDA pattern (Figure 4.18 (b)), 2 attractive SEIs and 2 repulsive SEIs result from such an arrangement;

therefore, there is no net effect of SEIs on binding strength, which leads to an increase in K_{asso} by an order of magnitude ($K_{\text{asso}} \sim 10^4 \text{ M}^{-1}$).⁷¹ Having all the hydrogen-bond donor sites in one partner and all acceptor sites in the other, i.e., AAA-DDD (Figure 4.18 (c)), as suggested by Jorgensen as the most favorable arrangement, renders all of the 4 possible SEIs attractive, and thus leads to a remarkably high value of K_{asso} ($\sim 10^7 \text{ M}^{-1}$ in CH_2Cl_2).⁸ The trend of K_{asso} clearly indicates the significance of SEIs in OHB-based hetero-complementary association. Sartorius and Schneider extended Jorgensen's SEI analysis by establishing an empirical relationship to correlate the binding free energy of DNA nucleobases and synthetic hydrogen-bonding host-guest complexes in CHCl_3 at 25°C (ΔG_{asso}) with the D/A site arrangements of these natural/synthetic hetero-complementary associative pairs, in order to provide a semi-quantitative way to estimate the effects of SEIs on the strengths of hetero-complementary associations.⁷³ They found that each primary interaction (i.e., hydrogen bond) contributes -7.9 kJ/mol to ΔG_{asso} , while the contribution from each repulsive SEI is $+2.9 \text{ kJ/mol}$, and that from each attractive SEI is -2.9 kJ/mol . For a set of 58 different complexes investigated in their work, the calculated values of ΔG_{asso} based on the above linear relationship were in remarkably good agreement with experimentally observed values with an average difference of 1.7 kJ/mol (which corresponds to an average factor of 2 in K_{asso} value).

From the perspective of SEI analysis, inspection on **THY/DAAP** and **HR/CA** pairs provides insights into the relationship between their binding strengths and D/A site arrangements. As shown in Figures 4.18 (a) and 4.19 (a), both pairs are based on alternating placement of D and A sites (**THY/DAAP**: ADA-DAD; **HR/CA**: DADDAD-ADAADA); therefore, SEIs in both pairs are all repulsive, and **THY/DAAP** and **HR/CA**

have 4 and 8 repulsive SEIs, respectively. Based on Schneider's empirical ΔG_{asso} formula, the three hydrogen bonds in the **THY/DAAP** pair contribute -23.7 kJ/mol to ΔG_{asso} , while the four repulsive SEIs contribute +11.6 kJ/mol. That is, the alternating D/A site arrangement ADA-DAD results in a staggering 48.9% loss of the binding free energy provided by the three hydrogen bonds between **THY** and **DAAP**. Similarly, the six hydrogen bonds in the **HR/CA** pair contribute -47.4 kJ/mol to ΔG_{asso} , whereas the eight repulsive SEIs contribute +23.2 kJ/mol, which is also 48.9% of the contribution of the primary interactions. The estimated values of net ΔG_{asso} for **THY/DAP** and **HR/CA** pairs, -12.1 and 24.2 kJ/mol respectively, can be converted to their K_{asso} in CHCl_3 at 25°C using the following thermodynamic relationship:

$$K_{\text{asso}} = \exp\left(-\frac{\Delta G_{\text{asso}}}{RT}\right)$$

The calculated values of K_{asso} for **THY/DAAP** and **HR/CA** based on Schneider's empirical formula are 1.48×10^2 and $2.21 \times 10^4 \text{ M}^{-1}$, respectively, and both are in good agreement with literature data (Table 4.1).

The above analysis on **THY/DAAP** and **HR/CA** pairs implicates a dilemma concerning the development of telechelic associative polymers as mist-control additives for kerosene using OHB-based hetero-complementary associative pairs as polymer end-groups. The MCK application demands for an inexpensive polymer formulation that imposes minimum increase on fuel cost, and thus complementary associative pairs that can be easily synthesized and attached to polymer chain ends, such as **THY/DAAP** and **HR/CA**, are preferred in this regard. The problem is, however, that they are both plagued by the reduction of association strength by repulsive SEIs resulting from the alternating

D/A site arrangement, which explains the finding that the **HR/CA** pair failed to enable the formation of supramolecular aggregates of telechelic 1,4-PB chains of $M_w \sim 200$ kg/mol stable at low-moderate shear rates (Figure 4.14). An OHB-based hetero-complementary associative pair stronger than **HR/CA** is therefore needed. Ideally, a D/A site arrangement that results in less or even no repulsive SEIs, for instance, ADDA-DAAD and AAAA-DDDD, would generate complementary association stronger than that of **HR/CA**. A representative example of the former pattern is the **UG/DAN** pair (Table 4.1 and Figure 4.19 (b)), in which there are 4 primary interactions, 2 attractive SEIs, and 4 repulsive SEIs. That is, the overall contribution of SEIs to the binding strength is 2 repulsive SEIs, which is significantly less than that in **HR/CA** (8 repulsive SEIs). The estimated ΔG_{asso} and K_{asso} in CHCl_3 at 25°C for the **UG/DAN** pair, based on Schneider's empirical formula, are -26.2 kJ/mol and $3.89 \times 10^4 \text{ M}^{-1}$ respectively, and these values are in good agreement with the literature.²¹ The calculated results also explain why the quadruple-hydrogen-bonding **UG/DAN** pair is stronger than the sextuple-hydrogen-bonding **HR/CA** pair. The problem is, however, that the synthesis of **DAN** unit requires the use of very expensive starting material (2,7-di-chloronathyrindine), palladium catalyst, and multiple cycles of chromatographic separation that counterbalance the benefit of strength provided by the **UG/DAN** pair.^{13,14,74,75} The issue of synthetic accessibility is even worse in the case of the ideal AAAA-DDDD pattern, and it can be illustrated by the hetero-complementary associative pair synthesized by Blight and coworkers (Figure 4.19 (c)).⁷² Although the AAAA-DDDD pattern results in six attractive SEIs that contribute considerably to the overall binding strength and leads to an exceptionally high K_{asso} ($> 3 \times 10^{12} \text{ M}^{-1}$ in CH_2Cl_2 at 25°C), these AAAA and DDDD clusters are prohibitively

complicated and costly to synthesize (a problem shared by the triple-hydrogen-bonding AAA-DDD pair), and it is even harder to prepare them in asymmetric forms that can be further functionalized and used as polymer end-groups. In addition, the fused heterocyclic structure of the DDDD cluster has been found photochemically unstable. The trade-off between binding strength and synthetic accessibility renders it difficult to implement multiple OHB-based hetero-complementary associations in the development of mist-control polymers for fuels.

On the other hand, CAHB-based **DA/DB** and **TA/TB** pairs both present a much greater feasibility compared to the multiple OHB-based complementary associative pairs in Figure 4.19. The superior strength of the CAHB between carboxyl and tertiary amine groups, which is nearly 4 times as strong as OHBs such as $\text{NH}\cdots\text{O}$ and $\text{NH}\cdots\text{N}$, provides a convenient way to pack plenty of strength into a compact configuration. To illustrate, the binding strength of the structure-wise simple **DA/DB** pair is roughly equivalent to that provided by 8 OHBs, and the **TA/TB** pair could deliver a strength equivalent to nearly 16 OHBs. Therefore, we can rank the strength of the four hetero-complementary associative pairs investigated in the present study as follows:



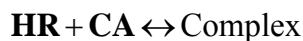
The design of dendritic end-groups we developed (Schemes 2.1 and 4.1) provides an inexpensive, simple and effective synthetic route to precisely control the number of CAHBs included in the carboxyl/tertiary-amine complementary end-association of telechelic 1,4-PB chains. Having all carboxyl groups on one dendritic end group and all tertiary-amine groups on the other also suggests the absence of repulsive SEIs. The shear viscosity data of **HR/CA** and **DA/DB** pairs reflect the superiority of CAHB-based design

(Figures 4.13 and 4.14): While the **HR/CA** pair failed to provide enough strength to hold polymer chains of $M_w \sim 200$ kg/mol together as supramolecules stable at low shear rates, the elegantly simple **DA/DB** pair was found effective in driving these polymer chains to form supramolecular aggregates stable at moderate shear rates. The above comparison also implicates that an OHB-based hetero-complementary associative pair that contains 8 OHBs and has a D/A site arrangement free of repulsive SEIs may possess sufficient binding strength for affording supramolecules stable at shear rates relevant to the MCK application. The problem is, however, that it is already difficult enough to synthesize an array of hydrogen-bond acceptors containing 4 acceptor sites and to use it as a polymer end group.⁷² To double the number of acceptors from 4 to 8 is a daunting task, and the accompanying cost and instability issues would further render the implementation of OHB-based hetero-complementary association in the development of mist-control polymers for fuels *impractical*.

4.3.2 Reconciliation between ¹H NMR Results and Viscosity Data

While ¹H NMR analysis indicates that all three complementary associative pairs (**THY/DAAP**, **HR/CA**, and **TA/TB**) could still associate when attached to chain ends of 1,4-PB chains of $M_w \sim 200$ kg/mol (Figures 4.10-4.12), only the **TA/TB** pair showed corresponding evidence of association in shear viscometry study (Figure 4.15). The trend observed in shear viscosity data is of no surprise, since the binding strength of the **TA/TB** pair, as discussed earlier, is considerably higher than those of **THY/DAP** and **HR/CA**. The trend also provides insights into the strength of complementary end-association required in the MCK application. Regarding the two OHB-based pairs, the discrepancy between the conclusions drawn from ¹H NMR and shear viscosity results can be

explained through the interplay between the equilibrium nature of such hetero-complementary association and hydrodynamic force. Take the **HR/CA** pair for example, and consider the complementary association of **HR** and **CA** units as an equilibrium reaction:



K_{asso} can thus be expressed as follows:

$$K_{\text{asso}} = \frac{[\text{Complex}]}{[\mathbf{HR}][\mathbf{CA}]} = \frac{k_{\text{asso}}}{k_{\text{disso}}}$$

Where $[\mathbf{HR}]$ and $[\mathbf{CA}]$ are the concentrations of free **HR** and **CA** end-groups, $[\text{Complex}]$ is the concentration of bound end groups, k_{asso} is the rate constant of the association process, and k_{disso} is the rate constant of the dissociation process. In this case, Arrhenius equation can be used to quantitate k_{disso} as follows:

$$k_{\text{disso}} = A_{\text{disso}} \exp\left(-\frac{E_{\text{disso}}}{RT}\right)$$

Where A_{disso} and E_{disso} are the pre-exponential factor and the activation energy of the dissociation process, respectively. In the ^1H NMR study of ~1wt% CDCl_3 solution of the mixture of 240K di-**HR** and 200K di-**CA** 1,4-PBs, the only energy source contributing to the dissociation process was the thermal energy of the polymer chains. The absence of the imide proton signal of the **CA** end-groups (Figure 4.11) indicates that **HR** and **CA** could still bind with each other, which suggests that the thermal energy of the polymer chains may not be sufficient to surpass E_{disso} . In shear viscometric study, however, mechanical energy was introduced into the 1wt% CDD solution of the polymer mixture as it was subjected to shear deformation, and the amount of such external energy was positively correlated to the applied shear deformation (expressed in terms of shear rate in

the present study). We believe it is possible that at higher shear rates ($>10 \text{ s}^{-1}$), the amount of introduced mechanical energy, combined with the thermal energy of the telechelic chains, may be sufficient to surpass E_{disso} . Consequently, the dissociation process could take place readily, leading to the absence of viscosity enhancement by mixing the 1wt% CDD solutions of 240K di-**HR** and 200K di-**CA** 1,4-PBs (Figure 4.14). We believe the above rationale can also apply to the case of the complementary pair of 288K di-**THY** and 219K di-**DAAP** 1,4-PBs (Figure 4.13).

The other feature of the equilibrium nature of **THY/DAAP** and **HR/CA** complementary associations concerning the discrepancy between the conclusions of ^1H NMR and shear viscometry data is that both the size of polymer backbone and the end-group concentration can affect the strength of complementary association. Numerous reports have revealed that the values of K_{asso} of **HR/CA** pair in polymeric systems ($\sim 2 \times 10^4 \text{ M}^{-1}$) can be lower than those in oligomeric and small-molecule systems ($\sim 10^5$ - 10^6 M^{-1}) by an order of magnitude,^{21,23,29,37} possibly due to the steric hindrance from the polymer chains during complexation.⁴⁹ A similar decrease in K_{asso} has also been reported on the stronger **UG/DAN** pair, which has a value of $K_{asso} \sim 10^7 \text{ M}^{-1}$ in small-molecule systems and a $K_{asso} \sim 2 \times 10^4 \text{ M}^{-1}$ in polymeric systems.^{14,21} As shown in Figure 4.2, **PA** ($M_w = 8.5 \text{ kg/mol}$, PDI = 1.30) and **PB** ($M_w = 11.4 \text{ kg/mol}$, PDI = 1.75) prepared by Yang and coworkers can form supramolecular diblock copolymer (evidenced by increase in η_{sp} at low shear rates ($<10 \text{ s}^{-1}$)) at 1.4-2.8 wt% in CH_2Cl_2 via **HR/CA** complementary association.²¹ In the present study, the average size of backbone is 20 times as high as those of **PA** and **PB**, and the concentration used in ^1H NMR and shear viscometry study is also lower ($\sim 1\text{wt}\%$). Consequently, [**HR**] and [**CA**] in this study is $\sim 1/20$ of those in

Yang and coworkers' work. From the viewpoint of equilibrium reactions, the above difference in [HR] and [CA] can be treated as dilution of HR and CA end-groups. According to *Le Chatelier's principle*, the equilibrium shifts to the left in order to counteract the effect of dilution, resulting in more free-standing HR and CA end groups. In other words, the binding strength of HR/CA end-association is weaker when a longer backbone and a lower polymer concentration are used. Supporting results for the above hypothesis are reported in Park and Zimmerman's work on supramolecular multi-block alternating copolymers from DAN-terminated telechelic poly(*n*-butylmethacrylate) ($M_w = 100$ kg/mol) and UG-terminated telechelic poly(ethylene oxide) ($M_w = 2$ kg/mol).³⁰ The shear rheology data of the polymer mixture in 1:1 DAN:UG end-group ratio in CHCl₃ at 26 °C showed that enhancement in η_{sp} was observable only at concentrations higher than a total polymer concentration of 6.25 g/dL (or 4wt%).

4.3.3 Connection between Shear Viscosity and Supramolecular Assembly

Currently in-depth investigation on the supramolecular self-assembly of DA/DB and TA/TB polymer pairs in non-polar media is underway. Nevertheless, a three-way comparison of shear viscosity data of 1wt% CDD solutions of 230K di-TA 1,4-PB, 1:1 (w/w) mixture of 230K di-TA 1,4-PB/250K di-TB 1,4-PB, and 1:1 (w/w) mixture of 230K di-DA 1,4-PB/204K di-DB 1,4-PB provides insights into the possible topology of such supramolecular polymer aggregates. As discussed earlier in Chapter 3, the self-association of TA end groups is strong enough to drive telechelic 1,4-PB chains of M_w up to 430 kg/mol to form supramolecular polymer aggregates with a concentration-dependent topology, which consists of compact flower-like micellar structures at low concentrations and micelles interconnected by bridging chains at concentrations near or

above c^* of the backbone (Figure 3.1). The considerable difference in specific viscosity (~ 4 in the shear-rate range $10\text{-}100\text{ s}^{-1}$) between the 1wt% CDD solution of 230K di-**TA** 1,4-PB and that of the non-associative 230K di-**TE** 1,4-PB evidences the presence of supramolecular polymer aggregates with the aforementioned topology of flower-like micelles interconnected by bridging chains (Figure 3.1). As shown in Figure 4.15, the 1:1 (w/w) mixture of 230K di-**TA** and 250K di-**TB** 1,4-PBs, at the same total polymer concentration (1wt%) in CDD, showed even higher values of η_{sp} (8.32-7.08 in the shear-rate range $10\text{-}100\text{ s}^{-1}$) compared to 230K di-**TA** 1,4-PB (6.16-5.7 in the same range of shear rate). Since the highly polar **TA** end groups are immiscible with the backbone and the solvent CDD, it is reasonable to infer that there was no free-standing **TA** end group in the 1wt% CDD solutions of 230K di-**TA** 1,4-PB; instead, they aggregated in certain numbers. The considerable higher η_{sp} of the 1wt% CDD solution of 1:1 mixture of 230K di-**TA** and 250K di-**TB** 1,4-PBs (compared to that of 230K di-**TA** 1,4-PB) suggests a different mode of end-group aggregation that led to more open supramolecular structures, resulting in higher η_{sp} . A possible scenario is that as the 1wt% CDD solutions of the two polymers were mixed together, **TB** end groups “reacted” with **TA** end groups and formed CAHB-based 1:1 complexes; consequently, the aggregates of **TA** groups were broken apart, and the 1:1 complexation of **TA** and **TB** led to the formation of linear and cyclic supramolecular polymer aggregates (Figure 1.9).

What is also worth noting is that there is no measurable difference in specific viscosity between the 1wt% CDD solution of 1:1 mixture of 230K di-**DA**/204K di-**DB** 1,4-PBs and that of the 1:1 mixture of 230K di-**TA**/250K di-**TB** 1,4-PBs (Figures 4.15 and 4.16). Given that the backbone sizes of the two pairs are virtually the same, these

results imply the possibility that the two pairs might form supramolecular polymer aggregates in a similar manner. Further characterizations, for example, dynamic and static light scattering (DLS and SLS), and small-angle neutron scattering (SANS), will be helpful to provide deeper insights into the supramolecular self-assembly of complementary associative pairs **di-DA/di-DB** and **di-TA/di-TB** 1,4-PBs in non-polar media.

4.4 Conclusions

The combination of two-stage ROMP, the use of dendritic CTAs, and post-polymerization click reaction presents an effective synthetic route to afford telechelic 1,4-PBs of $M_w > 200$ kg/mol with **DB** and **TB** end-groups. The results of shear viscometric study reveal critical information concerning the strength of complementary end-association required for telechelic 1,4-PB chains of $M_w \geq 200$ kg/mol to form supramolecules that are stable at moderate shear rates and potentially useful in MCK applications. Thanks to the superior strength of CAHBs and the lack of repulsive SEIs, **DA/DB** and **TA/TB** pairs outmatch their OHB-based counterparts **THY/DAAP** and **HR/CA** pairs and show efficacy in driving telechelic 1,4-PB chains of $M_w > 200$ kg/mol to form shear-stable supramolecular polymer aggregates effective in modulating rheological properties of such telechelic polymers in CDD and Jet-A. The ease of implementation of CAHB-based complementary end-association provides invaluable access to complementary pairs of telechelic associative polymers as potential mist-control additives for fuels, which is difficult to achieve *via* using OHB-based complementary associative pairs due to the trade-off between binding strength and synthetic feasibility. Future work may include in-depth study of the hetero-complementary association-driven,

supramolecular self-assembly of telechelic chains using various scattering techniques, including SANS, DLS and SLS.

4.5 Experimental

All reagents were obtained at 99% purity or above from Sigma-Aldrich, Alfa Aesar, J.T. Baker, BDH, EMD, or Mallinckrodt Chemicals except for thymine-1-acetic acid (Aldrich, 98%), *p*-toluenesulfonic acid monohydrate (Sigma-Aldrich, 98.5%), sodium amide (Aldrich, 95%), peracetic acid (Aldrich, 32%), 11-bromo-1-undecene (Aldrich, 95%), *cis*-2-butene-1,4-diol (Fluka, 96%), dimethyl 5-hydroxyisophthalate (Aldrich, 98%), allyl bromide (Aldrich, 97%), phosphorus tribromide (Aldrich, 97%), potassium hydroxide (Mallinckrodt Chemicals, 88%), oxalyl chloride (Aldrich, 98%), *cis*-1,4-dichloro-2-butene (Aldrich, 95%), lithium aluminum hydride (Aldrich, 95%), and cyanuric chloride (Aldrich, 98%).

¹H NMR spectra were obtained using a Varian Inova 500 spectrometer (500 MHz); all spectra were recorded in CDCl₃, acetone-d₆, and DMSO-d₆ at ambient temperature. Chemical shifts were reported in parts per million (ppm, δ) and were referenced to residual solvent resonances. Polymer molecular weight measurements were carried out in tetrahydrofuran (THF) at 35°C eluting at 0.9 mL/min (pump: Shimadzu LC-20AD Prominence HPLC Pump) through four PLgel 10- μ m analytical columns (Polymer Labs, 10⁶ to 10³ Å in pore size) connected in series to a DAWN EOS multi-angle laser light scattering (MALLS) detector (Wyatt Technology, Ar laser, λ = 690 nm) and a Waters 410 differential refractometer detector (λ = 930 nm).

4.5.1 Triple Hydrogen-Bonding THY/DAAP Pair

Allyl Thymine-1-acetate (2). Thymine-1-acetic acid (**1**, 1.00g, 5.32 mmol) and allyl alcohol (9.50 g, 0.16 mol) were reacted in the bulk in a 50 mL RBF at 95°C overnight with *p*-toluenesulfonic acid monohydrate (pTSA·H₂O, 0.21g, 1.1 mmol) as catalyst. Excess allyl alcohol was removed under reduced pressure at 40°C, and the remaining solid was dissolved with 50 mL of EA. The solution was poured into a 250 mL separatory funnel, and washed thrice with 50 mL of water + 1 g of NaHCO₃ (discarding the aqueous phase after each wash). The resultant organic phase was dried over 3 g of MgSO₄ and filtered, and the solvent was removed under reduced pressure to afford analytically pure **2** as fine, white crystals (0.61g, 2.72 mmol, 51.1% yield). ¹H NMR (500 MHz, acetone-d₆): δ = 10.16 (s, 1H), 7.45 (q, J = 1.2 Hz, 1H), 5.96 (ddt, J = 17.2, 10.5, 5.5 Hz, 1H), 5.51 – 5.04 (m, 2H), 4.68 (dt, J = 5.5, 1.5 Hz, 2H), 4.59 (s, 2H), 1.85 (d, J = 1.2 Hz, 3H).

THY-functional acid (3). **2** (0.71 g, 3.1 mmol) and 3-mercaptopropionic acid (3MPA, 0.50 g, 5.1 mmol) were mixed in 3 mL of THF and 3 mL of methanol in a 20 mL scintillation vial. After homogenization, the mixture was exposed to UV at room temperature for 4 h under vigorous stirring. The solvents were removed under reduced pressure, and the residual crude was purified by dissolving in 10 mL of boiling EA and allowing it to recrystallize in the freezer overnight. Vacuum filtration of the crystals and removal of solvents under reduced pressure at 40°C overnight afforded analytically pure **3** as fine, white crystals (0.91 g, 2.75 mmol, 80.6% yield). ¹H NMR (500 MHz, DMSO-d₆): δ = 12.28 (s, 1H), 11.41 (s, 1H), 7.50 (q, J = 1.2 Hz, 1H), 4.48 (s, 2H), 4.17 (t, J = 6.3

Hz, 2H), 2.67 (t, J = 7.1 Hz, 2H), 2.55 (t, J = 7.2 Hz, 2H), 2.50 (t, J = 7.2 Hz, 2H), 1.84 (dt, J = 7.6, 6.4 Hz, 2H), 1.76 (d, J = 1.2 Hz, 3H).

Di-THY macro CTA (5). Di-hydroxyl 1,4-PB (**4**, 0.40 g, $M_w = 9.8$ kg/mol, PDI = 2.36), **3** (0.25 g, 0.76 mmol) and DMAP (6 mg, 48.6 μ mol) were dissolved in 6 mL of anhydrous THF in a 50 mL Schlenk flask. The solution was degassed by 3 freeze-pump-thaw cycles. Degassed *N,N'*-diisopropylcarbodiimide (DIC, 0.11 g, 0.89 mmol) was injected into the flask, which was then placed in an oil bath at 40°C and left to stir overnight. The mixture was cooled and precipitated into 100 mL of methanol at 0°C. The collected polymer was further purified by 2 cycles of reprecipitation from THF (5 mL) into methanol (100 mL) at 0°C. Drying the precipitated polymer *in vacuo* at 35°C overnight afforded **5** (0.19 g, ~41.1% yield) as a clear, faint-yellow polymer. ¹H NMR (500 MHz, CDCl₃): δ = 8.15 (s, 2H), 7.30-7.27 (m, 4H), 6.95 (q, J = 1.2 Hz, 2H), 6.93 – 6.86 (m, 4H), 5.60-5.10 (br, =CHCH₂-, 347H, backbone), 5.08 (s, 4H), 4.57 (d, J = 4.4 Hz, =CHCH₂O, *trans* end group), 4.47 (d, J = 6.0 Hz, =CHCH₂O, *cis* end group), 4.42 (s, 4H), 4.29 (t, J = 6.2 Hz, 4H), 2.79 (t, J = 7.3 Hz, 4H), 2.64 (t, J = 7.3 Hz, 4H), 2.59 (t, J = 7.1 Hz, 4H), 2.20 – 1.95 (br, =CHCH₂-, 694H, backbone), 1.94 (d, J = 1.3 Hz, 6H).

288K di-THY 1,4-PB (6). Di-THY macro CTA **5** (46 mg) was dissolved in anhydrous DCM (1 mL) in a 50 mL Schlenk flask, and degassed by 3 freeze-pump-thaw cycles. After the flask was placed in a water bath at 40°C, 0.27 mL of 1 mg/mL DCM solution of Grubbs III was injected to reach equilibrium with the macro CTA for 1 min. A small amount of degassed, VCH-free COD (0.11 g, 0.98 mmol) was injected into the flask. 2 min later, a large amount of degassed, VCH-free COD (2.00 g, 18.3 mmol) and degassed DCM (4 mL) were injected. The mixture was stirred at 40°C for 2 min, and the reaction

was quenched by adding 25 mL of DCM + 0.1 g of BHT into the flask. The diluted mixture was precipitated into 300 mL of ethanol, and the collected polymer was dried *in vacuo* at 35°C overnight, yielding **6** as a clear, faint-yellow polymer (1.19 g, 58.2% yield). GPC-LS (THF, 35°C): $M_w = 288$ kg/mol, PDI = 1.80.

2,6-Diamino-4-methylpyridine (8). It was synthesized according to a literature procedure.⁵⁷ To a 1,2,3,4-tetrahydronaphthalene (tetralin, 300 mL) suspension of sodium amide (NaNH₂, 19.3 g, 0.65 mol) in a 500 mL RBF was added 4-picoline (**7**, 24.82 g, 0.267 mol). The RBF was placed in an oil bath to stir at 140°C for 6 h, and then at 190°C for 10 h. After the reaction mixture was cooled to room temperature, the RBF was placed in an ice bath, and 300 mL of ethanol was slowly added into the RBF to quench excess NaNH₂ and protonate the product. 30 g of silica gel was added, and the remaining ethanol was removed under reduced pressure. The resultant dark solid was added to the top of a 110 g column of silica gel and eluted with ~ 6 L of EA. The combined eluent was concentrated *via* rotary evaporation, and the resultant solid was dried *in vacuo* at 35°C overnight. The crude was purified by vacuum sublimation at 80~ 100°C at 60 mTorr to afford analytically pure **8** (12.94 g, 99.5 mmol, 37.3% yield). ¹H NMR (500 MHz, DMSO-d₆): $\delta = 5.44$ (s, 2H), 5.16 (s, 4H), 1.94 (s, 3H).

2,6-Diacetamido-4-methylpyridine (9). **8** (12.94 g, 99.5 mmol) and acetic anhydride (139.0 g, 1.36 mol) were stirred in the bulk in a 250 mL RBF at room temperature for 2 h. Removal of volatiles under reduced pressure at 60°C afforded analytically pure **9** as faint-yellow solid (18.95 g, 90.5 mmol, 91.0% yield). ¹H NMR (500 MHz, CDCl₃): $\delta = 7.88 - 7.53$ (br, 4H), 2.40 (s, 3H), 2.01 (s, 6H).

2,6-Diacetamido-4-methylpyridine-1-oxide (10). To an acetic acid (90 mL) solution of **9** (18.95 g, 90.5 mmol) in a 250 mL RBF was added 32 wt% acetic acid solution of peracetic acid (90 mL, 0.43 mol) at room temperature over a period of 30 min. The resultant solution was stirred at 60°C for 3 h and 70°C for 4 h. The reaction mixture was concentrated by removal ~60% of acetic acid under reduced pressure at 60°C, and the concentrated solution was precipitated into 300 mL of cold methanol at 0°C. Vacuum filtration of the precipitated solid and removal of solvents under reduced pressure at 70°C overnight afforded analytically pure **9** (11.51 g, 51.6 mmol, 57.0% yield) as fine, white crystals. ¹H NMR (500 MHz, DMSO-d₆): δ = 7.83 (s, 2H), 2.32 (s, 3H), 2.27 (s, 6H).

2-Diacetimido-6-acetamido-4-acetoxymethylpyridine (11). **10** (11.51 g, 51.6 mmol), acetic acid (25.2 g, 0.42 mol), and acetic anhydride (166.3 g, 1.63 mol) were stirred in a 500 mL RBF at 130°C for 20 min, and at reflux for 30 h. After the reaction mixture was cooled to room temperature, 40 g of silica gel was added to the mixture, and the volatiles were removed under reduced pressure at 70°C. The resultant dark solid was loaded to the top of 150 g column of silica gel, and eluted with ~ 4 L of 1:1 EA/petroleum ether mixture. The combined eluent was concentrated *via* rotary evaporation at 35°C, and the resultant crude was rinsed 5 times with ~ 10 mL of methanol to remove the oily, bright-yellow contaminant covering the crystalline crude (discarding the solvent after each rinse). Removal of solvents under reduced pressure at 35°C overnight afforded analytically pure **11** (4.76 g, 15.5 mmol, 30.0% yield) as fine, white crystals. ¹H NMR (500 MHz, CDCl₃): δ = 8.29 (s, 1H), 8.00 (s, 1H), 6.90 (s, 1H), 5.15 (s, 2H), 2.27 (s, 6H), 2.21 (s, 3H), 2.17 (s, 3H).

2,6-Diacetamido-4-hydroxymethylpyridine (DAAP-functional alcohol) (12). **11** (4.76 g, 15.5 mmol) and dry K_2CO_3 (3.01 g, 21.8 mmol) were stirred in 60 mL of methanol + 15 mL of water at room temperature for 8 h. 15 g of silica gel was added into the reaction mixture, and the solvents were removed under reduced pressure at 40°C. The resulting yellow solid was loaded to the top of a 100 g column of silica gel, and eluted with ~ 2 L of EA/ethanol 9:1 mixture. The combined eluent was concentrated *via* rotary evaporation at 35°C, and the resultant solid was rinsed 5 times with ~ 10 mL of THF (discarding the liquid after each rinse). Drying the resultant solid *in vacuo* afforded analytically pure **12** (1.73 g, 7.75 mmol, 50.0% yield) as fine, white crystals. 1H NMR (500 MHz, DMSO- d_6): δ = 9.99 (s, 2H), 7.70 (s, 2H), 5.39 (t, J = 5.8 Hz, 1H), 4.47 (d, J = 5.8, 2H), 2.10 (s, 6H).

DAAP-functional acid (13). **12** (0.40 g, 1.77 mmol) and succinic anhydride (0.23 g, 1.95 mmol) were stirred in THF (7 mL) in a 50 mL RBF at reflux temperature for 16 h with DMAP (0.025 g, 0.20 mmol) as the catalyst. The solvent was removed *via* rotary evaporation, and the remaining crude was purified by dissolving in 10 mL of EA/THF 1:1 mixture and allowing it to recrystallize in the freezer overnight. Vacuum filtration of the crystals and removal of solvents under reduced pressure afforded analytically pure **13** (0.55 g, 1.72 mmol, 88.2% yield). 1H NMR (500 MHz, DMSO- d_6): δ = 12.59 – 11.97 (br, 1H), 10.00 (s, 2H), 7.70 (s, 2H), 5.08 (s, 2H), 2.61 (m, 2H), 2.51 (m, 2H), 2.10 (s, 6H).

Di-DAAP macro CTA (14). Di-hydroxyl 1,4-PB **4** (0.30 g, M_w = 9.8 kg/mol, PDI = 2.36), **13** (0.187 g, 0.57 mmol) and DMAP (4 mg, 31.8 μ mol) were dissolved in 7.5 mL of anhydrous THF in a 50 mL Schlenk flask. The solution was degassed by 3 freeze-pump-thaw cycles. Degassed N,N'-diisopropylcarbodiimide (DIC, 0.089 g, 0.7 mmol)

was injected into the flask, which was then placed in an oil bath at 40°C and left to stir overnight. The mixture was cooled and precipitated into 100 mL of methanol at 0°C. The collected polymer was further purified by 2 cycles of reprecipitation from THF (5 mL) into methanol (100 mL) at 0°C. Drying the resultant polymer *in vacuo* at 35°C overnight afforded **14** (0.14 g, ~40.5% yield) as a clear, faint-yellow polymer. ¹H NMR (500 MHz, CDCl₃): δ = 7.86 (s, 4H), 7.58 (s, 4H), 7.26 (d, J = 8.7 Hz, 4H), 6.88 (d, J = 8.7 Hz, 4H), 5.60-5.10 (br, =C(H)CH₂-, 347H, backbone), 5.12 (s, 4H), 5.06 (s, 4H), 4.62 (d, J = 5.6 Hz, =CHCH₂O, *trans* end group), 4.48 – 4.43 (m, =CHCH₂O, *cis* end group), 2.79-2.69 (m, 8H), 2.19 (s, 12H), 2.14 – 1.94 (br, =C(H)CH₂-, 694H, backbone).

219K di-DAAP 1,4-PB (15). Di-DAAP macro CTA **14** (45 mg, M_w=10.5 kg/mol) was dissolved in anhydrous DCM (1 mL) in a 50 mL Schlenk flask, and degassed by 3 freeze-pump-thaw cycles. After the flask was placed in a water bath at 40°C, 0.27 mL of 1 mg/mL DCM solution of Grubbs III was injected to reach equilibrium with the macro CTA for 1 min. A small amount of degassed, VCH-free COD (0.11 g, 0.98 mmol) was injected into the flask. 2 min later, a large amount of degassed, VCH-free COD (2.00 g, 18.3 mmol) and degassed DCM (7 mL) were injected. The mixture was stirred at 40°C for 11 min, and 0.5 mL of 1 mg/mL DCM solution of Grubbs III was injected to the mixture to allow the polymerization to proceed further. The mixture was stirred for another 4 min at 40°C before it was quenched by adding 25 mL of THF + 0.1 g of BHT into the flask. The diluted mixture was precipitated into 300 mL of ethanol, and the collected polymer was dried *in vacuo* at 35°C overnight, yielding **15** as a clear, faint-yellow polymer (0.87 g, 42.5% yield). GPC-LS (THF, 35°C): M_w = 219 kg/mol, PDI = 1.64.

4.5.2 Sextuple Hydrogen-Bonding HR/CA Pair

11-Undecenyl isocyanurate (17). To a DMSO (170 mL) suspension of cyanuric acid (**16**, 40.86 g, 0.316 mol) and 1,8-diazabicyclo[5.4.0]undec-7-ene (DBU, 3.16 g, 20.3 mmol) in a 500 mL RBF was added 11-bromo-1-undecene (4.80 g, 20.6 mmol). The RBF was placed in an oil bath at 70°C and left to stir overnight. The reaction mixture was poured into a 1 L separatory funnel containing 300 mL of water, and extracted with 300 mL of hot EA. The organic phase was washed again with 300 mL water. The solvent was removed under reduced pressure, and the remaining crude was purified by 2 cycles of recrystallization from methanol to afford **17** as fine, white crystals (0.87 g, 3.09 mmol, 15% yield). ¹H NMR (500 MHz, DMSO-d₆): δ = 11.35 (s, 2H), 5.79 (ddt, J = 17.0, 10.2, 6.7 Hz, 1H), 4.97 (m, 2H), 3.62 (t, 2H), 2.05 – 1.96 (m, 2H), 1.50 (p, J = 7.0 Hz, 2H), 1.34 (p, J = 6.5, 6.1 Hz, 2H), 1.24 (s, 10H).

CA-functional acid (18). To a THF (3.5 mL) solution of **17** (0.41 g, 1.46 mmol) was added 3MPA (0.29 g, 2.73 mmol). The mixture was subject to UV irradiation at room temperature for 2 h. The solvent was removed under reduced pressure, and the remaining crude was purified by dissolving it in 6 mL of boiling methanol and allowing it to recrystallize in the freezer overnight. Vacuum filtration of the crystals and removal of solvents under reduced pressure at 35°C afforded analytically pure **18** (0.36 g, 0.93 mmol, 63.7% yield) as fine, white crystals. ¹H NMR (500 MHz, DMSO-d₆): δ = 13.04 – 10.47 (br, 3H), 3.61 (t, 2H), 2.65 (t, J = 7.2 Hz, 1H), 2.55 (m, 4H), 1.55 – 1.43 (m, 4H), 1.41 – 1.14 (m, 12H).

Di-CA CTA (19). *cis* 2-butene-1,4-diol (0.039 g, 0.42 mmol) was added to a solution of **18** (0.36 g, 0.92 mmol), 1-ethyl-3-(3-dimethylaminopropyl)carbodiimide hydrochloride (EDC·HCl, 0.20g, 1.03 mmol) and DMAP (6.0 mg, 50.6 μ mol) in 3 mL anhydrous DCM + 7 mL of anhydrous THF in a 50 mL RBF at room temperature. The mixture was stirred at room temperature overnight. The mixture was diluted with 30 mL of EA, and washed 4 times with 30 mL of 1M HCl_(aq) (discarding the aqueous phase after each wash), dried over 3 g of MgSO₄, and filtered. The solvent was removed under reduced pressure to afford **19** in ~ 80% purity (0.20 g, 0.19 mmol, ~45% yield), which was later used as is. ¹H NMR (500 MHz, DMSO-d₆): δ = 11.38 (s, 4H), 5.80 – 5.58 (m, 2H), 4.75 – 4.53 (m, 4H), 3.76 – 3.46 (m, 4H), 2.76 – 2.54 (m, 8H), 2.51 – 2.46 (m, 4H), 1.49 (dd, J = 8.7, 5.9 Hz, 4H), 1.40-1.10 (m, 30H).

Di-CA marco CTA (20). **19** (0.151 g, 0.15 mmol based on 80% purity) was loaded into a 50 mL Schlenk flask, degassed by 5 cycles of pulling vacuum/filling argon, and dissolved with degassed, anhydrous THF (6 mL). The flask was placed in a water bath at 40°C. 3.1 mg of Grubbs III in 2 mL of degassed, anhydrous THF was injected into the flask to equilibrate with the CTA for 1 min. Degassed, VCH-free COD (2.00 g, 18.3 mmol) was injected into the flask to start the polymerization reaction. The mixture was stirred at 40°C for 1 h. Before the reaction was terminated, an aliquot was taken and analyzed by ¹H NMR, which shows that monomer was completely consumed, and ~65% of CTA was incorporated into polymers. 20 mL THF + 0.1 g of BHT was added to the mixture to quench the reaction, and the mixture was precipitated into 300 mL of isopropanol. The precipitated polymer was further purified by 2 cycles of reprecipitation from THF (30 mL) into isopropanol (300 mL). The resultant polymer was dried in vacuo at room

temperature overnight, yielding **20** as a clear, faint-yellow polymer (1.00 g, 46.5% yield). GPC-LS (THF, 35°C): $M_w = 51.7$ kg/mol, PDI = 2.10.

200K di-CA 1,4-PB (21). Di-CA macro CTA **20** (0.30 g, $M_w = 51.7$ kg/mol, PDI = 2.10) was dissolved with anhydrous DCM (6 mL) in a 50 mL Schlenk flask. The solution was degassed by 3 freeze-pump-thaw cycles, and the flask was placed in a water bath at 40°C. 0.36 mL of 1 mg/mL DCM solution of Grubbs III was injected to reach equilibrium with the macro CTA for 1 min. A small amount of degassed, VCH-free COD (0.13 g, 1.22 mmol) was injected into the flask. 3 min later, a large amount of degassed, VCH-free COD (2.00 g, 18.3 mmol) was injected. The mixture was stirred at 40°C for 20 min, and 0.5 mL of 1 mg/mL DCM solution Grubbs III was injected to the mixture to allow the polymerization to go on. The mixture was stirred for another 36 min at 40°C before it was quenched by adding 20 mL of THF + 0.1 g of BHT into the flask. The diluted mixture was precipitated into 300 mL of ethanol, and the collected polymer was dried *in vacuo* at 35°C overnight, yielding **21** as a clear, faint-yellow polymer (2.17 g, 89.7%). GPC-LS: $M_w = 198.6$ kg/mol, PDI = 1.44.

Dimethyl 5-allyloxyisophthalate (23). Dimethyl 5-hydroxyisophthalate (**22**, 5.00 g, 23.3 mmol), dry K_2CO_3 (6.44 g, 46.6 mmol), and allyl bromide (3.49 g, 28.0 mmol) were stirred in 60 mL of DMF in a 250 mL RBF at 60°C overnight. Excess allyl bromide was vacuum-evaporated off the reaction mixture at 70°C. The mixture was diluted with 120 mL of DCM, poured into a 500 mL separatory funnel, washed twice with 120 mL of water, and washed thrice with 120 mL 1M $HCl_{(aq)}$ (discarding the aqueous phase after each wash). The organic phase was dried over $MgSO_4$ and filtered, and the solvent was

removed under reduced pressure. The remaining solid was purified by dissolving in 10 mL of boiling methanol and allowing it to recrystallize in the freezer overnight. Vacuum-filtration of the crystals and removal of solvents under reduced pressure at 40°C afforded analytically pure **23** (4.92 g, 19.7 mmol, 84.4% yield) as fine, white crystals. ¹H NMR (500 MHz, CDCl₃): δ = 8.28 (t, *J* = 1.5 Hz, 1H), 7.77 (d, *J* = 1.5 Hz, 2H), 6.06 (ddt, *J* = 17.2, 10.5, 5.2 Hz, 1H), 5.44 (dq, *J* = 17.2, 1.6 Hz, 1H), 5.32 (dq, *J* = 10.5, 1.4 Hz, 1H), 4.63 (dt, *J* = 5.2, 1.5 Hz, 2H), 3.94 (s, 6H).

Dimethyl 5-(3-((2-hydroxyethyl)thio)propoxy)isophthalate (24). The mixture of **23** (4.92 g, 19.7 mmol), 2-mercaptoethanol (3.84 g, 49.2 mmol) and DCM (5 mL) in a 50 mL RBF was subject to UV irradiation at room temperature for 7 h, resulting in quantitative conversion of the vinyl group of **23** (verified by ¹H NMR analysis). The reaction mixture was diluted with 100 mL of EA, poured into a 250 mL separatory funnel, and washed thrice with 100 mL water + 5 g of sodium carbonate (Na₂CO₃) (discarding the aqueous phase after each wash). The organic phase was dried over MgSO₄ and filtered, and the solvent was removed under reduced pressure at 35°C to afford analytically pure **24** (6.27 g, 19.1 mmol, 97.0% yield) as clean, yellow oil. ¹H NMR (500 MHz, CDCl₃): δ = 8.27 (t, *J* = 1.5 Hz, 1H), 7.75 (d, *J* = 1.5 Hz, 2H), 4.16 (t, *J* = 5.9 Hz, 2H), 3.94 (s, 6H), 3.75 (q, *J* = 4.9, 4.2 Hz, 2H), 2.75 (q, *J* = 7.2, 6.6 Hz, 4H), 2.16 (s, 1H), 2.14 – 2.06 (p, 2H).

Dimethyl 5-(3-((2-azidoethyl)thio)propoxy)isophthalate (25). To a THF (25 mL) solution of **24** (2.00 g, 6.03 mmol) in a 50 mL RBF was slowly added phosphorus tribromide (PBr₃, 2.02 g, 7.2 mmol) over 10 min. The mixture was stirred at room

temperature for 3 h. 6 mL of methanol was added to the mixture to quench excess PBr_3 . The solvent was removed under reduced pressure, and the remaining oil was dissolved with 100 mL of DCM, poured into a 250 mL separatory funnel, and washed thrice with 100 mL of water + 5 g of NaHCO_3 (discarding the aqueous phase after each wash). The resultant organic phase was dried over 7 g of MgSO_4 and filtered, and the solvent was removed under reduced pressure to afford analytically pure dimethyl 5-(3-((2-bromoethyl)thio)propoxy)isophthalate (1.93 g, 4.93 mmol, 81.8% yield) as colorless oil. ^1H NMR (500 MHz, CDCl_3): δ = 8.28 (t, J = 1.5 Hz, 1H), 7.74 (d, J = 1.5 Hz, 2H), 4.15 (t, J = 6.0 Hz, 2H), 3.94 (s, 6H), 3.50 (t, 2H), 2.96 (t, 2H), 2.78 (t, J = 7.2 Hz, 2H), 2.10 (ddd, J = 12.7, 7.0, 5.8 Hz, 2H). The intermediate bromide (1.93 g, 4.93 mmol) and sodium azide (NaN_3 , 0.64 g, 9.9 mmol) were stirred in 10 mL of DMF in a 50 mL RBF at 40°C overnight. The reaction mixture was cooled, diluted with 50 mL of EA, poured into a 250 mL separatory funnel, and washed twice with 50 mL of water, thrice with 50 mL of water + 5 g of NaCl , and thrice with 50 mL of 1M $\text{HCl}_{(\text{aq})}$ (discarding the aqueous phase after each wash). The organic phase was dried over 3 g of MgSO_4 and filtered, and the solvent was removed under reduced pressure to afford analytically pure **25** (1.50 g, 4.2 mmol, 86.1% yield). ^1H NMR (500 MHz, CDCl_3): δ = 8.28 (t, J = 1.5 Hz, 1H), 7.75 (d, J = 1.4 Hz, 2H), 4.16 (t, J = 5.9 Hz, 2H), 3.94 (s, 6H), 3.48 (t, J = 6.9 Hz, 2H), 2.79 (t, J = 7.1 Hz, 2H), 2.74 (t, J = 6.9 Hz, 2H), 2.11 (tt, J = 7.0, 5.9 Hz, 2H).

HR-functional azide (27). **25** (1.50 g, 4.2 mmol) and potassium hydroxide (KOH, 1.78 g, 28.0 mmol) were stirred in 22 mL of water + 25 mL of ethanol at 75°C overnight. 40 mL of 1M $\text{HCl}_{(\text{aq})}$ was slowly added to the reaction mixture at room temperature to quench excess KOH and protonate the product. The solvents were removed under reduced

pressure, and 60 mL of EA was added to the RBF. The mixture was poured into a 250 mL separatory funnel and washed thrice with 60 mL of water + 4 g of NaCl (discarding the aqueous phase after each wash). The organic phase was dried over 5 g of MgSO₄ and filtered, and the solvent was removed under reduced pressure at 40°C overnight to afford the isophthalic acid (1.03 g, 3.17 mmol, 75.4% yield) as fine, white powder. ¹H NMR (500 MHz, DMSO-d₆): δ = 8.07 (t, J = 1.4 Hz, 1H), 7.65 (d, J = 1.5 Hz, 2H), 4.17 (d, J = 12.2 Hz, 1H), 3.51 (t, J = 6.7 Hz, 2H), 2.74 (td, J = 7.5, 7.1, 6.0 Hz, 4H), 2.01 (tt, J = 7.0, 5.9 Hz, 2H). To a THF (10 mL) solution of the isophthalic acid (1.03 g, 3.17 mmol) with 3 drops of anhydrous DMF was added oxalyl chloride (1.60 g, 12.7 mmol) drop-wise over a period of 10 min. The mixture was stirred at reflux temperature for 3 h. The gaseous byproducts were scavenged by directing them into a water bath. The solvent and excess oxalyl chloride were removed under reduced pressure, which afforded **26**. The remaining oil was dissolved with 20 mL of anhydrous THF, and the resultant solution was added drop-wise through a 25 mL addition funnel to a THF (50 mL) solution of 2,6-diaminopyridine (2.76 g, 25.3 mmol) and triethylamine (TEA, 0.80 g, 7.9 mmol) over a period of 20 min. The reaction mixture was stirred at room temperature overnight. The solvent was removed under reduced pressure, and the remaining solid was dissolved in 50 mL of 3:1 EA/THF mixture, washed twice with 50 mL of water, and thrice with 50 mL water + 4 g of NaCl (discarding the aqueous phase after each wash). The organic phase was dried over 4 g of MgSO₄ and filtered, and the solvent was removed under reduced pressure. The resultant solid was dissolved in 10 mL of acetic anhydride (10.8 g, 0.105 mol), and the mixture was stirred at room temperature overnight. The volatiles were removed under reduced pressure at 70°C. The residue was purified by silica gel column

chromatography eluting with 15:1 DCM/methanol mixture, giving **27** in ~ 99% purity as orange-yellow powder (1.07 g, 1.81 mmol, 57.6% yield). ^1H NMR (500 MHz, DMSO- d_6): δ = 10.51 (s, 2H), 10.19 (s, 2H), 8.13 (t, J = 1.5 Hz, 1H) 7.89- 7.74 (m, 6H), 7.72 (d, J = 1.5 Hz, 2H), 4.23 (t, J = 6.1 Hz, 2H), 3.53 (t, J = 6.7 Hz, 2H), 2.80 – 2.75 (m, 4H), 2.12 (s, 6H).

Di-Propargyl 1,4-PB (28). Di-*tert*-butyl ester CTA (**3** in Scheme 2.1, 82.5 mg, 0.18 mmol) was dissolved in anhydrous THF (5 mL) in a 50 mL Schlenk flask, and the solution was deoxygenated by 3 freeze-pump-thaw cycles. The flask was placed in a water bath at 40°C. Under argon atmosphere, 2.4 mL of 1 mg/mL THF solution of Grubbs III (2.7 μmol) was syringe-transferred to the mixture and allowed to reach equilibrium with the CTA for 1 min. Degassed, VCH-free COD was syringe-transferred into the mixture to start the polymerization reaction. The mixture was stirred at 40°C for 4 h, resulting in quantitative consumption of the monomer and the CTA (verified by ^1H NMR analysis). Under argon purge, ground KOH (1.0g, 15.7 mmol) was added to the reaction mixture. The mixture was left to stir at room temperature overnight. 2 mL of 12 M HCl(aq) in 12 mL of THF was slowly added to the reaction mixture to quench excess KOH and protonate the carboxylate salts. The mixture was filtered, concentrated *via* rotary evaporation at 35°C, and dissolved with 5 mL of THF. The solution was drop-wise precipitated into 100 mL of methanol. The resultant polymer was further purified by two cycles of reprecipitation from THF (5 mL) into methanol (100 mL) at 0°C. Drying the collected polymer *in vacuo* at room temperature overnight afforded di-carboxyl 1,4-PB (1.50 g, ~75% yield) as a clear, colorless polymer. GPC-LS: M_w = 24.0 kg/mol, PDI = 2.03. ^1H NMR (500 MHz, CDCl_3): δ = 8.03 (dd, J = 9.1, 2.5 Hz, ArH, 4H), 6.94 (dd, J =

9.1, 2.5 Hz, ArH, 4H), 5.80 – 5.14 (br, =C(H)CH₂-, 800H, backbone), 4.64 (d, =CHCH₂O-, J = 4.7 Hz, *trans* end group), 4.54 (d, J = 6.0 Hz, =CHCH₂O-, *cis* end group), 2.26 – 1.84 (br, =C(H)CH₂-, 1600H, backbone).

To an anhydrous DCM (20 mL) solution of the di-carboxyl 1,4-PB (1.50 g) in a 50 mL Schlenk reaction were added propargyl alcohol (0.096 g, 1.7 mmol), EDC·HCl (0.198 g, 1.02 mmol), and DMAP (0.008 g, 64.8 μmol). The mixture was degassed by 1 freeze-pump-thaw cycle, and left to stir at room temperature overnight. The reaction mixture was concentrated and precipitated into 100 mL of methanol at 0°C. The resultant polymer was further purified by two cycles of reprecipitation from THF (6 mL) into methanol (100 mL) at 0°C. Drying the precipitated polymer *in vacuo* at room temperature overnight afforded **28** (1.30 g, ~ 86.7% yield) as a clear, yellow polymer. ¹H NMR (500 MHz, CDCl₃): δ = 8.02 (dd, J = 9.1, 2.5 Hz, ArH, 4H), 6.96 – 6.90 (dd, J = 9.1, 2.5 Hz, ArH, 4H), 5.80 – 5.14 (br, =C(H)CH₂-, 800H, backbone), 4.89 (d, J = 2.4 Hz, -OCH₂C≡CH, 4H), 4.63 (d, =CHCH₂O-, J = 4.7 Hz, *trans* end group), 4.53 (d, J = 6.1 Hz, =CHCH₂O-, *cis* end group), 2.50 (t, J = 2.5 Hz, -OCH₂C≡CH, 2H), 2.26 – 1.84 (br, =C(H)CH₂-, 1600H, backbone).

Di-HR macro CTA (29). **27** (0.3 g, 0.5 mmol), **28** (0.5 g), and *N,N,N',N',N''*-pentamethyldiethylenetriamine (PMDETA, 12.5 mg, 71.1 μmol) were dissolved in anhydrous THF (15 mL) in a 50 mL Schlenk flask. The mixture was degassed by 2 freeze-pump-thaw cycles. While the mixture was frozen, copper (I) bromide (Cu(I)Br, 9 mg, 62.8 μmol) was added to the top of the frozen mixture under argon purge. The flask was promptly resealed, pumped, thawed to room temperature, and refilled with argon.

The mixture was stirred at room temperature for 20 min to allow Cu(I)Br and PMDETA to form catalytic complex. The flask was placed in an oil bath at 50°C and left to stir overnight. The reaction mixture was cooled, concentrated *via* rotary evaporation, and precipitated into 100 mL of methanol. The precipitated polymer was further purified by 2 cycles of reprecipitation from THF (5 mL) into methanol (100 mL) at 0°C. Drying the precipitated polymer *in vacuo* at room temperature overnight afforded **29** (0.20 g, ~35% yield) as a brown-yellow polymer. ¹H NMR (500 MHz, CDCl₃) δ = 9.20-9.15 (br, 4H), 8.83 (s, 4H), 8.05 (d, J = 8.0 Hz, 4H), 8.01 (s, 2H), 7.99 – 7.95 (d, 4H), 7.93 (d, J = 8.7 Hz, 4H), 7.78 (t, J = 8.1 Hz, 4H), 7.73 (s, 2H), 7.66 (s, 4H), 6.89 – 6.81 (d, J = 8.7 Hz, 4H), 5.60-5.10 (br, =C(H)CH₂-, backbone), 4.59 (d, =CHCH₂O, trans end group), 4.54 (t, J = 6.4 Hz, 4H), 4.48 (d, =CHCH₂O, cis end group), 4.11 (t, J = 5.6 Hz, 4H), 3.05 (t, J = 6.4 Hz, 4H), 2.58 (t, J = 6.9 Hz, 4H), 2.26 (s, 12H), 2.20 – 1.76 (br, =C(H)CH₂-, backbone).

240K di-HR 1,4-PB (30). Di-HR macro CTA **29** (M_w = 24.0 kg/mol, 0.19g) was dissolved in anhydrous DCM (5 mL) in a 50 mL Schlenk flask. The solution was degassed by 3 freeze-pump-thaw cycles, and the flask was placed in a water bath at 40°C. 0.54 mL of 1 mg/mL DCM solution of Grubbs III was injected into the flask to reach equilibrium with the macro CTA for 1 min. A small amount of degassed, VCH-free COD (0.13 g, 1.22 mmol) was injected into the flask. 3 min later, a large amount of degassed, VCH-free COD (2.00 g, 18.3 mmol) was injected. The mixture was stirred at 40°C for 20 min, and 0.5 mL of 1 mg/mL DCM solution of Grubbs III was injected to the mixture to allow the polymerization to proceed further. The mixture was stirred for another 36 min at 40°C before it was quenched by adding 20 mL of THF + 0.1 g of BHT into the flask.

The diluted mixture was precipitated into 300 mL of ethanol, and the collected polymer was dried *in vacuo* at 35°C overnight, yield a clear, faint-yellow polymer (1.72 g, 74.6%). GPC-LS (THF, 35°C): $M_w = 241.6$ kg/mol, PDI = 1.45.

4.5.3 CAHB-Based DA/DB and TA/TB Pairs

24K di-TE 1,4-PB. Octa-functional tert-butyl ester CTA (0.81 g, 549 μ mol; refer to Section 2.2.1 and Scheme 2.1) was placed in 50 mL Schlenk flask (charged with a stir bar), and degassed by 5 cycles of pulling vacuum/filling argon. Deoxygenated, anhydrous DCM (16 mL) was syringe-transferred into the flask to dissolve the CTA. The flask was placed in an oil bath at 40°C. Grubbs II (4.6 mg, 549 μ mol) in deoxygenated, anhydrous DCM (1 mL) was injected into the mixture to equilibrate with the CTA, followed immediately by adding degassed, VCH-free COD (6.00 g, 54.9 mmol) to the mixture to start the polymerization reaction. The reaction mixture was stirred at 40°C for 16 h, and precipitated into 300 mL of methanol at room temperature. The precipitated polymer was collected and dried *in vacuo* at room temperature overnight. 5.80 g of faint-yellow polymer was afforded (85.3% yield). ^1H NMR (500 MHz, CDCl_3): $\delta = 8.20$ (t, $J = 1.4$ Hz, ArH), 7.76 (d, $J = 1.5$ Hz, ArH), 7.10 (t, $J = 1.5$ Hz, ArH), 6.99 (d, $J = 1.5$ Hz, ArH), 5.62 – 5.22 (br, =C(H)CH₂-, backbone), 5.11 (s, -O-(CH₂)-O-), 4.61 (d, $J = 4.3$ Hz, =CHCH₂O-, *trans* end group), 4.50 (d, $J = 6.0$ Hz, *cis* end group), 2.31 – 1.84 (br, =C(H)CH₂-, backbone). 1.60 (s, -C(CH₃)₃). GPC-LS: $M_w = 23.8$ kg/mol, PDI = 1.88.

24K di-TA 1,4-PB. 24K di-TE 1,4-PB (0.50 g, $M_w = 23.8$ kg/mol, PDI = 1.88) was dissolved in 20 mL of anhydrous THF in a 50 mL Schlenk reactor (charged with a magnetic stir bar). Ground KOH (0.27 g, 4.2 mmol) was added into the reactor. The

mixture was degassed by 2 freeze-pump-thaw cycles, and stirred vigorously at room temperature for 16 h. 1 mL of 12 M HCl(aq) in 6 mL of THF was slowly added to the reaction mixture to quench excess KOH and protonate the carboxylate salts. The mixture was filtered, concentrated *via* rotary evaporation at 35°C, and drop-wise precipitated into 100 mL of methanol at 0°C. The resultant polymer was further purified by two cycles of reprecipitation from THF (5 mL) into methanol (100 mL) at 0°C. Drying the collected polymer *in vacuo* at room temperature overnight afforded 24K di-TA 1,4-PB (0.36 g, ~72% yield) as a white, opaque polymer.

204K Tetra-functional azido-terminated 1,4-PB. Tetra-functional chloro-terminated 1,4-PB ($M_w = 204$ kg/mol, 0.50 g; see Appendix A) was dissolved in anhydrous THF (8 mL) in a 50 mL Schlenk flask. Anhydrous THF (2 mL) solution of azidotrimethylsilane (TMSN_3 , 0.12 g, 980 μmol) and tetrabutylammonium fluoride monohydrate ($\text{TBAF}\cdot\text{H}_2\text{O}$, 0.26 g, 1.0 mmol) was added to the polymer solution. The mixture was degassed by 3 freeze-pump-thaw cycles, and stirred at 60°C under argon atmosphere overnight. After cooling to room temperature, the reaction mixture was precipitated into 100 mL of acetone at room temperature. The precipitated polymer was re-dissolved in 10 mL of THF, and the resultant solution was precipitated into 100 mL of acetone at room temperature. The precipitated polymer was collected and dried *in vacuo* at room temperature overnight. 0.49 g of faint-yellow, transparent polymer was afforded (98.0% yield).

204K di-DB 1,4-PB. 204K tetra-functional azido-terminated 1,4-PB was dissolved in anhydrous THF (6 mL) in a 50 mL Schlenk flask, followed by the addition of *N,N*-

dimethyl propargylamine (0.15 g, 1.8 mmol) and PMDETA (8.5 mg, 49 μ mol). The mixture was degassed by 2 freeze-pump-thaw cycles, and then frozen again. Cu(I)Br (6 mg, 42 μ mol) was added into the flask under argon flow while the mixture was still frozen. The mixture was degassed again, and stirred at room temperature under argon atmosphere for 16 h. The resultant polymer was purified by 5 times of reprecipitation from 10 mL of THF into 150 mL of methanol at room temperature, followed by drying *in vacuo* at room temperature overnight. 0.39 g of faint-yellow, transparent polymer was afforded (78.0% yield).

22K Octa-functional azido-terminated 1,4-PB. 22K octa-functional chloro-terminated 1,4-PB ($M_w = 21.7$ kg/mol, 1.50 g; see Appendix A) was dissolved in anhydrous THF (25 mL) in a 50 mL Schlenk flask. An anhydrous THF (15 mL) solution of TMSN₃ (1.33 g, 11.0 mmol) and TBAF·H₂O (2.90 g, 11.2 mmol) was added to the polymer solution. The mixture was degassed by 2 freeze-pump-thaw cycles. The mixture was stirred at 60°C under argon atmosphere overnight. After cooling to room temperature, the reaction mixture was precipitated into 300 mL of acetone at room temperature. The precipitated polymer was re-dissolved in 20 mL of THF, and the resultant solution was precipitated into 300 mL of acetone at 0°C. The precipitated polymer was collected, purified by 2 more cycles of reprecipitation from THF (10 mL) into 200 mL of methanol at 0°C, and dried *in vacuo* at room temperature overnight. 1.30 g of faint-yellow, transparent polymer was afforded (94.9% yield). ¹H NMR (500 MHz, CDCl₃): $\delta = 7.07$ (s, ArH), 6.96 (d, J = 1.5 Hz, ArH), 6.90 (d, J = 1.5 Hz, ArH), 6.87 (d, J = 1.5 Hz, ArH), 5.55 – 5.22 (br, =C(H)CH₂-, backbone), 5.07 (s, -O-(CH₂)-O-), 4.60 (d, J = 4.3 Hz, =CHCH₂O-, *trans* end

group), 4.50 (d, $J = 6.0$ Hz, *cis* end group), 4.33 (s, $-\text{CH}_2\text{-N}_3$), 2.31 – 1.84 (br, $=\text{C}(\text{H})\text{CH}_2-$, backbone).

22K di-TB 1,4-PB. 22K octa-functional azido-terminated 1,4-PB was dissolved in anhydrous THF (20 mL) in a 50 mL Schlenk flask, followed by addition of *N,N*-dimethyl propargylamine (0.36 g, 4.2 mmol) and PMDETA (8.3 mg, 47.4 mmol). The mixture was degassed by 2 freeze-pump-thaw cycles, and then frozen again. Cu(I)Br (11 mg, 76.7 mmol) was added into the flask under argon flow while the mixture was still frozen. The mixture was degassed again, and stirred at room temperature under argon atmosphere for 16 h. The resultant polymer was purified by 3 times of reprecipitation from 20 mL of THF into 300 mL of methanol at room temperature, followed by drying *in vacuo* at room temperature overnight. 1.20 g of faint-yellow, transparent polymer was afforded (92.3% yield). ^1H NMR (500 MHz, CDCl_3): $\delta = 7.43$ (s, triazole proton), 6.95 (s, *ArH*), 6.88 (d, $J = 1.5$ Hz, *ArH*), 6.82 (d, $J = 1.5$ Hz, *ArH*), 6.77 (s, *ArH*), 5.63 – 5.18 (br, $=\text{CHCH}_2-$, backbone), 4.94 (s, $-\text{O}-\text{CH}_2-\text{O}-$), 4.58 (d, $J = 4.2$ Hz, $=\text{CHCH}_2\text{O}-$, *trans* end group), 4.47 (d, $J = 6.0$ Hz, $=\text{CHCH}_2\text{O}-$, *cis* end group), 3.59 (s, $-\text{CH}_2-\text{N}(\text{CH}_3)_2$), 2.26 (s, $-\text{CH}_2-\text{N}(\text{CH}_3)_2$), 2.18 – 1.89 (br, $=\text{CHCH}_2-$, backbone).

250K Octa-functional azido-terminated 1,4-PB. Octa-functional chloro-terminated 1,4-PB ($M_w = 254$ kg/mol, 1.37 g; see Appendix A) was dissolved in anhydrous THF (25 mL) in a 50 mL Schlenk flask. An anhydrous THF (15 mL) solution of TMSN_3 (1.33 g, 11.0 mmol) and TBAF $\cdot\text{H}_2\text{O}$ (2.90 g, 11.2 mmol) was added to the polymer solution. The mixture was degassed by 2 freeze-pump-thaw cycles. The mixture was stirred at 60°C under argon atmosphere overnight. After cooling to room temperature, the reaction

mixture was precipitated into 300 mL of acetone at room temperature. The precipitated polymer was re-dissolved with 20 mL of THF, and the polymer solution was precipitated into 300 mL of acetone. The precipitated polymer was collected and dried *in vacuo* at room temperature overnight. 1.30 g of faint-yellow, transparent polymer was afforded (94.9% yield).

250K di-TB 1,4-PB. Octa-functional azido-terminated 1,4-PB ($M_w = 254$ kg/mol, 1.30 g) was dissolved with anhydrous THF (20 mL) in a 50 mL Schlenk flask, followed by addition of *N,N*-dimethyl propargylamine (0.36 g, 4.2 mmol) and PMDETA (8.3 mg, 47.4 mmol). The mixture was degassed by 2 freeze-pump-thaw cycles, and then frozen again. Cu(I)Br (11 mg, 76.7 mmol) was added into the flask under argon flow while the mixture was still frozen. The mixture was degassed again, and stirred at room temperature under argon atmosphere for 16 h. The resultant polymer was purified by 3 times of reprecipitation from 20 mL of THF into 300 mL of methanol at room temperature, followed by drying *in vacuo* at room temperature overnight. 1.20 g of faint-yellow, transparent polymer was afforded (92.3% yield).

4.5.4 ^1H NMR Study of Hetero-Complementary End-Association

^1H NMR study of hetero-complementary end-association of telechelic 1,4-PB chains was carried out at a total polymer concentration of $\sim 1\text{wt}\%$ in deuterated chloroform (CDCl_3) at room temperature. ^1H NMR samples of individual telechelic associative polymers were prepared by combining polymer and CDCl_3 at a polymer concentration $\sim 1\text{wt}\%$ in 20 mL scintillation vials, which were placed on a Wrist-Action Shaker (Burrell Scientific) for up to 16 h to allow the polymer to completely dissolve. ^1H

NMR samples of complementary polymer pairs were prepared by mixing ~1wt% CDCl_3 solutions of their corresponding polymers in 20 mL scintillation vials in desired end-group ratios, except for the 1:1 (w/w) mixture of 24K di-**TA**/22K di-**TB** 1,4-PBs, of which the ^1H NMR sample was prepared by combining the two polymers at a 1:1 weight ratio and CDCl_3 at a total polymer concentration ~ 1wt% in a 20 mL scintillation vial that was placed on a Wrist-Action Shaker (Burrell Scientific) for 16 h at room temperature.

The investigation of hetero-complementary end-association by ^1H NMR spectroscopy was carried out by measuring the ^1H NMR spectra of individual telechelic associative polymers and those of complementary polymer pairs, followed by comparing signals of protons participating hetero-complementary end-association in ^1H NMR spectra of individual polymer solutions to those of the same protons in the spectra of corresponding polymer mixtures. Due to the inherent detection limit of ^1H NMR spectroscopy, either changes in chemical shifts or the disappearance of the signals of protons participating hetero-complementary association of polymer end-groups were followed as the evidence of end-association, depending on the sizes of polymer backbones. For telechelic associative polymers of $M_w \leq 50$ kg/mol, characteristic shifts of signals of associative end-groups were followed; for those of $M_w \geq 200$ kg/mol, the focus was whether the mixing of complementary partners caused the disappearance of the signals of protons participating hetero-complementary association of polymer end-groups.

4.5.5 Shear Viscometric Study of Hetero-Complementary End-Association

Shear viscometry was used as a complementary measure of ^1H NMR study to evaluate the strength of hetero-complementary pairs. 1-chlorododecane (CDD) was

chosen as the solvent due to its low interference with hydrogen bonding, low volatility at room temperature, high solvency for 1,4-PB backbones, and being a pure solvent. For all of the four hetero-complementary pairs (**THY/DAAP**, **HR/CA**, **DA/DB**, and **TA/TB**), telechelic polymers of $M_w \sim 200$ kg/mol were used. In addition to CDD, dodecane and Jet-A were also used in shear viscometric study of **THY/DAAP** and **HR/CA** pairs, respectively. Except for di-**DA** and di-**TA** 1,4-PBs, polymer solutions in 1-chlorododecane were prepared by combining polymer and solvent at a weight fraction of polymer = 1wt% in clean 20 mL scintillation vials, which were placed on a Wrist-Action Shaker (Burrell Scientific) at room temperature for up to 16 h to allow complete dissolution of polymers. 1wt% CDD solutions of di-**DA** and di-**TA** 1,4-PBs of $M_w \sim 200$ kg/mol were prepared according to the procedure described in Chapter 3 (Section 3.2.2). For each hetero-complementary associative pair, 1wt% solutions of polymer mixture were prepared by mixing 1wt% solutions of the individual polymers in desired weight ratios in 20 mL scintillation vials at room temperature. Shear viscosity of polymer solutions were measured according to the procedure described in Chapter 3 (Section 3.2.3).

4.6 Figures, Schemes, and Tables

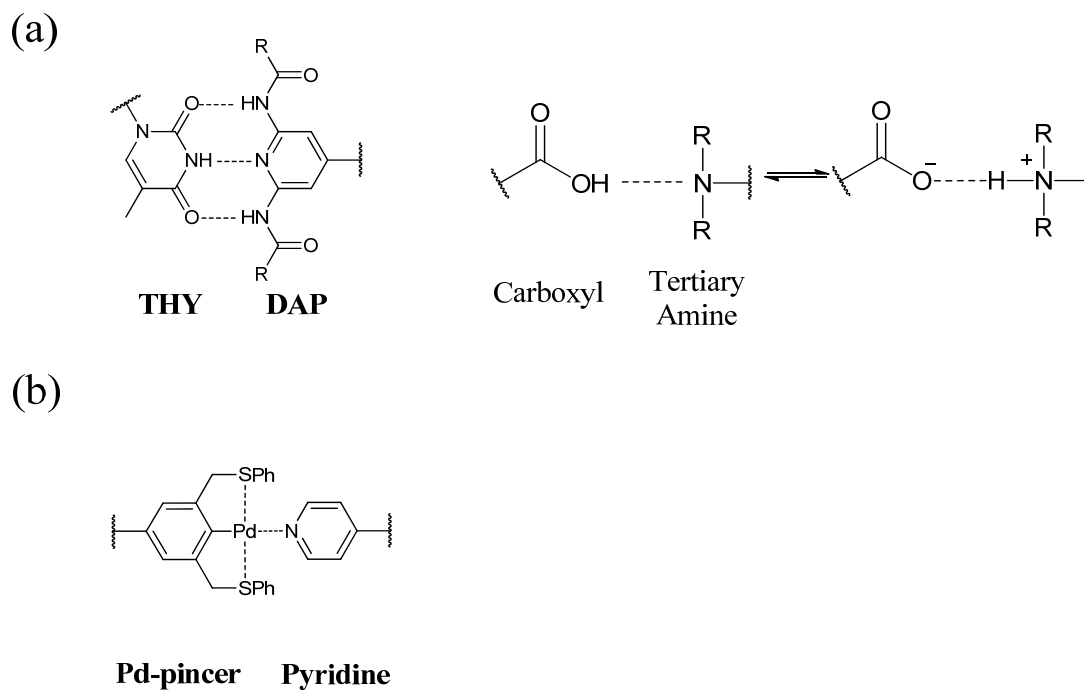


Figure 4.1 Representative examples of directional noncovalent bondings. (a) Directional hydrogen bonding (Left: hetero-complementary thymine (**THY**)/diamidopyridine (**DAP**) interaction;¹¹ Right: carboxyl/tertiary amine charge-assisted hydrogen bonding.² (b) Metal coordination interaction (palladated-pincer complex/pyridine interaction).⁹

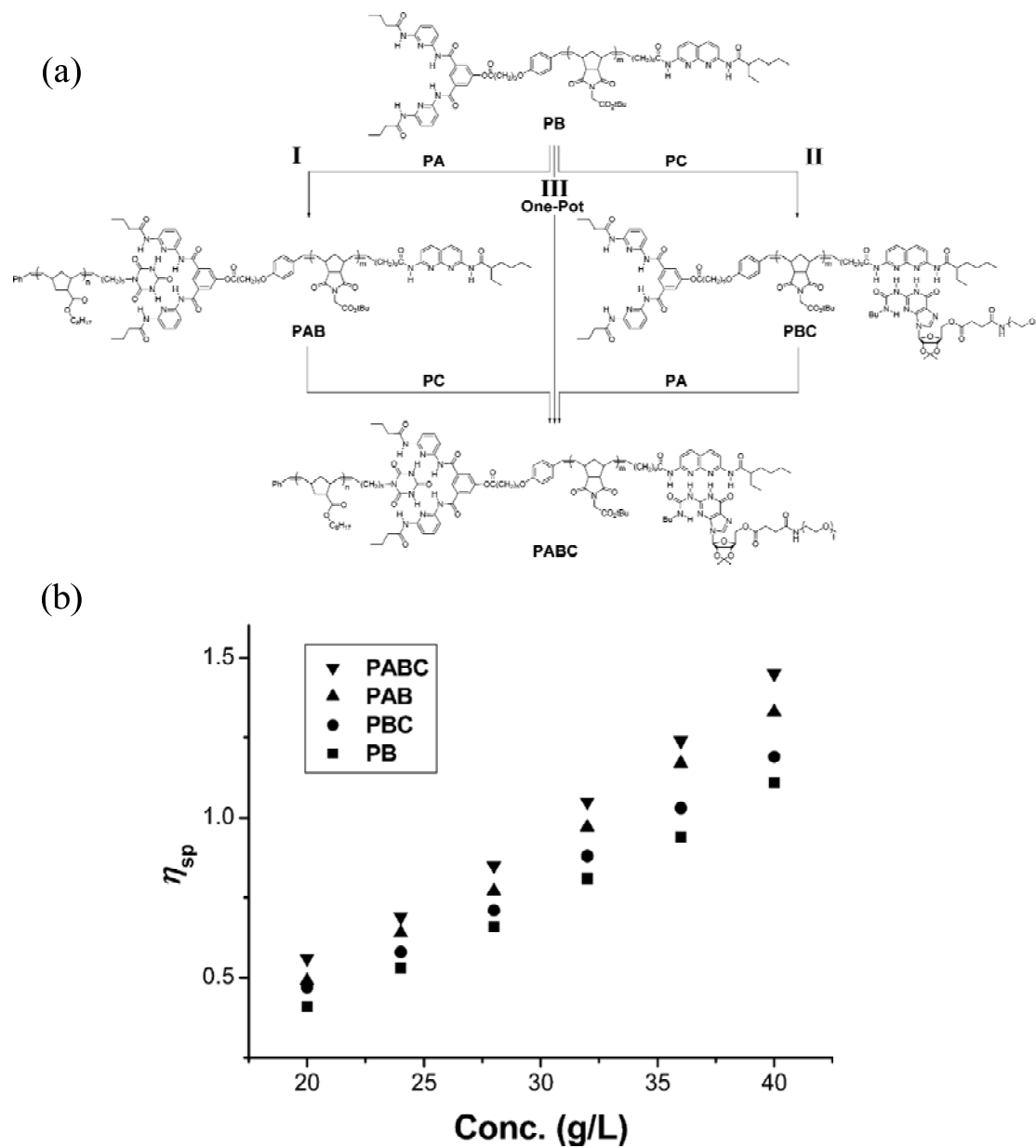


Figure 4.2 (a) Structures of polymers PA, PB, PC and step-wise self-assembly of supramolecular triblock copolymer. (b) Plot of specific viscosity versus concentration for PB and supramolecular block copolymers (Adapted from Yang et al.²¹ and reproduced with permission).

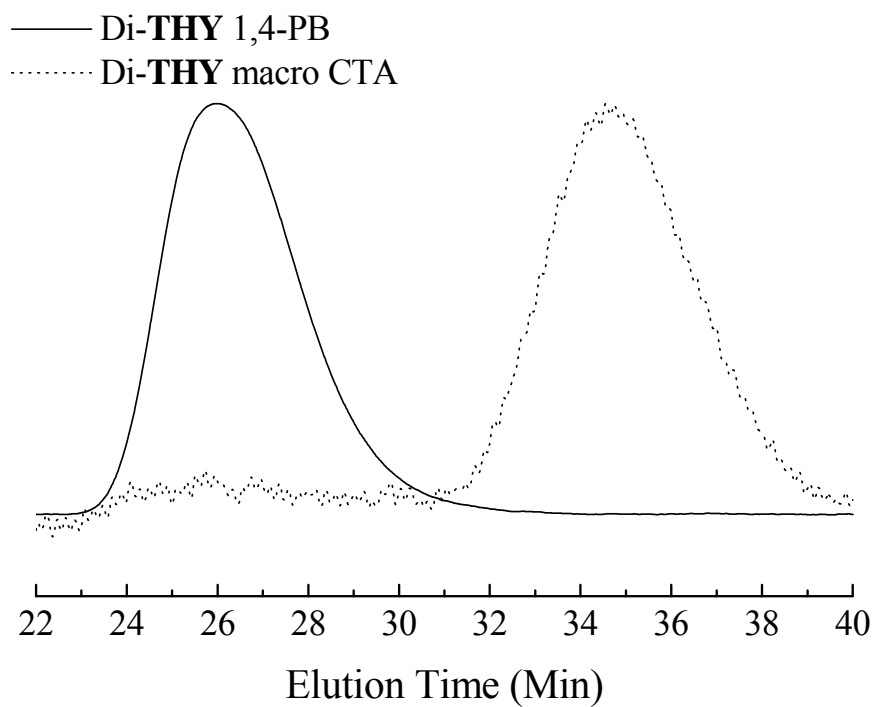


Figure 4.3 GPC-LS traces of di-**THY** macro CTA and the corresponding 288K di-**THY** 1,4-PB. Note that the superposition indicates complete consumption of di-**THY** macro CTA in the synthesis of 288K di-**THY** 1,4-PB.

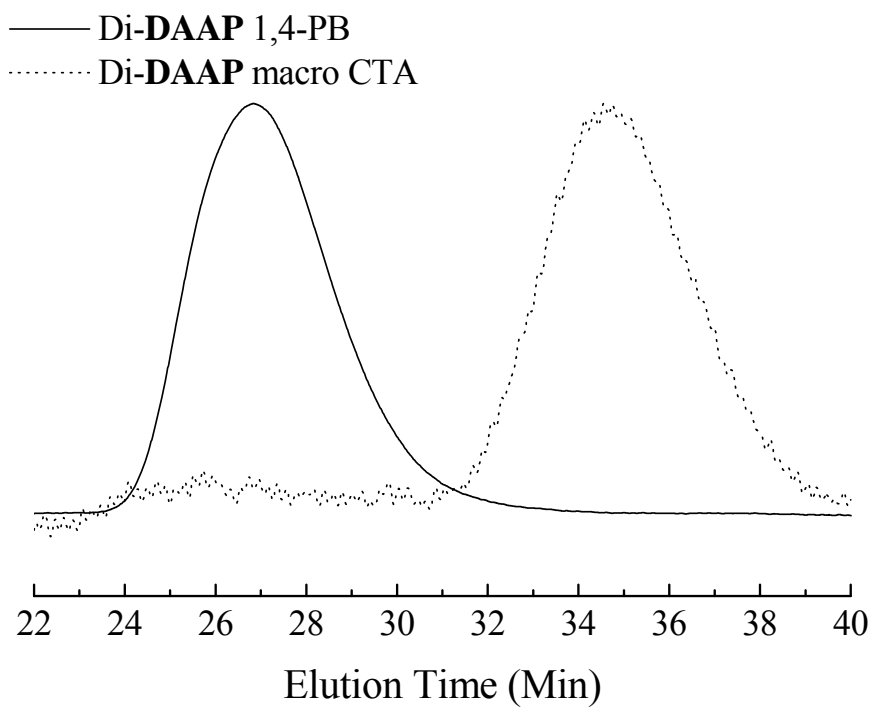


Figure 4.4 GPC-LS traces of di-**DAAP** macro CTA and the corresponding 219K di-**DAAP** 1,4-PB. Note that the superposition indicates complete consumption of di-**DAAP** macro CTA in the synthesis of 219K di-**DAAP** 1,4-PB.

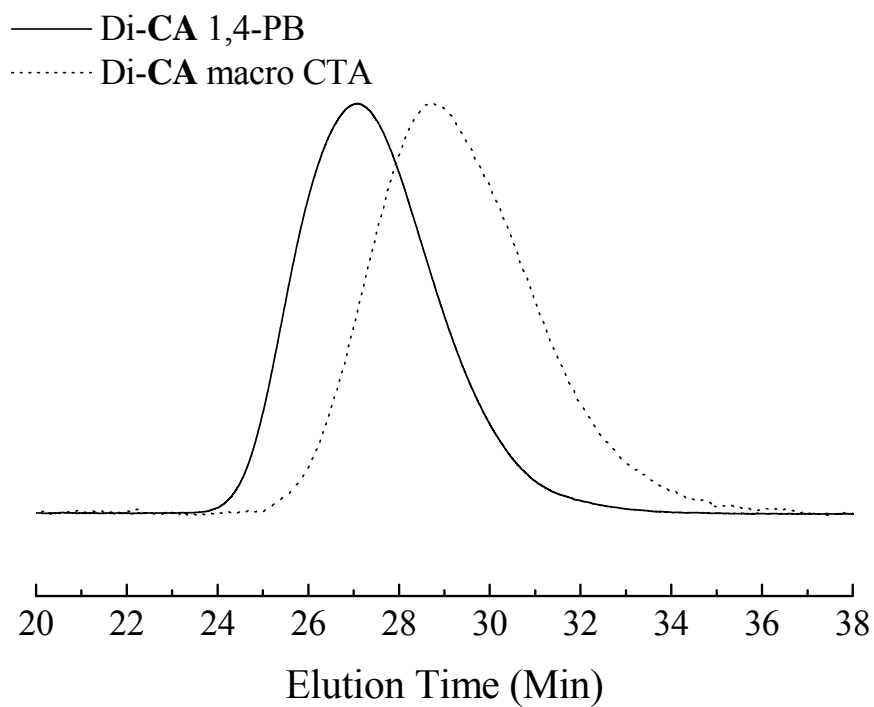


Figure 4.5 GPC-LS traces of di-CA macro CTA and the corresponding 200K di-CA 1,4-PB. Note that the superposition indicates complete consumption of di-CA macro CTA in the synthesis of 200K di-CA 1,4-PB.

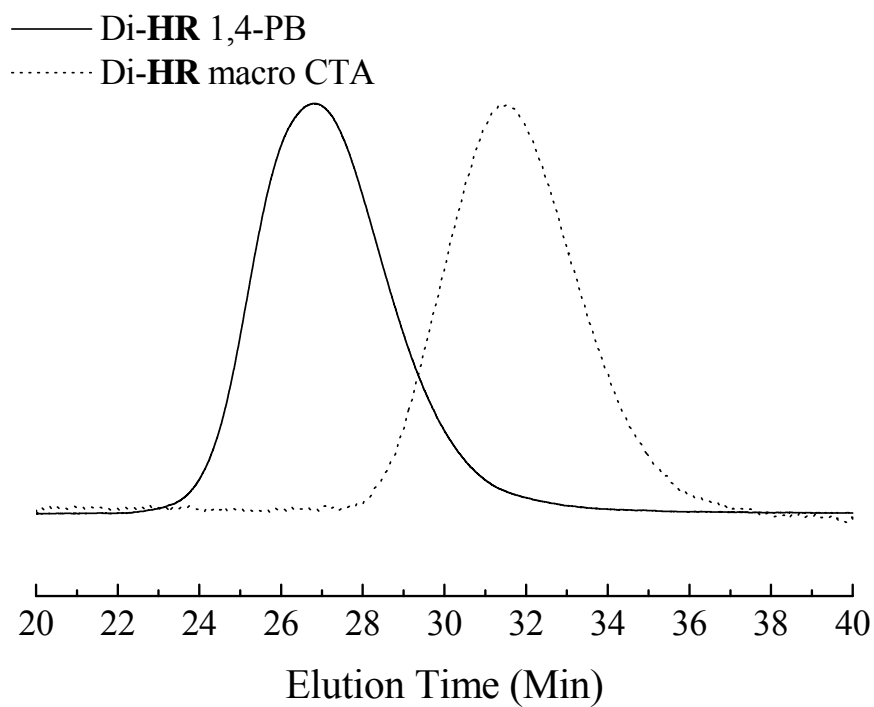


Figure 4.6 GPC-LS traces of di-**HR** macro CTA and the corresponding 240K di-**HR** 1,4-PB. Note that the superposition indicates complete consumption of di-**HR** macro CTA in the synthesis of 240K di-**HR** 1,4-PB.

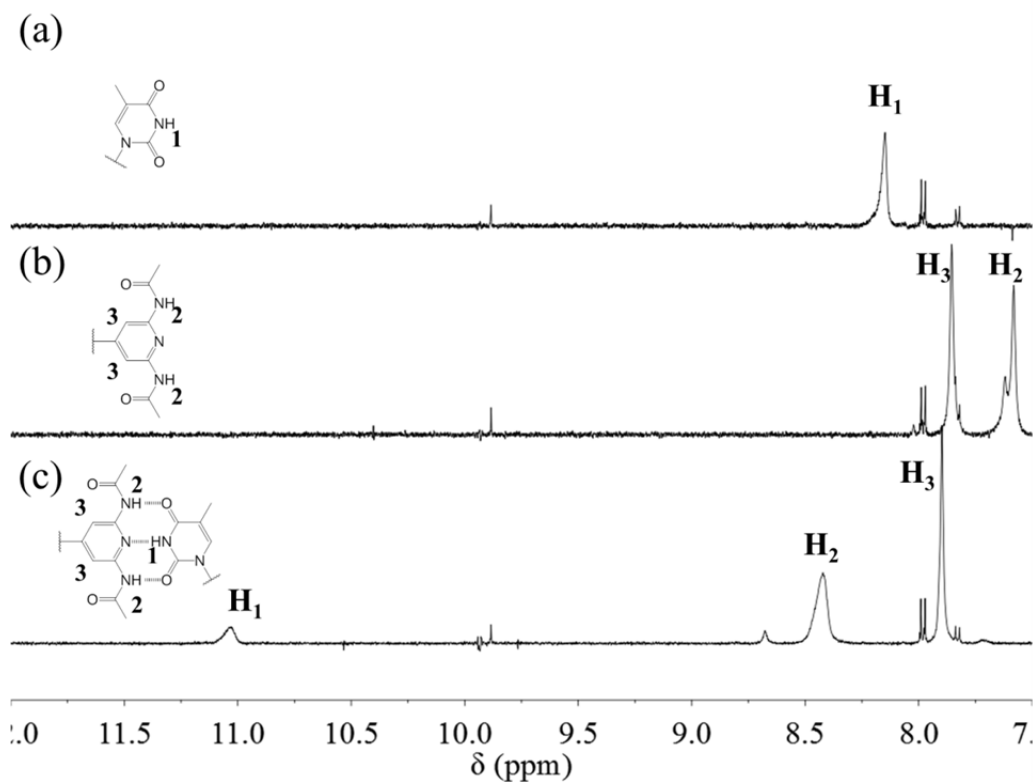


Figure 4.7 Expanded ^1H NMR (500 MHz) spectra of CDCl_3 solutions of telechelic polymers that have a 10 kg/mol 1,4-PB backbone with end groups that are (a) **THY**, (b) **DAAP**, and (c) a mixture of the two polymers with a mass ratio of 1:2, which represents a stoichiometric ratio of approximately 1:2. The concentration of polymer in solution is approximate 1wt%.

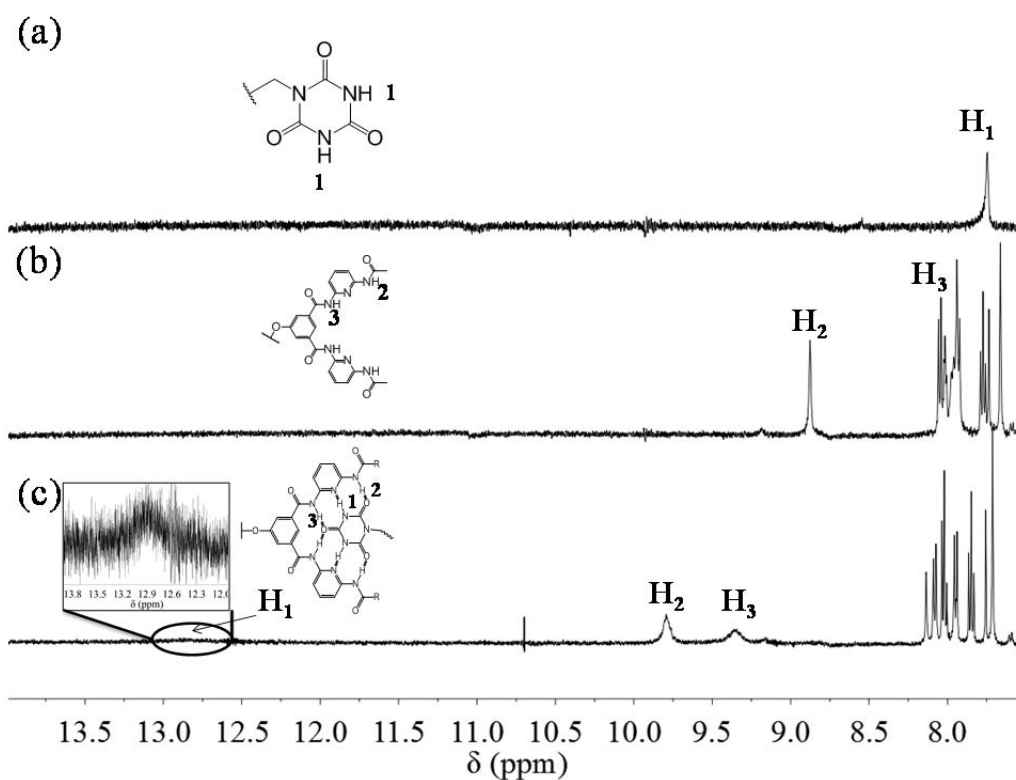


Figure 4.8 Expanded ^1H NMR (500 MHz) spectra of CDCl_3 solutions of telechelic polymers that are (a) 1,4-PB of $M_w = 50$ kg/mol with **CA** end groups, (b) 1,4-PB of $M_w = 24$ kg/mol with **HR** end groups, and (c) a mixture of the two polymers with a mass ratio of 1:1.4, which represents a stoichiometric ratio of **CA:HR** of approximately 1:2. The concentration of polymer in solution is approximate 1wt%.

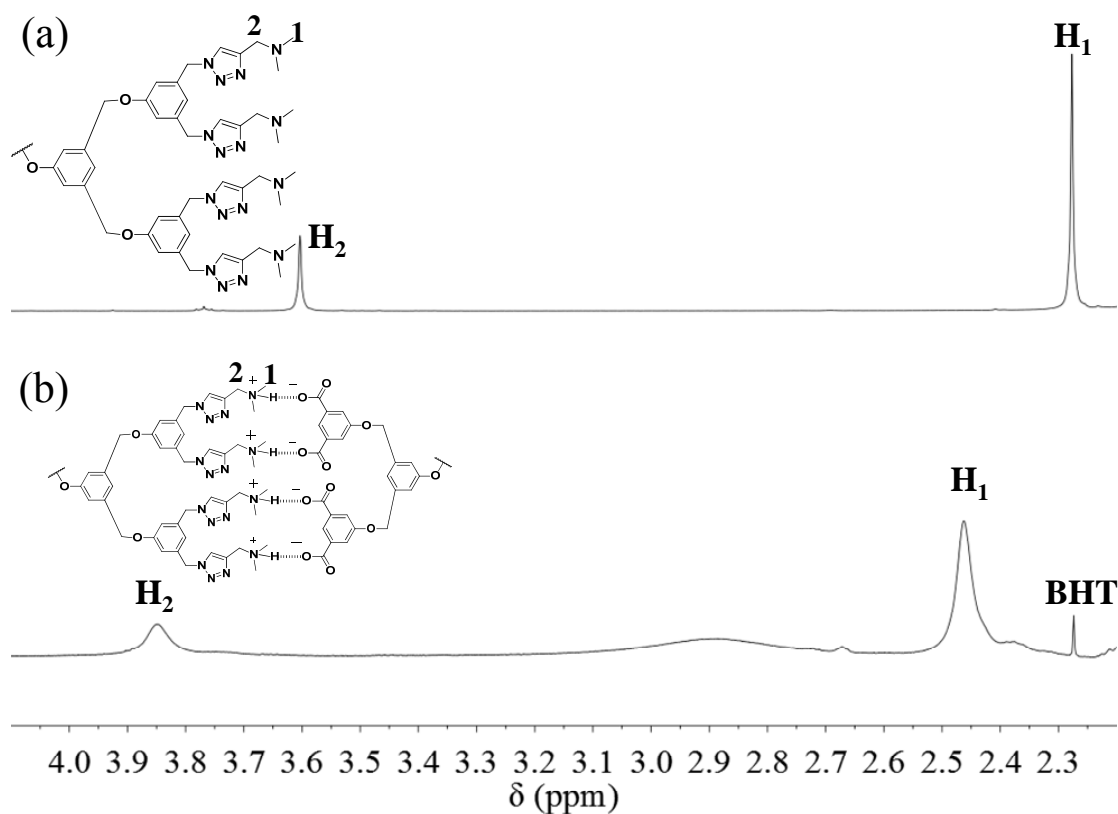


Figure 4.9 Expanded ^1H NMR (500 MHz) spectra of CDCl_3 solutions of telechelic polymers that are (a) 1,4-PB of $M_w = 22$ kg/mol with **TB** end groups, (b) a mixture of 1,4-PB of $M_w = 22$ kg/mol with **TB** end groups and 1,4-PB of $M_w = 22$ kg/mol with **TA** end groups two polymers with a mass ratio of 1:1. The concentration of polymer in solution is approximate 1wt%.

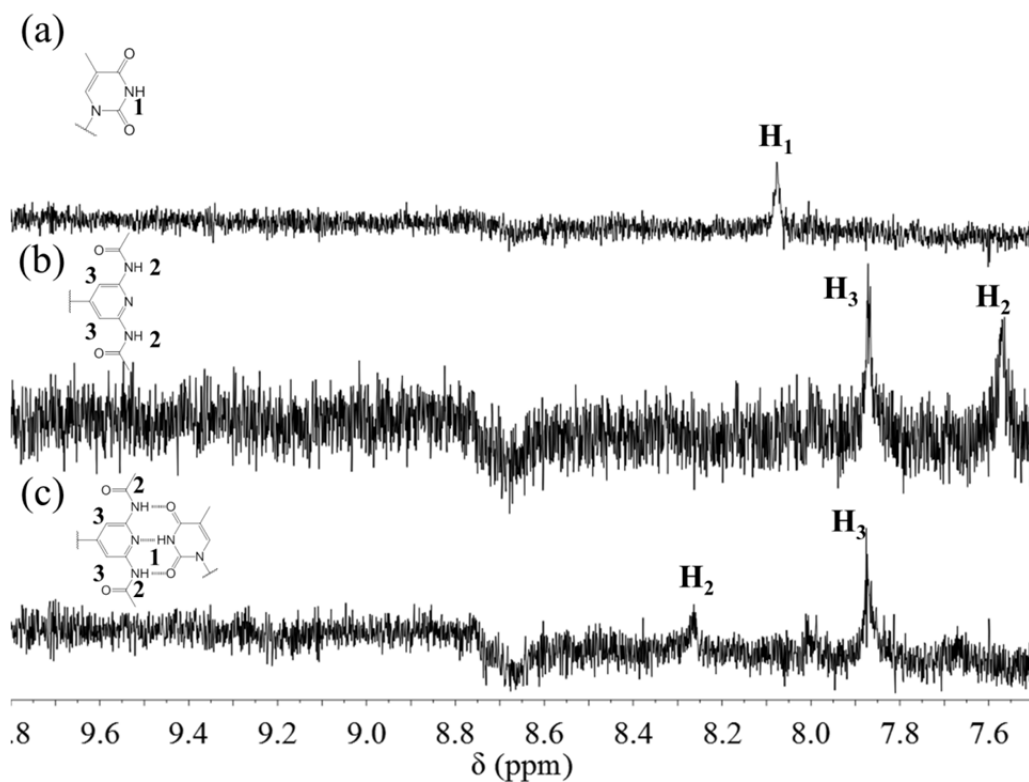


Figure 4.10 Expanded ^1H NMR (500 MHz) spectra of CDCl_3 solutions of telechelic polymers that are (a) 1,4-PB of $M_w = 288$ kg/mol with **THY** end groups, (b) 1,4-PB of $M_w = 219$ kg/mol with **DAAP** end groups, and (c) a mixture of the two polymers with a mass ratio of 1:2. The concentration of polymer in solution is approximate 1wt%.

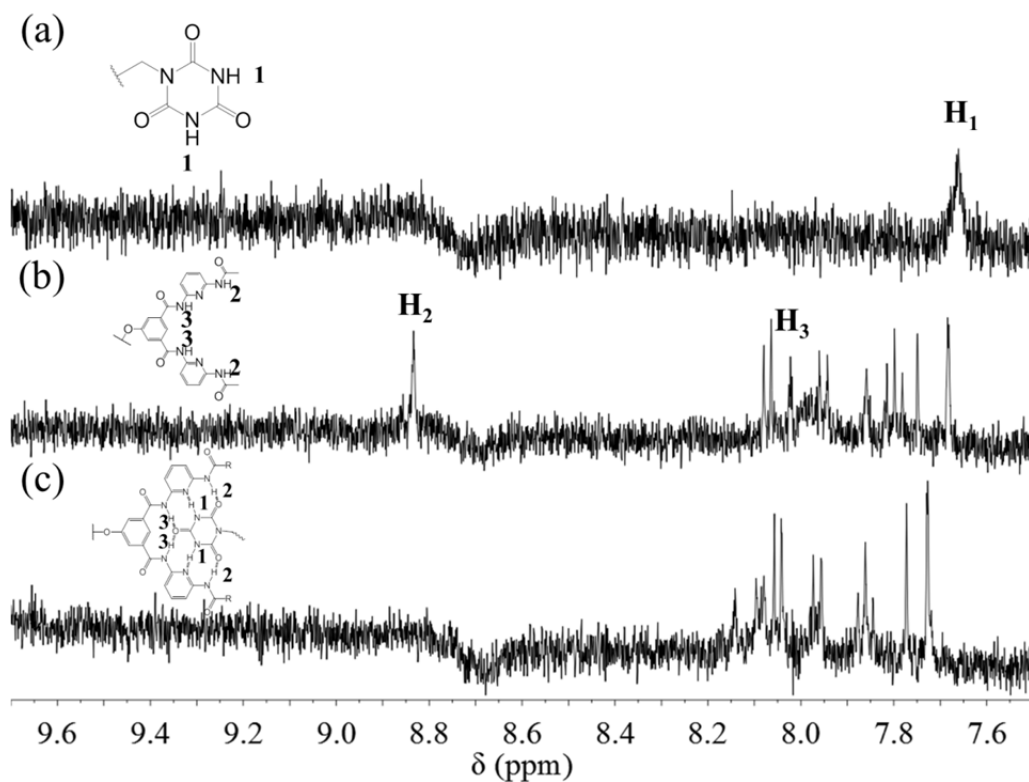


Figure 4.11 Expanded ^1H NMR (500 MHz) spectra of CDCl_3 solutions of telechelic polymers that are (a) 1,4-PB of $M_w = 200$ kg/mol with **CA** end groups, (b) 1,4-PB of $M_w = 240$ kg/mol with **HR** end groups, and (c) a mixture of the two polymers with a mass ratio of 1:2. The concentration of polymer in solution is approximate 1wt%.

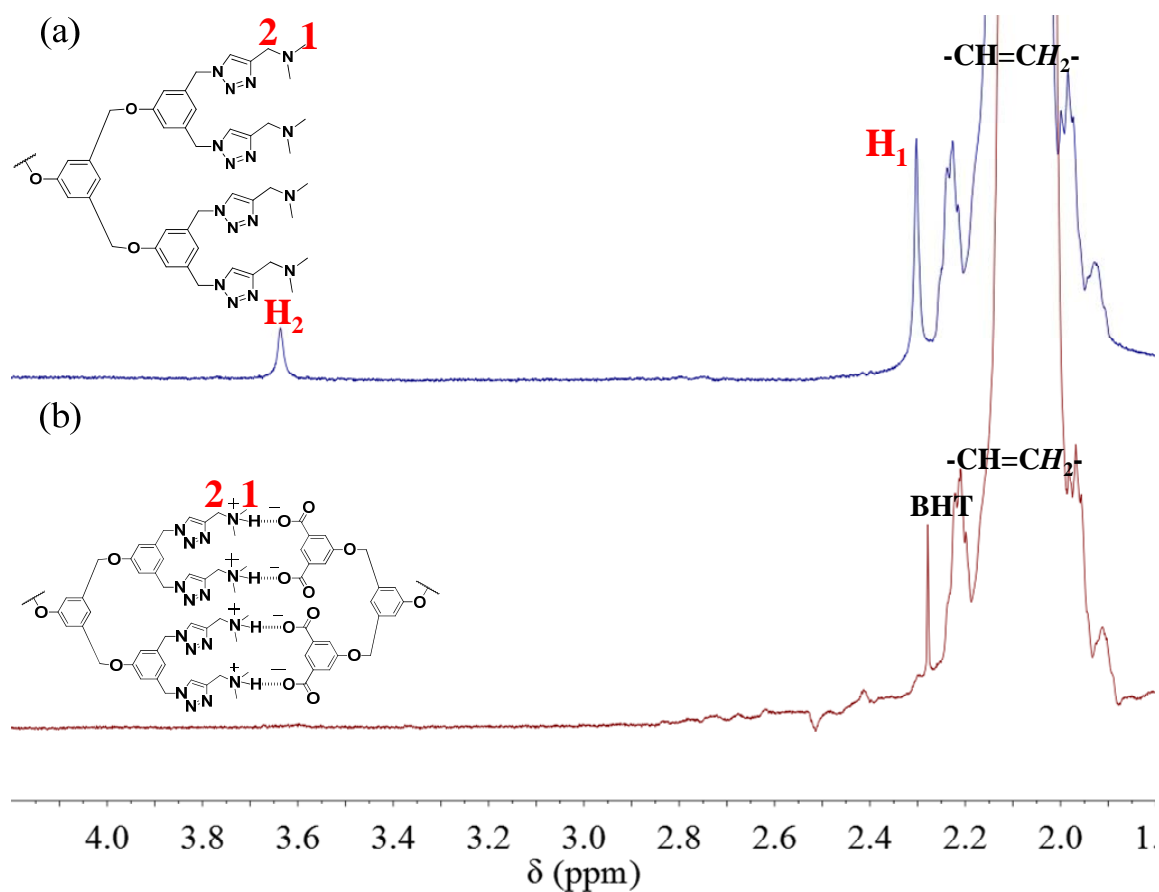


Figure 4.12 Expanded ^1H NMR (500 MHz) spectra of CDCl_3 solutions of telechelic polymers that are (a) 1,4-PB of $M_w = 250$ kg/mol with **TB** end groups, (b) a mixture of 1,4-PB of $M_w = 250$ kg/mol with **TB** end groups and 1,4-PB of $M_w = 230$ kg/mol with **TA** end groups two polymers with a mass ratio of 1:1. The concentration of polymer in solution is approximate 1wt%.

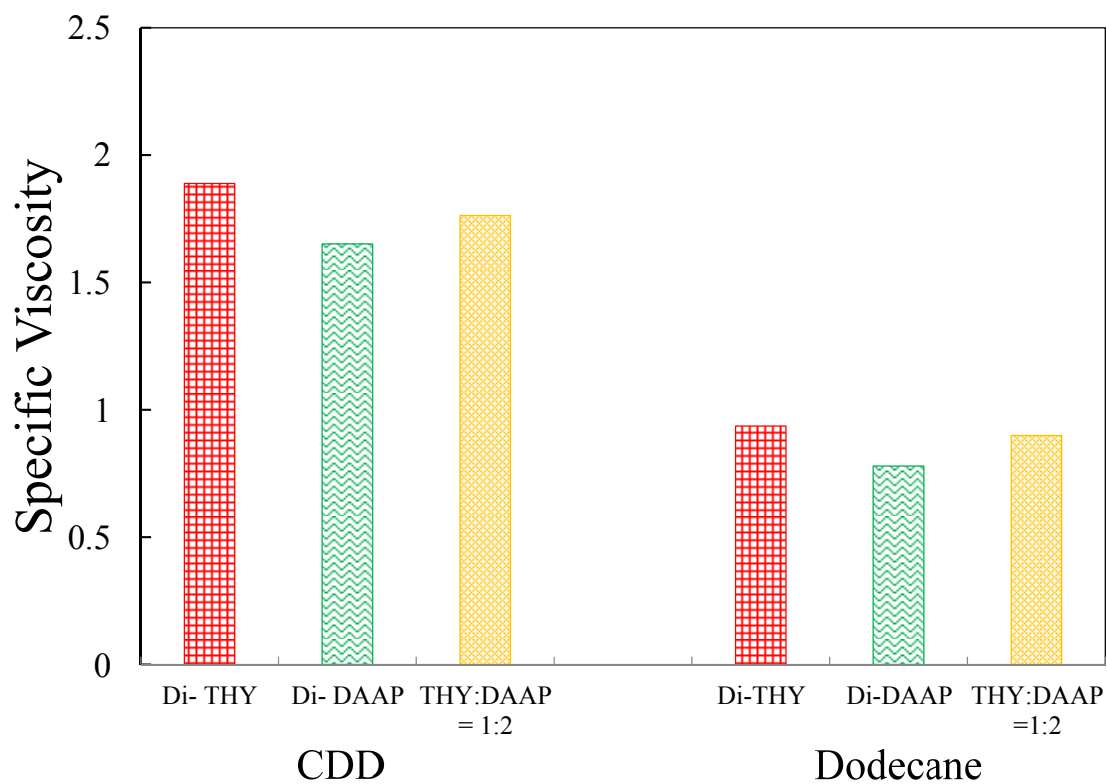


Figure 4.13 Specific viscosity (25°C) of 1wt% 1-chlorododecane (CDD) and dodecane solutions of 288K di-**THY** 1,4-PB, 219K di-**DAAP** 1,4-PB, and 1:2 (w/w) mixture of 288K di-**THY** 1,4-PB and 219K di-**DAAP** 1,4-PB.

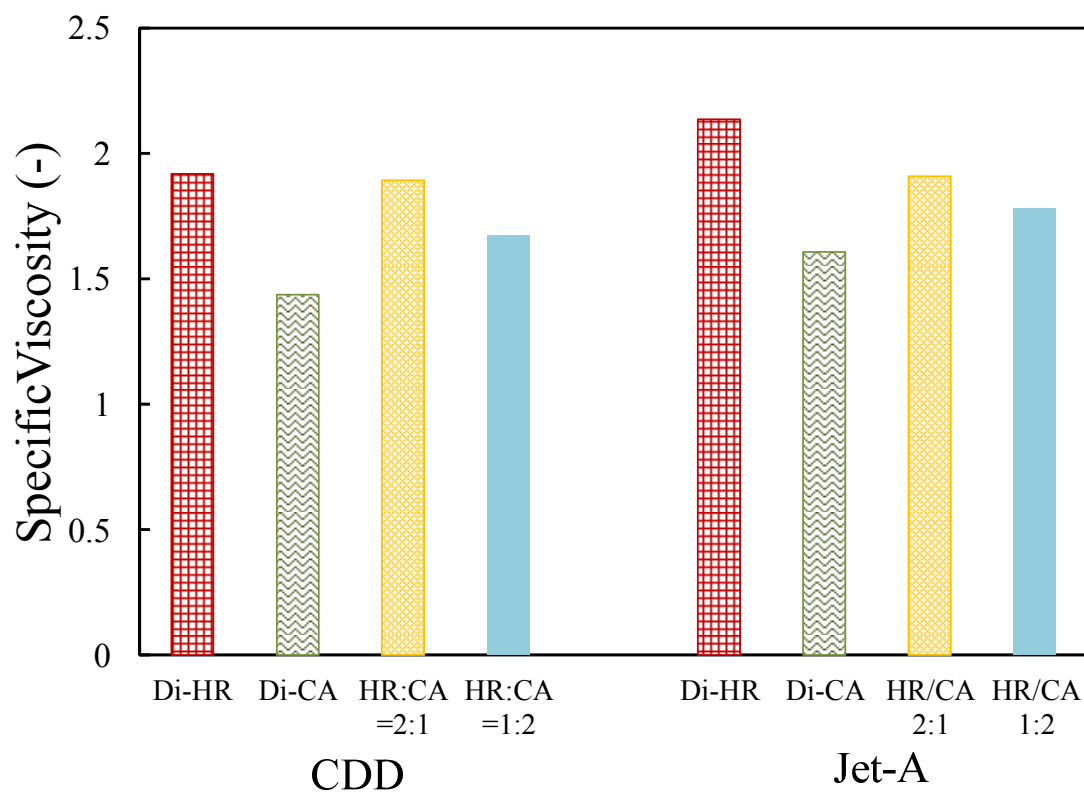


Figure 4.14 Specific viscosity (25°C) of 1wt% 1-chlorododecane (CDD) and Jet-A solutions of 240K di-**HR** 1,4-PB, 200K di-**CA** 1,4-PB, and 1:2 and 2:1 (w/w) mixtures of 240K di-**HR** 1,4-PB and 200K di-**CA** 1,4-PB.

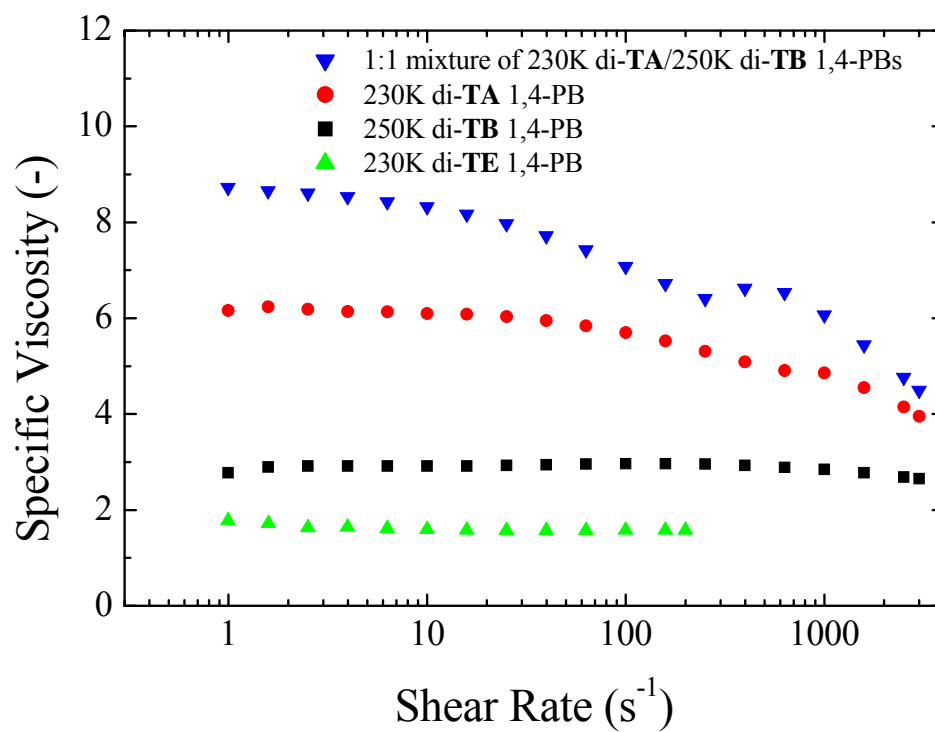


Figure 4.15 Specific viscosity (25°C) of 1wt% CDD solutions of 230K di-TE 1,4-PB, 230K di-TA 1,4-PB, 250K di-TB 1,4-PB, and the 1:1 (w/w) mixture of 230K di-TA 1,4-PB and 250K di-TB 1,4-PB at shear rates 1-3000 s⁻¹.

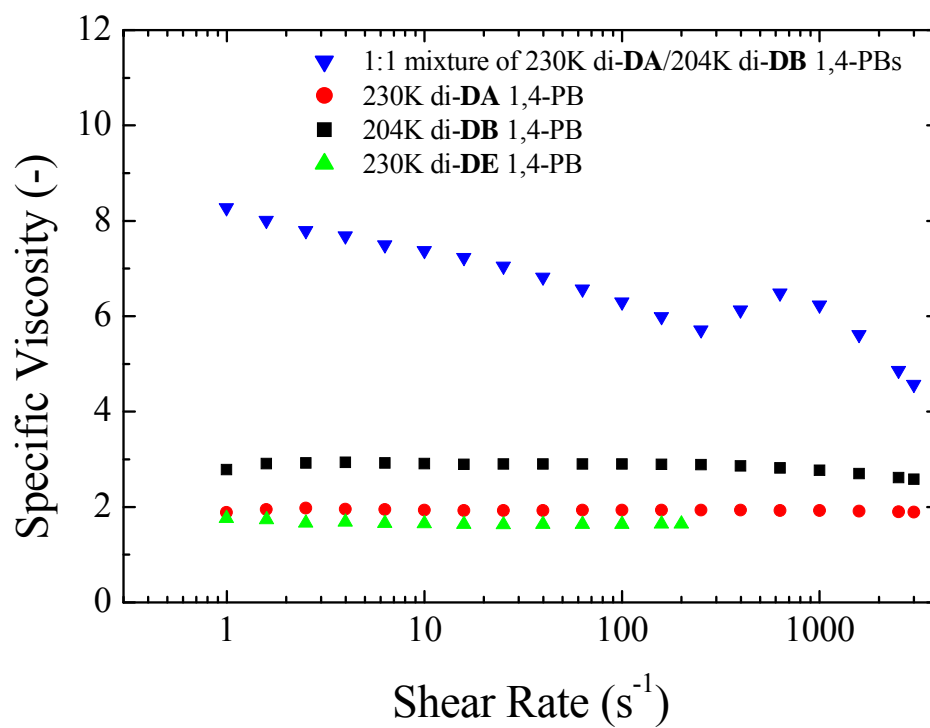


Figure 4.16 Specific viscosity (25°C) of 1wt% CDD solutions of 230K di-DE 1,4-PB, 230K di-DA 1,4-PB, 204K di-DB 1,4-PB, and the 1:1 (w/w) mixture of 230K di-DA 1,4-PB and 204K di-DB 1,4-PB at shear rates 1-3000 s⁻¹.

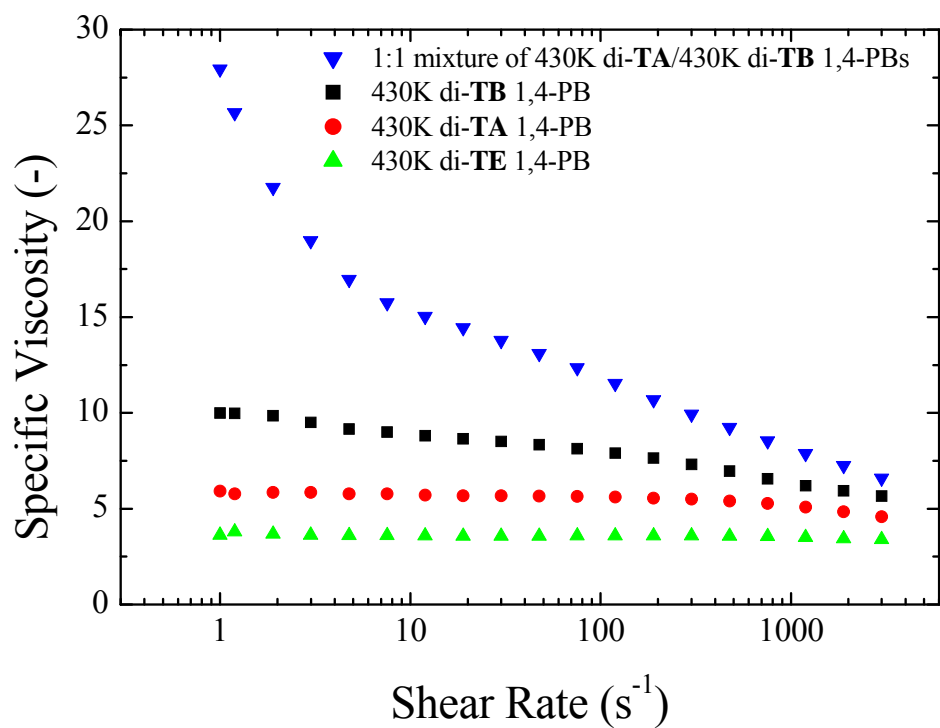


Figure 4.17 Specific viscosity (25°C) of 1wt% Jet-A solutions of 430K di-TE 1,4-PB, 430K di-TA 1,4-PB, 430K di-TB 1,4-PB, and the 1:1 (w/w) mixture of 430K di-TA 1,4-PB and 430K di-TB 1,4-PB at shear rates 1-3000 s^{-1} .

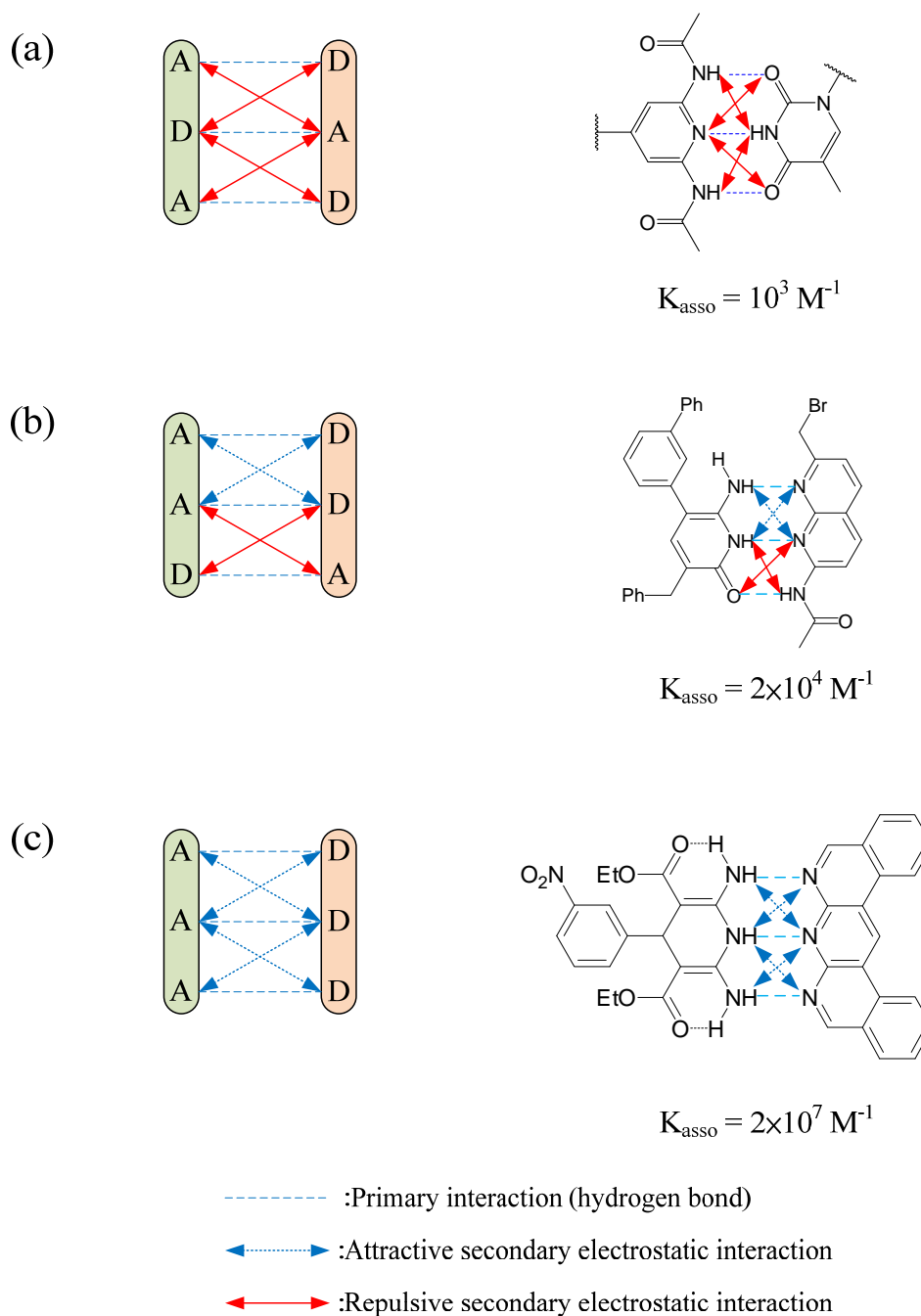


Figure 4.18 Secondary-electrostatic-interaction (SEI) analysis of all possible hydrogen-bond donor (D) and acceptor (A) site arrangements for triple-hydrogen-bonding hetero-complementary associative pairs and their representative examples. (a) ADA-DAD;⁷⁶ (b) AAD-DDD;⁷¹ (c) AAA-DDD.⁸

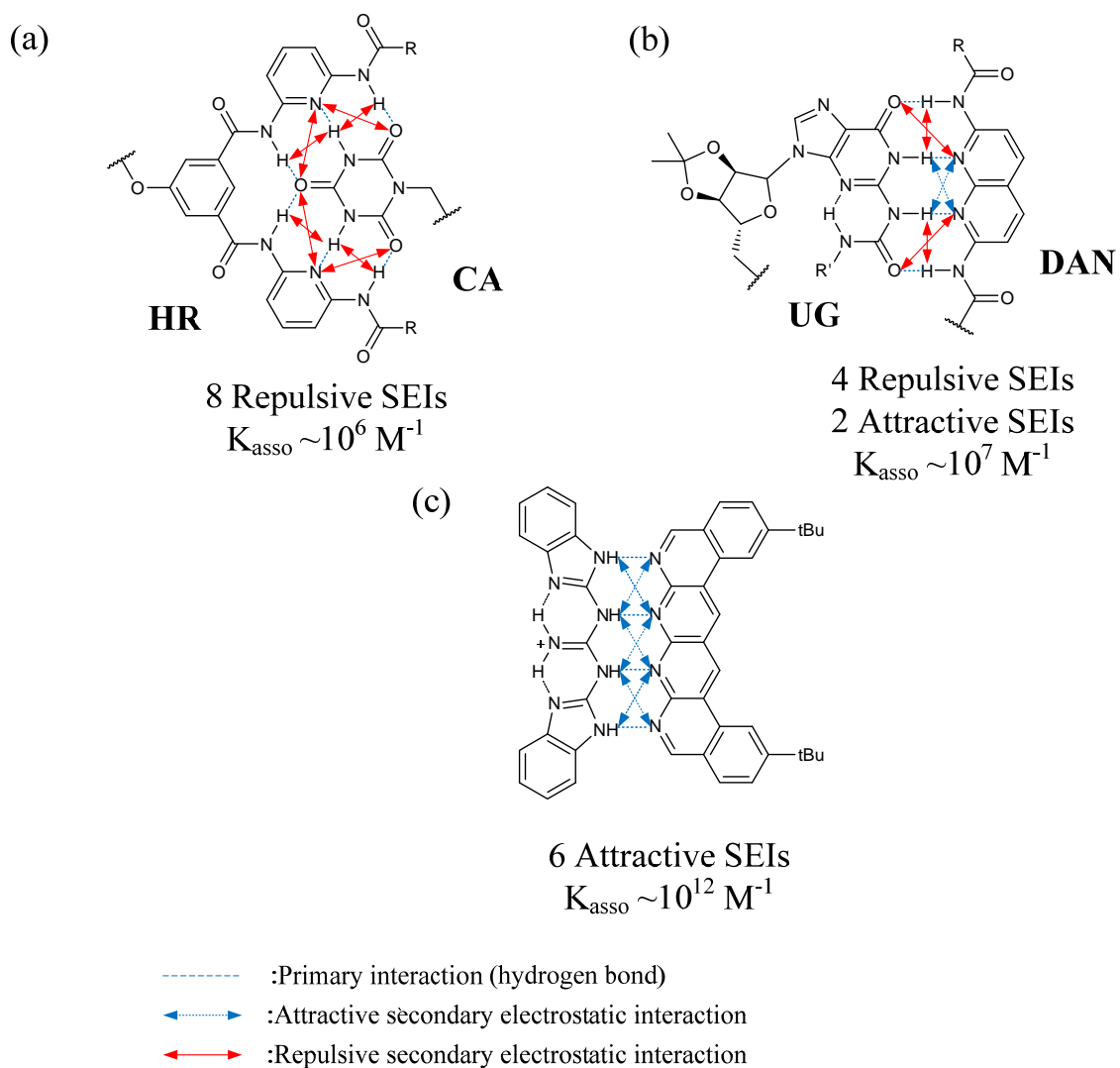
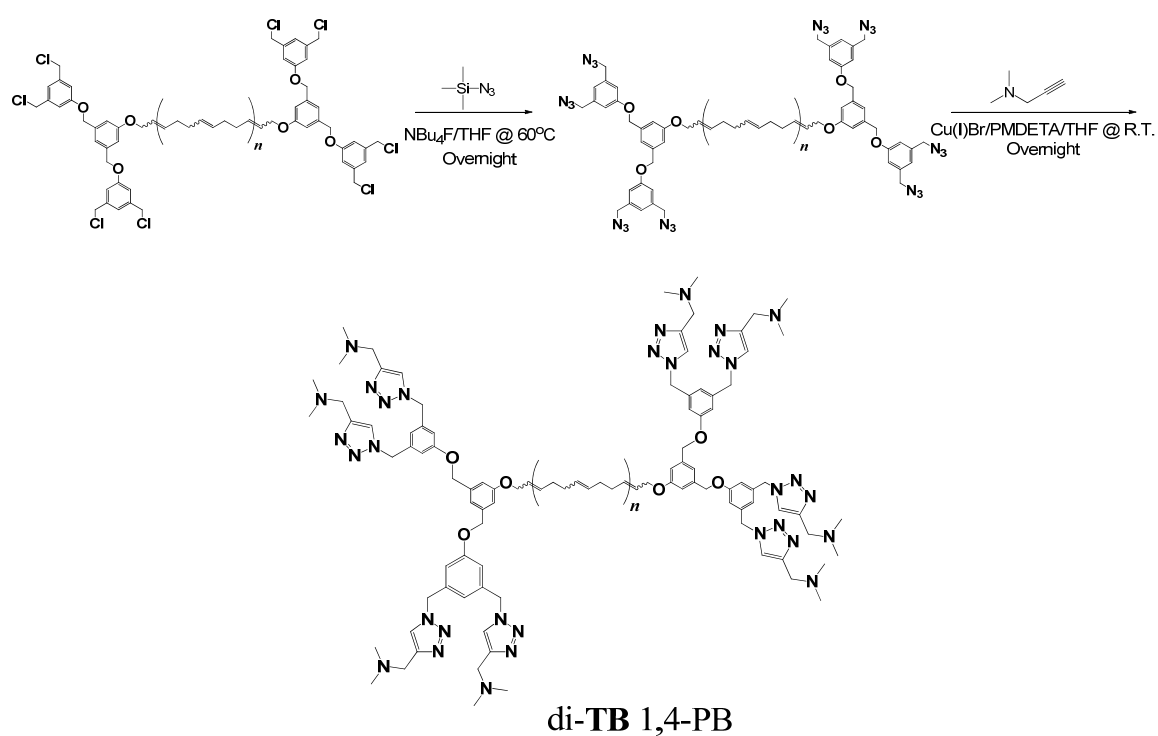
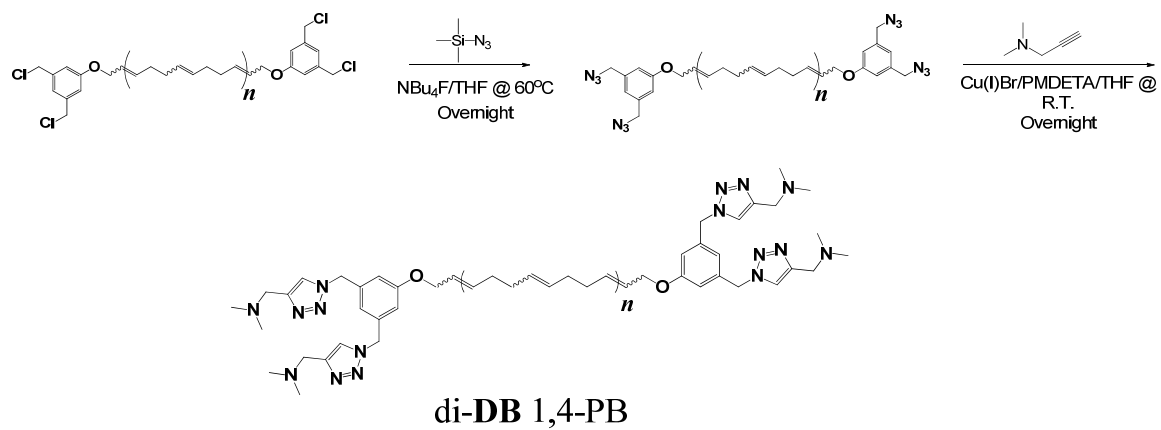
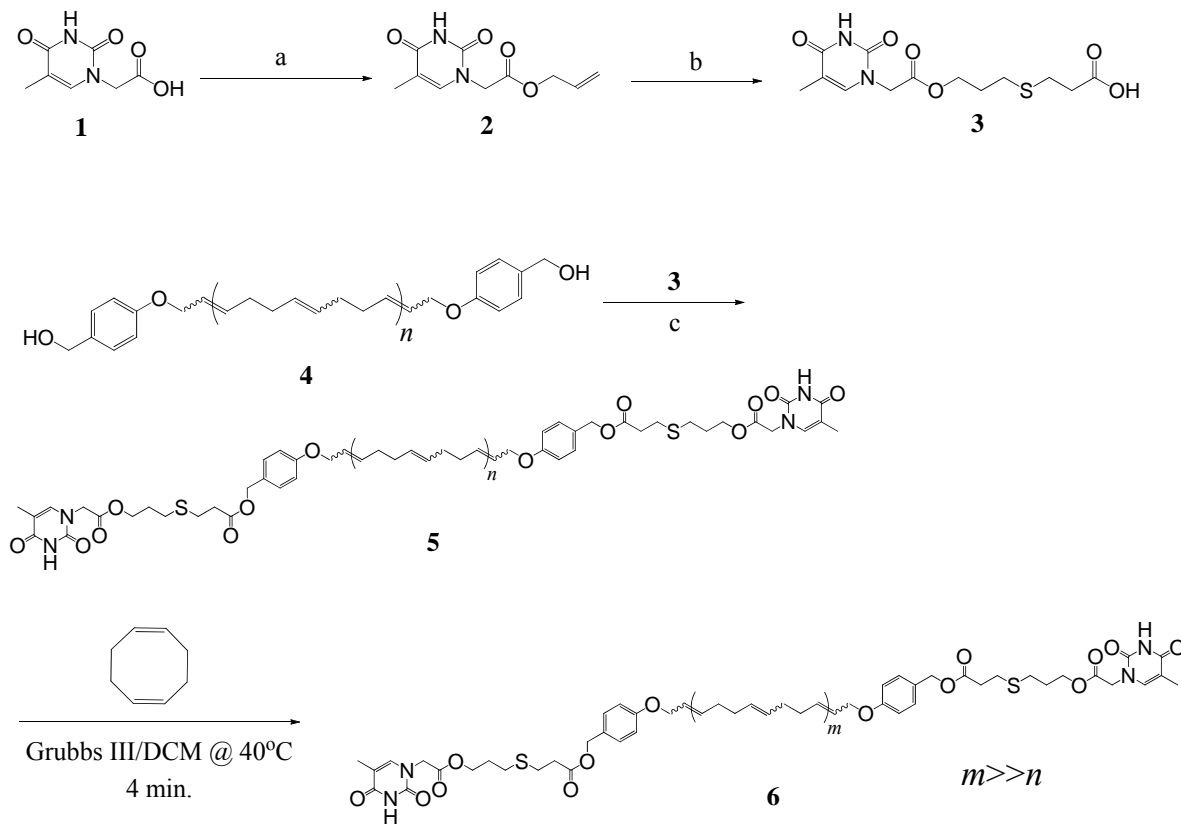


Figure 4.19 SEI analysis of D/A site arrangements for multiple-hydrogen-bonding hetero-complementary associative pairs. (a) **HR/CA** (ADAADA-DADDAD); (b) **UG/DAN** (ADDA-DAAD); (c) **AAAA-DDDD**.

Scheme 4.1 Synthesis of Di-DB and Di-TB 1,4-PBs *via* Two-Stage, Post-Polymerization End-Functionalization

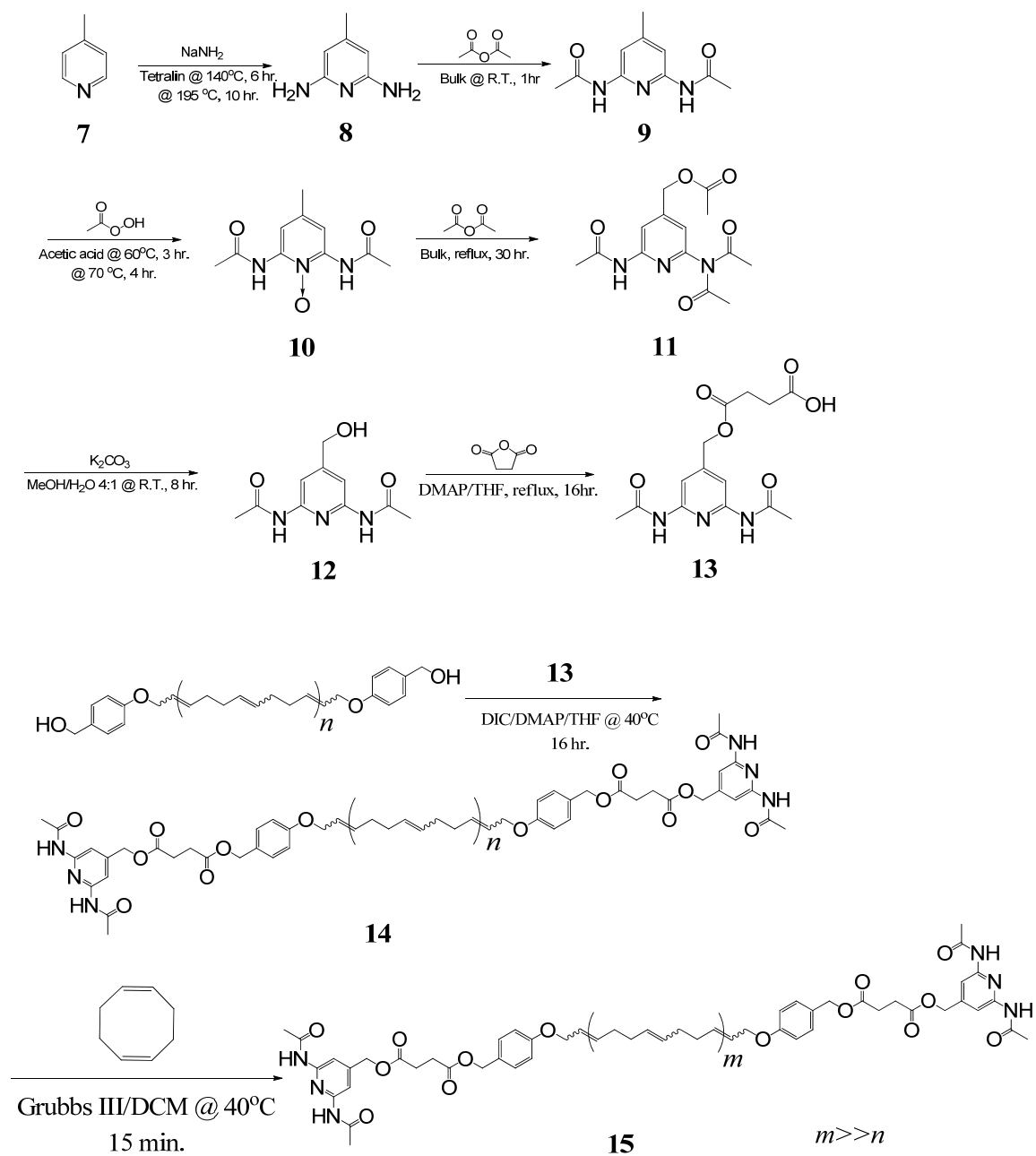


Scheme 4.2 Synthesis of **THY**-Functional Acid, Di-**THY** Macro CTA, and Di-**THY** 1,4-PB of $M_w \sim 200$ kg/mol

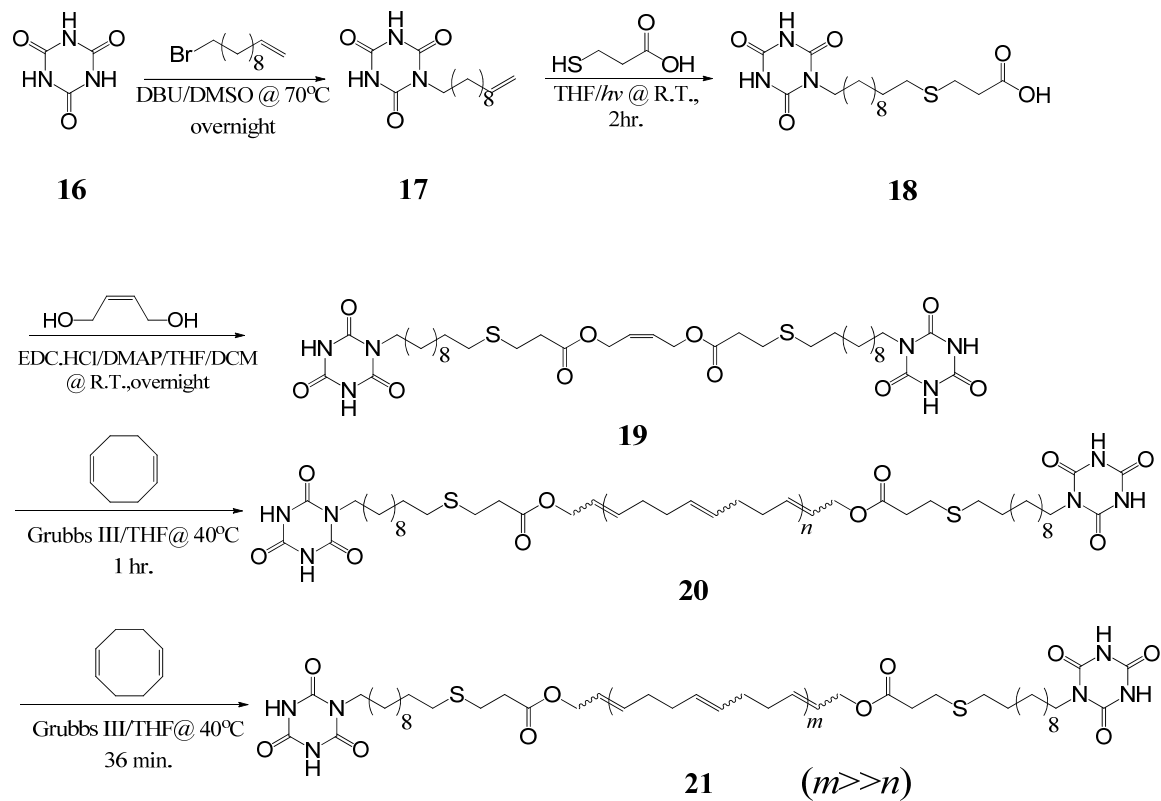


Key: a) allyl alcohol, *p*TSA·H₂O, bulk, reflux, overnight; b) 3MPA, *hν*, R.T., 4 h; c) DIC, DMAP, THF, 40°C, overnight.

Scheme 4.3 Synthesis of **DAAP**-Functional Acid, **Di-DAAP** Macro CTA, and **Di-DAAP** 1,4-PB of $M_w \sim 200$ kg/mol



Scheme 4.4 Synthesis of CA-Functional Acid, Di-CA CTA, Di-CA Macro CTA, and Di-CA 1,4-PB of $M_w \sim 200$ kg/mol



Scheme 4.5 Synthesis of **HR**-Functional Azide, Di-**HR** Macro CTA, and Di-**HR** 1,4-PB of $M_w \sim 200$ kg/mol

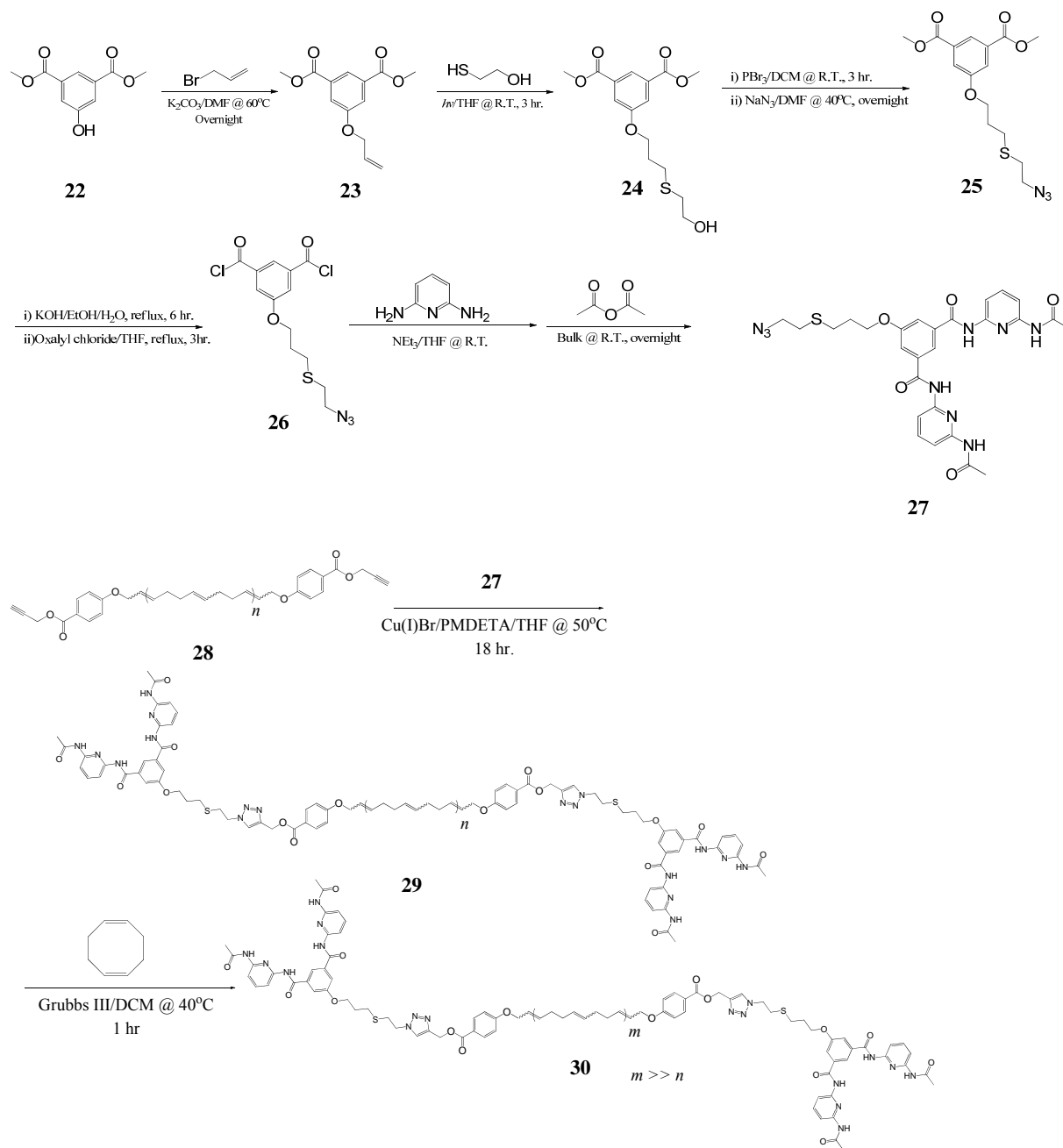
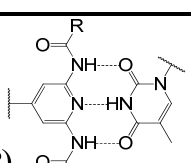
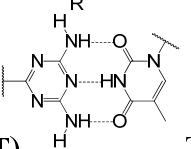
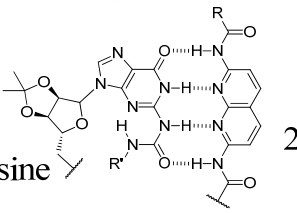
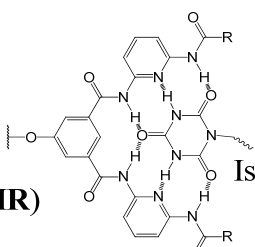


Table 4.1 Representative Examples of Multiple OHB-Based Hetero-Complementary Associative Pairs

Hetero-Complementary Associative Pair	Number of Hydrogen Bonds	$^aK_{\text{asso}}$ (M^{-1})	Reference
 Diamidopyridine (DAP) Thymine (THY)	3	$^b10^2$ $^c10^3$	9,10,36,76
 Diaminotriazine (DAT) Thymine (THY)	3	$^b10^2$ $^c10^3$	76,77
 Ureidoguanosine (UG) 2,7-diamido-1,8-naphthyridine (DAN)	4	$^b10^4$ $^c10^7$	13,14,21
 Hamilton Receptor (HR) Isocyanuric Acid (CA)	6	$^b10^4$ $^c10^6$	21, 23, 29

^a: measured by NMR titration or isothermal titration calorimetry (ITC); ^b: measured when bound to polymer chain ends; ^c: measured as small molecules.

Table 4.2 pK_a Values of Common Organic Acids and Conjugated Acids of Organic bases²

Compound	pK _a ^a
Ar ^b -Sulfonic acid	1-3
R ^c -Sulfonic acid	0-2
Ar-Nitroacids	2-3
Ar-Halogenoacids	2-4
Ar-Amino acids	2-2.5
Ar-Hydroxyacids	3-5
Benzoic acid	4.2
R-Carboxylic acid	3-5
2,4,6-trinitrophenol	0.33
Pentachlorophenol	5.25
R-SH	10-11
Amides	15-17
Anilines	25-31
Primary amines	10-11
Secondary amines	10-11
Tertiary amines	10-11
Pyridine	5.22
3-Chloropyridine	2.84
4,4'-Bipyridyl	4.71, 2.7
Quinoline	4.9
DABCO ^d	8.82, 2.97

^a: measured in aqueous environment; ^b: aromatic; ^c: aliphatic; ^d: 1,4-diazabicyclo-[2.2.2]octane.

Table 4.3 List of Attempted Strategies for Synthesizing Tertiary-amine-Terminated 1,4-PBs and Corresponding Problems

Approach	Synthetic Method	Problems
3° amine-functional CTA followed by ROMP	Functionalization of multi-functional α -bromoester CTA with dimethylaminoethanethiol <i>via</i> thiol-bromo coupling reaction in DMSO	Incorporation of the resultant CTA was found very poor, likely due to the interference of tertiary amines with Grubbs III.
	Functionalization of multi-functional azide with dimethylamino <i>via</i> alkyne-azide 1,3-cycloaddition	The (C+O)/(N in azide) ratio of multi-functional azide intermediate was too low. Thus it was unstable and possibly explosive.
ROMP with non-amino CTA then post-polymerization functionalization	Mitsunobu coupling of multi-functional carboxyl-terminated polymer with dimethylaminoethanol (DMAE)	The tertiary amine motif of DMAE interfered with the coupling reaction and thus resulted in very poor extent of functionalization of acid end groups even in the case of short backbones ($M_w \sim 20$ kg/mol).
	DCC/DMAP mediated esterification of carboxyl-terminated polymer with DMAE	The tertiary amine motif of DMAE interfered with the coupling reaction and thus resulted in very poor extent of functionalization of acid end groups even in the case of short backbone ($M_w \sim 20$ kg/mol).
	NaH mediated Williamson etherification of multi-functional chloro-terminated polymer with DMAE	Crosslinking of PB backbone was observed accompanying the end-functionalization.
	Azidation of multi-functional chloro-terminated polymer, followed by Cu(I) mediated 1,3 cycloaddition of the azide-terminated polymer with <i>N,N</i> -dimethyl propargylamine	No synthetic problems were observed. Tertiary amine-terminated PBs were successfully synthesized using this approach without crosslinking of backbone.

References

- (1) David, R. L. A. Dissertation (Ph.D.), California Institute of Technology, 2008.
- (2) Gilli, G.; Gilli, P. *The nature of the hydrogen bond : outline of a comprehensive hydrogen bond theory*; Oxford University Press: Oxford ; New York, 2009.
- (3) Fang, Y.; Nguyen, P.; Ivasenko, O.; Aviles, M. P.; Kebede, E.; Askari, M. S.; Ottenwaelder, X.; Ziener, U.; Siri, O.; Cuccia, L. A. *Chemical Communications* **2011**, 47, 11255.
- (4) Stuparu, M. C.; Khan, A.; Hawker, C. J. *Polym Chem-Uk* **2012**, 3, 3033.
- (5) Floudas, G.; Pispas, S.; Hadjichristidis, N.; Pakula, T. *Macromolecular Chemistry and Physics* **2001**, 202, 1488.
- (6) Pispas, S.; Floudas, G.; Pakula, T.; Lieser, G.; Sakellariou, S.; Hadjichristidis, N. *Macromolecules* **2003**, 36, 759.
- (7) Huh, J.; Park, H. J.; Kim, K. H.; Kim, K. H.; Park, C.; Jo, W. H. *Advanced Materials* **2006**, 18, 624.
- (8) Djurdjevic, S.; Leigh, D. A.; McNab, H.; Parsons, S.; Teobaldi, G.; Zerbetto, F. *J Am Chem Soc* **2007**, 129, 476.
- (9) Higley, M. N.; Pollino, J. M.; Hollembeak, E.; Weck, M. *Chemistry-a European Journal* **2005**, 11, 2946.
- (10) Burd, C.; Weck, M. *Macromolecules* **2005**, 38, 7225.
- (11) Beijer, F. H.; Sijbesma, R. P.; Vekemans, J. A. J. M.; Meijer, E. W.; Kooijman, H.; Spek, A. L. *J Org Chem* **1996**, 61, 9636.
- (12) Scherman, O. A.; Ligthart, G. B. W. L.; Ohkawa, H.; Sijbesma, R. P.; Meijer, E. *W. P Natl Acad Sci USA* **2006**, 103, 11850.
- (13) Park, T.; Zimmerman, S. C.; Nakashima, S. *J Am Chem Soc* **2005**, 127, 6520.
- (14) Park, T.; Todd, E. M.; Nakashima, S.; Zimmerman, S. C. *J Am Chem Soc* **2005**, 127, 18133.
- (15) Keizer, H. M.; Sijbesma, R. P.; Meijer, E. M. *Eur J Org Chem* **2004**, 2553.
- (16) Sijbesma, R. P.; Beijer, F. H.; Brunsveld, L.; Folmer, B. J. B.; Hirschberg, J. H. K.; Lange, R. F. M.; Lowe, J. K. L.; Meijer, E. W. *Science* **1997**, 278, 1601.

- (17) Altintas, O.; Schulze-Suenninghausen, D.; Luy, B.; Barner-Kowollik, C. *Acs Macro Lett* **2013**, *2*, 211.
- (18) Herbst, F.; Seiffert, S.; Binder, W. H. *Polym Chem-Uk* **2012**, *3*, 3084.
- (19) Chen, S.; Rocher, M.; Ladaviere, C.; Gerard, J.-F.; Lortie, F.; Bernard, J. *Polym Chem-Uk* **2012**, *3*, 3157.
- (20) Grimm, F.; Ulm, N.; Grohn, F.; During, J.; Hirsch, A. *Chemistry-a European Journal* **2011**, *17*, 9478.
- (21) Yang, S. K.; Ambade, A. V.; Weck, M. *J Am Chem Soc* **2010**, *132*, 1637.
- (22) Kolomiets, E.; Buhler, E.; Candau, S. J.; Lehn, J. M. *Macromolecules* **2006**, *39*, 1173.
- (23) Chang, S. K.; Hamilton, A. D. *J Am Chem Soc* **1988**, *110*, 1318.
- (24) Brunsveld, L.; Folmer, B. J. B.; Meijer, E. W.; Sijbesma, R. P. *Chemical Reviews* **2001**, *101*, 4071.
- (25) Rehm, T.; Schmuck, C. *Chemical Communications* **2008**, 801.
- (26) Pollino, J. M.; Nair, K. P.; Stubbs, L. P.; Adams, J.; Weck, M. *Tetrahedron* **2004**, *60*, 7205.
- (27) Altintas, O.; Rudolph, T.; Barner Kowollik, C. *Journal of polymer science. Part A, Polymer chemistry* **2011**, *49*, 2566.
- (28) Binder, W. H.; Kunz, M. J.; Kluger, C.; Hayn, G.; Saf, R. *Macromolecules* **2004**, *37*, 1749.
- (29) Binder, W. H.; Bernstorff, S.; Kluger, C.; Petraru, L.; Kunz, M. J. *Advanced Materials* **2005**, *17*, 2824.
- (30) Park, T.; Zimmerman, S. C. *J Am Chem Soc* **2006**, *128*, 13986.
- (31) Binder, W. H.; Kunz, M. J.; Ingolic, E. *J Polym Sci Pol Chem* **2004**, *42*, 162.
- (32) Altintas, O.; Tunca, U.; Barner Kowollik, C. *Polym Chem-Uk* **2011**, *2*, 1146.
- (33) Park, T.; Zimmerman, S. C. *J Am Chem Soc* **2006**, *128*, 11582.
- (34) Gilli, G.; Gilli, P. *J Mol Struct* **2000**, *552*, 1.
- (35) Sontjens, S. H. M.; Sijbesma, R. P.; van Genderen, M. H. P.; Meijer, E. W. *J Am Chem Soc* **2000**, *122*, 7487.
- (36) Stubbs, L. P.; Weck, M. *Chemistry-a European Journal* **2003**, *9*, 992.

- (37) Berl, V.; Schmutz, M.; Krische, M. J.; Khoury, R. G.; Lehn, J. M. *Chemistry-a European Journal* **2002**, *8*, 1227.
- (38) Kunz, M. J.; Hayn, G.; Saf, R.; Binder, W. H. *J Polym Sci Pol Chem* **2004**, *42*, 661.
- (39) Broeren, M. A. C.; de Waal, B. F. M.; van Genderen, M. H. P.; Sanders, H. M. H. F.; Fytas, G.; Meijer, E. W. *J Am Chem Soc* **2005**, *127*, 10334.
- (40) Manabe, K.; Okamura, K.; Date, T.; Koga, K. *J Am Chem Soc* **1993**, *115*, 9355.
- (41) Hudson, R. A.; Vinograd.Sn; Scott, R. M. *J Phys Chem-U.S.* **1972**, *76*, 1989.
- (42) DeTar, D. F.; Novak, R. W. *J Am Chem Soc* **1970**, *92*, 1361.
- (43) Davis, M. M. *Natl Bureau Stand M* **1968**, *1*.
- (44) Barrow, G. M.; Yerger, E. A. *J Am Chem Soc* **1954**, *76*, 5211.
- (45) Russell, T. P.; Jerome, R.; Charlier, P.; Foucart, M. *Macromolecules* **1988**, *21*, 1709.
- (46) Huh, J.; Jung, J. Y.; Lee, J. U.; Cho, H.; Park, S.; Park, C.; Jo, W. H. *Acs Nano* **2011**, *5*, 115.
- (47) Gao, J. P.; Li, X.; Li, B. Y.; Han, Y. C. *Polymer* **2010**, *51*, 2683.
- (48) Noro, A.; Hayashi, M.; Ohshika, A.; Matsushita, Y. *Soft Matter* **2011**, *7*, 1667.
- (49) Dethlefs, C.; Eckelmann, J.; Kobarg, H.; Weyrich, T.; Brammer, S.; Nather, C.; Luning, U. *Eur J Org Chem* **2011**, 2066.
- (50) Grimm, F.; Ulm, N.; Groehn, F.; Duering, J.; Hirsch, A. *Chemistry : a European Journal* **2011**, *17*, 9478.
- (51) Rubinstein, M.; Colby, R. H. *Polymer physics*; Oxford University Press: Oxford ; New York, 2003.
- (52) Smith, M.; March, J. *March's advanced organic chemistry : reactions, mechanisms, and structure*; 5th ed.; John Wiley: New York, 2001.
- (53) Kurosu, M.; Dey, S. S.; Crick, D. C. *Tetrahedron Lett* **2006**, *47*, 4871.
- (54) Frenzel, U. *Journal of polymer science. Part A, Polymer chemistry* **2002**, *40*, 2895.
- (55) Slugovc, C. *Macromolecular Rapid Communications* **2004**, *25*, 1283.
- (56) Alfred, S. F.; Lienkamp, K.; Madkour, A. E.; Tew, G. N. *J Polym Sci Pol Chem* **2008**, *46*, 6672.
- (57) Shi, X. X.; Barkigia, K. M.; Fajer, J.; Drain, C. M. *J Org Chem* **2001**, *66*, 6513.

- (58) Love, J. A.; Morgan, J. P.; Trnka, T. M.; Grubbs, R. H. *Angewandte Chemie-International Edition* **2002**, *41*, 4035.
- (59) Cheng, C. C.; Lin, I. H.; Yen, Y. C.; Chu, C. W.; Ko, F. H.; Wang, X. L.; Chang, F. C. *Rsc Adv* **2012**, *2*, 9952.
- (60) Altintas, O.; Lejeune, E.; Gerstel, P.; Barner-Kowollik, C. *Polym Chem-Uk* **2012**, *3*, 640.
- (61) Burd, C.; Weck, M. *J Polym Sci Pol Chem* **2008**, *46*, 1936.
- (62) Hietala, S.; Strandman, S.; Jarvi, P.; Torkkeli, M.; Jankova, K.; Hvilsted, S.; Tenhu, H. *Macromolecules* **2009**, *42*, 1726.
- (63) Stavrouli, N.; Aubry, T.; Tsitsilianis, C. *Polymer* **2008**, *49*, 1249.
- (64) Suzuki, S.; Uneyama, T.; Inoue, T.; Watanabe, H. *Macromolecules* **2012**, *45*, 888.
- (65) Chassenieux, C.; Nicolai, T.; Benyahia, L. *Curr Opin Colloid In* **2011**, *16*, 18.
- (66) Li, H. K.; Wang, J.; Sun, J. Z.; Hu, R. R.; Qin, A. J.; Tang, B. Z. *Polym Chem-Uk* **2012**, *3*, 1075.
- (67) Quinn, J. R.; Zimmerman, S. C.; Del Bene, J. E.; Shavitt, I. *J Am Chem Soc* **2007**, *129*, 934.
- (68) Pranata, J.; Wierschke, S. G.; Jorgensen, W. L. *J Am Chem Soc* **1991**, *113*, 2810.
- (69) Pranata, J.; Jorgensen, W. L. *Tetrahedron* **1991**, *47*, 2491.
- (70) Popelier, P. L. A.; Joubert, L. *J Am Chem Soc* **2002**, *124*, 8725.
- (71) Kyogoku, Y.; Lord, R. C.; Rich, A. *Biochim Biophys Acta* **1969**, *179*, 10.
- (72) Blight, B. A.; Hunter, C. A.; Leigh, D. A.; McNab, H.; Thomson, P. I. T. *Nature chemistry* **2011**, *3*, 244.
- (73) Sartorius, J.; Schneider, H. J. *Chemistry-a European Journal* **1996**, *2*, 1446.
- (74) Ligthart, G. B. W. L.; Ohkawa, H.; Sijbesma, R. P.; Meijer, E. W. *J Org Chem* **2006**, *71*, 375.
- (75) Park, T.; Mayer, M. F.; Nakashima, S.; Zimmerman, S. C. *Synlett* **2005**, 1435.
- (76) Beijer, F. H.; Sijbesma, R. P.; Vekemans, J. A. J. M.; Meijer, E. W.; Kooijman, H.; Spek, A. L. *J Org Chem* **1996**, *61*, 6371.
- (77) Herbst, F.; Schroter, K.; Gunkel, I.; Groger, S.; Thurn-Albrecht, T.; Balbach, J.; Binder, W. H. *Macromolecules* **2010**, *43*, 10006.

Chapter V Towards A Viable Fuel Additive to Mitigate Post-Impact Fires

5.1 Introduction

Thus far we have successfully developed a synthetic strategy to synthesize telechelic 1,4-PBs with unprecedentedly high M_w (up to 430 kg/mol) and precisely engineered chain-end structures *via* two-stage ROMP of rigorously purified COD in conjunction with the use of well-defined, bis-dendritic CTAs. We have also found that having 4 carboxyl groups on chain ends of telechelic 1,4-PBs results in strong end-association in non-polar solvents while keeping the polymers dissolvable in such media. In the investigation of telechelic polymer pairs end-capped with hetero-complementary associative groups, we have identified that in the ranges of M_w and polymer concentration for mist-control applications, carboxylic acid/tertiary amine interaction in dendritic configurations shows efficacy in driving the formation of supramolecules that can modify rheological properties of the solutions of the corresponding pairs of telechelic associative 1,4-PBs in non-polar solvents. These findings have enabled us to eventually move forwards to validate the design of end-associative telechelic polymers as mist-control additives for fuels. In this chapter, we choose Jet-A, the most widely used civil aviation fuel in the U.S., as the fuel of study, and a series of self-associative, telechelic 1,4-PBs end-capped with tetra-functional carboxyl-terminated dendrons (referred to as di-**TA** 1,4-PB hereinafter) with M_w ranging from 76 to 430 kg/mol are tested as mist-control additives for Jet-A.

5.2 Experimental

5.2.1 Materials

A precisely matched pair of non-associative (430K di-**TE** 1,4-PB with *tert*-butyl protecting groups intact) and self-associative, carboxyl-terminated (430K di-**TA** **1,4**-PB) telechelic 1,4-PBs, as well as a series of carboxyl-terminated telechelic 1,4-PBs of lower molecular weights (76K, 230K, 264K and 300K di-**TA** 1,4-PBs) were synthesized and purified as described earlier (Sections 2.3.3 and 2.3.4 for the 230K and 430K polymers; Appendix A for 76K, 264K and 300K di-**TA** 1,4-PBs). Polyisobutylene of $M_w = 4200$ kg/mol, hereafter referred to as 4.2M PIB, was purchased from Aldrich (product number 181498, with $M_w/M_n = 1.35$). 2,6-Di-*tert*-butyl-4-methylphenol (BHT) at 99% purity was obtained from Sigma-Aldrich. Jet-A was purchased from El Monte Airport (El Monte, California, USA) and used as received.

5.2.2 Preparation of Test Solutions

To prevent crosslinking of polymer, an air-free procedure was used for preparation of stock solutions, as illustrated by the following protocol for a 1wt% of 430K di-**TA** 1,4-PB in Jet-A. The carboxyl-terminated polymer 430K di-**TA** 1,4-PB was weighed (0.79 g) and loaded into a 250 mL Schlenk flask provided with a magnetic stir bar and charged with BHT (0.1 g, ca. 13 wt% of polymer) and Jet-A (77.77 g). Three freeze-pump-thaw cycles were performed on the mixture to remove dissolved oxygen. The mixture was stirred under argon atmosphere at 70°C for 16 h to ensure complete dissolution. Solutions of lower concentrations (0.15, 0.3, 0.5, and 0.7 wt%) were prepared by combining required amounts of 1wt% stock solution and Jet-A in clean 100 mL glass

jars that were placed on a Wrist-Acition Shaker (Burrell Scientific) for up to 1 h to allow full homogenization. The same air-free procedure described above was also applied in preparation of 0.5wt% Jet-A solutions of 76K, 230K and 300K di-**TA** 1,4-PBs. A solution of 4.2 M PIB at 0.35 wt% in Jet-A was prepared by combining required amounts of 4.2M PIB (0.57 g), BHT (0.1 g, ca. 18 wt% of polymer), and Jet-A (161.38 g) in a 250 mL glass jar (with a magnetic stir) and homogenizing with vigorous stirring at 70°C for two days. Each prepared solution was divided into two approximately equal portions and stored at -30°C until use. A small quantity of 1wt% 430K di-**TE** 1,4-PB solution in Jet-A was prepared as the control (polymer without association) by combining 0.1 g of 430K di-**TE** 1,4-PB, 0.02 g of BHT, and 9.9 g of Jet-A in a clear 20 mL vial which was placed on a Wrist-Acition Shaker for 16 h to allow the polymer to fully dissolve. The solution was also stored at -30°C until use.

5.2.3 Shear Stability Test

A recirculation setup consisting of a Bosch 69100 In-line Electric Fuel Pump and a MW122A 2AMP Regulated DC Power Supply (LKD Ind.) at 12 V (shown in Figure 5.1) was used to subject polymer solutions to a flow history that mimics, for example, recirculation of fuel through an engine's heat transfer system. Jet-A solutions of 430K di-**TA** 1,4-PB and 4.2M PIB at each concentration investigated in the present study (0.3, 0.5, and 0.7 wt% for 430K di-**TA** 1,4-PB; 0.35 wt% for 4.2M PIB) were recirculated through the setup at room temperature for 60 s (approximately 50 passes through the pump using 50-60 mL of solution and a flow rate of 3L/min). After recirculation, samples were collected in 100 mL glass jars and stored at -30°C for further tests. Between tests, the pump was rinsed 4 times with approximately 200 mL of hexanes, followed by drying *in*

vacuo at 40°C overnight to prevent cross-contamination among samples or dilution by hexanes. Shear stability was evaluated by comparing shear viscosities of recirculated samples to those of the corresponding unsheared controls.

5.2.4 Shear Viscosity Measurements

Shear viscosity as a function of shear rate was measured using an AR1000 rheometer from TA Instruments. An aluminum core of 60 mm diameter, 1° cone angle and 29 μm truncation was used as the geometry for all samples. A steady-state flow procedure was used to examine shear rates from 1 to 3000 s⁻¹ at 25°C.

5.2.5 Dewatering Test

Approximately 1mL of 0.5 wt% Jet-A solution of 264K di-TA 1,4-PB and ~ 1 mL of DI water were added to a 2 mL vial. The control was prepared by adding ~ 1 mL of Jet-A and ~ 1 mL of DI water in another 2 mL vial. Both vials were then shaken vigorously by hands for 20 s, and left to stand undisturbed for 60s to allow phase separation. Images of both samples were recorded (Figure 5.2) to evaluate the effect of 264K di-TA 1,4-PB in Jet-A on the dewatering process.

5.2.6 Impact/Flame Propagation Test

Efficacy of high molecular-weight end-associative polymers as mist-control additives for fuels was studied *via* high-speed imaging during an impact/flame propagation test (experiments courtesy of Dr. Virendra Sarohia and Mr. Thomas A. Wynne of Jet Propulsion Laboratory; Mr. Petros Arakelian of Aerospace Department, Caltech.) The apparatus (Figure 5.3) emulates the atomization and subsequent ignition of fuels released from ruptured fuel tanks in crash scenarios of ground vehicles/aircraft. An

aluminum canister (outer diameter = 23 mm, height = 140 mm) pre-loaded with a cylindrical aluminum filler (diameter = 22 mm, height = 40 mm) was used as a miniature fuel tank to hold ~30 mL of a test sample. The cap was tightly sealed with superglue and 2-3 wraps of electrical tape to keep it in place during the impact. A solid stainless steel cylinder (diameter = 24 mm, length = 50 mm) was used as a projectile to impact the canister and disperse the fuel. Compressed air at 6.89×10^5 Pa was used to propel the projectile through a 1.66 m-long barrel (inner diameter = 25.4 mm), resulting in a muzzle speed of 63 m/s. An array of three continuously burning propane torches was placed in the path of the ejected fuel to serve as ignition sources. The onset of impact, formation of mist, and the following ignition events and propagation of flame were captured at a frame rate of 10 kHz using a high-speed camera (Photron SA1.1). Image acquisition was triggered by a laser-motion detector attached to the end of muzzle (Figure 5.3 (b)). The high-speed images clearly revealed whether or not ignition events propagated and provided qualitative information about the efficacy of various polymers before and after being subjected to the intense shearing described above (Section 5.2.3). Tested samples include untreated Jet-A, unsheared and sheared 0.35wt% Jet-A solutions of 4.2M PIB, unsheared and sheared Jet-A solutions of 430K di-TA 1,4-PB at 0.3, 0.5 and 0.7 wt%, unsheared 0.15wt% Jet-A solution of 430K di-TA 1,4-PB, and unsheared 0.5wt% Jet-A solutions of 76K, 230K, and 300K di-TA 1,4-PBs.

5.3 Results

5.3.1 Phase Behavior

All Jet-A solutions of di-**TA** 1,4-PBs were homogenized by heating the mixtures at 70°C with magnetic stirring for 16 h. Without heating, we observed gel-like heterogeneities in each mixture after overnight mixing at room temperature. Heating to 70°C hastened dissolution of the polymer chains in the solvent (here, Jet-A). Once homogenized and cooled to room temperature, Jet-A solutions of carboxyl-terminated polymers at all concentrations of interest were found to remain homogeneous indefinitely even at -30°C (Figure 5.4).

5.3.2 Effect of End-Association in Jet-A

As discussed in preceding chapter (Section 3.3.2), the viscosity of solutions of 430K di-**TA** 1,4-PB in apolar solvents 1-chlorododecane and tetralin is much greater than that of the non-associative prepolymer 430K di-**TE** 1,4-PB at the same concentrations due to the strong association of **TA** end groups. Given that Jet-A is a mixture of hundreds of different chemicals, including some that could interfere with the end-association of polymers, shear rheology at 25°C was performed on 1wt% solutions of 430K di-**TA** 1,4-PB and 430K di-**TE** 1,4-PB in Jet-A so as to understand whether the association of **TA** end groups was still effective to drive the formation of supramolecular aggregates in Jet-A as it was in 1-chlorododecane and tetralin. Indeed, the results show that, while the carboxyl-terminated polymer still conferred higher viscosity than its non-associative counterpart, the increase in specific viscosity η_{sp} due to end-association was not as significant as that observed in single-component apolar solvents (Figure 5.5, compare

with Chapter 3). The shear-thinning behavior observed in apolar solvents was also observed in Jet-A at high shear-rates (300-3000 s⁻¹).

5.3.3 Shear Stability

Fuel is transported through pipes in highly turbulent flow, passes through pumps, and needs to be passed through filters in many engines, including aviation turbine engines and large diesel engines. It must be circulated repeatedly through heat exchangers that prevent the engine from overheating. In order to ensure that fire protection is retained up to the moment it is needed, the polymer must not degrade prior to fueling or during filtering and circulation during operation of the engine. Therefore, resistance to flow-induced chain scission (often called “shear degradation”) is among the most crucial requirements for mist-control additives for fuels. For linear polymers dissolved in θ - and good solvents, the correlation between shear viscosity and average molecular weight of polymer (MW) is well-described by the following scaling relationship:¹

$$\eta_s \propto (\text{MW})^a$$

where η_s is the shear viscosity and a is the Mark-Houwink constant (0.5 for θ -solvents; 0.76 for good solvents). Shear viscosity at low shear rate provides a reliable, simple and straightforward method to evaluate shear degradation of polymers after recirculation tests. The recirculation apparatus (Figure 5.1) was validated with 0.35wt% Jet-A solution of 4.2M PIB: After 60s of recirculation, the viscosity at low shear rates decreased ~40% (Figure 5.6), indicating that this protocol is capable of degrading 4.2M PIB at 0.35wt% in Jet-A. The Jet-A solutions of longest of the end-associative polymers in this study 430K di-TA 1,4-PB at 0.3, 0.5 and 0.7wt% were tested using the same protocol, and none of the three solutions showed detectable decrease in shear viscosity (Figure 5.6).

5.3.4 De-Watering

Using the simple, bench-top dewatering experiment (Section 5.2.5), no significant difference between Jet-A and a 0.5wt% Jet-A solution of 264K di-TA 1,4-PB in the rate and extent of aqueous-organic phase separation was observed (Figure 5.2).

5.3.5 Impact/Flame Propagation Test

The small-scale high-speed impact test (Figure 5.3) was validated using Jet-A and a solution of 4.2M PIB at 0.35wt%, an effective mist-control polymer. The test method correctly mimicked the atomization after high-speed impact and the explosive ignition of the resulting cloud of Jet-A (Figure 5.7): 30 ms after the impact, a cloud of very fine mist of Jet-A was observed, which was ignited approximately 60ms after impact (Figure 5.7 (c)) and the flame propagated to engulf the entire cloud of fuel within a further 60ms. The resultant fireball lasted for over 400 ms and appeared to consume all visible droplets of fuel. In the case of (unsheared) 0.35wt% Jet-A solution of 4.2M PIB, much larger droplets interconnected by fluid filaments were observed after impact ((b) and (c) in Figure 5.8). As ejected fluid flew over the propane torches, localized ignition events were observed, which soon self-extinguished. In accord with prior literature, the presence of 4.2M PIB at 0.35wt% in Jet-A suppressed droplet breakup of Jet-A and thus imparted fire protection. A “sheared” sample of the 0.35wt% Jet-A solution of 4.2M PIB (treated as described in Section 5.2.3), however, showed a significantly different pattern of ejection of fluid after impact (Figure 5.8 (e)): Fine droplets formed and interconnecting filaments were no longer observed. Ignition events observed at 30 ms after impact quickly propagated and engulfed the fuel cloud in fireball ((f) in Figure 5.8), although it was not

as large and long-lasting as the one observed in the case of Jet-A. The results confirm that the method is capable of creating a post-impact fuel mist that propagates fire from any ignition event, correctly captures the fire protection that is known to be conferred by 4.2M PIB at 0.35wt% and the loss of fire protection that is known to occur after fuel is passed through pumps, filters or turbulent pipe flow (section 5.3.4).

Successfully validated, the setup was used to test the efficacy of 430K di-**TA** 1,4-PB as a mist-control additive in Jet-A, and the change in fire protection (if any) after recirculation. High-speed imaging analysis showed that in the tests of all three unsheared solutions, 430K di-**TA** 1,4-PB at 0.3, 0.5 and 0.7wt% suppressed mist formation of Jet-A (Figures 5.9-5.11): Ignition events self-extinguished and, as a result, no propagating fireballs were observed. “Sheared” solutions of 430K di-**TA** 1,4-PB (treated as described in Section 5.2.3), were tested ((d)~(f) in Figure 5.9-5.11). We found that in the case of the 0.3wt% solution, the post-impact ignition events propagated to a very limited extent; they did not evolve into a propagating fireball at all, indicating the retention of fire protection provide by 430K di-**TA** 1,4-PB at this concentration. Interestingly, the results of recirculated 0.5 and 0.7wt% solutions suggest that increasing concentration makes the solution more sensitive to intense shear (the flame lifetime after ignition was longer for sheared solutions than their unsheared counterparts); nevertheless, post-impact ignition events did self-extinguish.

To explore the lower bound of fire-protection efficacy of 430K di-**TA** 1,4-PB in Jet-A, unsheared 0.15wt% Jet-A solution of 430K di-**TA** 1,4-PB was also tested, and its result at 60 ms after impact was compared along with those of unsheared 0.3, 0.5 and 0.7

wt% (Figure 5.12). The propagating fireball shown in Figure 5.12 (a) suggests that the lowest effective concentration of 430K di-**TA** 1,4-PB as a mist-control additive for Jet-A falls between 0.15 and 0.3wt%.

The effect of molecular weight of di-**TA** 1,4-PB on fire-protection efficacy for Jet-A was studied using unsheared 0.5wt% Jet-A solutions of 76K, 230K, 300K and 430K di-**TA** 1,4-PBs. A strong positive correlation was observed between the polymer molecular weight and the extent of fire suppression (Figure 5.13). Complete suppression of fire propagation was only observed in the case of the longest telechelic associative polymer, 430K di-**TA** 1,4-PB.

5.4 Discussions

5.4.1 Successful Molecular Design

The engineering tests performed on Jet-A solutions of di-**TA** 1,4-PBs demonstrate the success of the molecular design we developed in four respects: 1) they avoid chain collapse, 2) they form large supramolecular assemblies that suppress misting, 3) they are compatible with essential fuel handling operations (including dewatering), and 4) they resist shear degradation.

1. The results show that *telechelic* associative polymers avoid the problem of chain collapse that results from randomly placing associative groups along polymer backbone.^{2,3}
2. In accord with theoretical predictions that very long backbones reduce cyclic association and favor intermolecular association even at low concentration, the results show that increasing the length of long telechelic associative polymers

favors formation elastic supramolecules at low concentrations and confers mist control.⁴ Thus, overcoming the synthetic obstacles to long (>300 kg/mol) telechelic associative polymers (Section 2.3.3) was essential, because it gave us access to the unexplored regime of very long telechelics (DP ca. 4000 in 430K di-**TA** 1,4-PB) where we discovered end-associative polymers that inhibit misting with as little as 0.3wt% polymer (Figures 5.7-5.9).

3. By using a very low content of polar groups (e.g., 430K di-**TA** 1,4-PB contains approximately one oxygen atom per 1000 carbon atoms), the present polymers do *not* reduce the fuel's energy content, phase separate at low temperature or interfere with "dewatering" (Section 5.3.4). Two of the prohibitive problems with the mist-control polymer that received the most intensive study to date, FM-9, was its tendency to phase separate during storage and its interference with dewatering, which resulted from the high content of carboxyl groups (~ 5 mol% acrylic acid).⁵ At concentrations that confer mist control (e.g. 0.5 wt%), the present polymers (di-**TA** 1,4-PBs) in Jet-A do *not* emulsify water-in-oil nor oil-in-water (Figure 5.2).
4. While the present polymers are very long with respect to prior telechelics, they are deliberately kept short enough so that they are not vulnerable to shear degradation (Figure 5.6). The quest for mist-control polymers that survive passage through pumps, filters, and turbulent pipe flow has remained a major unsolved problem despite decades of research. Routine handling of fuel degrades ultrahigh-molecular-weight (UHMW) polymers, such as UHMW PIB (Figure 5.6) and FM-9,^{5,6} rendering them ineffective (Figure 5.8). The literature on shear degradation

of polymers in dilute (i.e., ~ 0.1 wt%) solutions indicates that there is a threshold backbone length (M_{∞}) below which chain scission does not occur during turbulent pipe flow: For example, polystyrene chains shorter 10^6 g/mol resist shear degradation.^{7,8} By deliberately keeping the M_w of the individual chains less than 10^6 g/mol and using association strengths that are substantially weaker than covalent bonds (i.e., much less than $84 k_B T$), we obtained polymers that resist shear degradation (Figure 5.6).

Even though the backbone size of 430Kdi-**TA** 1,4-PB is merely 1/10 of that of 4.2M PIB, this telechelic associative polymer still shows remarkable fire-protection efficacy. Thus, the reversible association of **TA** end groups is strong enough to drive formation of supramolecular structures that suppress misting, yet weak enough that the supramolecules can break at the noncovalent linkages, dissociating into individual chains in response to intense hydrodynamic forces. They re-associate into supramolecular structures quickly when the high force is removed. Thus, proper molecular design combines two seemingly mutually exclusive properties, mist-control ability and shear stability, in one family of polymers. The present results also show that, within this family of long, end-associative polymers, there are particularly favorable choices of the association strength and chemical structure of the polymer backbone.

5.4.2 Optimizing the Strength of Association

The number of carboxyl groups on the chain ends has a profound effect on the strength of end-association and the solubility of the polymer in non-polar organic solvents (Chapter 3). Theoretical work conducted in our group examined the effect of the

association energy ($\epsilon k_B T$) on the equilibrium distribution of supramolecules. When all chains have both ends functionalized (“perfectly telechelic”), the model predicts that the range of ϵ that is useful in mist control is surprisingly narrow (e.g., for telechelics of molecular weight of 500-1000 kg/mol at a concentration of approximately 0.1wt%, formation of 50ppm of supramolecules of 5000 kg/mol or more requires $16 \leq \epsilon \leq 18$).⁴ When ϵ is below the optimal range, aggregates are few and contain small numbers of supramolecular chains. When ϵ is above the optimal range, the dominant components are cyclics that contain a small number of chains. Only when ϵ falls in the optimal range, there is a balance of interactions strong enough to drive formation of large supramolecules and weak enough to accommodate a significant population of chains with an unpaired end (i.e., *linear* supramolecules).

Although, that model treats pairwise, donor-acceptor interactions, there are significant parallels between the model predictions and the observed behavior of the carboxyl-terminated (self-associative) telechelic polymers. As a function the number of carboxyl groups at each chain end (N), polymers with either too few ($N = 1$ and 2) or too many ($N = 8$) were observed to have little effect. When the association strength is in a particularly favorable range ($N = 4$), a profound increase in shear viscosity is observed and the desired combination of mist suppression and resistance to shear degradation is achieved. As a first approximation for the energy of association of carboxyl-terminated telechelic polymers, consider the strength of end-association as roughly proportional to N . Previously discussed in Section 3.4.1, the estimated energy of end-association of carboxyl-terminated end groups for $N = 1$, 2 , and 4 are 7.6 , 15.2 , and $30.4 k_B T$, respectively. In reality the energy of association in each case may be lower due to species

in fuel that can compete for hydrogen bonds (will be discussed below) and possible steric frustration when multiple carboxylate groups are in close proximity. Thus, it is reasonable that $N = 4$ is the one closest to the theoretical optimal range of energy of association.

The survival of end association in Jet-A is non-trivial. Although the majority of the chemical species in fuel do not disrupt hydrogen bonds (70-80% are saturated hydrocarbons in the forms of paraffins and cycloparaffins, 17-20% are aromatic hydrocarbons, 3-6% are unsaturated olefins), the concentration of chain ends is extremely low (15 μM in a 0.3wt% solution of 430K di-TA 1,4-PB). The concentration of chain ends is less than the concentrations of various additives present in Jet-A, many of which carry hydrogen-bond capable functional groups (e.g., sulfonic acid groups in the anti-static agent dinonylnaphthylsulfonic acid and hydroxyl groups in the fuel system icing inhibitor (FSII) diethylene glycol monomethyl ether (Di-EGME)). It is significant that the TA end groups of 430K di-TA 1,4-PB clearly associate in Jet-A (Figure 5.6), despite the presence of species that could potentially interfere with end-association of di-TA 1,4-PBs.

5.4.3 The Advantages of An Unsaturated Hydrocarbon Backbone

Backbone length is a key parameter for telechelic associative polymers as mist-control agents for fuels: Increasing the chain length suppresses “ring closure” hydrogen bonding of a chain with itself.⁴ Specifically, our model predicts that when a sufficiently long backbone (i.e., >400 kg/mol) is used, even at modest aggregation number (4-10 chains per aggregate), supramolecules with effective molecular weight well above 10^6 g/mol can form and provide mist suppression (Figure 5.13).

The unsaturated 1,4-PB backbone also makes crucial contribution to the success of the molecular design. First of all, we found that the 1,4-PB backbones grant the resultant polymers excellent solubility in Jet-A. Similar to PIBs, di-TA 1,4-PBs were found to remain in solution at -30°C indefinitely without the need of any surfactant or stabilizer. This property renders di-TA 1,4-PBs far superior to ICI's proprietary FM-9 polymer, the associative polymer extensively studied in the 1980's as a mist-control additive for kerosene, since FM-9 would not stay in solution at sub-ambient temperatures even with the use of a package of "carrier fluid" made of water, glycerol, ethylene glycol, and formic or acetic acid.^{5,9}

Another important benefit of an unsaturated backbone is that it improves resistance to chain scission relative to backbones that have only single carbon-carbon bonds in the backbone, particularly with quaternary carbons (such as PIB). Reactive molecular dynamics simulation clearly shows the effect of the number of carbon neighbors on the scission of C-C bonds in saturated polymer backbones: The activation energy for chain scission (E_a) decreases strongly from polyethylene (PE, backbone with 100% 2° -carbons, $E_a=181$ kJ/mol) to polypropylene (PP, backbone with 50% 3° -carbons, $E_a = 99$ kJ/mol) to polyisobutylene (PIB, backbone with 50% 4° -carbons, $E_a=42$ kJ/mol).¹⁰ Nyden and coworkers' finding explain the well-known susceptibility of PIB to chain scission by mechanical force, irradiation, and high temperature even at low molecular weights due to the fact that 50% of its backbone carbons are quaternary.¹¹⁻¹⁴ The present backbone has two distinct advantages: It excludes tertiary/quaternary carbons that serve as weak links and 33% of the backbone is comprised of C=C double bonds that are stronger than even the strongest C-C single bonds.¹⁵

5.4.4 Factors That Affect Resistance to Mechanical Degradation

In addition to the effects of chain length and the types of carbon-carbon bonds in the backbone, the resistance to mechanical degradation also depends on polymer concentration. While all three concentrations of 430K di-TA 1,4-PB retained efficacy after exposure to the shear degradation protocol, there was a significant difference in performance for the highest concentration (0.7 wt%): In the impact/flame propagation test, compared to its as-prepared control, partial loss of fire protection was observed after the shear degradation protocol for 0.7 wt% Jet-A solution of 430K di-TA 1,4-PB, but negligible change occurred for the 0.3 wt% solution. (Figure 5.14). This is reminiscent of the findings of Yu and coworkers that for high molecular weight PIBs dissolved in oil, the threshold backbone length below which chain scission does not occur (M_{∞}) decreases as polymer concentration increases: M_{∞} decreases from 230 kg/mol at 0.15 wt%, to 200 kg/mol at 0.25 wt%, and 185 kg/mol at 0.5 wt%.¹⁶ Based on their findings, we infer that the high molecular weight species in the polydisperse polymer 430K di-TA 1,4-PB (Figure 5.15) largely survived during the recirculation test at 0.3 wt%, but underwent some amount of chain scission at 0.5 and 0.7 wt%.

Interestingly, no detectable decrease in shear viscosity was observed for any of the three “sheared” samples of 430K di-TA 1,4-PB at 0.3, 0.5 and 0.7 wt% (Figure 5.6). To reconcile this with the effects seen in the fire resistance test, we hypothesize that the loss of the longest chains in the 0.7 wt% 430K di-TA 1,4-PB solution had a very subtle effect on the average molecular weight (making it difficult to detect in the shear viscosity), but had a significant effect on the concentration of ultralong supramolecules (which is strongly affected by addition of monotelechelic chains, which would result

from chain scission). As discussed in the preceding section, chains of high molecular weights are the major contributors to the fire protection imparted by the polymer additive. Further in-depth investigations, for instance, GPC analysis of unsheared and sheared samples over the range of concentrations of interest and *in situ* SANS study on solutions of di-TA 1,4-PBs under high shear stress, could clarify the effects of the shear degradation protocol on individual telechelic chains and, consequently, on the supramolecular aggregates of di-TA 1,4-PBs.

In relation to optimization of the supramolecular aggregation of high-molecular-weight telechelic associative polymers for mist control of fuels, theory predicts that, for a given backbone length, a design that uses hetero-complementary association provides relatively more open, more elastic supramolecular aggregates. If confirmed, this prediction indicates that mist control could be achieved at concentrations well below 0.3wt%, which would further improve resistance to shear degradation. Therefore, future work will include study of high-molecular-weight telechelic associative polymers with tertiary-amine-terminated end group in solution with their carboxyl-terminated counterparts as mist-control additives for fuels (Chapter 4).

5.4.5 Anti-Misting or Mist-Control?

In the 70's and 80's, the prevailing concept for improving fire safety of fuels was that it could be achieved through the addition of then-known *anti-misting* polymers (such as UHMW PIBs and FM-9) into fuels to eliminate the impact-induced atomization of fuels and the subsequent fire/explosion hazards.^{5,9,17-19} However, more recent studies indicate that simply shifting the drop size distribution to higher values can prevent flame

propagation through a fuel mist. For example, the critical values of Sauter mean diameter of droplets of military fuel JP-8 in a droplet/air (aerosol) mixture to propagate a flame from an ignition source is approximately 52 μm ; at lower droplet sizes than this critical values the aerosol becomes entirely engulfed in flame.²⁰ Thus, complete elimination of mist formation is not necessary. Since the 9/11/2001 terrorist attack on the World Trade Center, a new concept, referred to as mist-*control* kerosene (MCK), has been investigated by the Jet Propulsion Laboratory, California Institute of Technology, and Southwest Research Institute in an attempt to develop a fire-safe fuel that would prevent another catastrophic event and neutralize terrorist threats based on high-speed impact of fuels.⁶ This approach is validated by the results of impact/flame propagation test of unsheared 0.3 wt% Jet-A solution of 430K di-**TA** 1,4-PB and 0.35 wt% Jet-A solution of 4.2M PIB (Figures 5.8 and 5.9): Fire resistance was observed in both cases, even though impact on 0.3 wt% Jet-A solution of 430K di-**TA** 1,4-PB resulted in a cloud of droplets, whereas unsheared 0.35 wt% Jet-A solution of 4.2M PIB formed much larger droplets interconnected by fluid filaments after impact. The observed fire-protection efficacy conferred by 430K di-**TA** 1,4-PB clearly indicates that it does not require complete elimination of misting to achieve fire-safe fuels; instead, the goal can be achieved *via* proper control of misting.

5.4.6 Potential for Large-Scale Production

Ring-opening metathesis polymerization (ROMP) provides a synthetic route that not only opens an unexplored class of molecules—very long end-associative polymers—for research, but also holds the potential for large-scale commercial production of such mist-control polymers. Typically ROMP reactions are carried out at or near room

temperature (e.g., 40°C) and are weakly exothermic, which simplifies scale-up and suggests that the energy cost associated with the polymerization reactor is expected to be insignificant. ROMP proceeds efficiently in both chlorinated (e.g., dichloromethane) and non-chlorinated solvents (e.g., toluene),²¹ so large-scale production can be achieved without the use of toxic chlorinated solvents. In terms of the cost of reagents: (1) the monomer COD is commercially available at low prices (\$9-13/kg); (2) A very low load of Grubbs II (e.g., 0.01wt% of monomer for 430K di-TE 1,4-PB, Table 2.2) is needed (\$32 per kg 430K di-TE 1,4-PB); (3) the octa-functional bis-dendritic CTA, which is synthesized *via* a multi-step route (Scheme 2.1) and expected to be far more expensive than the monomer, is quantitatively incorporated into polymers (Table 2.2) and an extremely small amount of CTA is needed because the target M_w is > 400 kg/mol (1/10,000 eq of monomer in the case of 430K di-TE 1,4-PB); (4) two-stage ROMP is compatible with continuous production in a two consecutive reactors (the first with small volume and long residence time and the second with large volume and short residence time). For large scale production, the tedious and comparatively expensive procedure for monomer purification can be replaced by distillation using an industrial-scale vacuum distillation apparatus with a sufficient effective length to remove VCH from COD. Therefore, the use of borane and the subsequent loss of monomer and multiple-step purification could be eliminated (refer to Section 2.2.3). As for deprotection of carboxyl-terminated end groups, possible approaches of optimization include (1) performing a kinetic study that would guide optimization of the reaction time for TFA-catalyzed deprotection, and (2) removing TFA from the reaction mixture of end-group deprotection of di-TA 1,4-PBs by gas stripping so as to eliminate reprecipitation.²²

5.5 Conclusions

At a concentration as low as 0.3wt% in Jet-A, self-associative telechelic polymer 430K di-TA 1,4-PB provides remarkable fire protection—comparable to that by the “gold standard” 4.2M PIB at 0.35wt%—and overcomes the decades old problem of shear degradation. The results prove that clustering associative groups at polymer chain ends overcomes the problem of chain collapse and affords elastic supramolecules that control misting. The molecular design of the present end-associative telechelic polymers with 1,4-PB backbones meets other crucial requirements for effective mist-control additives for fuels, such as superior long-term solubility in Jet-A over a wide range of temperature (-30°C ~ +70°C), acceptably small increase in shear viscosity, and compatibility with pumping, filtering and dewatering operations.

Future work may include optimization of the size of 1,4-PB backbone, study of high-molecular-weight complementary pair of telechelic associative polymers based on charge-assisted hydrogen bonding (i.e., carboxylic acid/amine interaction) as mist-control additives, further engineering tests of the influence of mist-control additives on fuel efficiency and emissions, and the impact of environmental parameters (e.g., temperature and humidity) on the efficacy of fire protection imparted by mist-control additives.

5.6 Figures

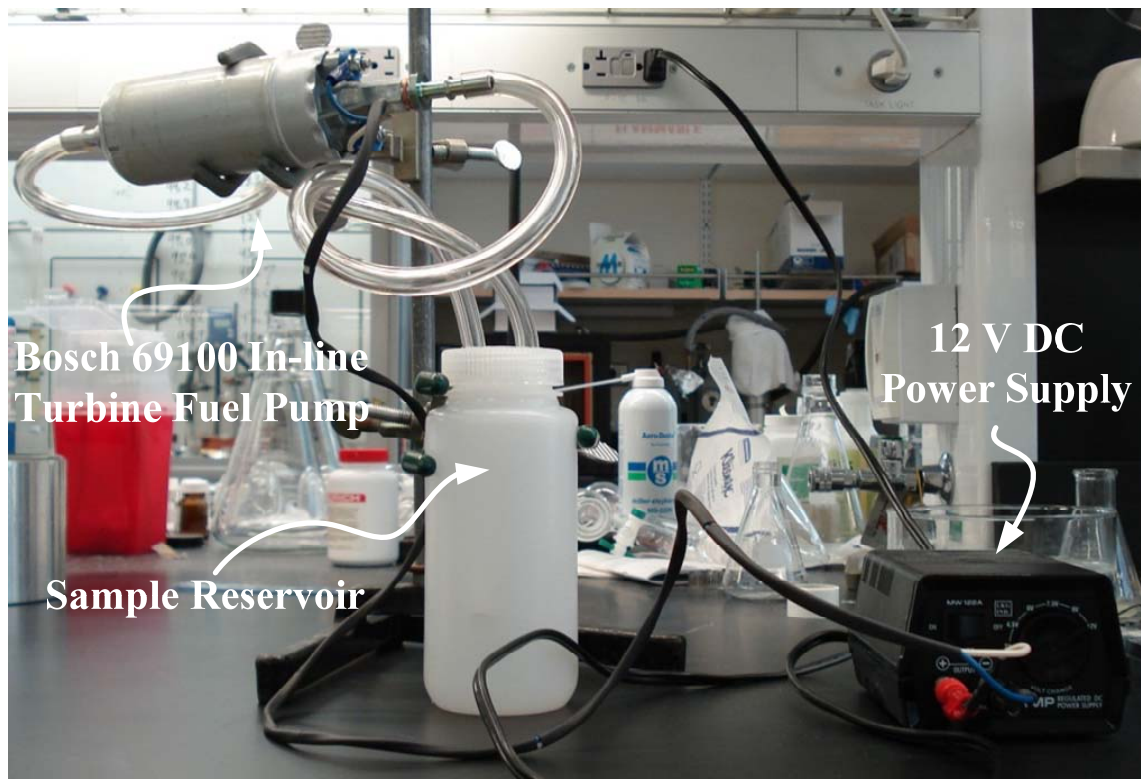


Figure 5.1 Experimental setup for shear stability test.



Figure 5.2 Results of de-watering test. Left: 0.5wt% Jet-A solution of 264K di-TA 1,4-PB; Right: Jet-A

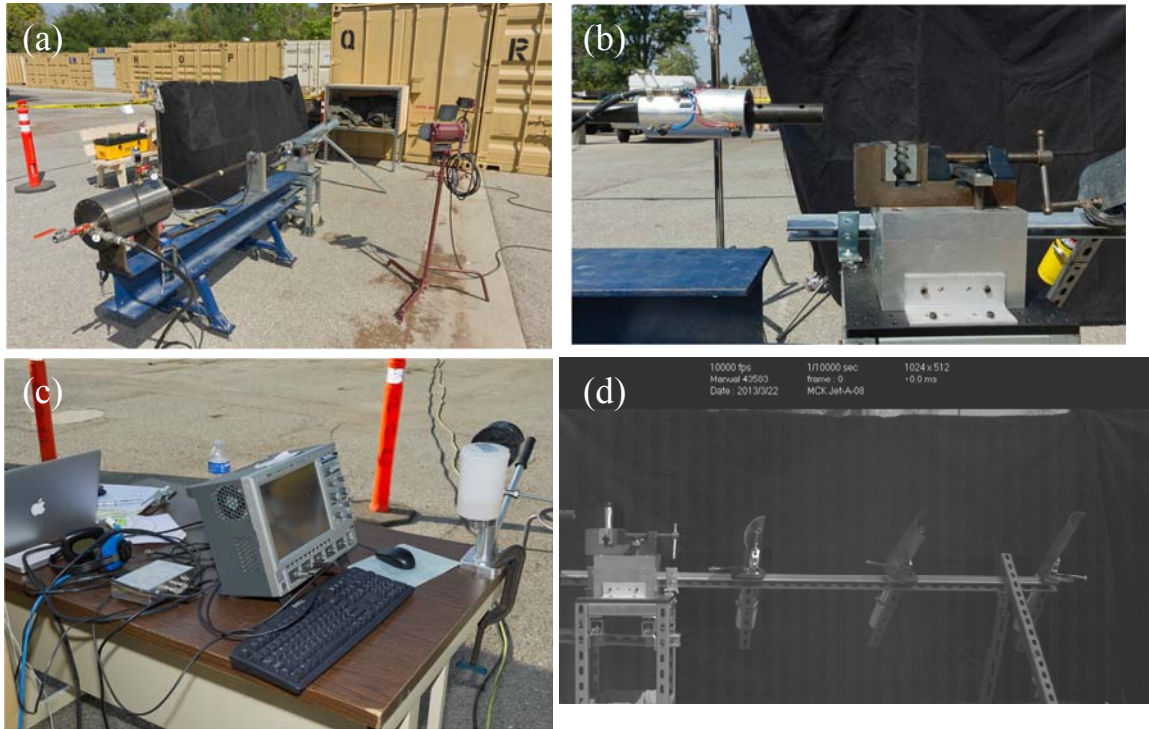


Figure 5.3 Experimental setup for high-speed impact and flame propagation test. (a) Barrel, reservoir of compressed air and light source. (b) Laser-motion detector and sample holder. (c) Oscilloscope as a part of synchronizing mechanism. (d) Side-view of the setup.

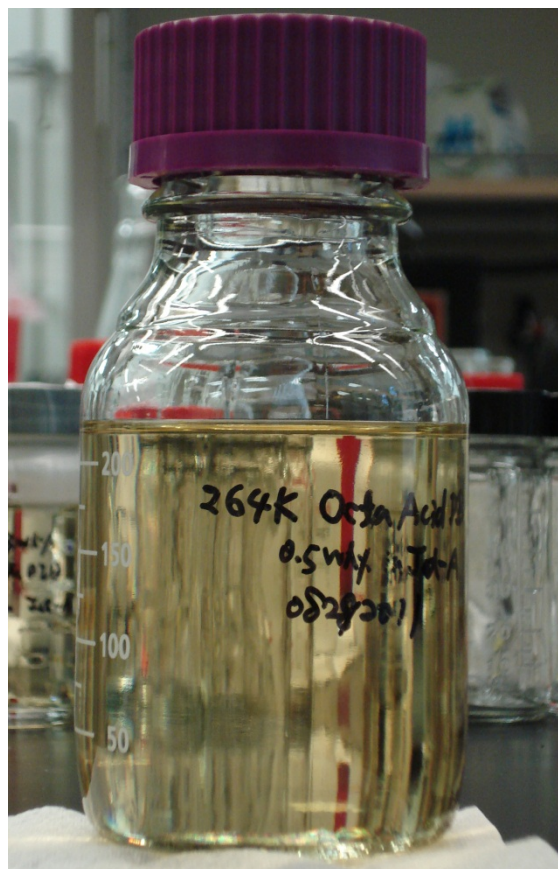


Figure 5.4 Appearance of 0.5wt% Jet-A solution of 264K di-TA 1,4-PB stored at -30°C for 18 months.

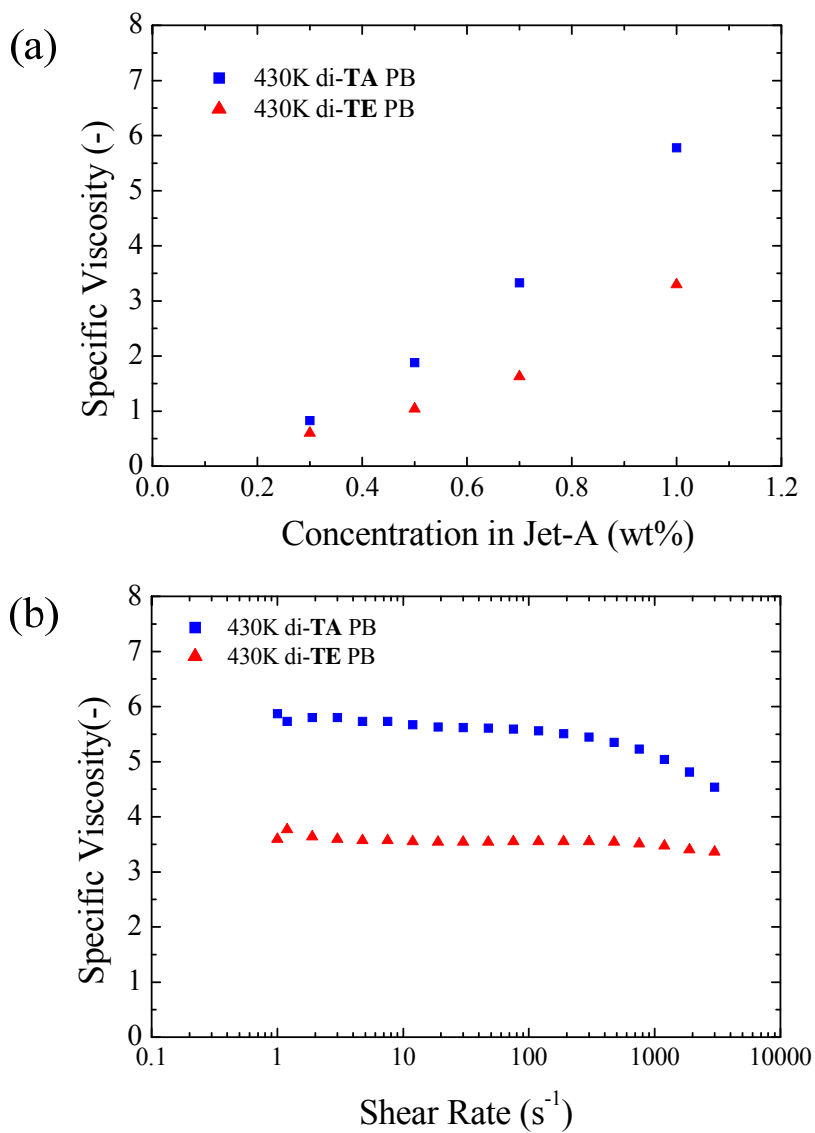


Figure 5.5 Shear viscosity of Jet-A solutions of 430K di-TE 1,4-PB and 430K di-TA 1,4-PB. (a) Specific viscosity as a function of concentration. (b) Specific viscosity of 1wt% Jet-A solutions as a function of shear rate.

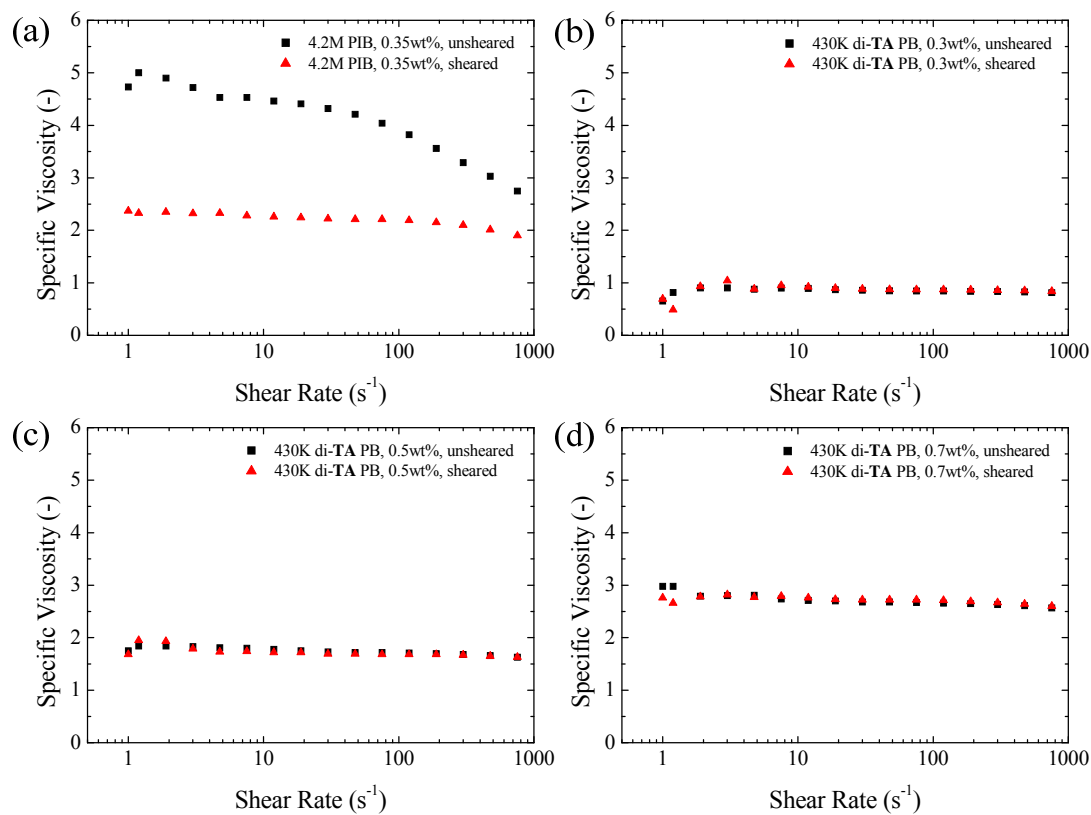


Figure 5.6 Shear viscosity of samples from shear stability test and their unsheared controls. (a) 0.35wt% Jet-A solution of 4.2M PIB. (b) 0.3wt% Jet-A solution of 430K di-TA 1,4-PB. (c) 0.5wt% Jet-A solution of 430K di-TA 1,4-PB. (d) 0.7wt% Jet-A solution of 430K di-TA 1,4-PB.

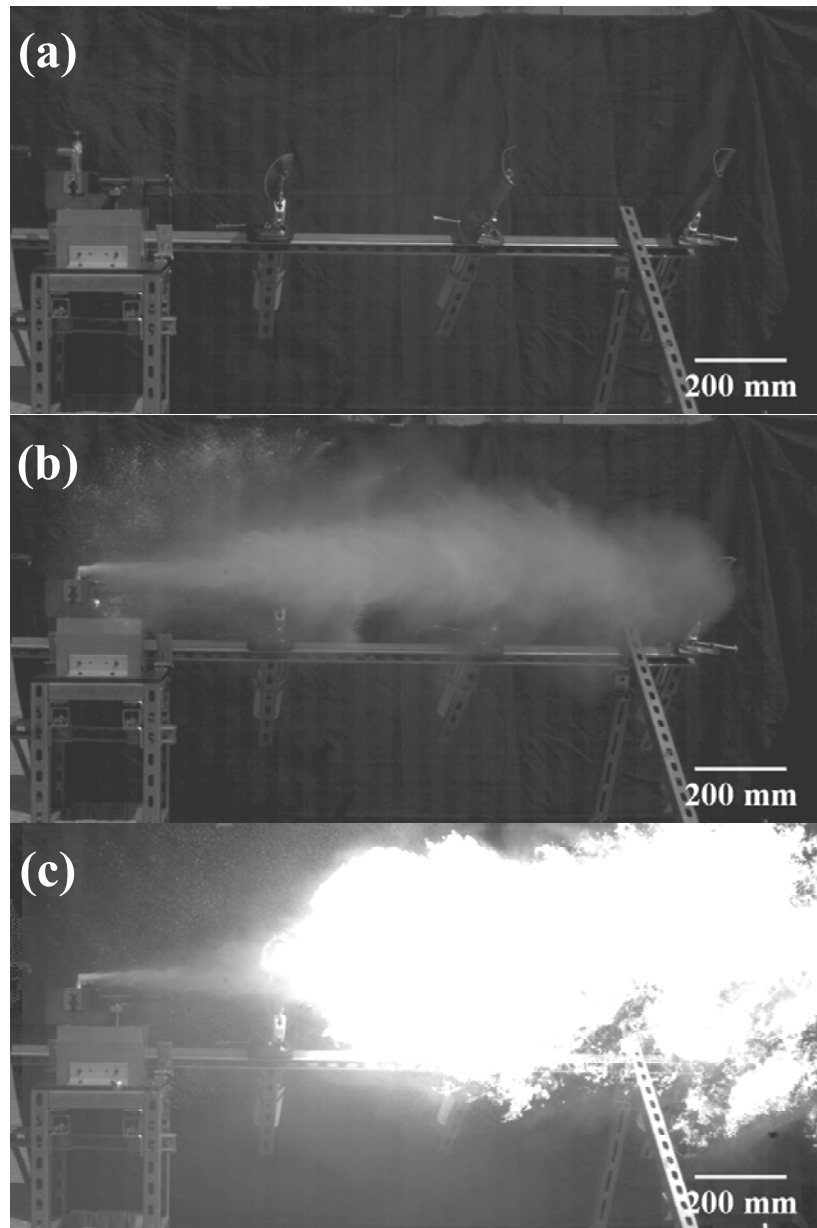


Figure 5.7 Results of Jet-A in impact/flame propagation test. (a) Impact ($t = 0$) (b) $t = 30$ ms after impact (c) $t = 60$ ms after impact.

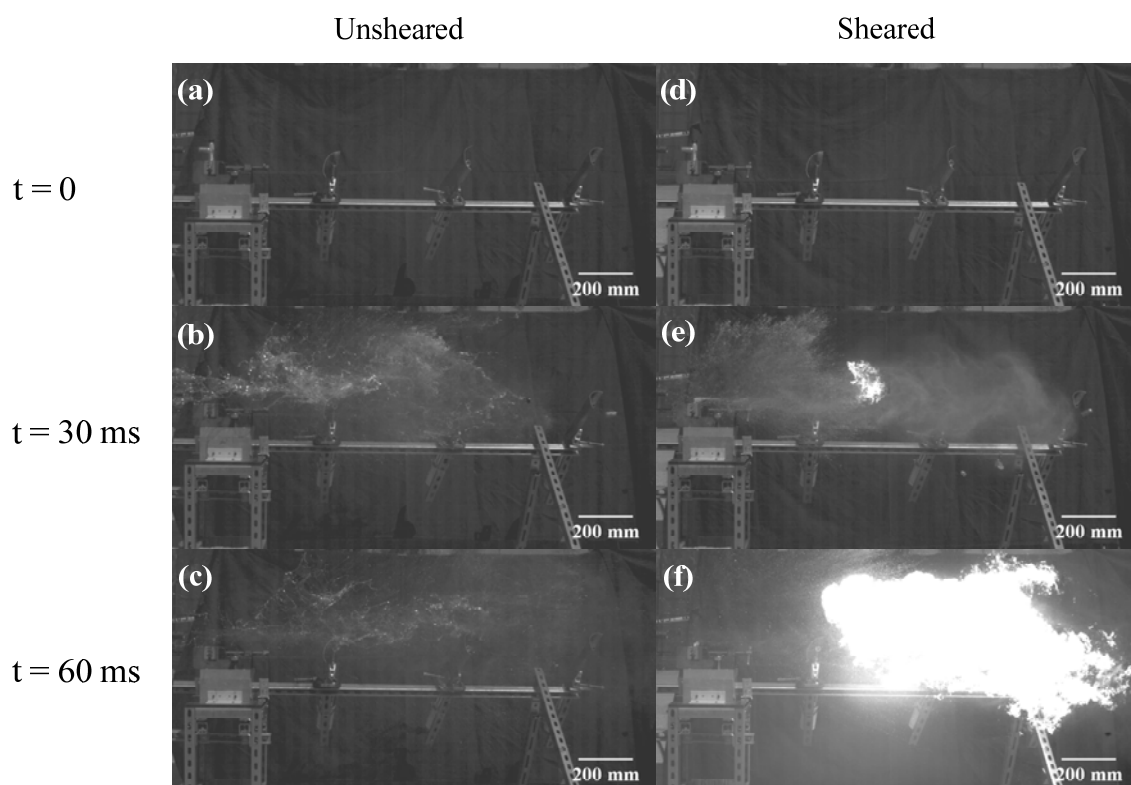


Figure 5.8 Results of 0.35wt% Jet-A solution of 4.2M PIB in flame propagation test. Left: results of unsheared solution. Right: results of sheared solution.

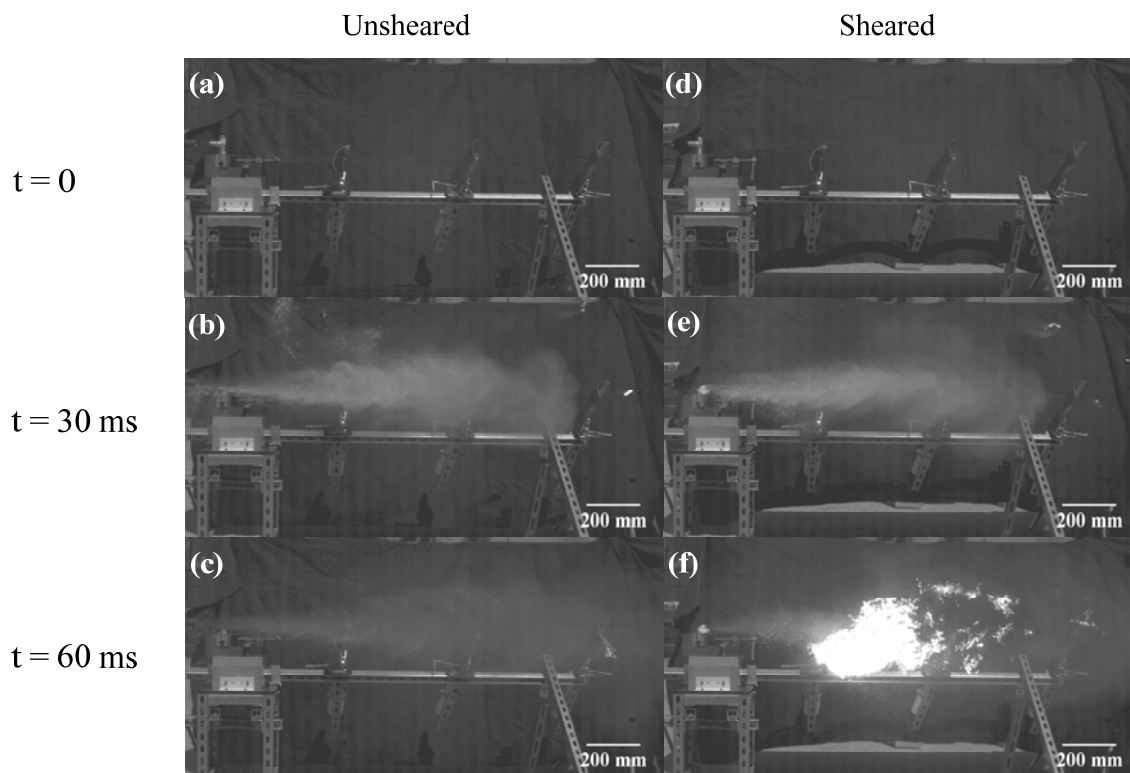


Figure 5.10 Results of 0.5wt% Jet-A solution of 430K di-TA 1,4-PB in flame propagation test. Left: results of unsheared solution. Right: results of sheared solution.

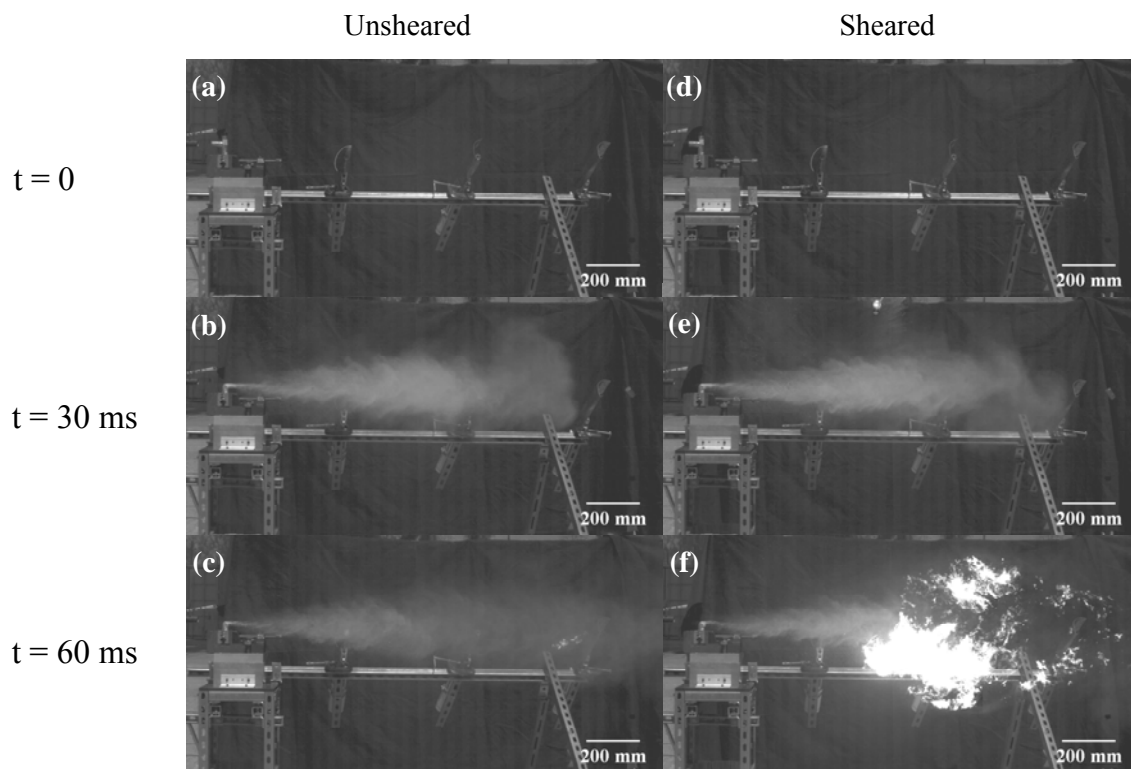


Figure 5.11 Results of 0.7wt% Jet-A solution of 430K di-TA 1,4-PB in flame propagation test. Left: results of unsheared solution. Right: results of sheared solution.

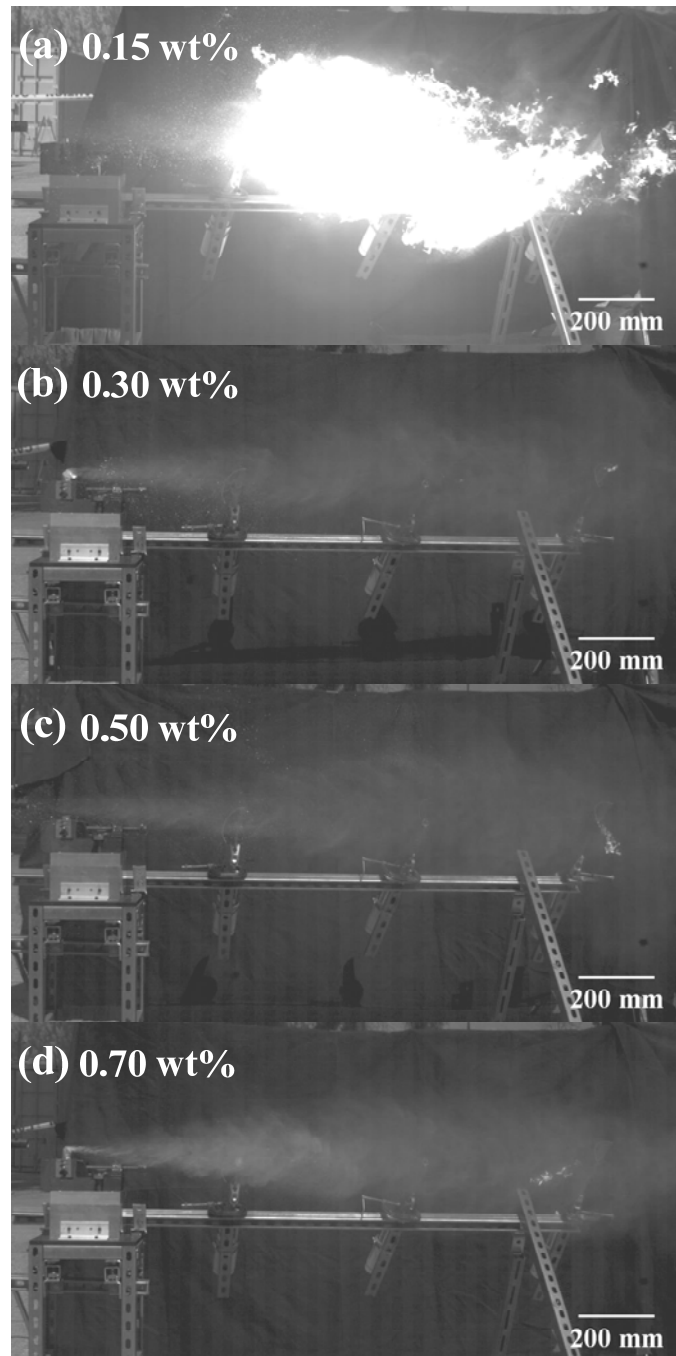


Figure 5.12 Effect of concentration of 430K di-TA 1,4-PB in Jet-A on fire suppression. (a) 0.15wt% (b) 0.3wt% (c) 0.5wt% (d) 0.7wt%. All selected frames are results at $t = 60$ ms after impact.

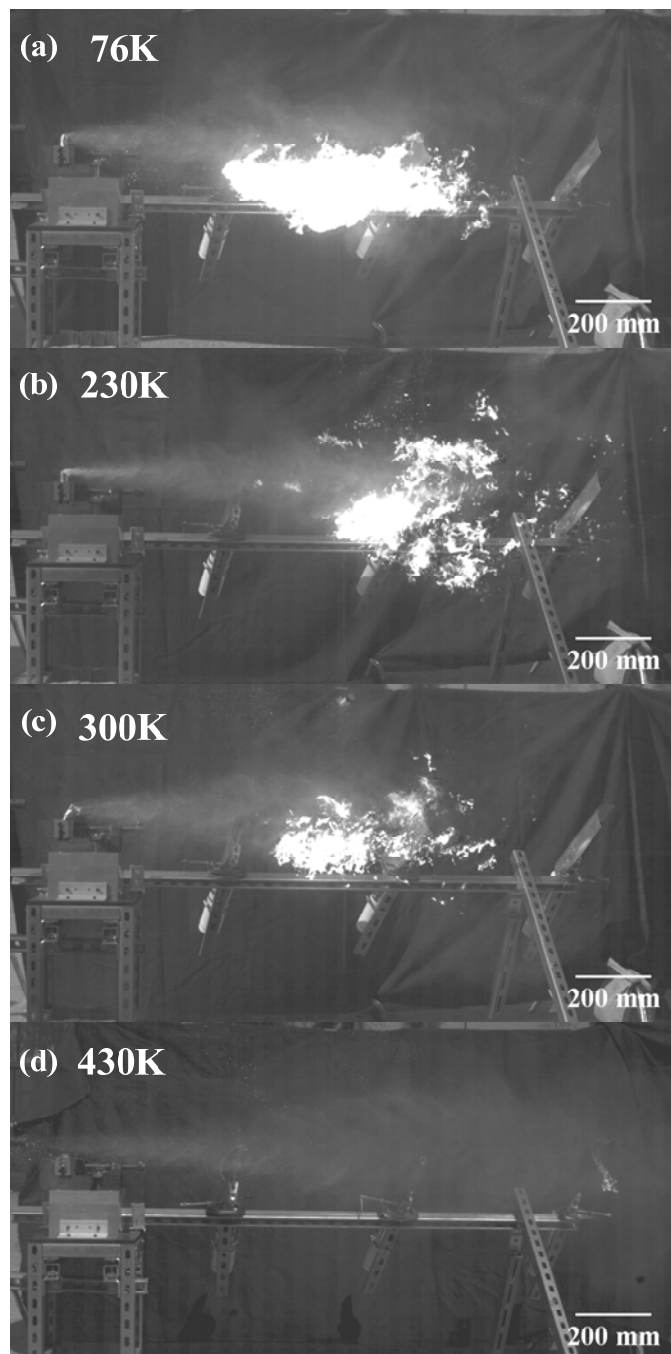


Figure 5.13 Effect of M_w on fire resistance of unsheared 0.5wt% Jet-A solutions of di-TA 1,4-PBs. (a) 76 kg/mol (b) 230 kg/mol (c) 300 kg/mol (d) 430 kg/mol. Note that all selected frames are results at $t = 60$ ms after impact.

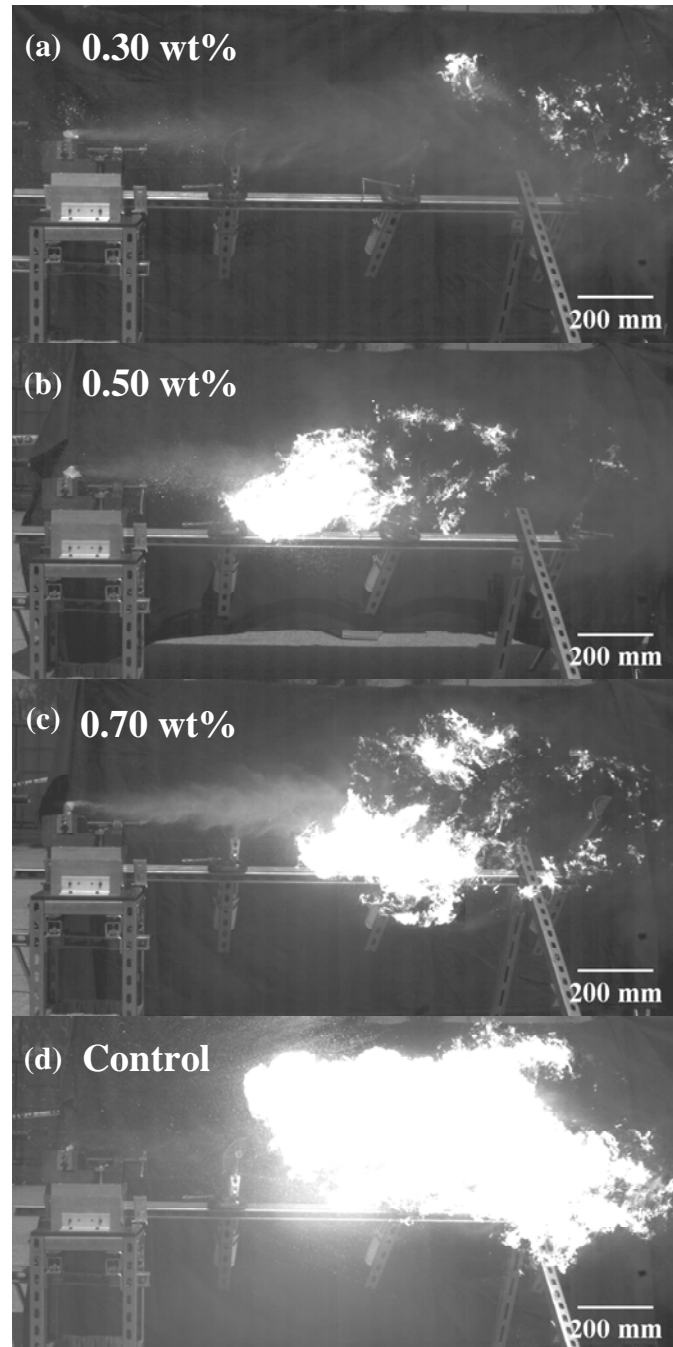


Figure 5.14 Effect of concentration on fire resistance of sheared Jet-A solutions of 430K di-TA 1,4-PB. (a) 0.3wt% (b) 0.5wt% (c) 0.7wt% (d) Control: 0.35wt% Jet-A solution of 4.2MPIB. Note that all selected frames are results at $t = 60$ ms after impact.

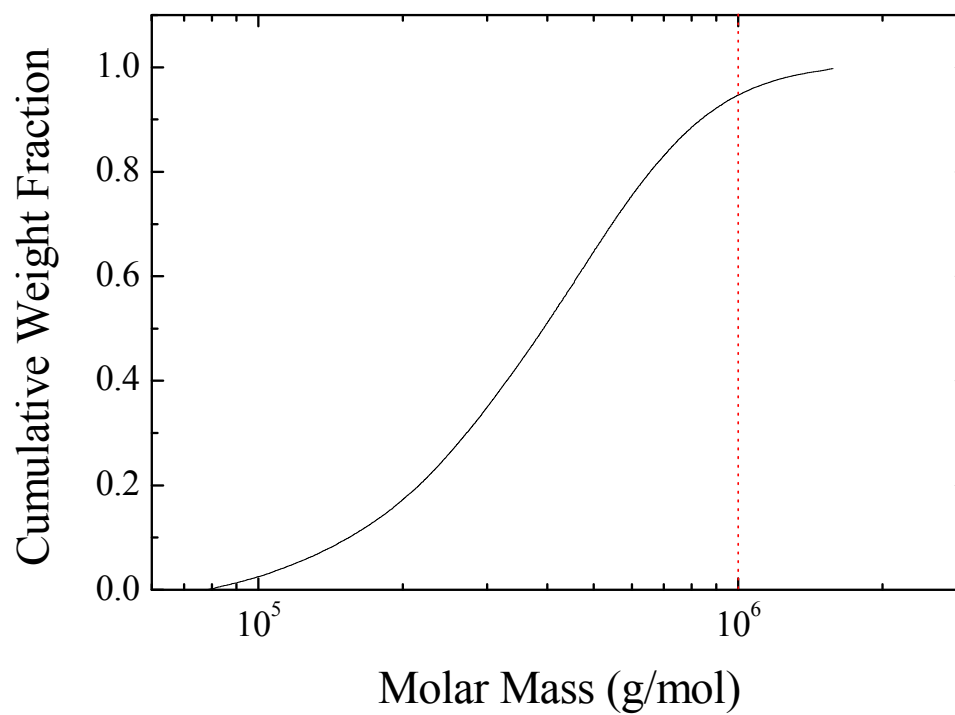


Figure 5.15 Cumulative weight-average molecular weight distribution of 430K di-TE 1,4-PB. The dash line represents the cut-off of the shear-resistant regime of molecular weight.

References

- (1) Rubinstein, M.; Colby, R. H. *Polymer physics*; Oxford University Press: Oxford ; New York, 2003.
- (2) David, R. L. A.; Wei, M. H.; Liu, D.; Bathel, B. F.; Plog, J. P.; Ratner, A.; Kornfield, J. A. *Macromolecules* **2009**, *42*, 1380.
- (3) David, R. L. A.; Wei, M. H.; Kornfield, J. A. *Polymer* **2009**, *50*, 6323.
- (4) David, R. L. A. Dissertation (Ph.D.), California Institute of Technology, 2008.
- (5) John Knight, F.: US, 1983; Vol. 06305736.
- (6) Wright, B. R. *The Forensic Examiner* **2004**, *13*, 14.
- (7) Brostow, W. *Polymer* **1983**, *24*, 631.
- (8) Hunston, D. L.; Zakin, J. L. *Polymer Engineering and Science* **1980**, *20*, 517.
- (9) Peng, S. T. J.; Landel, R. F. *Journal of Non-Newtonian Fluid Mechanics* **1983**, *12*, 95.
- (10) Nyden, M. R.; Stoliarov, S. I.; Westmoreland, P. R.; Guo, Z. X.; Jee, C. *Mat Sci Eng a-Struct* **2004**, *365*, 114.
- (11) Lee, K.; Kim, C. A.; Lim, S. T.; Kwon, D. H.; Choi, H. J.; Jhon, M. S. *Colloid Polym Sci* **2002**, *280*, 779.
- (12) Odell, J. A.; Muller, A. J.; Narh, K. A.; Keller, A. *Macromolecules* **1990**, *23*, 3092.
- (13) Sawaguchi, T.; Seno, M. *Polymer* **1998**, *39*, 4249.
- (14) Bremner, T.; Hill, D. J. T.; O'Donnell, J. H.; Perera, M. C. S.; Pomery, P. J. *J Polym Sci Pol Chem* **1996**, *34*, 971.
- (15) Smith, M.; March, J. *March's advanced organic chemistry : reactions, mechanisms, and structure*; 5th ed.; John Wiley: New York, 2001.
- (16) Yu, J. F. S.; Zakin, J. L.; Patterson, G. K. *J Appl Polym Sci* **1979**, *23*, 2493.
- (17) Henry F. Hamil, N. B. T. X.; William D. Weatherford, J. S. A. T. X.; George E. Fodor, S. A. T. X. Hydrocarbon compositions of high elongational viscosity and process for making the same. US 4731096, 1988.

- (18) Ilan Duvdevani, L. N. J.; Dennis G. Peiffer, E. B. N. J.; John A. Eckert, M. N. J.; Robert D. Lundberg, B. N. J. Antimisting system for hydrocarbon fluids. US 4516982, 1985.
- (19) Chao, K. K.; Child, C. A.; Grens, E. A.; Williams, M. C. *Aiche Journal* **1984**, *30*, 111.
- (20) Willauer, H. D.; Ananth, R.; Hoover, J. B.; Foote, A. B.; Whitehurst, C. L.; Williams, F. W. *Combust Sci Technol* **2007**, *179*, 1303.
- (21) Schrodi, Y.; Pederson, R. L. *Aldrichim Acta* **2007**, *40*, 45.
- (22) Michael A. Taylor, H. T. N.; Ajay V. Bapat, S. Removal of organic volatiles from polymer solutions and dispersions. US 5414193, 1995.

Appendix A Supplemental Information

A.1 Measurements of Polymer Molecular Weights

The determination of molecular weight and molecular weight distribution is of central interest in polymer analysis, as the molecular weight of a polymer directly relates to its physical properties.¹ Take telechelic associative polymers as mist-control additives for kerosene for example, their efficacy in providing fire protection and resistance to shear degradation rely on proper choice of backbone length, which falls in the range $M_w = 5 \times 10^5 - 10^6$ g/mol (refer to Chapter 5). Table A.1 summarizes common characterization methods for determining different average molecular weights (MWs) and molecular weight distributions (MWDs) of polymers.¹⁻³

Table A.1 Molecular Weight Measurement Methods¹⁻³

Method	Absolute	Relative	M_n	M_w	Range (g/mol)
Proton NMR end-group analysis	×		×		$M_n < 2.5 \times 10^4$
Vapor pressure osmometry	×		×		$M_n < 3 \times 10^4$
Ebulliometry	×		×		$M_n < 3 \times 10^4$
Light Scattering (LS)	×			×	$10^4 < M_w < 10^7$
Intrinsic Viscosity		×			$M < 10^6$
GPC ^a with concentration detectors		×	×	×	$10^3 < M_w < 10^7$
GPC ^a with concentration and LS detectors	×		×	×	$10^4 < M_w < 10^7$
MALDI-TOF-MS ^b	×		×	×	$M < 3 \times 10^4$

^aGPC, gel permeation chromatography. ^bMALDI-TOF-MS, matrix-assisted laser desorption/ionization times -of-flight mass spectroscopy.

Among the methods in Table A.1, GPC with concentration and LS detectors (referred to as “GPC-LS “hereinafter) was chosen in the present study for determining MW and MWD of telechelic associative 1,4-PBs due to the following reasons: (1) it allows measurements of absolute weight-average MWs and corresponding MWDs; (2) it has a wide applicable range (10^4 - 10^7 g/mol) which covers the MW range of interest (5×10^5 - 10^6 g/mol) for mist-control applications; (3) it is comparatively easy to implement. Although MALDI-TOF-MS is capable of measuring absolute MWs and MWDs of polymers with accuracy that GPC-LS can hardly match, it is not practically useful in analyzing polymers of $MW > 30$ kg/mol;⁴ selection of matrix compounds, sample preparation and interpretation of the mass spectra become difficult in the case of synthetic polymers of $MW > 30$ kg/mol and thus detract from the benefits associated with the unrivalled accuracy provided by MALDI-TOF-MS.^{1,3,5} Given that what we pursued are telechelic 1,4-PBs of $MW \gg 30$ kg/mol, it is clear that GPC-LS presents as a better option to measure MWs than MALDI-TOF-MS in the present study. The same rationale also applies to the other competing method, proton NMR end-group analysis, which has been widely used in determining number-average MWs (i.e., M_n) of synthetic polymers *via* comparing the integration values of signals of backbone protons to those of the end-group protons.^{1,6,7} The implementation of proton NMR end-group analysis is straightforward: the M_n value of a polymer can be simply derived from its ^1H NMR spectrum without any additional experimental work. However, the determination of M_n by proton NMR end-group analysis for polymers of $MW > 25$ kg/mol loses its accuracy due to a diminished resolution resulting from the inherent detection limit of proton NMR spectroscopy, and the uncertainty in the M_n values becomes greater for polymers of

higher MWs.¹ The other issue of this method is that it lacks the ability to measure MWDs of polymers. These shortcomings render proton NMR end-group analysis an *ineffective* method to characterize high-MW (i.e., MW > 100 kg/mol) telechelic 1,4-PBs as potential mist-control additives for kerosene.

In the case that associative groups are attached onto the chain ends of telechelic 1,4-PBs, measuring of MWs and MWDs of such polymers by GPC-LS becomes challenging, since the associative chain ends could possibly interact with the column packing, or drive the formation of supramolecular aggregates in THF, leading to false reading of MWs and MWDs. As discussed earlier in Chapter 2, we did observe confusing GPC-LS results as we characterized 230K di-**TE** 1,4-PB and its corresponding carboxyl-terminated polymer after TFA hydrolysis, 230K di-**TA** 1,4-PB (Section 2.4.3): compared to the non-associative 230K di-**TE** 1,4-PB, the apparent M_w of 230K di-**TA** 1,4-PB was found higher by 63% (Table 2.3 and Figure A.1). We hypothesized that the apparent increase in M_w resulted from the aggregate of associative **TA** end groups in THF, rather than crosslinking of 1,4-PB backbone during TFA hydrolysis of *tert*-butyl ester groups. To test our hypothesis, we treated 230K di-**TA** 1,4-PB with LiAlH_4 in THF so as to reduce the highly associative carboxyl groups to *much less* associative hydroxyl groups. The GPC-LS result of the resultant hydroxyl-terminated 230K telechelic 1,4-PB, as shown in Figure A.1, virtually overlaps with that of 230K di-**TE** 1,4-PB, although the former seems slightly broadened compared to the latter. Comparison of the three GPC-LS traces in Figure A.1 verified our hypothesis: the apparent increase in M_w after TFA hydrolysis of 230K di-**TE** 1,4-PB was due to aggregation of associative **TA** end groups, since the increase in M_w disappeared after the carboxyl groups on polymer chain ends

were reduced to hydroxyl groups. It also suggests that the mild condition of TFA hydrolysis does not cause appreciable amount of crosslinking of 1,4-PB backbone. As for the broadening of GPC-LS trace of hydroxyl-terminated 230K telechelic 1,4-PB, it might result from interaction of hydroxyl-terminated chain ends with column packing. The results in Figure A.1 also reveal the importance of interpreting GPC-LS results of telechelic associative polymers with scrutiny, since association of chain ends and chain-end/column interaction can both result in false reading of MWs and MWDs. In other words, using the *non-associative* forms of telechelic associative polymers in GPC-LS analysis yields more accurate information concerning the MWs and MWDs of polymer backbones on the condition that the transformation of associative chain ends to non-associative counterparts does not damage the backbones.

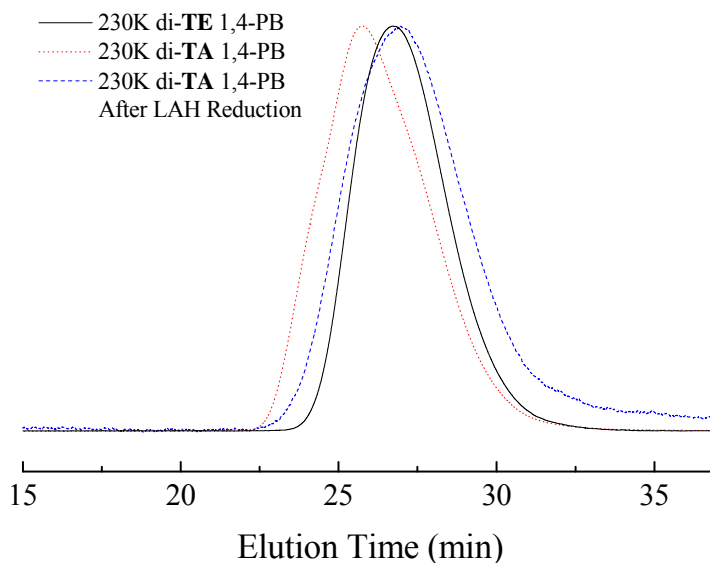


Figure A.1 GPC-LS (THF, 35°C) traces of 230K di-TE 1,4-PB, 230K di-TA 1,4-PB and the resultant polymer of LAH reduction of 230K di-TA 1,4-PB.

A.2 Effect of COD Purity on the Proceeding of ROMP with CTAs

In the preceding chapter (Section 2.3.2), we reported that the purity of VCH-free COD has a profound effect on the synthesis of telechelic 1,4-1,4-PBs *via* ROMP of COD using Grubbs II: peroxides and *n*-butanol (introduced during $\text{BH}_3 \cdot \text{THF}$ treatment of COD according to the Macosko protocol) can also adversely affect the metathetical activity of Grubbs II by reacting with it and irreversibly transforming it into inactive species. In response to the issues associated with peroxides and *n*-butanol, we developed a multi-stage process (Section 2.2.3) to rigorously purify COD. To illustrate the influence of the purity of VCH-free COD on the preparation of telechelic 1,4-PBs *via* ROMP of COD, we chose the synthesis of di-**TE** 1,4-PB *via* the two-stage ROMP of COD with octa-functional *tert*-butyl ester-terminated bis-dendritic CTA (compound **8** in Scheme 2.1) as the benchmark reaction (Figure A.2). Two different batches of VCH-free COD were prepared: the first (i.e., the control, COD I) was afforded *via* purification according to only the Macosko protocol, whereas the second one (COD II) was prepared according to the procedure described in Section 2.2.3. The implementation of two-stage ROMP using both batches of COD was the same as the procedure in Section 2.2.3, in which the total monomer:CTA ratio was 2000:1, and 100 eq of COD was used in the first stage of ROMP; the load of Grubbs II was 1/30 eq of the CTA. Here we chose the following properties to quantitate the effect of the purity of COD: (1) the period of time during which the reaction mixture develops enough viscosity to stop the magnetic stir bar from moving after the addition of 1900 eq of COD (t_v) (2) the overall conversion of COD (X_f , measured by ^1H NMR analysis of the aliquot of reaction mixture) (3) the *cis/trans* ratio of the polymeric species in the aliquot (measure by ^1H NMR analysis) (4) M_w of the

resultant polymer (measured by GPC-LS). The results for COD I and COD II were summarized in Table A.2.

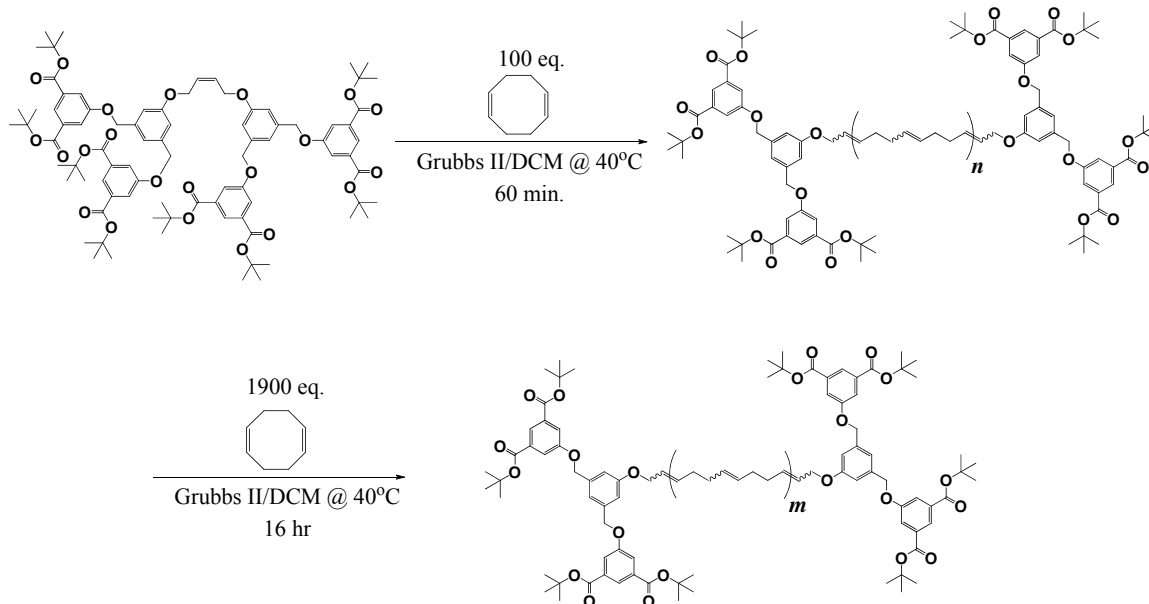


Figure A.2 Synthesis of di-TE 1,4-PB *via* two-stage ROMP of COD as the benchmark reaction for the influence of the purity of VCH-free COD.

Table A.2 Results of Synthesis of Di-TE 1,4-PB *via* ROMP of Batch 1 and Batch 2 VCH-free COD

	COD I	COD II
t_v (min)	40.0	1.5
X_f (mol%)	85.0	97.6
<i>cis/trans</i> ratio	2.20	1.73
M_w (kg/mol)	264	142
PDI	1.58	1.43

Table A.2 shows that the second stage of ROMP of COD II proceeded significantly faster ($t_v = 1.5$ min) compared to that of COD I ($t_v = 40$ min); the conversion

of COD II was nearly quantitative ($X_f = 97.6\%$), whereas the reaction stopped at $X_f = 85\%$ in the case of COD I. In addition, ^1H NMR analysis of aliquots taken in the end of polymerization reactions also revealed that the use of COD II led to a lower *cis/trans* ratio (1.73) compared to the case of COD I (2.20). The M_w of the resultant polymer of ROMP of COD II (142 kg/mol), as revealed by GPC-LS analysis, was found significantly lower than that of ROMP of COD I (264 kg/mol). When considered as a whole, these results clearly indicate that Grubbs II possesses a *higher* metathetical activity (or a higher turnover number) when impurities in VCH-free COD that can interfere with Grubbs II are removed. This explains the much faster reaction rate of the second stage of ROMP of COD II. Similarly, Grubbs II in the presence of COD II could perform more cycles of metathesis reactions compared to in COD I, and thus a nearly quantitative $X_f = 97.6\%$ was achieved in the case of COD II. The low *cis/trans* ratio (1.73) and M_w (142 kg/mol) resulting from ROMP of COD II suggest that a considerable fraction of ruthenium complexes on polymer chain ends remained metathetically active when COD II was mostly consumed, and as a result they continued to react with available C=C bonds present in the reaction mixture (in this case, C=C on polymer backbones) till they reached their maximum turnover number. The consumption of backbone by active ruthenium centers on chain ends (i.e., back-biting) led to the decreases in *cis/ratio* ratio and M_w .

In sum, the significantly enhanced activity of Grubbs II observed in the present study validates our effort to develop the multi-stage rigorous purification of COD (Section 2.2.3).

A.3 Synthesis of 76K, 264K and 300K Di-TE 1,4-PBs

In Chapter 3, we reported the rheological properties of 76K di-TA 1,4-PB in 1-chlorododecane (CDD) and tetralin (TL); in Chapter 5, we demonstrated the negligible interference of di-TA 1,4-PB with dewatering of Jet-A using 264K di-TA 1,4-PB, and we also included 0.5wt% Jet-A solution of 300K di-TA 1,4-PB in the high-speed impact/flame propagation test as a part of the study on the effect of the length of 1,4-PB backbone on mist-control of Jet-A. The protected forms of the three aforementioned di-TA 1,4-PBs were not synthesized exactly according to the synthetic strategy we reported in Chapter 2; as a result, we did not include them in Chapter 2. Here we report the syntheses of 76K, 264K, and 300K di-TE 1,4-PBs in detail.

76K di-TE 1,4-PB. Octa-functional *tert*-butyl ester terminated bis-dendritic CTA (12.6 mg, 8.7 μmol , refer to Scheme 2.1) was loaded into a 50 mL Schlenk reactor (charged with a magnetic stir bar). The content was degassed by 5 cycles of pulling vacuum/filling argon, and the reactor was placed in an oil bath at 40°C. Grubbs II (0.8 mg, 0.92 μmol) was dissolved with 1 mL of deoxygenated anhydrous toluene under argon atmosphere, and the resultant solution was syringe-transferred into the reactor. The catalyst and CTA were given 5 min reach equilibrium, and 0.12 mL of freshly vacuum-distilled COD (0.1 g, 0.98 mmol) purified according to the Macosko protocol was injected into the reactor to allow the formation of macro CTA. 55 min later, 2.25 mL of COD (1.98 g, 18.2 mmol) and 5 mL of deoxygenated anhydrous toluene were injected into the reactor to start chain extension. The reaction mixture was stirred at 40°C for 16 h, and 20 mL of DCM (with 0.1 g of BHT) was added to dilute the mixture. The diluted solution was precipitated into 300 mL of methanol at room temperature. Drying the precipitated polymer *in vacuo* at

room temperature overnight afforded 1.60 g (76.6% yield) of white, opaque polymer. GPC-LS (THF, 35°C): $M_w = 76$ kg/mol, PDI = 1.46.

264K di-TE 1,4-PB. Octa-functional *tert*-butyl ester terminated bis-dendritic CTA (13.0 mg, 9.15 μ mol, refer to Scheme 2.1) was loaded into a 50 mL Schlenk reactor (charged with a magnetic stir bar). The content was degassed by 5 cycles of pulling vacuum/filling argon, and the reactor was placed in an oil bath at 40°C. 0.26 mL of 1 mg/mL anhydrous DCM solution of Grubbs II (0.26 mg, 0.31 μ mol) was injected into the mixture to equilibrate with the CTA, followed immediately by adding a small amount of degassed, freshly vacuum-distilled VCH-free COD (0.10 g, 0.92 mmol; purified according to the Macosko protocol) to the mixture to start the polymerization reaction. The mixture was stirred at 40°C for 1 hr. A large amount of degassed, freshly vacuum-distilled purified COD (2.00 g, 18.3 mmol; purified according to the Macosko protocol) in degassed, anhydrous DCM (4 mL) was injected into the mixture. The mixture was stirred at 40°C for 15 h. Additional DCM (20 mL) and 0.1 g of BHT were added, and the mixture was precipitated into 300 mL of acetone at room temperature. Drying the precipitated polymer *in vacuo* at 35°C overnight afforded 1.60 g (80.0% yield) of transparent, pale-yellow polymer. ^1H NMR analysis (500 MHz, CDCl_3) showed that the conversion of COD was 85%, and the *cis/trans* ratio (refer to Table 2.2) was 2.20. GPC-LS (THF, 35°C): $M_w = 264$ kg/mol, PDI = 1.58.

300K di-TE 1,4-PB. 142K di-TE 1,4-PB (0.44 g, $M_w = 142$ kg/mol, PDI = 1.43; entry 4 in Table 2.2) was used as a macro CTA, and it was loaded into a 50 mL Schlenk reactor (charged with a magnetic stir bar). The content was degassed by 5 cycles of pulling

vacuum/filling argon, followed by homogenization with 6 mL of deoxygenated, anhydrous DCM at R.T. The reactor was placed in a water bath at 40°C. 0.06 mL of 0.5 mg/mL anhydrous DCM was injected into the solution *via* a 0.1 mL Hamilton Gastight precision syringe. 2.2 mL of freshly vacuum-distilled, rigorously purified COD (refer to Section 2.2.3) was immediately injected into the reaction mixture to start chain extension reaction. The mixture was stirred at 40°C for 30 min, and an aliquot was taken for ¹H NMR analysis. The reaction was then immediately terminated by the addition of 30 mL of oxygen-containing DCM (with 0.12 g of BHT). The diluted mixture was precipitated into 300 mL of acetone at room temperature. Drying the precipitated polymer *in vacuo* at 35°C overnight afforded 1.61 g (66.0% yield) of transparent, pale-yellow polymer. ¹H NMR analysis (500 MHz, CDCl₃) showed that the conversion of COD was 78.9%, and the *cis/trans* ratio (refer to Table 2.2) was 2.25. GPC-LS (THF, 35°C): M_w = 304 kg/mol, PDI = 1.44.

A.4 Hydrolysis of *tert*-Butyl Ester-Terminated Telechelic 1,4-PBs Using Ground KOH

This part of the present study was aimed to investigate the feasibility of recovering the carboxyl groups on chain ends of di-**TE** 1,4-PBs *via* treating the *tert*-butyl ester terminated polymers with ground KOH in THF followed by acidification using HCl (Figure A.3). 0.5 g of di-**TE** 1,4-PB (M_w = 287 kg/mol, PDI = 1.69; referred to as 287K di-**TE** 1,4-PB hereinafter) was loaded into a 50 mL Schlenk reactor (charged with a magnetic stir bar) and dissolved with 25 mL of THF. Ground KOH (0.4 g, 6.3 mmol) was loaded into the reactor. The mixture was degassed by 3 freeze-pump-thaw cycles, and then stirred at room temperature for 16 h. 1 mL of 12 M HCl_(aq) in 20 mL of THF was

drop-wise added into the reaction mixture to neutralize unreacted KOH and acidify the resultant carboxylate groups on the chain ends. After filtering the salt, the polymer solution was concentrated *via* rotary-evaporation of THF under reduced pressure. The concentrated solution was precipitated into 300 mL of methanol at room temperature. The precipitated polymer was further purified by 2 more cycles of reprecipitation from THF into methanol at room temperature. Drying the precipitated polymer *in vacuo* at room temperature overnight afforded 0.35 g (70.0% yield) of transparent, faint-yellow polymer.



Figure A.3 Reaction scheme of hydrolysis of di-TE 1,4-PBs using the KOH/HCl protocol.

The efficacy of hydrolysis of *tert*-butyl ester end groups using ground KOH/HCl was initially evaluated by ^1H NMR analysis of the resultant polymer in CDCl_3 ; trace amount of acetone- d_6 was added into the sample to facilitate the dissolution of polymer. The signal of *tert*-butyl groups on polymer chain ends ($\delta = 1.61$ ppm) was not observed in the ^1H NMR spectrum of the resultant polymer 287K di-TA 1,4-PB ((Figure A.4), suggesting the possibility of complete recovery of carboxyl groups.

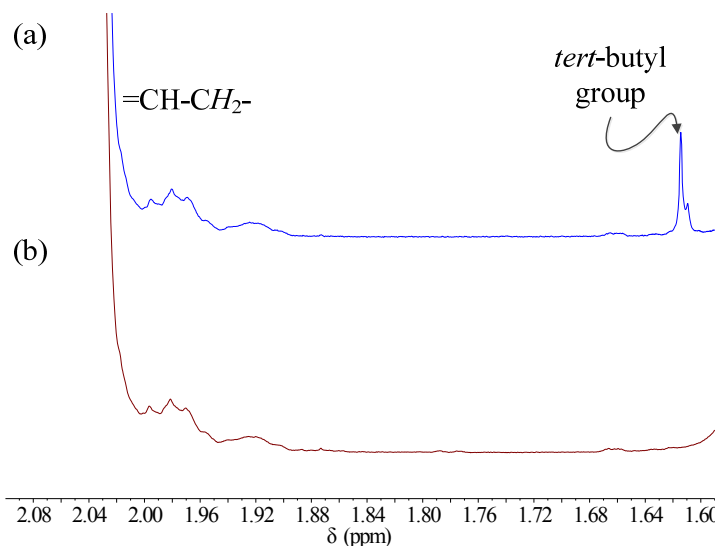


Figure A.4 Expanded ^1H NMR (500 MHz) spectra of CDCl_3 solutions of 287K di-**TE** 1,4-PB and 287K di-**TA** 1,4-PB prepared *via* the KOH/HCl protocol. (a) 287K di-**TE** 1,4-PB (b) 287K di-**TA** 1,4-PB.

Steady-flow shear rheology was also adopted as a complementary method to investigate the efficacy of the KOH/HCl protocol. Similar to the study described in Chapter 3, we prepared 1wt% 1-chlorododecane (CDD) solutions of 287K di-**TE** 1,4-PB and 287K di-**TA** 1,4-PB resulting from the KOH/HCl protocol, and measured their shear viscosity according to the protocol described in Section 3.3.2. We found that the specific viscosity of the 1wt% CDD solution of 287K di-**TA** 1,4-PB was higher than that of 287K di-**TE** 1,4-PB by 0.56, whereas the difference in shear viscosity between the 1wt% CDD solutions of 230K di-**TE** 1,4-PB and its corresponding polymer after TFA treatment (230K di-**TA** 1,4-PB, refer to Sections 2.2.3 and 3.3.2) was 4.34 (Figure A.5). As discussed earlier in Section 2.4.3, treating *tert*-butyl ester terminated telechelic 1,4-PBs with TFA in DCM does not cause crosslinking of 1,4-PB backbones. Therefore, the results in Figure A.x suggest that the deprotection of 287K di-**TE** 1,4-PB using ground

KOH was *incomplete*. As discussed earlier in Chapter 2, the heterogeneous nature of this protocol may limit the mass transfer of polymer chain ends to the surface of ground KOH. The other factor contributing to the incomplete conversion of *tert*-butyl ester groups is the gelation of reaction mixture occurred within 1 h after 287K di-**TE** 1,4-PB was stirred with ground KOH in THF, which resulted from the aggregation of resultant carboxylate potassium salt on chain ends. We believe the gelation further hindered unreacted *tert*-butyl ester end groups from reaching the surface of KOH and eventually stopped the reaction from going to completion. These disadvantages render the KOH/HCl protocol a *less* effective way to hydrolyze the *tert*-butyl ester groups on chain ends of di-**TE** 1,4-PBs.

Why did ^1H NMR analysis and steady-flow shear rheology give contradicting conclusions concerning the efficacy of removing *tert*-butyl groups using ground KOH? We noticed that the signals of the aromatic protons of the poly (benzyl ether) dendron on polymer chain ends were not observed either. A possible explanation is that partial recovery of carboxyl groups on the dendritic chain ends provides enough hydrophilicity to render the chain ends insoluble in CDCl_3 , which leads to the absence of signals of the poly (benzyl ether) dendrons on chain ends. We believe that using more acetone- d_6 in the ^1H NMR sample of the polymer resulting from ground KOH treatment of 287K di-**TE** 1,4-PB would improve the solubility of polymer chain ends in CDCl_3 and thus provide information concerning the conversion of *tert*-butyl ester groups on polymer chain ends with better accuracy.

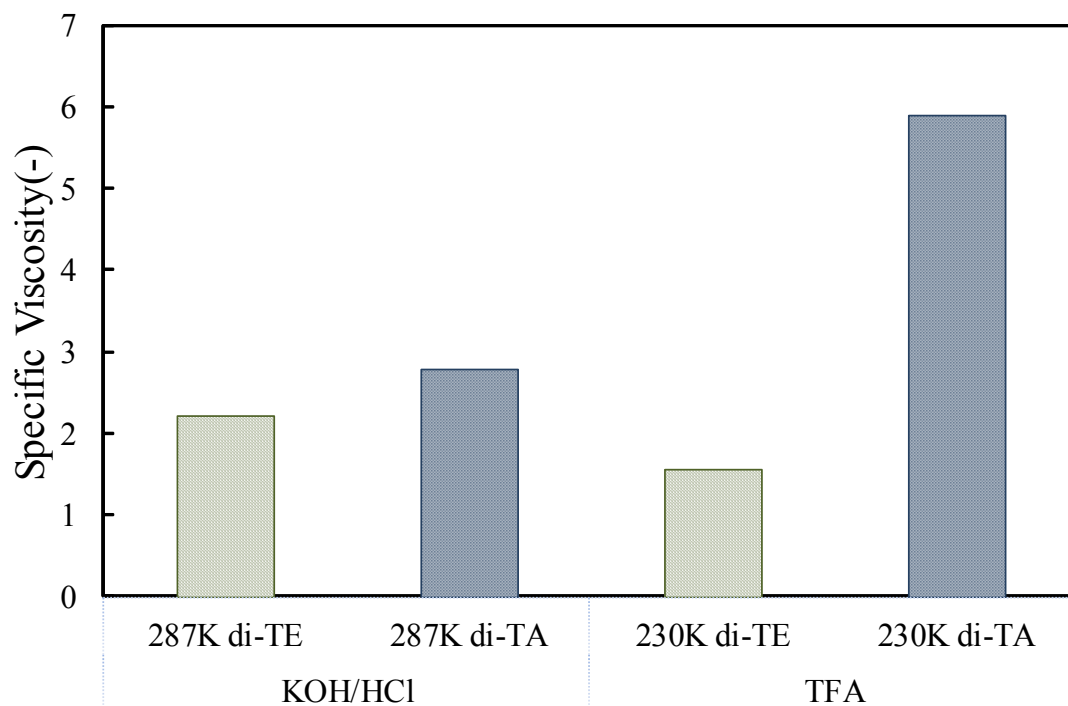


Figure A.5 Specific viscosity of 1wt% solutions of test polymers in 1-chlorododecane (CDD). Left: 287K di-TE 1,4-PB and its corresponding carboxyl-terminated polymer 287K di-TA 1,4-PB prepared *via* the KOH/HCl protocol; right: 230K di-TE 1,4-PB and its corresponding carboxyl-terminated polymer 230K di-TA 1,4-PB prepared *via* the TFA protocol.

A.5 Synthesis of Multi-Functional Chloro-Terminated 1,4-PBs

In Chapter 3, we reported the success of synthesizing tertiary amine-terminated telechelic 1,4-PBs *via* two-stage post-polymerization end-functionalization of chloro-terminated telechelic prepolymers. Here we report the details of the syntheses of the CTAs, and the following preparation of chloro-terminated telechelic prepolymers *via* two-stage ROMP of COD with these CTAs.

Tetra-functional Chloro-Terminated Bis-dendritic CTA (A1) (Figure A.6). To an anhydrous THF (20 mL) of cyanuric chloride (2.62 g, 14.1 mmol) in a 100 mL RBF was

slowly added an anhydrous DMF (4.5 mL) solution of compound **6** in Scheme 2.1 (1.00 g, 2.75 mmol). The mixture was stirred at room temperature overnight. 30 mL of THF was added to the mixture, and it was filtered to remove precipitated cyanuric acid-DMF complex. The filtrate was concentrated *via* rotary evaporation, and extracted with 50 mL of EA and 50 mL of 1M HCl_(aq). The organic phase was washed twice with 1M HCl_(aq) (discarding the aqueous phase after each wash), and the solvent was removed under reduced pressure. The remaining solid was purified by dissolving in 20 mL of boiling ethanol and allowing it to recrystallize in the freezer overnight. Vacuum filtration and removal of solvents under reduced pressure afford analytically pure **A1** (1.03 g, 2.37 mmol, 86.2% yield) as fine, white crystals. ¹H NMR (500 MHz, CDCl₃): δ = 7.02 (t, J = 1.5 Hz, 2H), 6.91 (d, J = 1.5 Hz, 4H), 5.96 (ddd, J = 4.3, 3.2, 0.9 Hz, 2H), 4.75 – 4.67 (m, 4H), 4.55 (s, 8H).

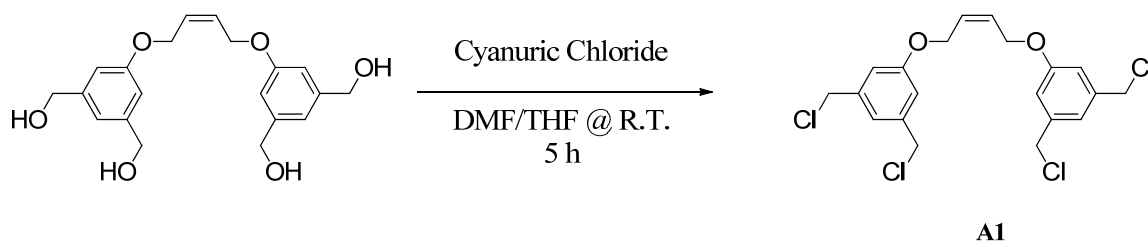


Figure A.6 Synthesis of tetra-functional chloro-terminated bis-dendritic CTA.

Octa-functional Chloro-Terminated Bis-dendritic CTA (A2) (Figure A.7). To cyanuric chloride (9.72 g, 52.2 mL) in 60 mL of anhydrous THF + 8 mL of anhydrous DMF in a 250 mL RBF was slowly added an anhydrous THF (35 mL) solution of compound **9** in Scheme 2.1 (3.92 g, 4.33 mmol) over a 5-min period. The mixture was stirred at room temperature overnight. The mixture was diluted with 40 mL of THF and filtered to remove precipitated cyanuric chloride-DMF complex, and the solvent was

freshly vacuum-distilled, rigorously purified COD (0.10 g, 0.92 mmol) to the mixture to start the polymerization reaction. The mixture was stirred at 40°C for 1 h. A large amount of degassed, freshly vacuum-distilled purified COD (1.94 g, 17.8 mmol) in degassed, anhydrous DCM (4 mL) was injected into the mixture. The mixture was stirred at 40°C for 16 h. An aliquot was taken for ^1H NMR analysis before the addition of 20 mL oxygen-containing DCM and 0.1 g of BHT. The mixture was precipitated into 300 mL of methanol at room temperature. The precipitated polymer was collected and dried *in vacuo* at room temperature overnight. 1.56 g of faint-yellow, transparent polymer was afforded (74.1% yield). Conversion of COD was 94.1%, and the *cis/trans* ratio was 1.98 (determined by ^1H NMR of the aliquot). GPC-LS: $M_w = 204$ kg/mol, PDI = 1.50.

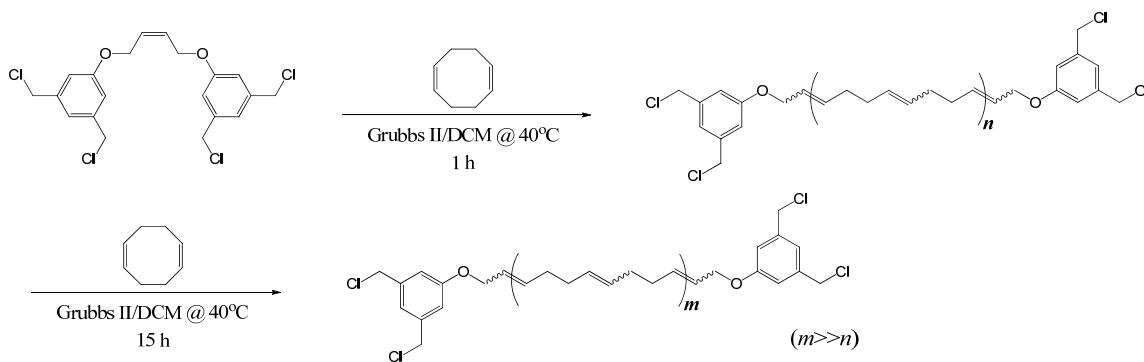


Figure A.8 Two-stage synthesis of telechelic 1,4-PB of $M_w = 204$ kg/mol with difunctional chloro-terminated dendritic end groups.

22K Telechelic 1,4-PB with Tetra-Functional Chloro-Terminated Dendritic End

Groups (Figure A.9). CTA A2 (0.259 g, 247 μmol) was placed in 50 mL Schlenk flask (charged with a stir bar), and degassed by 5 cycles of pulling vacuum/filling argon. Deoxygenated, anhydrous DCM (4 mL) was syringe-transferred into the flask to dissolve the CTA. The flask was placed in an oil bath at 40°C. The second-generation Grubbs

Catalyst (2.1 mg, 2.47 μmol) in deoxygenated, anhydrous DCM (1 mL) was injected into the mixture to equilibrate with the CTA, followed immediately by adding degassed purified *cis,cis,trans*-1,5,9-cyclododecatriene (CDDT, 2.00 g, 12.3 mmol) to the mixture to start the polymerization reaction. The reaction mixture was stirred at 40°C for 16 h, and precipitated into 150 mL of methanol at room temperature. The precipitated polymer was collected and dried *in vacuo* at room temperature overnight. 1.66 g of white polymer was afforded (73.5% yield). ^1H NMR (500 MHz, CDCl_3): δ = 7.07 (s, ArH), 7.02 (d, J = 1.5 Hz, ArH), 6.97 (d, J = 1.5 Hz, ArH), 6.96 (d, J = 1.5 Hz, ArH), 5.55 – 5.22 (br, =C(H)CH₂-, backbone), 5.06 (s, -O-(CH₂)-O-), 4.61 (d, J = 4.3 Hz, =CHCH₂O-, *trans* end group), 4.55 (s, -CH₂-Cl), 4.50 (d, J = 6.0 Hz, *cis* end group), 2.31 – 1.84 (br, =C(H)CH₂-, backbone). GPC-LS: M_w = 21.7 Kg/mol, PDI = 1.98.

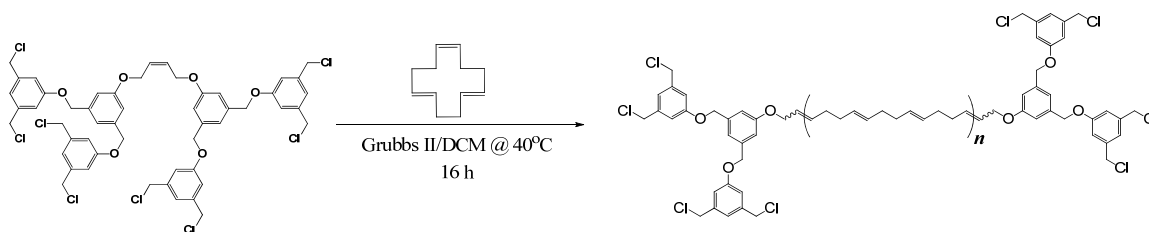


Figure A.9 Synthesis of telechelic 1,4-PB of M_w = 22 kg/mol with tetra-functional chloro-terminated dendritic end groups.

250K Telechelic 1,4-PB with Tetra-Functional Chloro-Terminated Dendritic End

Groups (Figure A.10). CTA **A2** (10.0 mg, 9.15 μmol) was placed in 50 mL Schlenk flask (charged with a stir bar), and degassed by 5 cycles of pulling vacuum/filling argon. Deoxygenated, anhydrous DCM (0.74 mL) was syringe-transferred into the flask to dissolve the CTA. The flask was placed in an oil bath at 40°C. 0.26 mL of 1 mg/mL anhydrous DCM solution of Grubbs II (0.26 mg, 0.31 μmol) was injected into the

mixture to equilibrate with the CTA for 5 min, followed immediately by adding a small amount of degassed, freshly vacuum-distilled purified COD (0.10 g, 0.92 mmol) to the mixture to start the polymerization reaction. The mixture was stirred at 40°C for 1 h. A large amount of degassed, freshly vacuum-distilled purified COD (2.00 g, 18.3 mmol) and degassed, anhydrous DCM (4 mL) were injected into the reactor. The reaction mixture was stirred at 40°C for 2 h. An aliquot was taken for ^1H NMR analysis before the reaction was terminated by the addition of butyl vinyl ether. Additional DCM (20 mL) and 0.1 g of BHT were added, and the mixture was precipitated into 300 mL of methanol at room temperature. Drying the collected polymer *in vacuo* at 35°C overnight afforded 1.60 g of faint-yellow, transparent polymer (78.7% yield). Conversion of COD was 82.1%, and the *cis/trans* ratio was 2.20 (determined by ^1H NMR of the aliquot). GPC-LS (THF, 35°C): $M_w = 254$ kg/mol, PDI = 1.58.

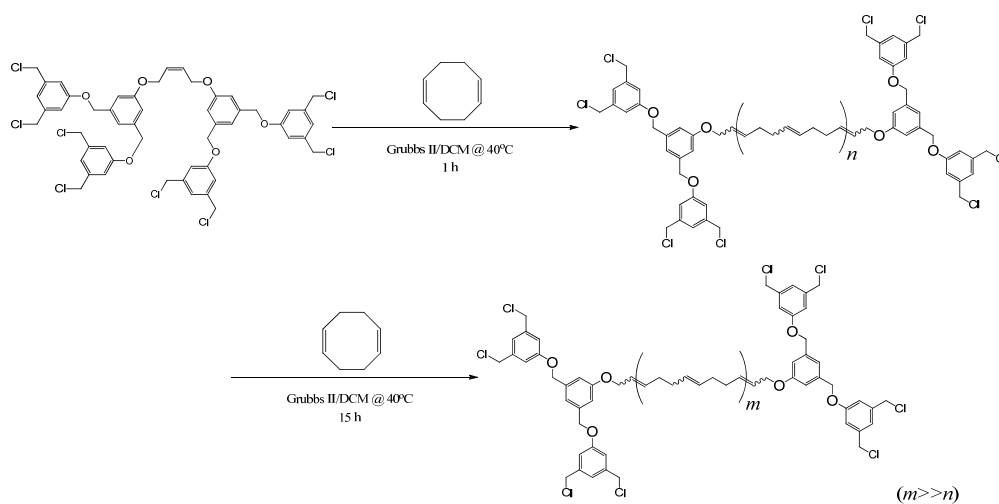


Figure A.10 Two-stage synthesis of telechelic 1,4-PBs of $M_w = 254$ and 430 kg/mol with tetra-functional chloro-terminated dendritic end groups.

430K Telechelic 1,4-PB with Tetra-Functional Chloro-Terminated Dendritic End Groups (Figure A.10). CTA A2 (10.0 mg, 9.15 μmol) was placed in 50 mL Schlenk flask (charged with a stir bar), and degassed by 5 cycles of pulling vacuum/filling argon. Deoxygenated, anhydrous DCM was syringe-transferred into the flask to dissolve the CTA. The flask was placed in an oil bath at 40°C. 0.26 mL of 1 mg/mL anhydrous DCM solution of second-generation Grubbs Catalyst (0.26 mg, 0.31 μmol) was injected into the mixture to equilibrate with the CTA for 7 min, followed immediately by adding a small amount of degassed, freshly vacuum-distilled purified COD (0.10 g, 0.92 mmol) to the mixture to start the polymerization reaction. The mixture was stirred at 40°C for 1 h. A large amount of degassed, freshly vacuum-distilled purified COD (2.00 g, 18.3 mmol) in degassed, anhydrous DCM (4 mL) was injected into the mixture. The mixture was stirred at 40°C for 4 h. An aliquot was taken for ^1H NMR analysis before the reaction was terminated. Additional DCM (20 mL) and 0.1 g of BHT were added, and the mixture was precipitated into 300 mL of methanol at room temperature. The precipitated polymer was collected and dried *in vacuo* at room temperature overnight. 0.73 g of faint-yellow, transparent polymer was afforded (14.7% yield). ^1H NMR (500 MHz, CDCl_3) of the aliquot showed that conversion of COD was 19%, and the *cis/trans* ratio was 3.26. GPC-LS (THF, 35°C): $M_w = 429 \text{ kg/mol}$, PDI = 1.49.

References

- (1) Izunobi, J. U.; Higginbotham, C. L. *J Chem Educ* **2011**, *88*, 1098.
- (2) Rubinstein, M.; Colby, R. H. *Polymer physics*; Oxford University Press: Oxford ; New York, 2003.
- (3) Nielen, M. W. F. *Mass Spectrom Rev* **1999**, *18*, 309.
- (4) Meyers, R. A. *Encyclopedia of analytical chemistry : applications, theory, and instrumentation*; Wiley: Chichester ; New York, 2000.
- (5) Yalcin, T.; Schriemer, D. C.; Li, L. *J Am Soc Mass Spectr* **1997**, *8*, 1220.
- (6) Pitet, L. M.; Hillmyer, M. A. *Macromolecules* **2011**, *44*, 2378.
- (7) Morita, T.; Maughon, B. R.; Bielawski, C. W.; Grubbs, R. H. *Macromolecules* **2000**, *33*, 6621.